

12

ESL-TR-82-47

FOD GENERATION BY AIRCRAFT TIRES

S.J. BLESS, L. CROSS,
A.J. PIEKUTOWSKI, H.F. SWIFT
UNIVERSITY OF DAYTON RESEARCH INSTITUTE
300 COLLEGE PARK AVE.
DAYTON, OHIO 45469

AUGUST 1983

FINAL REPORT
NOV 1981 - OCT 1982

OCT 06 83

APPROVED FOR PUBLIC RELEASE; DISTRIBUTION UNLIMITED



ENGINEERING AND SERVICES LABORATORY
AIR FORCE ENGINEERING AND SERVICES CENTER
TYNDALL AIR FORCE BASE, FLORIDA 32403

118 5011-011

NOTICE

PLEASE DO NOT REQUEST COPIES OF THIS REPORT FROM
HQ AFESC/RD (ENGINEERING AND SERVICES LABORATORY).
ADDITIONAL COPIES MAY BE PURCHASED FROM:

NATIONAL TECHNICAL INFORMATION SERVICE
5285 PORT ROYAL ROAD
SPRINGFIELD, VIRGINIA 22161

FEDERAL GOVERNMENT AGENCIES AND THEIR CONTRACTORS
REGISTERED WITH DEFENSE TECHNICAL INFORMATION CENTER
SHOULD DIRECT REQUESTS FOR COPIES OF THIS REPORT TO:

DEFENSE TECHNICAL INFORMATION CENTER
CAMERON STATION
ALEXANDRIA, VIRGINIA 22314

UNCLASSIFIED

SECURITY CLASSIFICATION OF THIS PAGE (When Data Entered)

REPORT DOCUMENTATION PAGE		READ INSTRUCTIONS BEFORE COMPLETING FORM
1. REPORT NUMBER ESL-TR-82-47	2. GOVT ACCESSION NO. 15-12277	3. RECIPIENT'S CATALOG NUMBER
4. TITLE (and Subtitle) FOD Generation by Aircraft Tires		5. TYPE OF REPORT & PERIOD COVERED Final Report Nov. 1981 - Oct. 1982
		6. PERFORMING ORG. REPORT NUMBER UDR-TR-82-136
7. AUTHOR(s) S. J. Bless, L. Cross, A. J. Piekutowski, H. F. Swift		8. CONTRACT OR GRANT NUMBER(s) F08635-82-K-0102
		10. PROGRAM ELEMENT, PROJECT, TASK AREA & WORK UNIT NUMBERS PE - 63723F JON - 21042B69
9. PERFORMING ORGANIZATION NAME AND ADDRESS University of Dayton Research Institute 300 College Park Ave. Dayton, Ohio 45469		12. REPORT DATE August 1983
11. CONTROLLING OFFICE NAME AND ADDRESS Air Force Engineering and Services Center Engineering and Services Laboratory (RDCR) Tyndall Air Force Base, FL 32403		
14. MONITORING AGENCY NAME & ADDRESS (if different from Controlling Office)		13. NUMBER OF PAGES 235
		15. SECURITY CLASS. (of this report) Unclassified
		15a. DECLASSIFICATION/DOWNGRADING SCHEDULE
16. DISTRIBUTION STATEMENT (of this Report) Approved for public release; distribution unlimited.		
17. DISTRIBUTION STATEMENT (of the abstract entered in Block 20, if different from Report)		
18. SUPPLEMENTARY NOTES The availability of the report is specified on reverse of front cover.		
19. KEY WORDS (Continue on reverse side if necessary and identify by block number) Runway Repair, FOD (foreign object damage), Stereophotography, Tire Mechanics, Debris Lofting, FOD Lofting Modelling, Debris Lofting Trajectories, Tire Scaling		
20. ABSTRACT (Continue on reverse side if necessary and identify by block number) Lofting of loose debris by overrolling tires was investigated by experiments and analysis. Trajectories of lofted particles were determined with a stereoscopic camera system. Tire speeds ranged up to 40 mph; single- and dual-wheel carriages were used. Debris was mostly stones, 1 inch and smaller. Concrete and packed dirt surfaces, both wet and dry, were included.		

UNCLASSIFIED

SECURITY CLASSIFICATION OF THIS PAGE (When Data Entered)

UNCLASSIFIED

SECURITY CLASSIFICATION OF THIS PAGE(When Data Entered)

The probability of lofting a stone, given an encounter, was typically 15 percent, until the stone density exceeded one stone per footprint area; then the lofting probability was much less. Launch directions were mainly within 20 degrees of the direction defined by the wheel axle. Launch velocities were mainly less than 2.5 m/s. The probability of launching debris to above 4 m/s was about 0.03. Angularity and size both increase lofting probability. Water did not greatly affect stone lofting, except for very small stones (6 mm).

Extrapolations of these results to airfield scenarios predict that the danger of engine ingestion of nosewheel generated debris is minimal. The worst case considered was the F-4, which was less than 0.17 stones/km ingestion. These conclusions are based on extrapolations and need to be checked with experiments at higher tire speeds and loads.

UNCLASSIFIED

SECURITY CLASSIFICATION OF THIS PAGE(When Data Entered)

TABLE OF CONTENTS

Section	Title	Page
I	INTRODUCTION	1
	A. BACKGROUND	1
	B. OBJECTIVES OF PROGRAM	1
	C. APPROACH	2
II	EXPERIMENTAL TECHNIQUES	4
	A. TEST BED	4
	B. TIRE CARRIAGE	4
	C. TV MONITOR	6
	D. INSTRUMENTATION	6
III	ANALYTICAL FRAMEWORK	11
	A. SELECTION OF TEST PARAMETERS	11
	B. SCALING CONSIDERATIONS	13
	1. Linear Size Scaling	15
	2. Viscosity Scaling	16
	3. Selection of Test Matrix Parameters	16
	C. INTERPRETATION OF RESULTS	19
	D. UNCERTAINTIES IN DATA	20
	E. FORM OF VELOCITY DISTRIBUTION	22
IV	FIRST-PHASE TESTS	24
	A. DESCRIPTION OF TESTS	24
	B. RESULTS OF TESTS	27
	C. ANALYSIS OF RESULTS	46
V	SECOND-PHASE TESTS	53
	A. LOFTING MECHANISMS FILMS	53
	B. RESULTS	55
	1. Single-Versus Dual-Wheel Comparison	55
	2. Saturation Effects	56
	3. Effects of Tire Velocity	59
	4. Effect of Tire Pressure	59
	5. Effect of Load (L_T)	60

TABLE OF CONTENTS (CONTINUED)

Section	Title	Page
	6. Effect of Stone Shape	61
	7. Effect of Stone Size	62
	8. Characteristics of High Speed Stones	62
	9. Effect of Wheel Suspension	63
	10. Effect of Debris Type	63
VI	THIRD-PHASE TESTS	66
	A. STONE VISUALIZATION TECHNIQUE	66
	B. HIGH-SPEED MOVIES	68
	C. STONE TRAJECTORY DATA AND ANALYSIS	70
	1. Baseline Data for Small Rocks	70
	2. Effect of Tire Velocity	70
	3. Effect of Tire Pressure	72
	4. Effect of Rock Size	72
	5. Effect of Load	72
	6. Effect of Coverage (Saturation)	73
	7. Effect of Water Depth	73
	8. Effect of Rock Placement Patterns	74
	9. Inside-Outside Bias	75
	10. Trajectory Statistics	76
	11. Water Suppression of Lofting	79
	12. General Review of Water Effects	79
VII	ANALYTICAL MODELLING OF LOFTING FROM AIRCRAFT RUNWAYS	81
	A. INFERENCES FROM THE DATA	81
	B. ENGINE CAPTURE CRITERIA	82
	C. PINCH STONE LOFTING MODELS	83
	D. HAMMER-LOFTING MODEL	86
	E. APPLICATION TO RUNWAY SCENARIOS	87
VIII	SUMMARY AND CONCLUSIONS	90
	A. TECHNIQUES	90
	B. GENERAL CHARACTERISTICS OF LOFTED DEBRIS	90
	C. CONCLUSIONS FOR LOFTING MECHANISMS	92
	D. CONCLUSIONS FOR AIRFIELD OPERATIONS	92
	E. RECOMMENDATIONS	94
IX	REFERENCES	95

TABLE OF CONTENTS (CONCLUDED)

Appendix	Title	Page
A	MODELLING SUPPORT FOR THE UDRI/USAF FDL STONE-LOFTING PROGRAM	97
B	TEST DATA FOR STONE-LOFTING PROGRAM	161

LIST OF FIGURES

Figure	Title	Page
1	Test Section with Concrete Bed, Prior to Test.	5
2	Single-Tire Carriage and Weight Bucket.	7
3	Dual-Tire Carriage.	7
4	Footprint of Tire.	9
5	Instrumentation Plan for Orthogonal Cameras.	9
6	General Forms of Stone Velocity Distribution.	23
7	Data Reporting Form.	26
8	Average Number of Stones Present Before Each Pass During Test IC1A.	28
9	Wooden Grid Used to Place Rocks.	29
10	Test IC7, Pass 1, Left Camera.	29
11	Test IC7, Pass 1, Right Camera.	30
12	Test IC7, Pass 2, Left Camera.	30
13	Test IC7, Pass 2, Right Camera.	31
14	Black and White Test Picture of Splash from Puddle on Concrete.	31
15	Test IA16, Pass 13, Left View.	33
16	Test IA16, Pass 13, Right View.	33
17	Photograph from Video Tape Showing Condition of Compacted Bed After 10 Consecutive Passes in Test IA15/SM.	34
18	Trough Array.	34
19	Trough Calibration.	35
20	Appearance of Bed Used in Test IWCA1, Before Test Started.	37
21	IWCA1 Bed After Three Passes (First Run).	37
22	Velocity Distribution of Lofted Rocks in Test IC4A (Test on Concrete at 25 mph).	39
23	Distribution of Velocities for All Rocks, Test IC1A.	41
24	Distribution of Velocities for All Rocks, Test IC1A, Semilog Plot.	42
25	Distribution of Launch Directions Observed in Test IC1A.	44

LIST OF FIGURES (CONTINUED)

Figure	Title	Page
26	Distribution of Velocity with Direction Angle for Baseline Test (ICLA).	45
27	Distribution of Elevation Angles for Baseline Test.	45
28	Trajectory Height Category vs. Launch Probability for the Baseline Experiment Conducted on a Hard, Dry Surface.	48
29	Trajectory Heights for All Large Stones Launched During Second and Third Passes.	50
30	Trajectory Heights for All Large Stones Launched During First Passes.	51
31	Trajectory Heights for All Small Stones Launched During Second and Third Passes.	52
32	Probability of Lofting Large Stones to $z > 125$ mm as a Function of Coverage (Dual Wheels).	57
33	Number of Large Stones Lofted Per Meter of Travel as a Function of Coverage (Dual Wheels).	57
34	Variation of Number of Lofted Stones with Contact Area.	61
35	Elevation Angle Distributions for Fast Stones.	64
36	Direction Distribution for Fast Stones.	64
37	Small Stones Lofted in Test III-9.	69
38	Probability of Lofting versus Coverage.	73
39	Normal 10 Percent Rock Placement Pattern.	74
40	Rock Placement Patterns for Comparison Tests.	75
41	Maximum Height Distribution of All Large Rocks Launched from Wet Pavement in Third Test Matrix.	78
42	Floating Objects After Launch.	80
43	Minimum Vertical Velocity, U_z , vs. Aircraft Speed, U_p , For Ingestion of Debris Lofted By The Nosewheel of An F-4E Aircraft.	84
44	Minimum Outward Velocity, U_x , vs. Aircraft Velocity, U_p , For Ingestion of Debris Lofted By The Nosewheel of An F-4E Aircraft.	84

LIST OF FIGURES (CONCLUDED)

Figure	Title	Page
45	Minimum Vertical Velocity, U_z , vs. Aircraft Speed, U_p , For Capture of Stone Lofted By The Nosewheel of An F-15 Aircraft	85
46	Minimum Outward Velocity Component vs. Aircraft Velocity for Ingestion of Stone Lofted By The Nosewheel of An F-15 Aircraft	85

LIST OF TABLES

Table	Title	Page
1	THREE TEST PHASES	3
2	NOMINAL VALUES OF VARIABLES FOR TIRE LOFTING TESTS	12
3	SCALING RELATIONSHIPS FOR NOMINAL VALUES WITH LINEAR SCALING	18
4	FIRST TEST MATRIX	25
5	RESULTS FOR WET AGGREGATE TESTS (AVERAGE VALUES PER RUN)	38
6	SECOND TEST MATRIX	54
7	PARTS I AND II RUNWAY FOD SUMMARY - PHASE III	67
8	SUMMARY OF OBSERVATIONS FROM THIRD TEST MATRIX	71
9	SUMMARY OF TRAJECTORY DATA	77

SYMBOLS

A	contact area
C*	saturation coverage
d	stone diameter
D	tire diameter
g	acceleration of gravity
L	load
L _s	roll distance
N	number of stones lofted
P	inflation pressure, probability
Q	probability of lofting
s	scale factor
S	fraction of stones with $v > v_{co}$
t	time
u	material velocity
v	stone velocity
V	tire velocity
W	load
x	distance, variable
z	vertical distance
σ	stress, standard deviation
μ	viscosity, mean
ω	angular frequency of tire
ρ	density

SYMBOLS (CONCLUDED)

Superscripts:

- * normalized value
- l values for laboratory tests

Subscripts

- o initial value
- co cut off
- T tire

SECTION I
INTRODUCTION

A. BACKGROUND

Because airfield runways will be prime targets in future military conflicts, the United States Air Force Engineering and Services Center (AFESC), Rapid Runway Repair Branch (AFESC/RDCR) is engaged in a program to upgrade ability to recover from attacks on runways. Postattack runways are likely to be very dirty by conventional standards. Debris sources will include crater ejecta, fill material from runway repair, and shell case fragments.

The presence of runway debris raises the potential of foreign object damage (FOD) to aircraft. Material lofted from runways may damage tactical aircraft to cause immediate mission loss (Reference 1). The primary aircraft vulnerability is ingestion of foreign objects by jet engines.

B. OBJECTIVES OF PROGRAM

We have conducted a research program to investigate tire-lofting mechanics and provide information to analyze and solve the problem of operating aircraft effectively from runways during intense combat. The objectives of the research program were as follows.

1. Reveal the mechanisms responsible for lofting of debris by tires for debris characteristic of damaged runways.

2. Develop an analytical model for debris lofting. The model should be based on physical understanding of the lofting problem and calibrated by empirical data.

3. Quantitatively show how debris lofting is affected by tire and debris parameters. Develop and evaluate concepts for suppressing debris lofting.

4. Quantitatively predict consequences of aircraft operation on debris-covered runways.

5. Identify need for additional investigations to evaluate FOD hazards from operation on unconventional runways.

C. APPROACH

Lofting action of tires was studied on a reduced-scale test track using high-speed photography. The facility used was the Air Force Mobility Development Laboratory (MDL) located at Wright-Patterson Air Force Base. The MDL test track is 27 meters in diameter, and test vehicles can be transported at speeds up to 20 meters/second relative to the track. Loads of up to 1,000 pounds may be imposed on the tire. This indoor facility can be operated with delicate instrumentation in any weather. It is also located near the University of Dayton, so that equipment and other experimental components could be quickly brought to the site, and data could be speedily returned to the University for processing.

The University helped to adapt the MDL for the proposed program. The adaptation included design and fabrication of a carriage for the tire, shielding to protect the facility from lofted stones, and a test track section suitable for simulating runway surfaces. The facility was operated by Air Force personnel, but the instrumentation was operated by University personnel.

Tire-induced particle lofting was investigated under conditions simulating important current and candidate runway repair materials. Configurations included: loose stones on hard pavements, beds of particles packed to various depths and densities, presence of standing water, and debris particles of various shapes and sizes. Likewise, tire configurations resembled those found on present or future fighter aircraft; both single and dual wheels were employed.

The matrix of experiments included combinations and permutations of the following variables.

- stone shape (smooth or angular)
- pebble size
- load
- tire pressure
- pebble number density
- tire speed
- single or dual tires
- presence or absence of standing water

Special diagnostic equipment was developed and deployed. Analysis of the data provided quantitative values of the trajectory parameters of stones lofted by overrolling tires.

The testing was conducted in three phases, each dedicated to a particular set of encounter parameters. The test phases are listed in Table 1.

The results of the experimental program led to the development of analytical models for debris-lofting processes. The experimental and analytical results were used to develop predictive equations for numbers of lofted stones and stone trajectories. The predictive equations resulting from the proposed program were used to investigate and evaluate several operational scenarios for F-4, F-16 and F-16 aircraft.

TABLE 1. THREE TEST PHASES

- | |
|--|
| I. Single wheels on concrete and aggregate, dry and wet test tracks. |
| II. Dual wheels on dry concrete and aggregate test tracks. |
| III. Wet concrete test tracks. |

SECTION II EXPERIMENTAL TECHNIQUES

Preparation for the test program required completion of a number of complex tasks:

- a. modification of a test track section,
- b. fabrication of a tire carriage to mount on the MDL whirling arm,
- c. assembly of an orthogonal photographic system for trajectory diagnostics,
- d. composition of a computer program for reducing the data,
- e. setup of video monitor and recording units, and
- f. installation of screening to protect MDL equipment from lofted water and stones.

Details of the experimental setup vary slightly in each of the three test phases.

A. TEST BED

One test section from the MDL track was modified for the present program. The 68-inch long 24-inch wide central plywood deck was removed, and the aluminum track section framework was modified. The altered sections could be fitted with a 6-inch thick concrete slab, or a 6-inch deep bed of graded aggregate. Figure 1 illustrates the modified section in place. A water connection was provided to a holding tank to permit the aggregate beds to be saturated from below. This was done to assure that downward drainage would not lead to variations in bed properties during the tests.

B. TIRE CARRIAGE

Two aluminum struts and a steel weight bucket were constructed. One strut was used for single-tire tests, and the other for dual-tire tests. These were rigidly attached to the heavepost on the MDL apparatus. The heavepost was free to move vertically as it



Figure 1. Test Section with Concrete Bed, Prior to Test.

was pushed around the track by the drive motor. Figures 2 and 3 show photographs of the tire carriages and weight bucket.

The test wheel is a standard commercial unit (although it is no longer manufactured) for a 13x5.0-4 tire. Goodyear tires were used. The 14-ply rating assured safe operation at 200 psi. This tire has a chine that was ground off. The tread is rib type; tread width is 1 inch and groove width is 0.18 inch. Figure 4 shows the footprint obtained with this tire at 200 psi inflation pressure and under a total load of 1,000 pounds.

Dual-tapered roller bearings supported the wheel on the axle. Temperatures of the tire and bearings were monitored during the tests; the rise was never more than 10°C.

The weight bucket was designed to hold up to 850 pounds of lead bricks. The single-tire carriage, empty weight bucket and heavepost, weighed 150 pounds. All aspects of the tire carriage were designed with a safety factor of two.

C. TV MONITOR

A color video monitor and 3/4-inch video tape recorder were used to record the appearance of the track between tire encounters during the first and second test passes. The video recorder could be used to count how many stones were available to be lofted.

D. INSTRUMENTATION

Pebble trajectories were recorded by orthogonal Nikon type EM 35 millimeter cameras. The cameras were fixed to a 6-meter long rigid box beam. The box beam has a three-point suspension system for leveling. Each camera was mounted on an individually adjustable platform so that its optic axis could be precisely aligned. The box beam was positioned parallel to the test track. The cameras had motor advance units. Lens focal lengths were 135 millimeters, and the field of view in the tire plane was approximately 1 square meter. A special flash unit was constructed

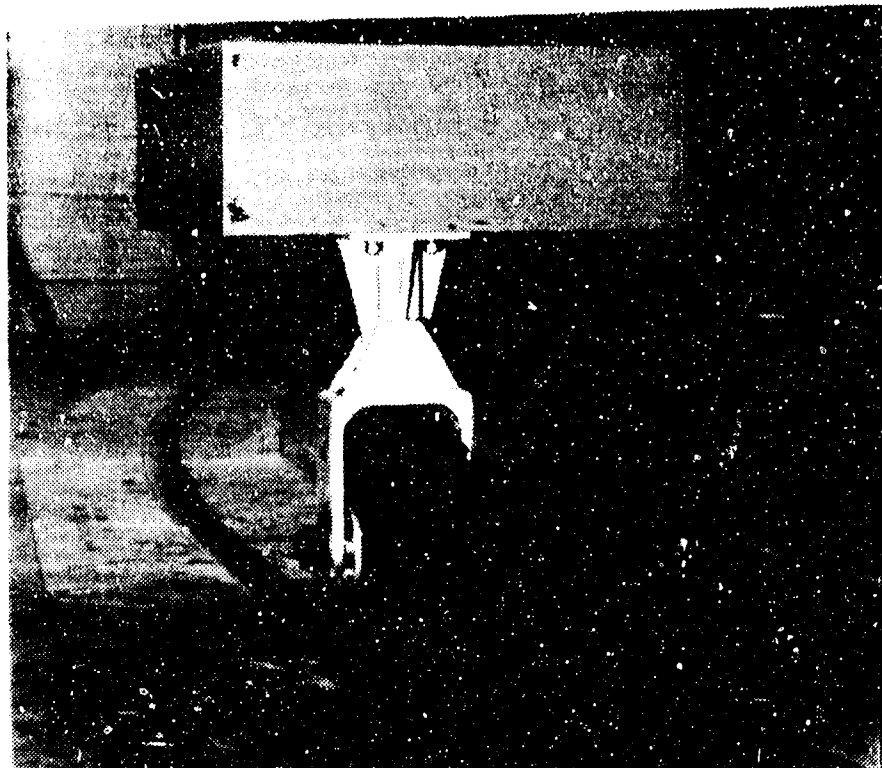


Figure 2. Single-Tire Carriage and Weight Bucket.

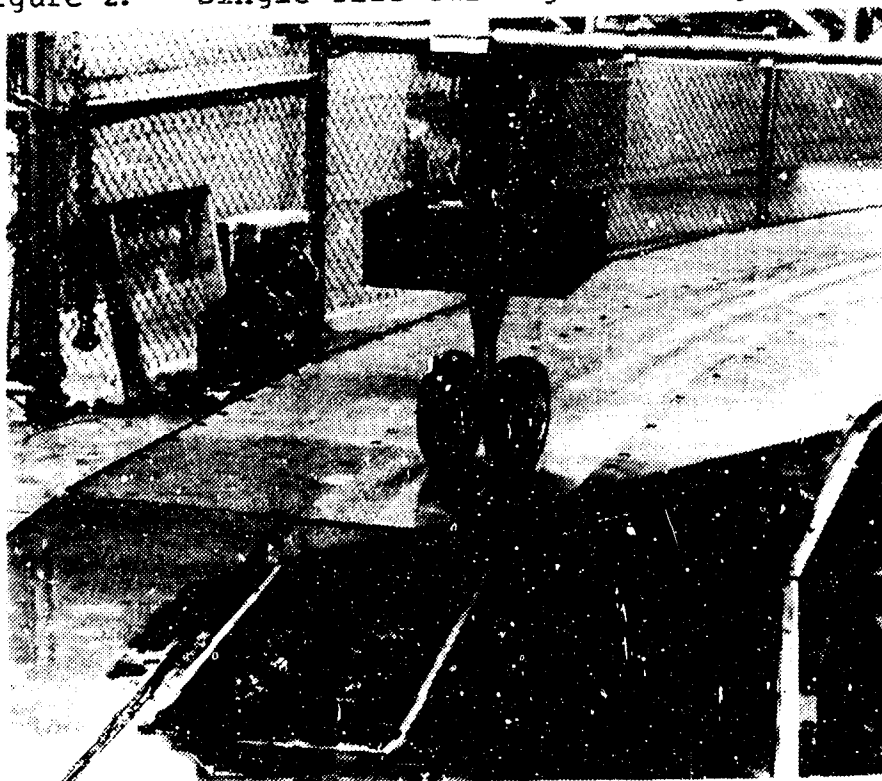


Figure 3. Dual-Tire Carriage.

that produced any number of 10 μ s duration flashes at rates of up to 500 hertz. Pulses were generated by a Hewlett-Packard type 8011B generator, and the Xenon flash bulb was fired via a Unitrode type GA201A SCR. Figure 5 shows a schematic of this system.

Each time that the tire passed the field, up to eight flashes were initiated. It was found that 50 hertz was an adequate rate for most tests. The camera shutters were opened, so that multiple exposures were obtained. It was necessary to conduct the tests in a darkened room at night. Later sections of the report contain many examples of these photographs. Kodak[®] RAR 2479 film was used, processed for ASA 2000. The usual aperture was f/5.6. In a few cases, High Speed Ektachrome[®] film was used. Resolution in the tire plane was approximately 0.3 mm; there was no motion blur.

The fence between the tire plane and the camera was painted black. It was so far out of focus that rocks behind it could be easily distinguished. It was also necessary to place a black backdrop behind the object plane. Room lights were dimmed for the tests, although there was still enough light for video monitors.

In the third test phase, the photography technique was modified to visualize the lofted stones through the clutter of lofted water drops. The special techniques employed and results are discussed in a later section of this report.

A 0.5 mm HeNe laser was used to trigger the strobe unit. Microswitches were placed on the center post of the MDL rotating arm to obtain trigger signals for opening and closing the camera shutters, which operated in the "bulb" mode. These trigger signals were also used to extinguish and turn on a spotlight that illuminated the test area for a video camera.

A computer program was written to reduce the stereo data. The program iteratively solves the optical transfer matrices that relate images in the film plane to objects in space. The program was repeatedly tested by photographing static fiducial

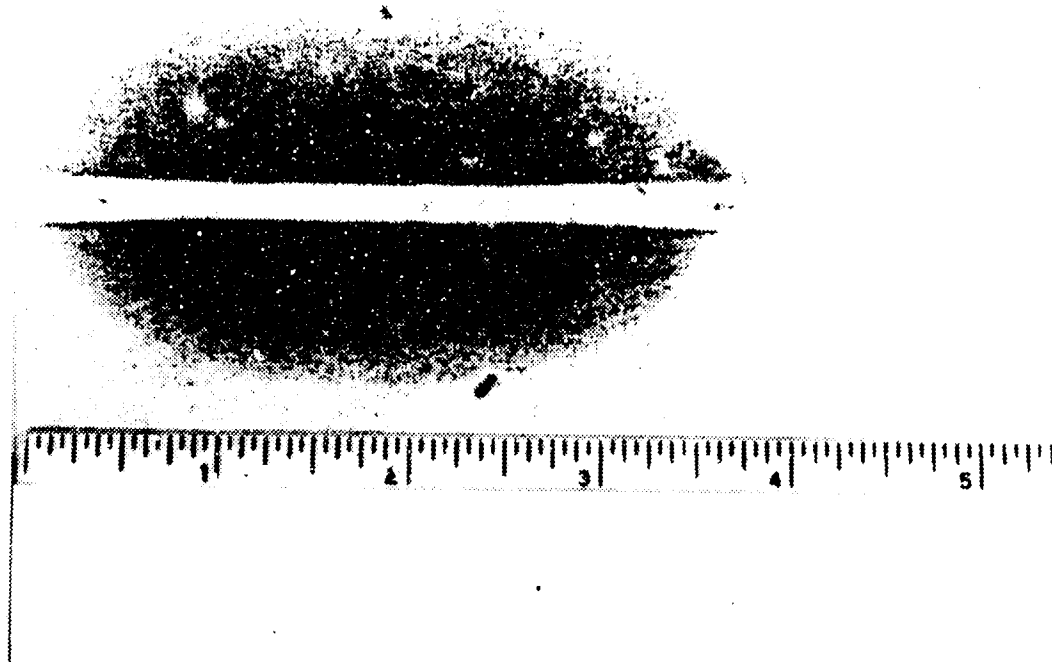
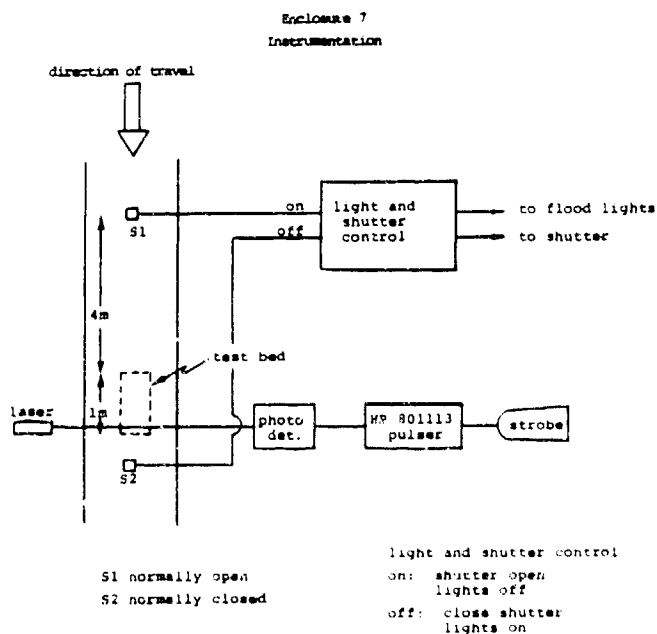


Figure 4. Footprint of Tire. 200 psi Inflation Pressure, 1000-pound Load.



NOTE: S1 and S2 are placed on central shaft.

Figure 5. Instrumentation Plan For Orthogonal Cameras.

structures. It was found to be accurate to ± 2 mm. (Somewhat larger errors were often encountered in reducing actual data because of the ambiguity in rock centers of mass.)

Data reduction began with a survey of the negatives. Frames in which stones were present above a specified height were designated. Those negatives were printed on 3x5 or 5x7 photographic paper. Stadia posts in the field of view were used to construct orthogonal coordinate axes whose origin was also the intersection of the two camera axes. These posts also provided fiducials for magnification. Lofted rocks were labeled on each print. The prints were then laid on a Talos[®] digitizing tablet, and the coordinate axes, magnification references, and pebble coordinates are read into a VAX computer.

The computer program operated on the digitized data to compute the following information for each rock:

- position in real space at each exposure time
- velocity between points, all components, and total
- a second-order curve fit through the points, extrapolated to the ground plane
- the launch velocity
- the launch elevation angle
- the launch direction
- the initial position
- the maximum height.

SECTION III ANALYTICAL FRAMEWORK

The goal of the test program was to acquire empirical support data for a quantitative understanding of processes associated with lofting of runway debris by aircraft tires.

To that end, the test program consisted of a variety of scaled experiments. In these scaled experiments, a small aircraft tire was run over several types of specially prepared test surfaces. The test surfaces were representative of those encountered in the Bomb-Damaged Runway (BDR) environment. Measurements of the velocity and frequency of debris lofted by the tire were the prime experimentally determined data.

A. SELECTION OF TEST PARAMETERS

The basic organization of the test matrices for the three test phases was based on variations from a nominal condition which was judged to represent the best approach to overall scaling of experimental results. Test variables considered included the following: tire type and size, tire velocity, tire inflation pressure, test bed particle size and shape, test bed strength (California Bearing Ratio, CBR), effect of standing water on test bed surface, use of single or dual tires, and number density of debris. Values taken as nominal (baseline) are listed in Table 2. Other values used in the various test phases are also listed.

The test tire was a 13-inch diameter tire used on the Falcon jet. Concrete slabs, 6 inches thick, were used to model hard surfaces. The concrete slabs were installed above a suitable sand substrate. A dry surface was the nominal test condition. Surfaces with standing water were modeled by placing a 1/2-inch flexible berm around the test section and filling the resulting cavity with water.

TABLE 2. NOMINAL VALUES OF VARIABLES FOR TIRE-LOFTING TESTS

Variable	Nominal Value	Other Values
CBR	∞	100
Velocity	40 mph	25 mph, 30 mph
Maximum stone size (inch)	1.0	0.5, 0.25
Shape	Angular	smooth
Inflation pressure (psi)	200	150, 75
Water level (inch)	dry	0.35, 0.5
Load (pounds)	1000	500
Coverage (area 1)	20%	1, 2, 5, 10%
Number of wheels	1	2

Back-filled craters were modeled with beds of well-graded crushed limestone. The particle sizes were scaled from the fill used in current practice. The coefficient of gradation* was 60, and the maximum particle had characteristic dimensions of 1.0 inch. Test beds of these materials were tamped to a CBR of 100, using a pneumatic tamper. CBR was measured by using a plunger with a 5-in² cross section. When loaded to 100 lbs/in², this plunger had no measurable sinkage into the tamped beds. The aggregate test beds were 12 inches thick, 24 inches wide, and 6 feet long. When they were water saturated, the water was let in from beneath until there was standing water on top.

Particle shape was both angular or rounded. The angular particles were composed of crushed limestone and the smooth ones were granite.

Two wheel loads were used. The nominal wheel load was 1,000 pounds, the maximum that the carriage could accommodate. Other tests used 500 pounds.

* This is defined in Reference 2.

B. SCALING CONSIDERATIONS

The MDL could not exactly simulate an aircraft nosewheel during takeoff roll or landing. The facility is limited in maximum speed and maximum applied load. Therefore, it was necessary to use appropriate scaling relationships to relate tests at the MDL to the phenomena that would occur with an actual aircraft tire.

Scaling relationships are based on theoretical assumptions regarding dominant physical mechanics. Equations of motion for continua are written in the form:

$$(\text{acceleration} \times \text{unit mass/unit volume}) = \Sigma(\text{force/unit volume}) \quad (1)$$

The forces that play a role in tire lofting may arise from viscosity effects in the tire or ground materials, elastic deformation of the tire, hydrodynamic drag, gravity, centrifugal acceleration, friction, etc. To develop an appropriate scaling relationship, it is not necessary to solve Equation (1), only to correctly represent the functional relationships between independent and dependent variables.

Scaling relationships for the variables in Equation (1) are clarified by introducing nondimensional variables. The process is nicely illustrated by application to the well-known phenomena of hydrodynamic drag. When the dominant forces causing fluid to move are viscous, then Equation (1) equates viscous forces proportional to gradients of velocity gradients ($\nabla^2 u$) to inertial forces ($\rho \, du/dt$). For steady flow, the mathematical expression of this relationship is

$$\rho(\mathbf{u} \cdot \nabla)\mathbf{u} = \mu \nabla^2 \mathbf{u}, \quad (2)$$

where μ is the viscosity. In order to show under what conditions two flows are similar, we introduce nondimensional variables. Then if two solutions are identical, it does not matter what size the system actually is. Let $u^* = u/u_0$, $x^* = x/x_0$, where u_0 and x_0 are characteristic velocities and lengths.

It is convenient here to take u_0 as the value of u when $x = x_0$. Now Equation (2) becomes

$$(\vec{u}^* \cdot \nabla) \vec{u}^* = \frac{\mu}{\rho x_0 u_0} \nabla^2 \vec{u}^* . \quad (3)$$

Regardless of what the actual solution to Equation (3) is, two systems will behave in geometrically similar ways if the term $\mu/\rho x_0 u_0$ is the same in both systems. This term is the Reynold's number, which is well known to scale drag phenomena in fluids.

The equation of motion for the continua (tires, stones, and ground) involved in a tire/ground encounter may be written as

$$\rho \frac{d\vec{u}}{dt} = -\nabla\sigma + \rho\omega x\vec{u} + \rho g + \mu\nabla^2\vec{u} . \quad (4)$$

The terms on the right represent stress gradients, centrifugal forces, gravity, and viscous forces. There are more terms if stress is not a linear function of strain or depends on strain rate. Nondimensionalization of Equation (4) yields the following scaling parameters:

- (a) $\frac{P_0 t_0}{\rho u_0 x_0}$ for conventional elastic-plastic forces
- (b) ωt_0 for centrifugal forces
- (c) $\frac{g t_0}{u_0}$ for gravity.

If it were possible to find two systems in which terms (a), (b), and (c) were the same in both systems, then scaling would be complete, as long as Equation (4) was complete. Unfortunately, that is not possible; all forces cannot be scaled at once.

1. Linear Size Scaling

The most commonly used scaling is based on term (a) above. Let superscript l denote the laboratory-scale experiment, and unscripted variables denote real values. The scaling is:

$$P_0^l t_0^l / \rho^l u_0^l x_0^l = P_0 t_0 / \rho u_0 x_0 \quad (5)$$

The conventional way to obtain this equality is:

$$\begin{aligned} \rho^l &= \rho \\ P_0^l &= P_0 \\ u_0^l &= u_0 \\ x^l/x &= t^l/t \equiv s . \end{aligned} \quad (6)$$

Thus, lengths and times are multiplied by a factor, s , and other variables are left unscripted. If the tire is pushed down by a weight, W , then:

$$\begin{aligned} W &= P_0 A \\ W^l &= P_0^l A^l = s^2 P_0 A = s^2 W . \end{aligned} \quad (7)$$

Thus, the scaled wheel loading is s^2 times the real wheel loading.

Gravity effects are reduced in subscale systems. It can be seen from term (b) that a gravitational acceleration equal to g/s would have to be present (where $s < 1$) for gravity to be correctly scaled.

Centrifugal force is correctly scaled by this technique. The tire angular velocity is $\omega = V/D$, and $\omega^l = V^l/D^l$. Since $V^l = V$ and $D^l = sD$, $\omega^l = \omega/s$. For example, the tire in a half-scale system turns twice as fast. Since $t_0^l = s t_0$, term (b) does not depend on s . Hence, centrifugal forces also result

in the same velocities at scaled times and distance as the real system.

Interfacial friction is also scaled correctly by linear scaling. The friction force is proportional to the force on the ground, P_0A . Thus, during the contact time which is proportional to D/V , friction may impart momentum PAD/V to a particle. The particle then has momentum proportional to ρd^3u . Evidently the particle velocity, u , is proportional to $PAD/\rho d^3$, and is unchanged by linear scaling.

Hydroplaning, as expected, also scales by linear scaling. A frequently used empirical formula for hydroplaning onset is:

$$V_H = 10.35 P \quad (8)$$

where P is in psi and V_H in mph. A 200 psi aircraft tire hydroplanes at 146 mph, regardless of its size.

2. Viscosity Scaling

Experiments involving standing water may be scaled by the Reynold's number:

$$\mu^l/V^l D^l \rho^l = \mu/VD\rho. \quad (9)$$

For the same materials ($\mu^l = \mu$, $\rho^l = \rho$), this reduces to:

$$\frac{V^l}{V} = \frac{D}{D^l}. \quad (10)$$

Equation (10) means that viscosity effects are correctly scaled when the tire test velocity is increased by the same proportion by which the tire diameter is decreased.

3. Selection of Test Matrix Parameters

Linear scaling was the principal consideration in test matrix design. Thus, the results can be related to larger tires, but not faster tires.

The requirement $s = D^{\ell}/D$ and $W^{\ell} < 1,000$ pounds led us to select as small a value of D^{ℓ} as practical. On the other hand, the requirements that $P_O^{\ell} = P_O$ mean that the tire must have a relatively high inflation pressure. There are very few such small high-pressure tires. The best one identified has $D^{\ell} = 13.0$ inches.

Linear scaling implies that the actual tire velocity be reproduced in the laboratory model. The maximum speed of the carriage at the MDL was about 40 mph. Boeing found that generation of lofted debris seemed especially efficient for $V \sim 40$ mph. Therefore, 40 mph was selected as the nominal carriage velocity in the test program.

The scale factor may be taken as D^{ℓ}/D . It varies according to which full-tire size is being modelled. The debris size should be scaled the same way as the tire size. In Table 3, scaling is detailed for an 18-inch full-scale tire. Thus, the scale factor is $s = 0.69$. The maximum stone size for the well-graded gravel fill in a runway repair is 1.5 inches. Thus, the maximum stone size to be used in the tests would be 1.04 inches. In fact, we specify the nearest sieve size as 1.0 inch. The CBR is unchanged in the scaled and full-size systems, since stresses are scaled 1:1. The experiments may be regarded as scaled models for other tire sizes that interact with other particle sizes.

The tire shape is less well scaled than other parameters. Linear scaling would require that the tire wall thickness be reduced in proportion to its diameter. For example, an F-4 tire is tubeless, 18 x 5.5 x 8.0 (O.D. x width x I.D.) with 14 plies. The test tire is also tubeless, but it is 12.5 x 4.7 x 4.5, and also 14 plies (apparently). Thus, the test tire is a little squattier than a truly scaled down F-4 tire, which would be 12.5 x 3.8 x 5.5. In addition, the test tire has a nearly semicircular tread cross section rather than a nearly flat one characteristic of nosewheel tires for modern

TABLE 3. SCALING RELATIONSHIPS FOR NOMINAL VALUES WITH LINEAR SCALING

Quantity	Nominal Test Values	Full Scale Values
p (psi)	200	200
D (in)	12.5	18
d (in)	1.0	1.5
V (mph)	40	40
water depth (in)	0.35	0.5
weight (lbs)	1000	2100

tactical aircraft. A flat-tread tire footprint increases to full width as light loads are applied and footprint length grows as loads are increased to full operational levels. Both the width and length of the test tire's footprint increase as load levels are increased within the tire's load-carrying capability.

Viscosity scaling is accomplished by increasing the velocity by s . Thus, for the nominal test condition ($v^0 = 40$ mph), viscosity effects are the same as for an aircraft velocity of 28 mph. A particle that is accelerated by fluid drag to a certain velocity in the lab test would be accelerated to $1/s$ times that velocity in a full-scale encounter. The variation of viscous effects with Reynolds number can be determined by running at a higher velocity, to obtain a value of the Reynolds number close to that characteristic of water flow under a full-scale tire.

C. INTERPRETATION OF RESULTS

Before describing the results of the experiments, it is helpful to review briefly the mathematical concepts that

underpin statements about how lofting parameters are affected by encounter parameters. Consider:

$$y = f(x_1, x_2, \dots, x_n) , \quad (11)$$

which indicates a functional dependence of a lofting parameter y (which can be maximum height, maximum velocity or direction, number of stones at various heights, etc.) that depends on the encounter parameters (x_1, x_2, \dots, x_n) . Encounter parameters are, for example, tire speed, tire shape, ground hardness, stone size, and so forth. We established a baseline condition that is of interest:

$$y_0 = f(x_{10}, x_{20}, \dots, x_{n0}) . \quad (12)$$

Here, x_{n0} denotes the baseline value of the parameter x_n . Baseline values are 200 psi pressure, 1000 pounds load, 40 mph, etc. The objective is to evaluate variations around the baseline. Given the limited number of tests, we changed each of the encounter parameters one at a time (by an increment h), and there results a different value of the observed parameter, given in general by a Taylor expansion:

$$y(x_i+h) = y_0 + h \frac{\partial f}{\partial x_i} + \frac{h^2}{2} \frac{\partial^2 f}{\partial x_i^2} . \quad (13)$$

In practice, only the leading derivative in Equation (3) was assumed to be of significance:

$$\frac{\partial f}{\partial x_i} = \frac{\Delta y}{\Delta x_i} . \quad (14)$$

Assumption of linearity is standard when the data are insufficient to evaluate higher order terms, unless there are compelling theoretical arguments that the first-order term is unimportant. For example, we might say that five more stones are lofted when the tire pressure changes 50 psi, so this partial derivative is 0.1 stone per psi.

It seems more reasonable, since our results have more validity for comparisons than they do for absolute numbers, to look at fractional changes, $\frac{\Delta y/y_0}{\Delta x/x_0}$. A statement that velocity of lofted stones increases by 10 percent when the tire pressure increases by 50 psi assumes that the measured quantity depends exponentially on the encounter parameter.

$$y = y_0 e^{x/x_0}. \quad (15)$$

Another common way to express results is as the logarithmic derivative,

$$\frac{\Delta y/y_0}{\Delta x/x_0} = \frac{\partial \ln y}{\partial \ln x} = n, \quad (16)$$

for example, the number of stones lofted changes by 15 percent when the tire speed changes by 40 percent. Such a statement assumes that the measured quantity is proportional to the encounter parameter,

$$y = (\text{const}) x^n. \quad (17)$$

D. UNCERTAINTIES IN DATA

Several of the test results were examined in detail to assess confidence levels that may reasonably be assigned to measure values of lofting variables. The particular variable considered was the probability that a given stone is lofted to $z > 125$ mm. This variable was selected because 125 mm is well above the threshold for counting stones, and thus this variable is less susceptible to sampling errors. The computed maximum heights were used for tests IIC2, IIC3, and IIC5. (These test conditions are described in a subsequent section.)

Let p denote the probability that a given stone is lofted to $z > 125$ mm. The probability that in a series of tests in which n stones are overrun, exactly x of them will be lofted to $z > 125$ mm is given by the binomial distribution:

$$p(x, n, p) = \frac{n!}{x!(n-x)!} p^x (1-p)^{n-x}. \quad (18)$$

The mean number of stones observed, μ , will be

$$\mu = np, \quad (19)$$

and the variance is

$$\sigma^2 = np(1-p). \quad (20)$$

These formulas were applied to the three tests mentioned above. For IIC2, $n = 80$, $\mu = 11$, $p = 0.14$, $\sigma = 3.1$, and the relative uncertainty is $\sigma/\mu = 0.28$. For IIC3, there were two wheels, so $n = 160$, and $\mu = 15$, $p = 0.093$, $\sigma = 3.67$, and the relative uncertainty is $\sigma/\mu = 0.25$. For IIC5, which was 20 percent coverage, $n = 1600$, $\mu = 19$, $p = 0.119$, $\sigma = 4.34$, and the relative uncertainty is $\sigma/\mu = 0.23$. The relative uncertainty is not very sensitive to n . If in IIC3, for example, we decide to ignore one rock because it was always missed by the tire, then $n = 120$, $p = 0.125$, but σ/μ is still 0.24. The conclusion is that the relative precision of the measurements of the number of stones lofted in these tests is about +25 percent.

The relative unimportance of n can be derived. It is easy to show that:

$$\sigma/\mu = \sqrt{(n-\mu)/n\mu}. \quad (21)$$

In most tests, $n \gg \mu$. Hence, to a good approximation,

$$\sigma/\mu = \sqrt{1/\mu}. \quad (22)$$

The implication of this analysis for the present program is as follows. The value of μ (the mean number of stones that would be lofted in a very large number of tests) may be approximated by the number actually observed in a small number of tests. The uncertainty in the approximation is equal to the square root of the number of stones observed.

E. FORM OF VELOCITY DISTRIBUTION

In order to conveniently describe the effects of velocity, and other encounter parameters as well, we introduce a shorthand description for the distribution of stone velocities, shown in Figure 6. In the simplified model, we consider that a large number of stones are more or less uniformly distributed at velocities up to some cutoff velocity, which we designate v_{CO} . For $v > v_{CO}$, the number of stones lofted decays approximately exponentially with velocity, except for a few stones thrown in what can be referred to as a "high-velocity tail." S denotes the fraction of the total stones thrown that are in this high-velocity tail. We denote by $N(z)$ the total number of stones lofted. Usually, we use $N(75 \text{ mm})$ or $N(125 \text{ mm})$.

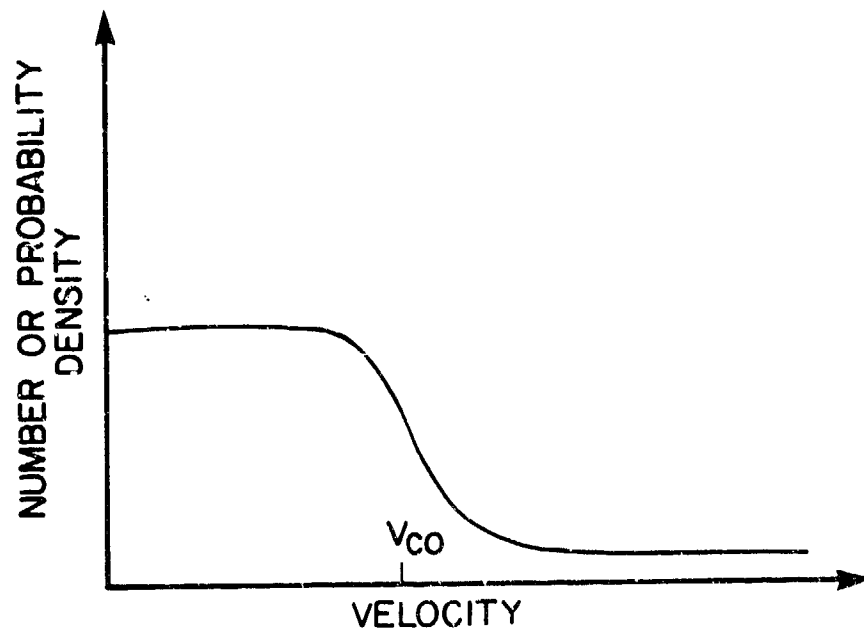


Figure 6. General Forms of Stone Velocity Distribution.
S is the Fraction of Stones with Velocities
Above v_{co} .

SECTION IV
FIRST-PHASE TESTS

A. DESCRIPTION OF TESTS

Table 4 presents the first test matrix. This test matrix was derived after consultation with AFESC and MDL personnel. The test designation nomenclature is as follows:

(I,II, or III) (C,A,WC,CA, or WCA) (1-25) (blank or A).

I, II, or III designates first, second, or third test matrix; C or A denotes concrete or aggregate substrate, WC indicates standing water on concrete, CA denotes catcher array and aggregate, and WCA is catcher array with wet aggregate bed; the third number corresponds to the test number from the test matrix; A denotes repeat of a test.

A pass was defined as a passage of the tire over the test track, resulting in one set of orthogonal photographs of lofted stones. The number of passes per test varied. Eighteen was usual.

Standard forms were used for recording essential parameters of each test. Figure 7 shows an example. The form includes the test parameter, the diagnostic equipment settings, the footage on the video tape showing the encounter ground, the stone array (numbers refer to tests in the test matrix), and the tire speeds.

The maximum velocity at which tests were conducted was 40 mph. The velocity was limited to this value because the carriage could not be accelerated to a higher speed in one revolution, and it was felt to be unsafe to drop the wheel while running near maximum speed.

TABLE 4. FIRST TEST MATRIX

Test Number	Remarks	CBR	V (mph)	P (psi)	Load (lbs)	Water Level (in)	Loose Stones (1)
IC1A	baseline, dry	∞	40	200	1000	0	LR, LA, SR, SA
IC2A	effect of stone size	∞	40	200	1000	0	½LR, ½LA, ½SR, ½SA
IC4A	effect of velocity	∞	25	200	1000	0	LR, LA, SR, SA
IC5	effect of weight	∞	40	200	500	0	LR, LA, SR, SA
IC6	effect of pressure	∞	40	150	1000	0	LR, LA, SR, SA
IC7	pressure, patch scale	∞	40	70	1000	0	LR, LA, SR, SA
IWC6	baseline, wet	∞	40	200	1000	0.36	½LA, ½LR, LA LR*
IWC9	effect of pressure	∞	25	70	1000	0.36	LA, LR*
IWC11	effect of velocity	∞	25	200	1000	0.36	½LA, ½LR, LA, LR*
IWC12	Pressure, patch scale	∞	40	70	1000	0.36	½LA, ½LR, LA, LR*
IA13	baseline, bed	100	40	200	1000	0	LA, LR, ½LA, ½LR*
IA14	effect of velocity	100	25	200	1000	0	LA, LR, ½LA, ½LR*
IA15	effect of weight	100	40	200	500	0	LA, LR, ½LA, ½LR*
IA15/SM	effect of stone size	100	40	200	1000	0	SA
IA16	effect of velocity	100	30	200	1000	0	LA, LR, ½LA, ½LR*
IA17	effect of pressure	100	40	150	1000	0	LA, LR, ½LA, ½LR*
IA18	Pressure, patch scale	100	40	70	1000	0	LA, LR, ½LA, ½LR*
ISA1	effect of stone size	100	40	200	1000	0	SA, SR, ½SA, ½SR
ISA2	effect of stone size+	100	40	200	1000	0	SA, SR, ½SA, ½SR
ICal	calibration+	100	40	200	1000	0	½LA, ½LR
IWCAl	baseline, wet bed+	100	40	200	1000	0.36	½LA, ½LR

1. L or S refers to large (approximately 1 inch) or small (tread size). A or R refers to angular (brushed limestone) or smooth (gravel). 1/2 refers to half-size.

* Segregated by size.

+ Trough catcher used instead of orthogonal cameras.

RUNWAY FOD

TEST NUMBER _____

DATE _____

TEST BED DESCRIPTION _____

TEST TIRE / LOAD DESCRIPTION

Tire Type _____

Inflation Pressure _____

Load (total) _____

LIGHT SOURCE / CAMERA DATA

Light Source Trigger _____

Light Source Frequency _____

Number of Pulses per Pass _____

Camera Aperture _____

Film Type _____

Total Exposures for Test _____

SPEED CONTROLLER SETTING _____

SPECIFIC TEST DATA

Run No.	Image Nos.	Time Hrs	Tape Start/Stop	Stone Array	Indicated Test Tire Speed, fps			
					1	2	3	4

COMMENTS _____

Figure 7. Data Reporting Form

B. RESULTS OF TESTS

The TV monitor was used to record the residual rocks after each pass. It was observed in almost all cases that after three passes so few rocks remained in the tire path that it was not useful to continue the test. Typical results are shown in Figure 8. Most of the stones were rolled, not thrown, out of the tire path. A standard procedure was developed according to which passes were conducted in triads. Each group of three passes counted as one run. After each run of three passes, the carriage was stopped, and the rock array was replaced.

In all tests, loose stones were distributed over the test surface. A wooden grid was constructed for placing the stones, shown in Figure 9. The grid spacing was 2 inches. The fraction of the area covered by the stones (coverage) was approximately 20 percent. Figures 10 through 13 illustrate typical photographic records obtained during these tests.

The first pass of each run lofted mainly large stones and the second and third pass lofted the remaining small stones. Therefore, starting with Test 8, stones of different sizes were no longer intermingled.

The tests with standing water (Test numbers 8 through 12) presented overwhelming problems for the photographic diagnostics. Figure 14 illustrates a sample photograph obtained in a test pass. It was not possible to distinguish the stones from the myriad of tiny water droplets. In tests I-WC8-12, ASA 800 speed color film was used and the stones were painted fluorescent green. In some passes, some larger colored stones could be identified. However, it was clear that a fine opaque mist obscured most of the view. It was not possible to reduce any of the photographs from these tests. Thus, no quantitative data were obtained in the first phase tests for stones in standing water. However, based on recovery of stones launched out of the test bed, it appeared that the probability of lofting was not significantly enhanced by the presence of water.

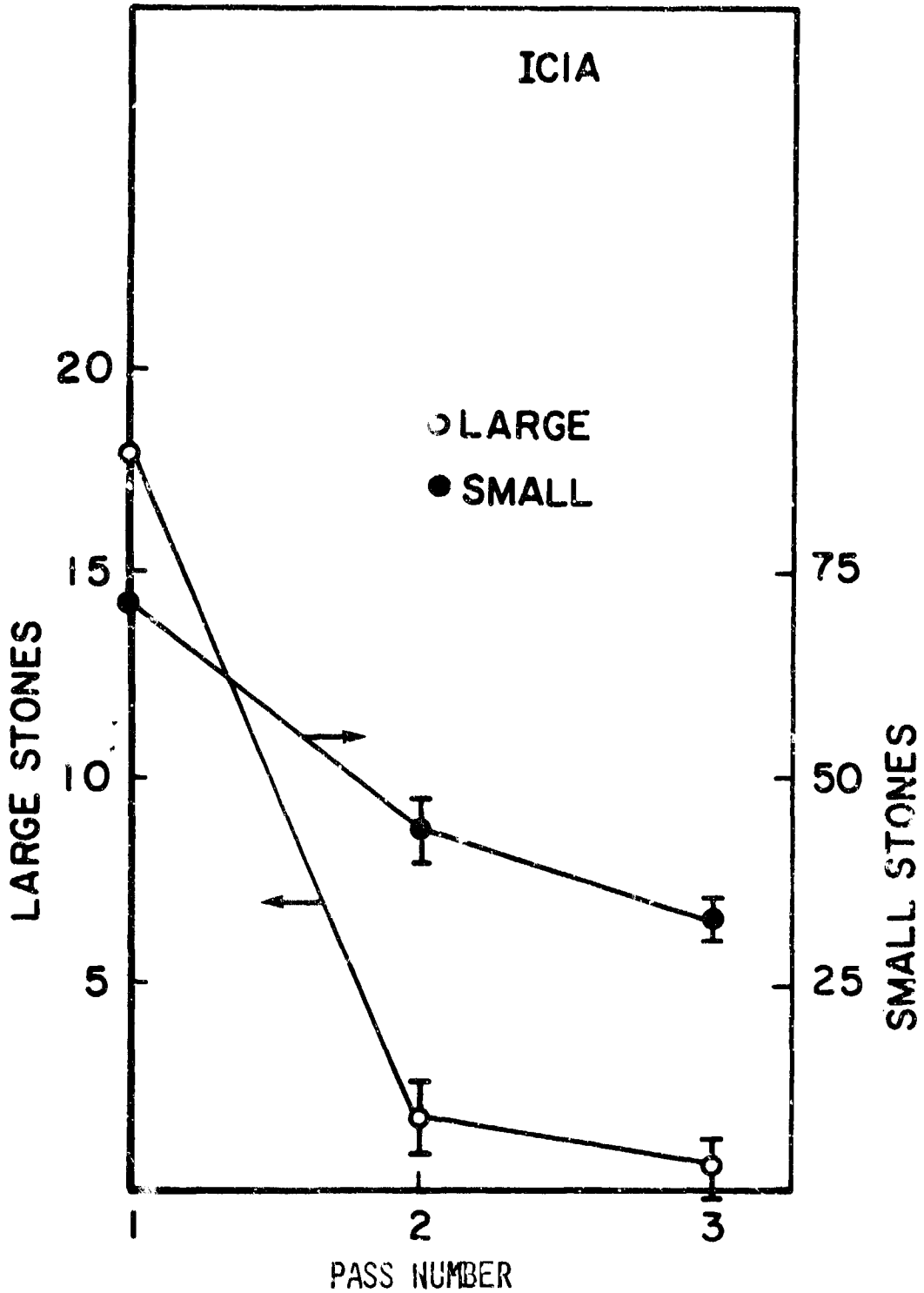


Figure 8. Average Number of Stones Present Before Each Pass During Test 1C1A. (Angular and Smooth Stones are Averaged Together.)

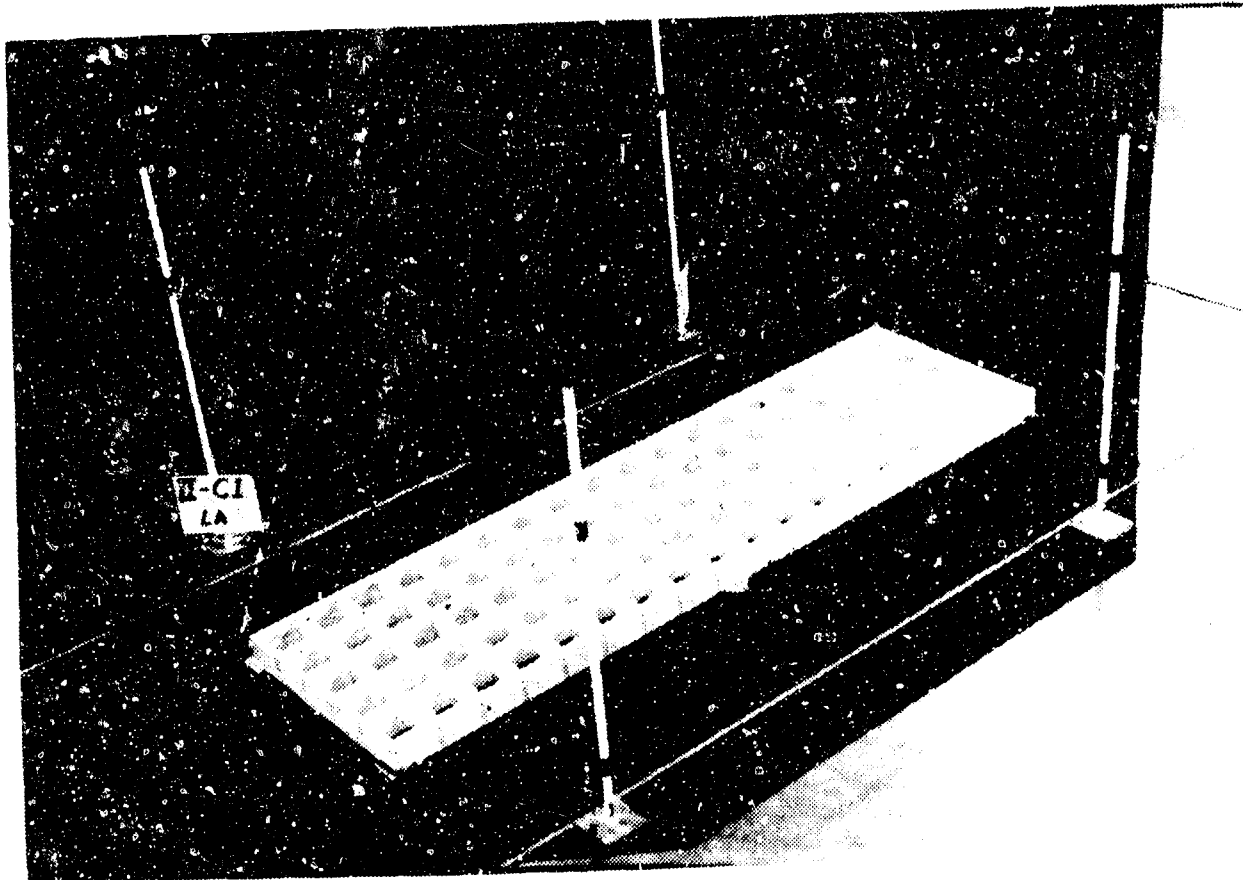


Figure 9. Wooden Grid Used to Place Rocks.

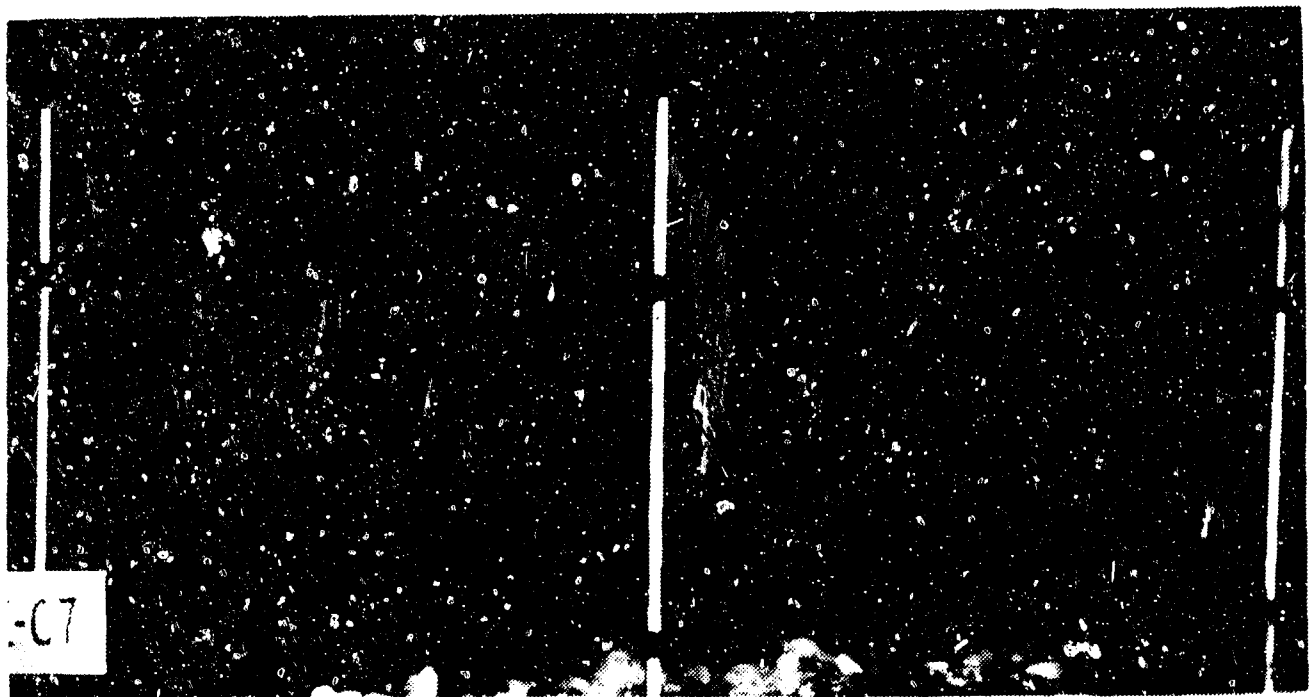


Figure 10. Test IC7, Pass 1, Left Camera.

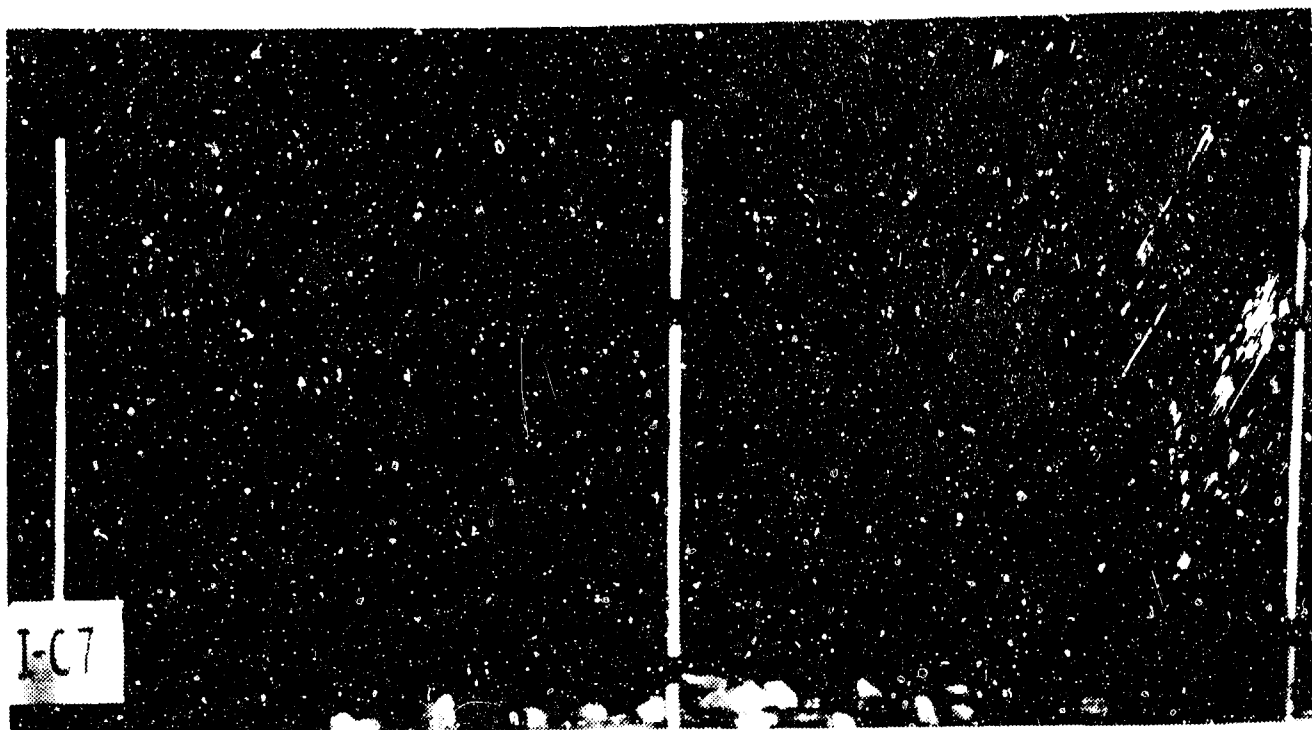


Figure 11. Test IC7, Pass 1, Right Camera.

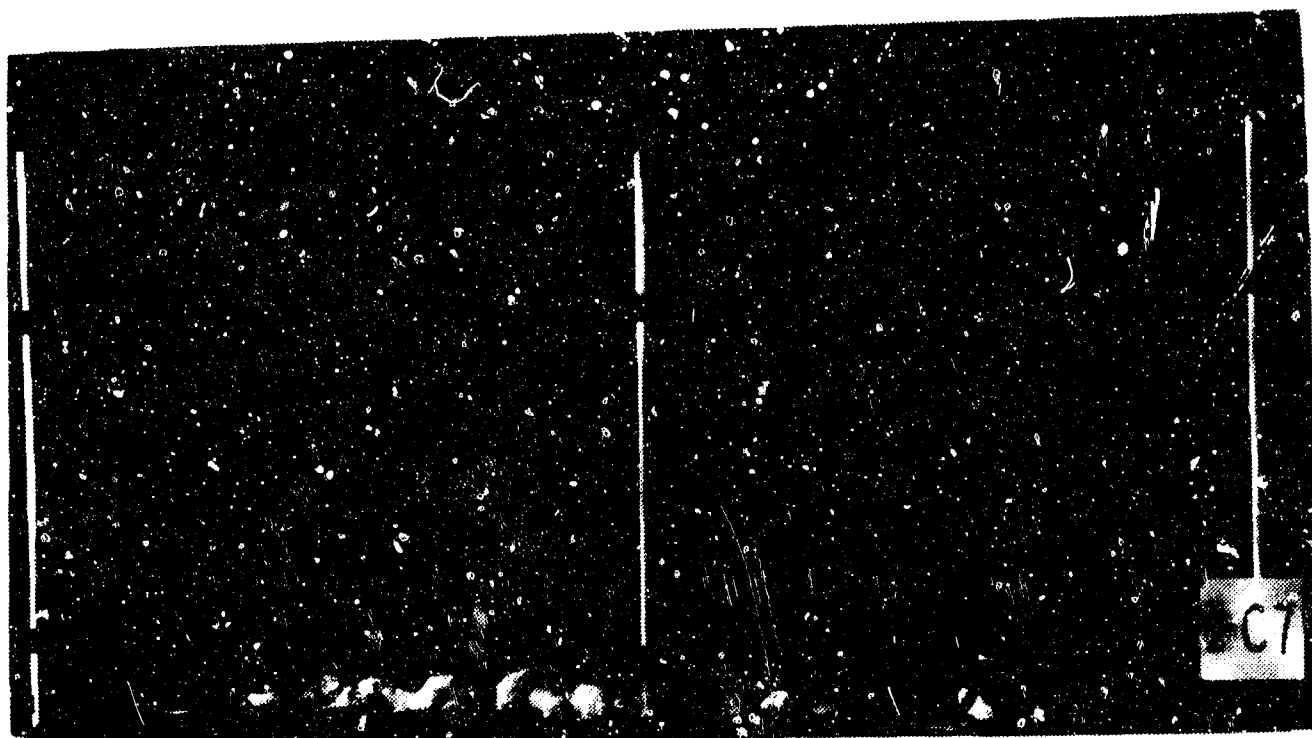


Figure 12. Test IC7, Pass 2, Left Camera.

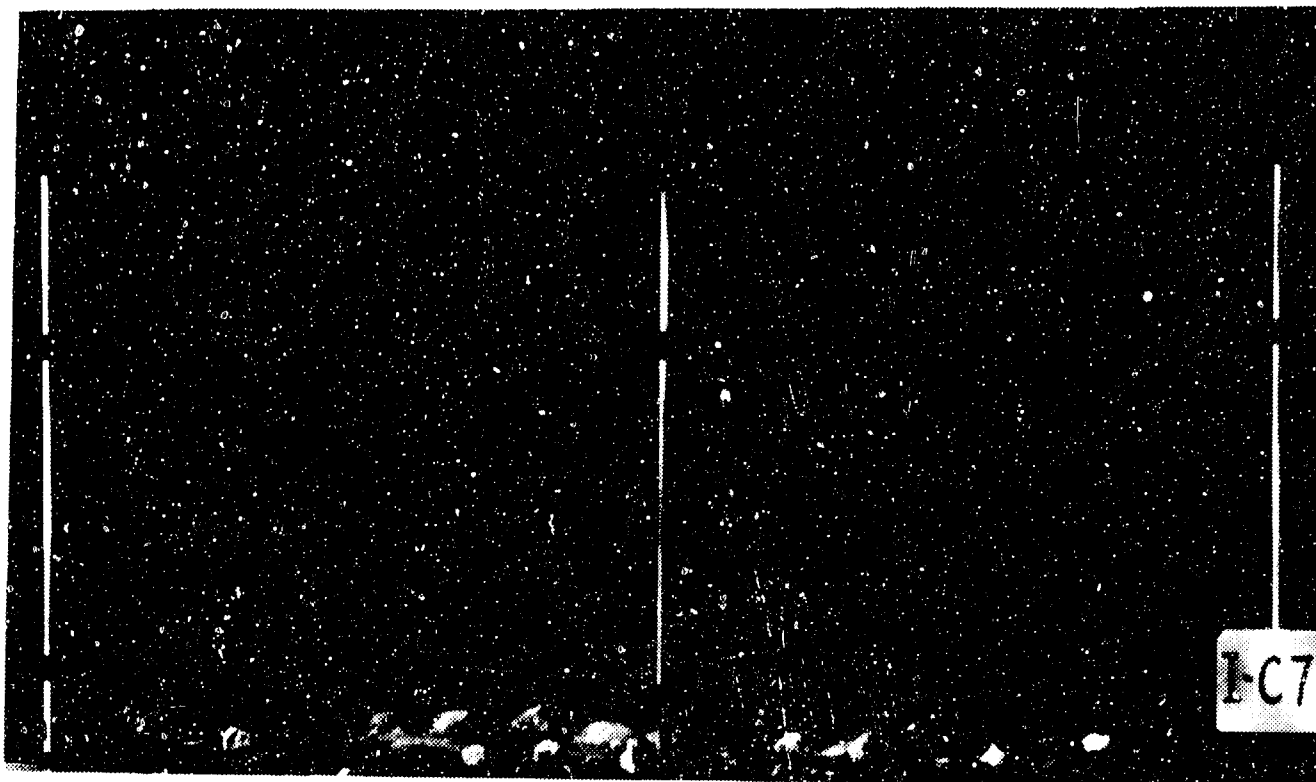


Figure 13. Test IC7, Pass 2, Right Camera.

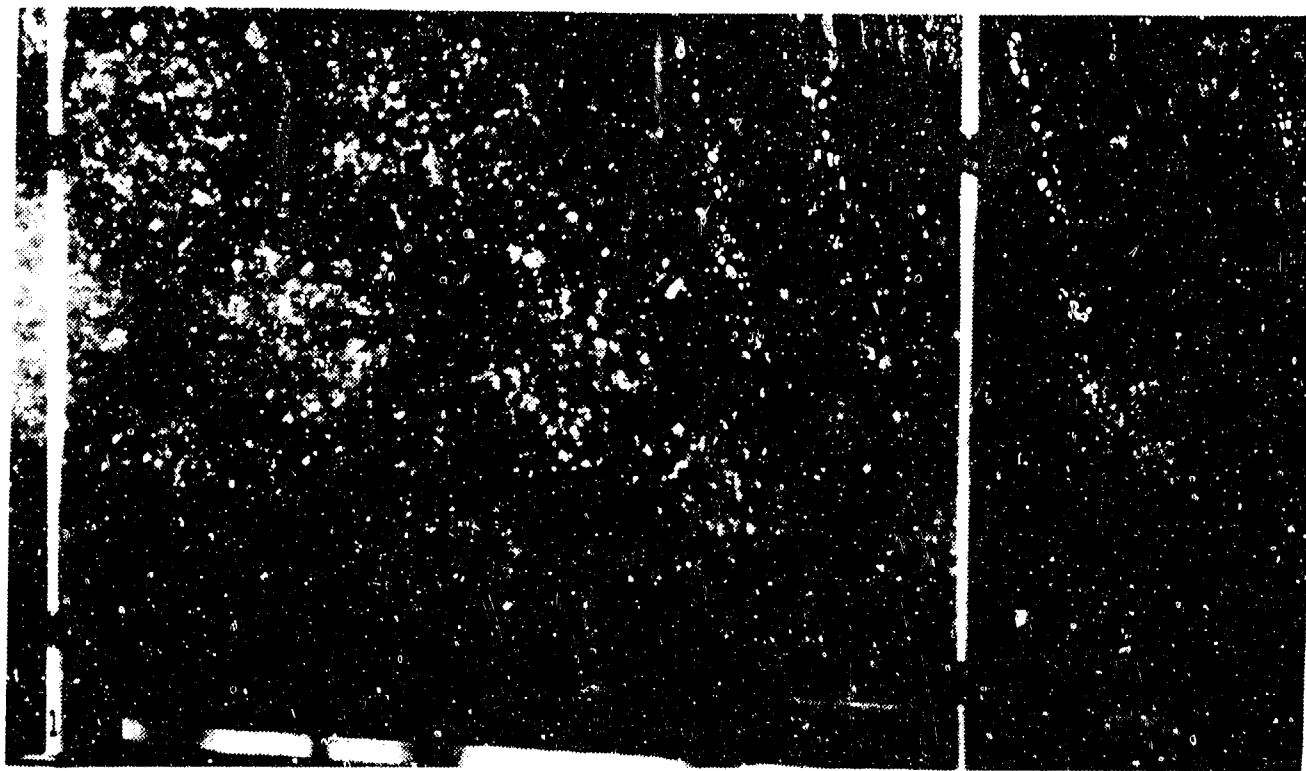


Figure 14. Black and White Test Picture of Splash from Puddle on Concrete.

Starting with test IA 13, a sting was added to the wheel strut to obtain earlier triggering of the flash unit. Figures 15 and 16 show the results obtained. The first two exposures capture the wheel as it traverses the bed. The large disparity between stone velocity and tire velocity is very apparent. Our motivation for earlier triggering was to check that no high-velocity forward or rearward stones were being missed; with the new timing, none were observed.

Tests 13 through 18 were conducted with the compacted aggregate bed. Groove-width size pebbles were not used for these tests, since it was felt that many small pebbles were already present in the bed, and that tread-size pebbles would be embedded in the bed. Instead, full-scale and half-inch rocks were employed, except in Test IA15/SM.

A test was conducted to check bed degradation. For the last 10 passes in IA15/SM, no additional rocks were placed. After the fifth pass, no stones were lofted. Thus, for five consecutive passes on a clean bed, there were no lofting events. Figure 17 shows the appearance of the bed after this test.

The tests on wet aggregate beds were conducted differently. It had been established that the photographic techniques were inadequate to capture the particle trajectories. Therefore, a catch system was deployed. A section of horizontal troughs was placed near the fire path. Rocks falling into the troughs were captured and counted. The troughs were moved away from the tire path in 2-inch increments, so that statistics were obtained for the number of rocks at each height, as a function of range. The trough spacings were 3 inches in height. Their width was 1 meter. Figure 18 shows the trough array in place.

Tests ISA1 and ISA2 were designed to calibrate the trough array, since it was expected to have a bias from rocks hitting the edge. These tests were conducted with the tiniest stones which were felt to be most likely to become entrained in the flow. Figure 19 shows the results. Contours are drawn for

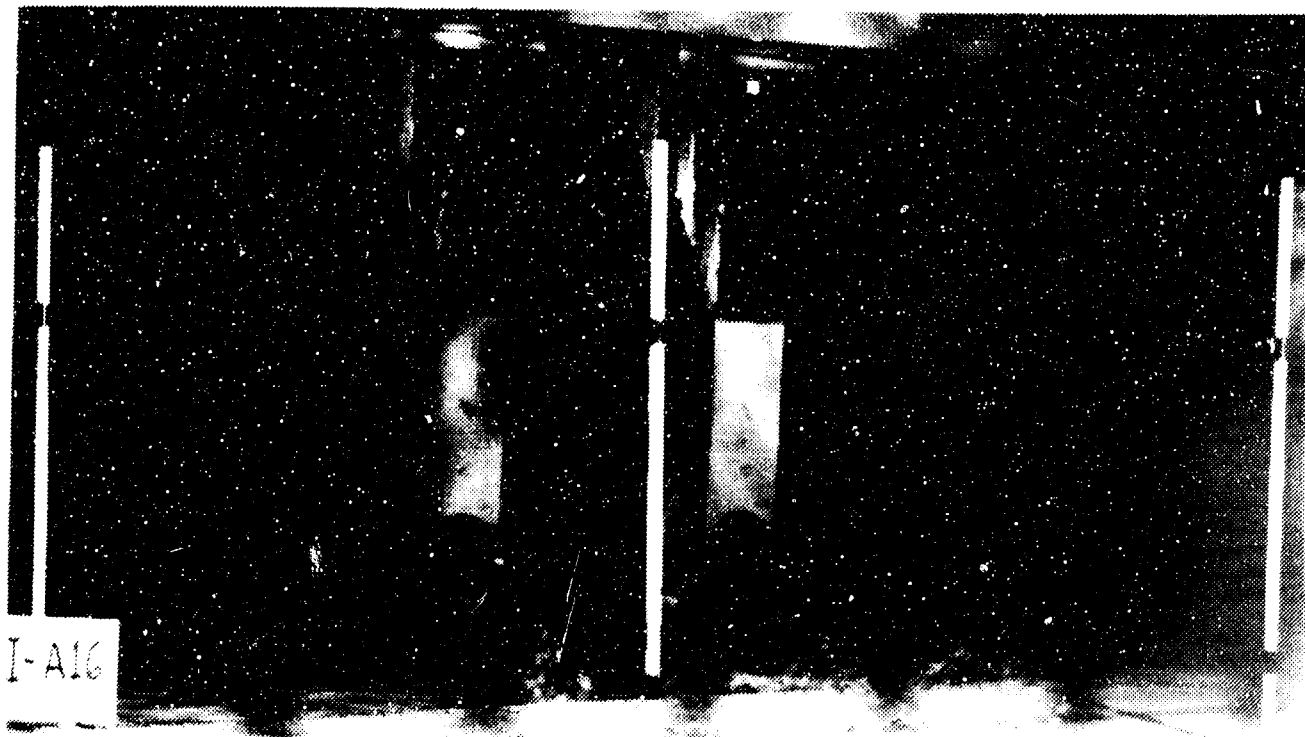


Figure 15. Test IA16, Pass 13, Left View.

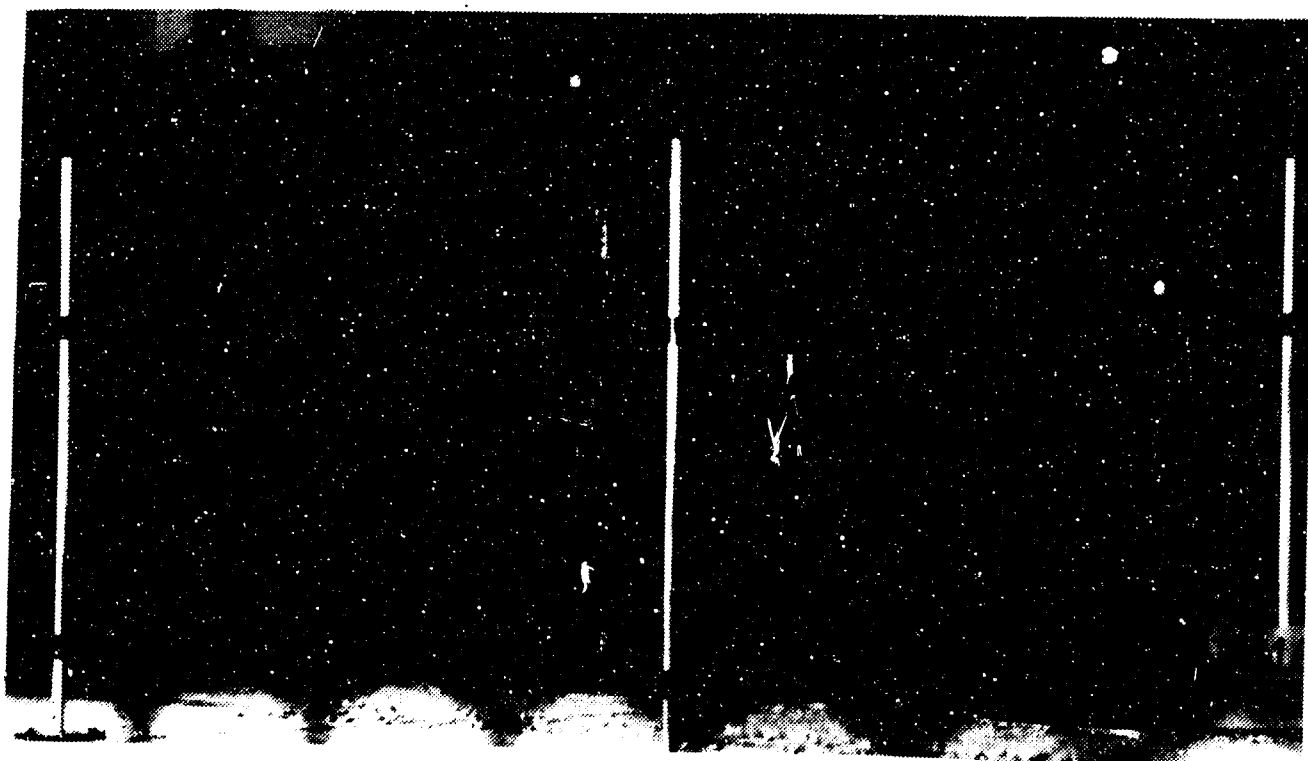


Figure 16. Test IA16, Pass 13, Right View.

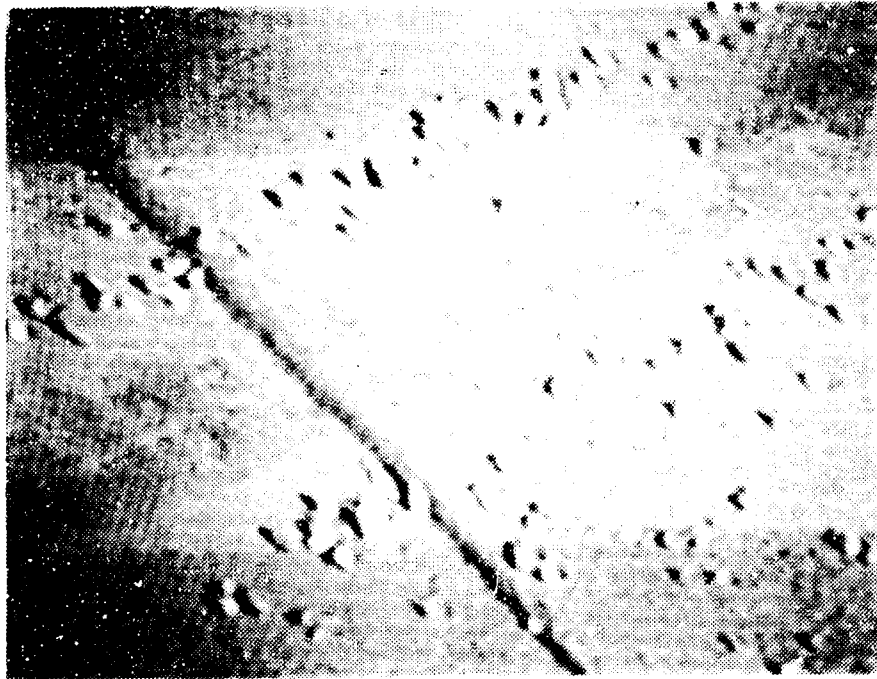


Figure 17. Photograph from Video Tape Showing Condition of Compacted Bed After 10 Consecutive Passes in Test IA15/SM.

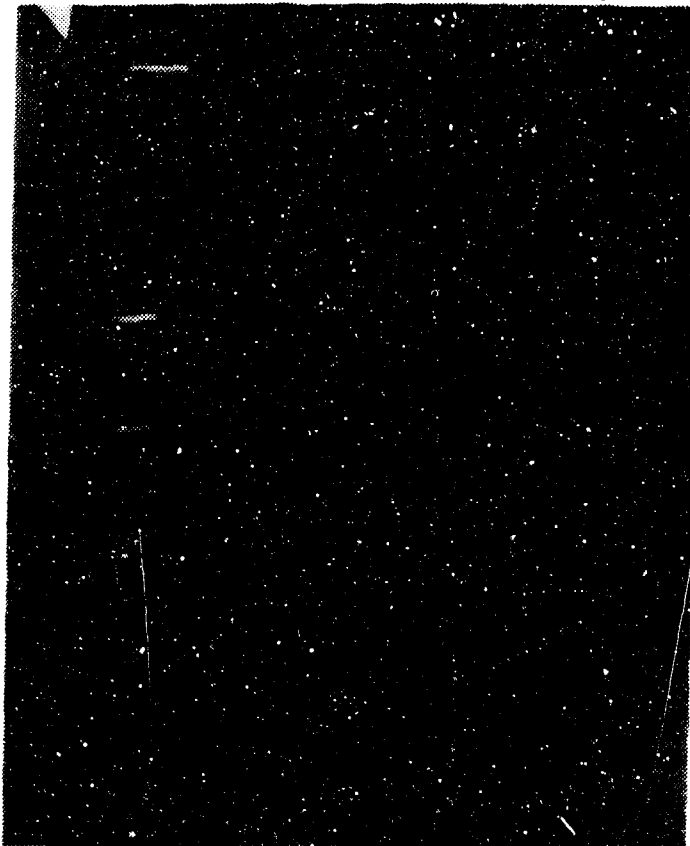


Figure 18. Trough Array.

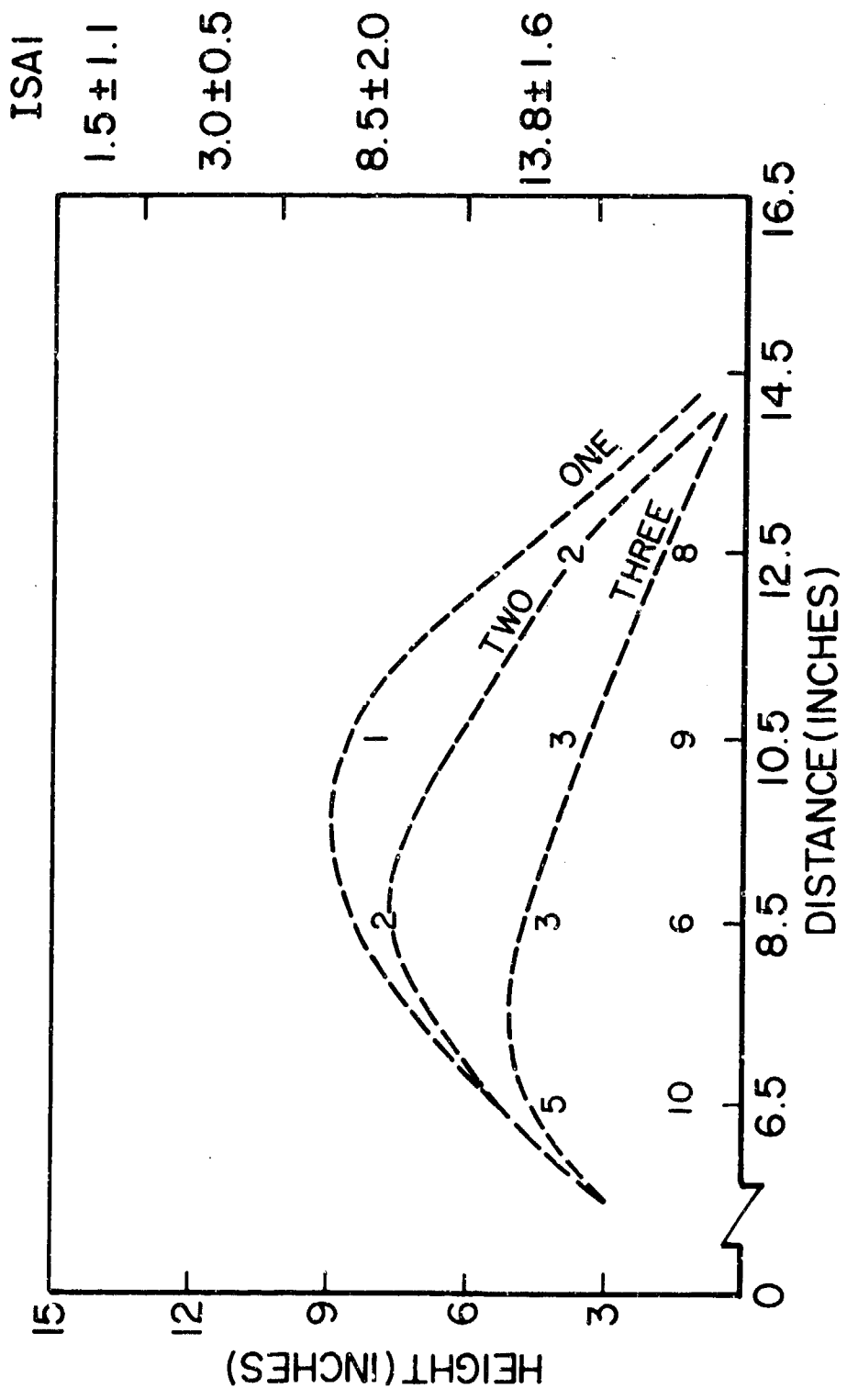


Figure 19. Trough Calibration.

the number of rocks at each height at each range. The catcher data are biased low. Two rocks were observed to bounce off the lower dividing edges. The tentative conclusion from Figure 19 is that the actual number of rocks lofted to mid-heights was about three times higher than indicated by the trough analysis. The causes of this discrepancy are probably poor collection efficiency and rocks missing the array.

It turned out to be possible to conduct only one test on a saturated bed. The problem was that the bed fluidized when it was recompacted after the first three passes. Thus, it was necessary to unsaturate the bed by draining out water before recompaction could take place. This was so time consuming that only one test could be completed in the 8 hours dedicated to wet bed testing. Moreover, it seems highly unlikely that aircraft could operate on beds as soft as those saturated patches. Figures 20 and 21 illustrate the appearance of a saturated bed before and after three passes.

Only the baseline saturated bed test was conducted, and even for that test, only 12 passes could be completed. A calibration test was also conducted with the same stones and catcher for a dry bed. Colored stones were used for some of the wet tests to distinguish lofted debris from bed particles. The data acquired in these tests are summarized in Table 5. The data for test ICA1 are averages for three runs. Only one run (three passes) was conducted for each trough position during test IWCA1. Values reported are the average number per run. Stones were redistributed two per cell (4 in^2) after each run, which consisted of three passes. The data in Table 5 clearly show that there is no augmentation of lofting caused by the presence of standing water.

Trajectory data were computed from the orthogonal camera data for most tests. Figure 22 shows the total velocity distribution for test IC4A. Sample photographic data that have been analyzed indicated that very few lofted rocks have speeds



Figure 20. Appearance of Bed Used in Test IWCA1, Before Test Started.



Figure 21. IWCA1 Bed After Three Passes (First Run).

TABLE 5. RESULTS FOR WET AGGREGATE TESTS (AVERAGE VALUES PER RUN)

Number	Range (in.)	Height (in.)					
		<3	3-6	6-9	9-12	12-15	>15
ICAL (dry)	6.5	44±10.7	13.3±2.5	4.3±0.7	0.7±0.5	0	0
	8.5	40.3±5.7	10.3±0.9	3.3±2.4	1.7±1.2	0.7±0.9	0
	10.5	37.7±4.0	9±2.2	4.3±2.5	0.3±0.5	0.3±0.5	0
	12.5	24.3±5.2	8.7±0.9	2.3±1.9	0.3±0.5	0.7±0.9	0.3±5
IWCL (wet)	6.5	45	9	2	0	0	0
	8.5	34	14	1	1	0	0
	10.5	13	5*	1*	0*	0*	0
	12.5	8	2*	3*	1	0	0

*Additional stones dislodged from bed not counted.

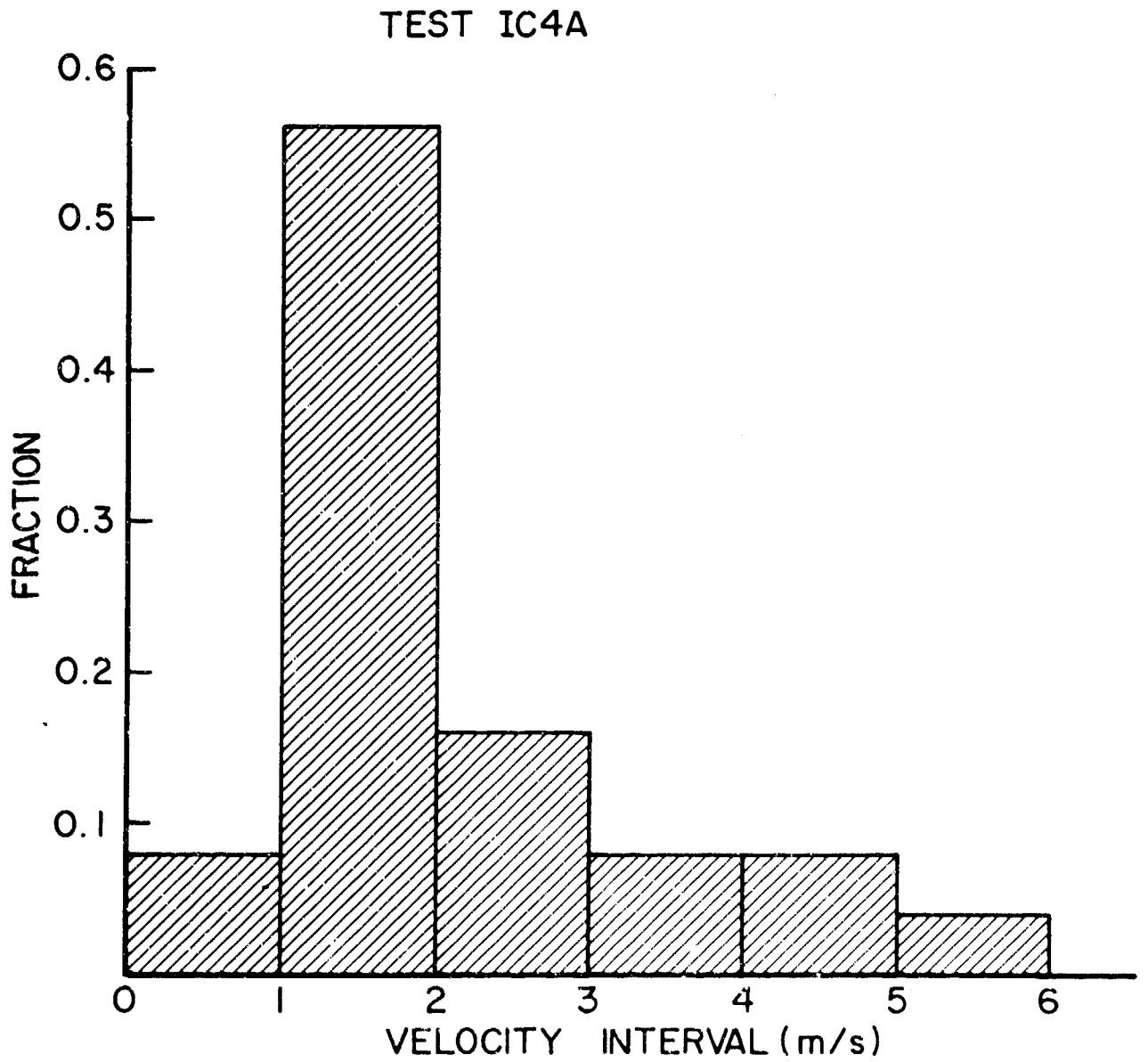


Figure 22. Velocity Distribution of Lofted Rocks in Test IC4A (Test on Concrete at 25 mph).

exceeding 10 percent of the tire speed. Figures 23 and 24 show this result for the baseline test IClA. The distribution of velocities is approximately exponential, with a cutoff below about 1 m/s. The cutoff is presumably due to the fact that trajectories below 3 inches were not considered. The horizontal component of the velocity vectors of most rocks is contained in a wedge ± 45 degrees of the outward normal to the tire path. Quantitative trends in the trajectory data are discussed in Section V, where the first and second phase results are compared.

Appendix B summarizes most of the trajectory data analyzed. Almost all of the shots were analyzed for the distribution of heights obtained by stones. For the tests which lofted the most rocks, the data have been further reduced to produce graphs showing: either the distribution of velocity of stones or sometimes the absolute number of stones at each velocity interval, the direction loft angles in the x-y plane, and the elevation angle. These graphs are collected in the appendix. We discuss here the most important conclusions that can be gleaned from these data.

The distribution of velocities observed in the baseline single wheel test, IClA, is shown in Figure 23. Data for large and small stones were similar, as detailed in Appendix B. The tire speed in this test was 18 m/s, yet very few stones had a velocity higher than 2.5 m/s. Only three stones had velocities of higher than 5 m/s. In no test was a stone observed with a velocity of more than half the tire speed, and in most of the tests the great majority of velocities were less than 2.5 m/s. The observations were generally consistent with an exponential velocity distribution, as shown in Figure 24, especially if it is assumed that many low velocity stones were not counted. (Stones that did not travel at least 2 or 3 inches high were not counted.)

Almost all of the tests in the first and second phases are characterized by stone launch directions that are skewed to

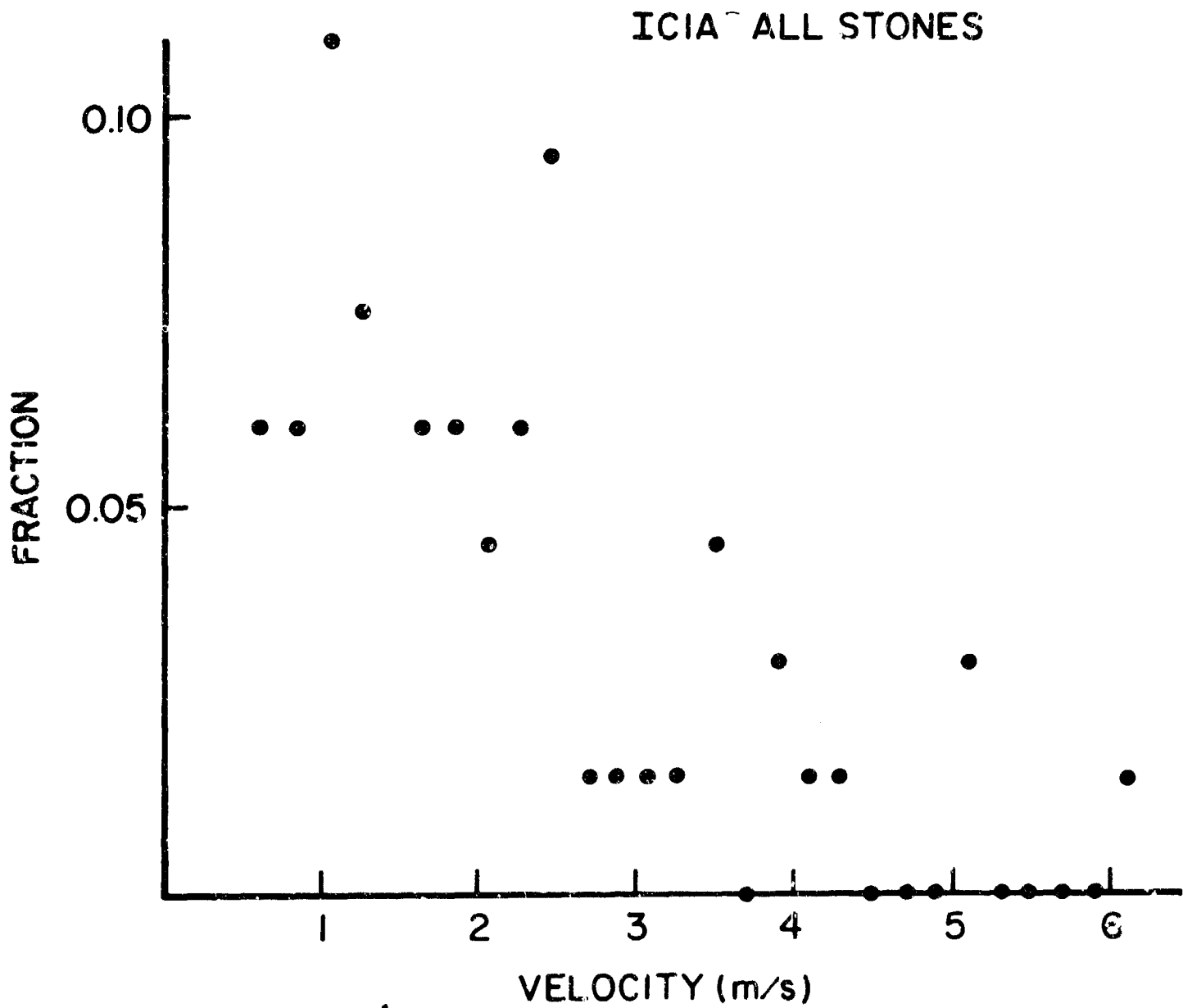


Figure 23. Distribution of Velocities for All Rocks, Test ICIA.

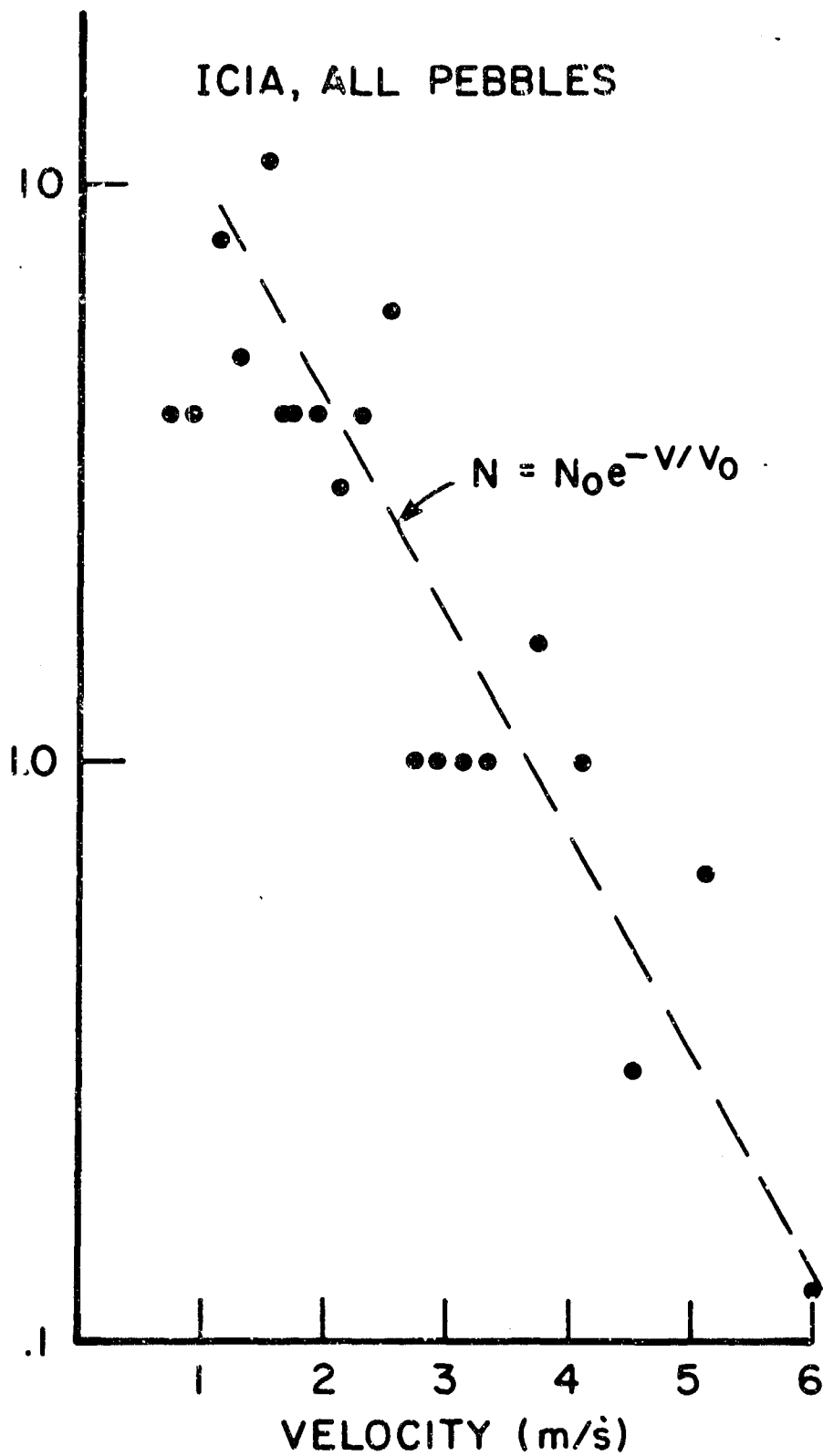


Figure 24. Distribution of Velocities for All Rocks, Test IC1A, Semilog Plot. Vertical Axis is Number of Stones per 0.2 m/s Velocity Interval.

the outside of the track. A typical example is shown in Figure 25. Approximately twice as many stones are thrown out as are thrown in. This is true for both large stones and small stones.

More insight is obtained by examining only the stones in Passes 2 and 3 of Test IC1A. (These tests were done in groups of three passes. After every third pass, the rock pattern was reset.) Consequently, in the first pass the coverage was 20 percent, and in the second and third passes the coverage was, on the average, 2 percent. It turned out that in Passes 2 and 3 (low coverage), all the rocks were thrown outward. Only in the first pass are any rocks thrown inward. This is characteristic of the pattern which is observed in many of the tests.

Figure 26 shows how velocity is distributed with direction angle for the baseline test. The results for this test are similar to those of other tests, although here they are better defined for the baseline because there are more data. There are apparently two high velocity lobes. Every example of a velocity over 4.5 m/s, was lofted in the direction of either ± 45 degrees to the direction of travel.

Figure 27 shows the distribution of elevation angles for the baseline. The data collection technique screens out the small angles, but unquestionably there is a peak around 45 degrees. The peak for this test is between 50 degrees and 60 degrees. The peak of the elevation angle shifts in different types of tests as discussed later.

Some of the other data in Appendix B, such as the plot for test IC4 (concrete/low velocity), show that even when the data set is much smaller, certain conclusions seem to be warranted. In IC4, for example, while the small number of samples makes it difficult to say much about the distribution of velocity at low velocities, it is clear that stones lofted by this test favored high velocities. For example, whereas in Test IC1A ten times more large rocks were thrown,

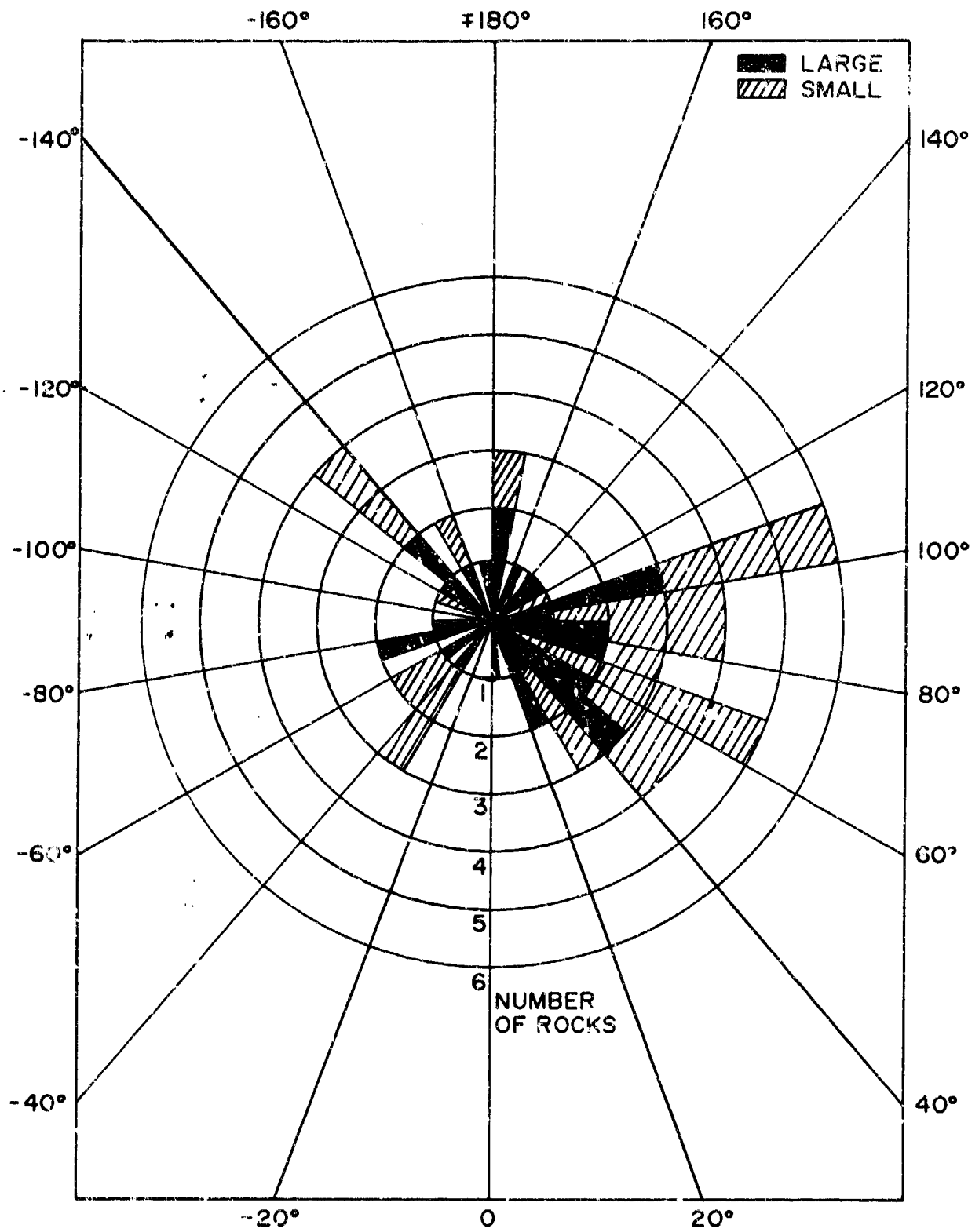


Figure 25. Distribution of Launch Directions Observed in Test IClA.
 (Wind Direction of Travel is 0 Degrees.)

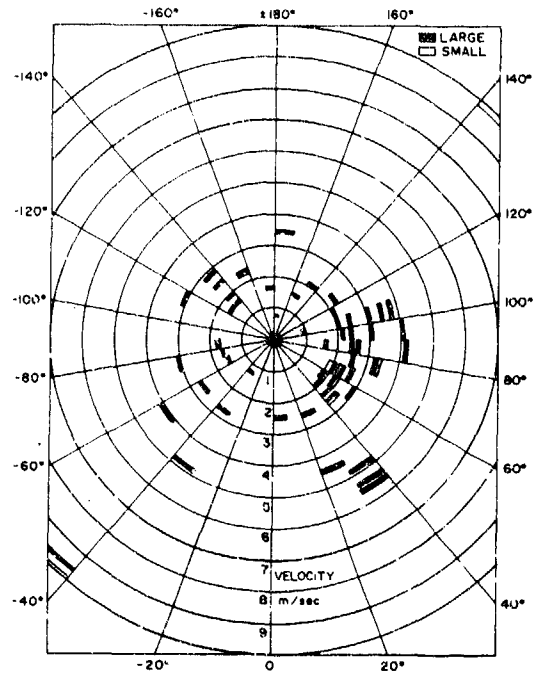


Figure 26. Distribution of Velocity with Direction Angle for Baseline Test (IC1A).

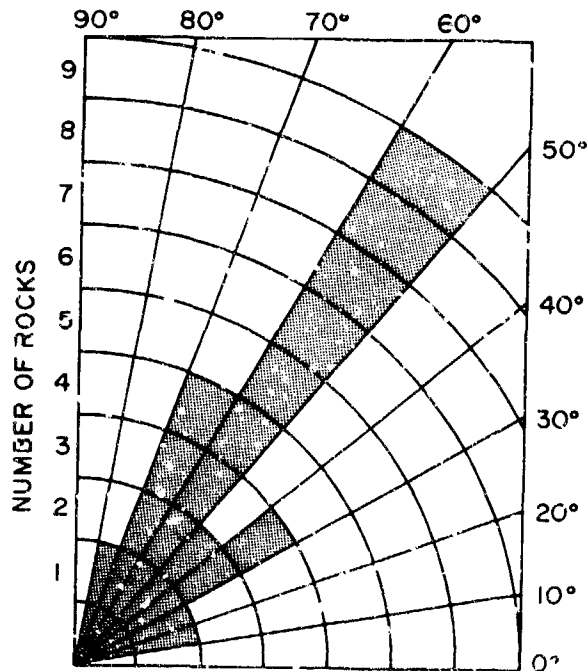


Figure 27. Distribution of Elevation Angles for Baseline Test.

none were thrown above 5 m/s. In IC4 practically one-third of the large rocks had velocities over 5 meters/second.

C. ANALYSIS OF RESULTS

Major trends in the data from the first phase tests were first revealed by a simplified data analysis procedure. The data considered consisted of video tape sequences showing the bed before and after each tire pass, and pairs of orthogonal still photographs which provided views of the individual stones lofted by the tire. Complete analyses of the orthogonal photographs reveal the velocity (speed and direction) of all lofted stones. More than a thousand stones were observed in flight, and the cost of analyzing all those trajectories was prohibitive. Therefore, the initial trend analysis employed a simpler data reduction process in which only peak altitudes of the stones (both observed and estimated) were recorded. Together with the direction, the height determines whether or not the stones can be entrained in an aircraft engine's air intake flow.

It was surprising to discover the relatively small number of stones lofted to heights of interest (above 1 meter). Trajectories were grouped according to maximum height, as follows:

<u>TRAJECTORY CATEGORY</u>	<u>PEAK HEIGHT</u>
A	350 mm or greater
B	254 mm - 350 mm
C	152 mm - 254 mm
D	95 mm - 152 mm

Data were recorded as far as possible in the form of large angular, large smooth, small angular, and small smooth stones versus trajectory height category. Separate entries were made for each pass. The trajectory data were compared with the number of stones available to be thrown, i.e., number of stones on the track in the path of the tire before the tire passes. This number was, simply, the number laid down for Pass 1

and the number for each other data run as observed on the TV tape recording prior to each of the subsequent passes.

The analyses were initially carried out for the hard dry beds, since these data are extremely important to the overall program. We have analyzed the baseline Test I-C-1A and enough other tests so that the effects of shifts in each encounter variable (tire speed, pressure, load, stone size, etc.) could be evaluated.

Figure 28 shows the probability of launching stones to various heights in the baseline test. Data from large stones versus small stones, and Pass 1 (virgin stone array) versus Passes 2 and 3 are separately displayed. The figure shows that large stones are launched with considerably higher probabilities than small ones. The launch probabilities of both large and small stones are much less in the first pass than in the second and third passes. Finally, the launch probabilities fall monotonically with peak trajectory heights.

The relative suppression of launch probability in the first pass was an unexpected result. However, all of the tests conducted on dry surfaces during the first phase testing consistently showed this effect. The probability for launch in a second or third pass was divided by the probability for launch during the first pass, for each test for which data were available. The average was 10.36 with a standard deviation of ± 0.56 (5.4 percent). When data from Passes 2 and 3 were ratioed in the same manner, the result was 1.34 with a standard deviation of ± 0.35 (26 percent); there was no statistically significant difference between Passes 2 and 3.

These results have been interpreted as a saturation effect. When the number of stones on the ground exceeds a critical value, the stones shield each other from the action of the tire, and the probability of launching any particular stone decreases (although not the total number of stones lofted). Between Passes 1 (20 percent areal coverage) and 2 and 3 (average 2 percent

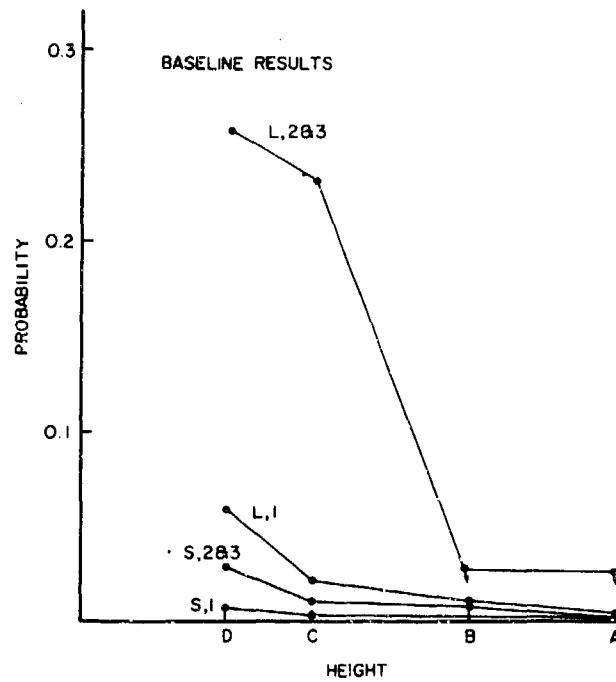


Figure 28. Trajectory Height Category vs. Launch Probability for the Baseline Experiment Conducted on a Hard, Dry Surface.

coverage) the launch probability was decreased by approximately a factor of 10.

Interest was focussed on Passes 2 and 3, since the lower coverage in those passes is probably more relevant to airfield scenarios. Figure 29 is a plot of large stones launched from a concrete surface during Passes 2 and 3. Note that the data from Test 1 (the baseline) and Test 7, where the tire pressure was reduced to approximately one-third of its standard value, produced comparable results within the relatively large data scatter. Reducing the stone size in Test 2 or reducing tire velocity in Test 4 yields slightly fewer stones launched. These trends are consistent with the data from large stones launched during the first pass as shown in Figure 30 but the effects are not nearly as striking. Data for small stones are considerably scarcer than that for large stones and the trends are somewhat less distinct as shown in Figure 31. The probability of launching small stones is definitely less than large stones.

The effects of tire speed, stone size, and tire pressure were also studied in the second test phase. The tentative conclusions reached in this analysis were substantiated and quantified when data from the first and second phases were combined, as revealed in the following section.

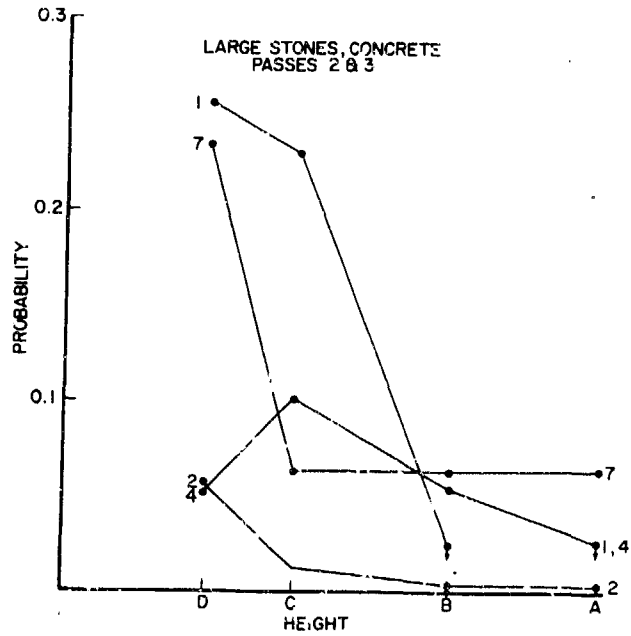


Figure 29. Trajectory Heights for all Large Stones Launched During Second and Third Passes. (Key to Tests: 1-Baseline, 2-Smaller Stones, 4-Lower Speed, 7-Lower Pressure).

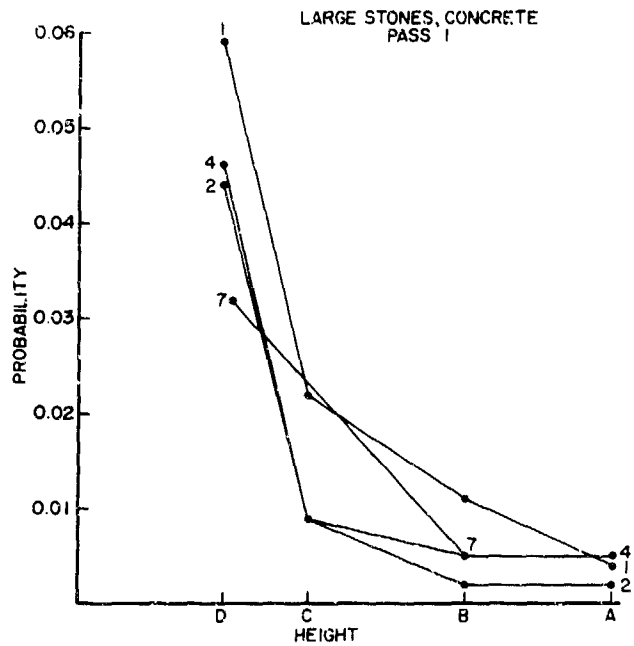


Figure 30. Trajectory Heights for All Large Stones Launched During First Passes.

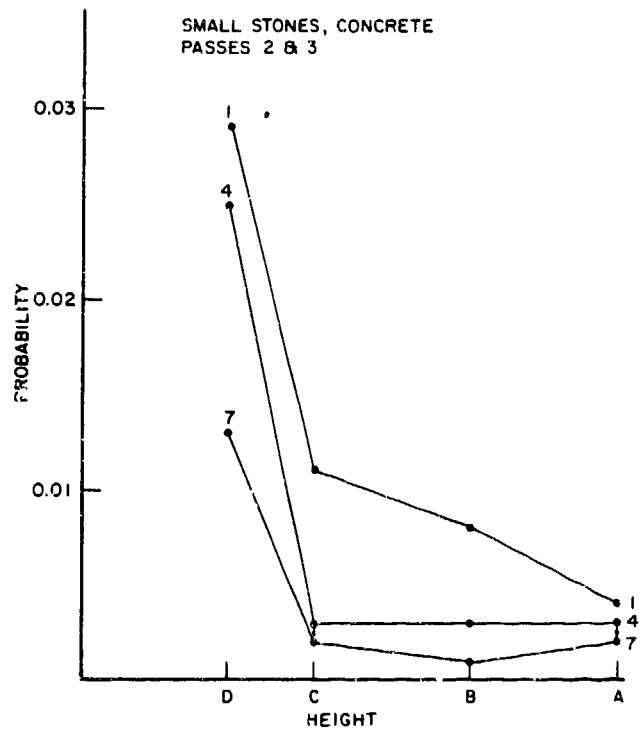


Figure 31. Trajectory Heights for All Small Stones Launched During Second and Third Passes.

SECTION V
SECOND-PHASE TESTS

Table 6 shows the Second Test Matrix. The objectives of the second-phase tests were to determine the effects of wheel configuration, to explicitly determine the variations of lofting probability with coverage, and to enhance the data base for evaluation of the effects of tire speed, load, and pressure. The first item in the matrix, Test 1, was done with a T37 wheel and its motive was to test the effects of a drastically different tire profile, as well as suspension system on lofting. Test 2 repeated the single-wheel baseline test to obtain more data for low coverage. Test 3 was the baseline test for dual-wheel consideration, 40 miles per hour (mph)/200 psi/1,000 pound load/2 percent coverage. Test 3 was with large angular stones which we found to be the most lively; Test 4 was a repeat with small angular stones. The next four tests were designed to explore the effects of saturation when the coverage ranges from 1 percent, which means only two rocks per tire per pass, to 20 percent, which was similar to that used in the First Test Matrix. Test 9 examined the effects of shape (in particular, marbles) on lofting. Test 10 was to study the effect of tire velocity, and Test 11 the effect of pressure (decreased to 75 psi). Test 12 was the baseline case for two wheels on the aggregate. Test 13 explored the effects of decrease in pressure, Test 14 the effects of stone size, Test 15 the effects of stone shape (using large round stones), and Test 16 the effects of velocity (namely 25 mph). The last four tests in the matrix were devoted to high speed photography, for which we used a 16 mm, high-speed camera running at 500 frames/second.

A. LOFTING MECHANISMS FILMS

A series of movies taken at 500 frames/second showed in some detail the interaction between the tire and the stones. The films

TABLE 6. SECOND TEST MATRIX

Test	Remarks	Wheel	CBR	V (mph)	P (psi)	L (lbs)	Cov. (%)	Stones
II1	effect of tire shape	T37	∞	40	nom	nom	2	LA, SA
II2	baseline	Falcon	∞	40	200	1000	2	LA, SA
II3	dual baseline	dual	∞	40	200	1000	2	LA
II4	dual baseline	dual	∞	40	200	1000	2	SA
II5	saturation	dual	∞	40	200	1000	20	LA
II6	saturation	dual	∞	40	200	1000	10	LA
II7	saturation	dual	∞	40	200	1000	5	LA
II8	saturation	dual	∞	40	200	1000	1	LA
II9	shape effect	dual	∞	40	200	1000	2	MARBLES
II10	velocity effect	dual	∞	30	200	1000	2	LA
II11	pressure effect	dual	∞	40	75	1000	2	LA
II12	aggregate	dual	100	40	200	1000	2	LA
II13	pressure effect	dual	100	40	75	1000	2	LA
II14	hi-speed photo	dual	100	40	200	1000	20	LA
II15	hi-speed photo	dual	100	40	200	1000	2	LA

were of an aggregate bed. Stones were launched just after the tire cleared them. All the stones observed were relatively slow. Almost all the stones had a forward tumble (e.g., they rotated in the same sense as they would were they rolling on the ground). Some stones appeared to be lofted that the tire passed squarely over, while others were just skimmed by the tire. A large amount of fine debris rose from the bed after the tire passed.

B. RESULTS

The trajectory data gathered in these tests are contained in Appendix B (separately bound). The data can be used to systematically evaluate the importance of each encounter parameter.

1. Single-Versus Dual-Wheel Comparison

The major objective of the second test program was to determine whether there were systematic differences between dual wheels and single wheels and, in particular, to discover if there were any synergisms between the two wheels. The clearest evidence bearing on this question comes from comparing Test IIC2 with Test IIC3. It was found that there was no significant interaction between the two wheels. The number of stones lofted by the dual wheels was 1.8 times that lofted by one wheel.

Tire loads are less for dual wheels than single wheels because the load is divided between the wheels. On the curved track, there is also a possible load shift to the outside wheel. (The inside tire also had a slightly smaller diameter because it had been used in the First Test Matrix.) Separate studies of the effects of load indicate that load by itself is not a very important parameter and cannot be expected to significantly bias these results.

Most of the stones were thrown outward in the dual-wheel tests, consistent with observations of the First Test

Matrix. It is interesting to note that some of the stones that were thrown inward in the dual-wheel tests were thrown by the outside tire. It also appears that some of the stones that were thrown outside in these tests were actually encountered by the inside half of the tires, and vice versa.

There is an overall bias in the dual-wheel tests that most stones are lofted by the outside wheel. This was strongest in the baseline test (IIC3), where 82 percent of the stones lofted were lofted by the outside wheel. However, this result may be influenced by rock placement. The outer tire consistently lofted two of the four rocks it encountered, while the inner tire only lofted one. The other was so placed that it could not be launched. Neglect of one of the inside rocks reduces the ratio of outer/inner tire loftings to 2.2.

In Tests IIC6, IIC7, and IIC11, the lofting of the two tires was essentially balanced. In IIC5 and IIC8, between two and three times more rocks were lofted by the outside tire. The total for the six tests (128 rocks lofted above 75 mm) was an outer/inner lofting ratio of 1.67.

2. Saturation Effects

Much of the Second Test Matrix was dedicated to determining the effects on lofting of the areal density of rocks on the track. There were indeed several significant effects. Low coverage promoted lofting in the forward direction and at lower angles. This can be most clearly seen by comparing the results of the 1-percent coverage tests with any of the other tests at higher coverage. It also seems to be true that if there were fewer stones, more stones were lofted to the outside, as mentioned previously.

The most important observation concerning saturation is that saturation occurs at coverage fractions on the ground between 10 and 20 percent. This is shown rather dramatically in Figures 32 and 33. Figure 32 shows the probability

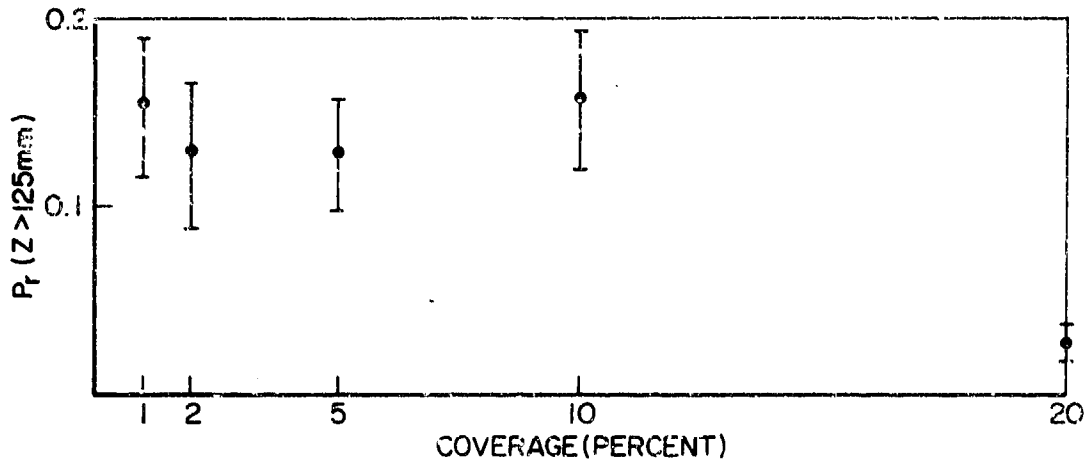


Figure 32. Probability of Lofting Large Stones to $z > 125$ mm as a Function of Coverage (Dual Wheels).

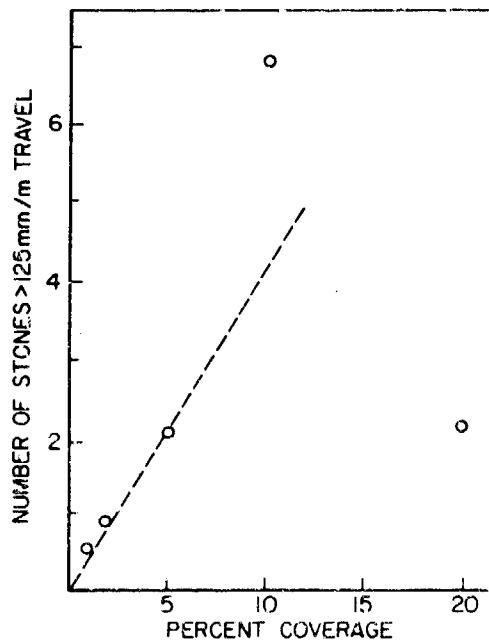


Figure 33. Number of Large Stones Lofted Per Meter of Travel as a Function of Coverage (Dual Wheels).

that any given stone will be lofted to a height of greater than 125 mm as a function of the percent of coverage. For low coverage, up to 10 percent, the probability is about 0.15. However, at 20 percent it is much less than that, only about 0.02. Hence, there is a dramatic drop in the probability of lofting between 10- and 20-percent coverage. It is more enlightening to look at Figure 32, in which the number of stones that would be expected to be lofted from 1 meter of travel is plotted versus the percent coverage. Where the probability of lofting is constant, the number of stones lofted versus percent of coverage will just be a straight line, drawn dashed in Figure 32. The line is drawn through the first three points, suggesting that the point at 10 percent is slightly high. The point at 20 percent is way below the curve. The trend in Figure 32 is an important and unavoidable consequence of a saturation phenomenon: that there is a worst coverage. Here it appears to be about 10 percent. That is, more stones are lofted per unit of distance traveled at 10-percent coverage than when there are either more or less stones.

Two caveats should be placed on the saturation data presented above. Since the stones are not randomly placed, changes in coverage imply slight changes in placement. This is most likely to affect low-coverage data (1 and 2 percent), because the rocks may be placed in positions more or less vulnerable to tire lofting. Startup and exit effects would tend to improve lofting at 20-percent coverage; however, since the rock spacing is about 5 percent of the track length, it is unlikely that the errors in N are more than 5 percent. Thus, the conclusion regarding saturated effects observed here are unlikely to be changed by additional analyses, although the relative lofting probabilities may be altered slightly.

The observed saturation effects are consistent with the hypothesis that saturation occurs when there is more than one rock per contact area. The contact area, A_T , for the

saturation tests was 5 in². The number of rocks in an area A, N_A(A), is equal to

$$N_A(A) = CA/100 A_R, \quad (23)$$

where C is the percent coverage and A_R is the area of the rock. Assume A_R = $\frac{1}{4}\pi d^2$, where d is the rock diameter. We predict saturation at C*, equal to

$$C^* = \frac{100\pi N_A d^2}{4A_T} = \frac{100 \times 1 \times \pi \times 1}{4 \times 5} = 15.7. \quad (24)$$

This is within the uncertainty range of the actual value.

3. Effects of Tire Velocity

Tire velocity (V_T) turned out to be the encounter parameter that most affects lofting. The most striking effect of tire velocity was on the total number of stones lofted, N (75 mm). N was at least proportional to V_T. In fact, most of the evidence indicates $(\Delta N/N)/(\Delta V_T/V_T) > \sim 1.5$. When the velocity dropped from 40 to 25 mph the number of stones lofted dropped from 17 to 6 for the baseline single wheel on concrete and from 28 to 12 for the single wheel on aggregate.

However, the velocity of the stones lofted did not depend on tire velocity. V_{CO} in our measurements was essentially independent of tire velocity. V_{CO} was always about 2.5 m/s, both when the tire velocity is 1.8 m/s and when the tire velocity is 11 m/s. There does appear to be evidence that s might be larger when V_T is smaller; at least for the concrete case it is clear that many more rocks were lofted at high velocity than were expected when the tire speed was decreased. This result is consistent with separate mechanisms for lofting at speeds below V_{CO} and in the high-velocity tail.

4. Effect of Tire Pressure

Four comparisons in the data base allow assessment of the effects of tire pressure--single wheel on concrete and

aggregate, and dual wheels on concrete and aggregate. For the single-wheel cases, there are data at three different pressures: 200, 150, and 70 psi. For the dual wheels on aggregate tests, too few stones were lofted to contribute to this analysis. If a plot is prepared for the number of stones lofted, normalized to the baseline conditions, for the single-wheel concrete, single-wheel aggregate, and dual-wheel concrete cases, then for the single wheel on concrete there is no variation with pressure within the uncertainty of the data. However, for single wheels operating on aggregate and dual wheels on concrete, the number of stones lofted decreases systematically as the pressure decreases. The most prudent approach is to average all of the data, which leads to the conclusion:

$$\frac{\partial \ln N(75)}{\partial \ln P} = 1.5. \quad (25)$$

The lofting distribution parameters V_{CO} and S were not affected by tire pressure in any detectable way.

5. Effect of Load (L_T)

Three comparisons were ideally available to assess the effect of load on lofting parameters: the single wheel operating on concrete, the single wheel operating on aggregate, and the single-wheel versus the dual-wheel baseline case. The latter case was complicated by shifts in weight on the dual-wheel tires. The data show that the effect of load was slight. Apparently, for the concrete single-wheel case, as the load was decreased by a factor of two, the number of stones lofted to the reference height dropped from 17 to 13; for the aggregate case, N dropped from 17 to 10. Thus N decreased slightly with decreasing load and the partial derivative $\partial N / \partial L_T$ was 0.1 ± 0.03 per psi for concrete and 0.14 ± 0.05 per psi for aggregate.

The load studies apparently showed that the tire contact area is not a very important encounter parameter. Figure 34 illustrates this statement. Tire contact area, A_T , depends

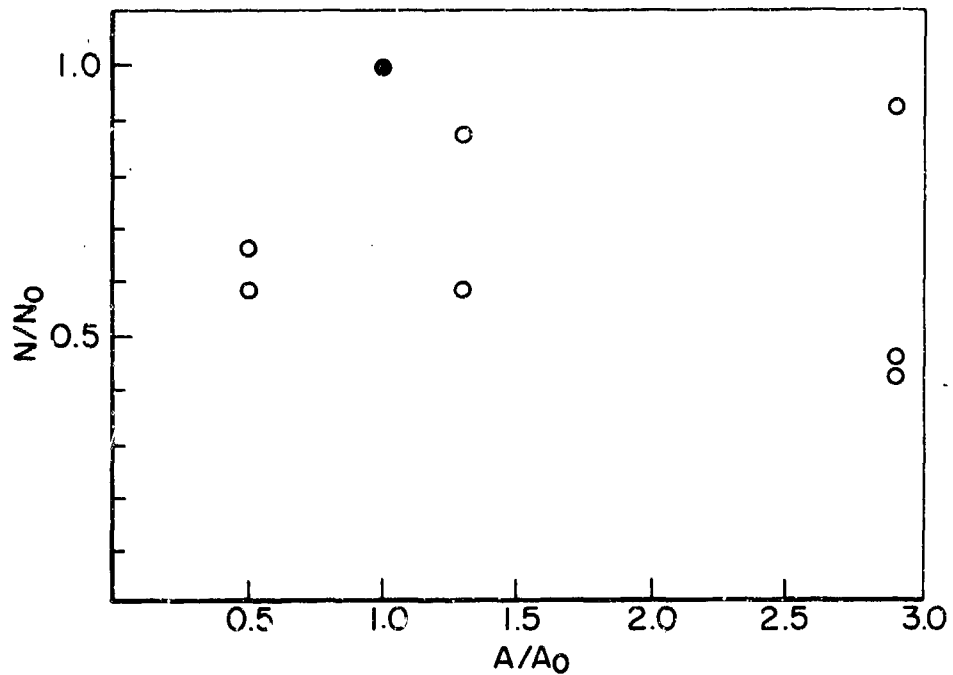


Figure 34. Variation of Number of Lofted Stones with Contact Area. (Both Axes Are Normalized to Baseline Values.)

on both load and pressure, $A_T = L_T/P_T$. The figure shows the combined effects of variation in L_T and P_T on $N(75)$. The data scattered badly, and the number of stones lofted was less for footprint areas greater than and less than the baseline case. Thus, tire contact area by itself did not appear to be a very important lofting parameter.

6. Effect of Stone Shape

The First Test Matrix provided extensive data for evaluating the effects of stone shape, since equal concentrations of both angular stones and smooth stones were mixed together. The conclusions are that: the angular stones are much more likely to be lofted than the smooth stones; the frequency of lofting angular stones from concrete is at least three times higher than for the smooth stones; and the frequency of lofting angular stones from aggregate gravel beds is at least twice as high as for smooth stones.

While angular stones are more likely to be lofted, however, it is not clear that the high velocity stones are more likely to be angular. There were so few high velocity stones that it is difficult or impossible to state categorical conclusions. Nonetheless, a substantial fraction of the highest velocity stones were round.

7. Effect of Stone Size

Results of several tests were examined to assess the effects of size on stone lofting. The best comparison for determining how size affected N was the baseline dual wheel Tests IIC3 and IIC4. The number of large stones lofted above 75 mm was 44 (IIC3), and the number of small stones was 43 (IIC4). The number of encounter sites was identical in these two tests; however, about six small stones were clumped at each site, versus one large stone. Results from IIC2 also show effects of stone size; however, the observations differ from those of the dual-wheel tests. Ten passes over large stones and ten over small stones were conducted. There were 21 large stones and 39 small stones lofted. Pictures from both Tests IIC2 and IIC4 show multiple small stone loftings from the same sites.

Interpretation of these data was clouded somewhat by uncertainty over saturation effects among the small stones. Nevertheless, considering that there were approximately six times as many small as large stones, the results established that the probability of lofting individual stones was much less for small than for large stones.

Velocity distributions from Test 1C1A showed no change with stone size. Both the V_{CO} and S parameters were similar for 1-inch and tread-size stones.

8. Characteristics of High-Speed Stones

A study was conducted of all the rocks in the first and second phase tests that were launched at velocities

exceeding 4 m/s. Direction distributions for these stones differed from the global distributions, as shown in Figures 35 and 36. Elevation angles of the fast stones were depressed, with virtually no stones above 50 degrees. A few appeared below 20 degrees, but fast low stones were difficult to detect, and many may have been missed. Similarly, the dearth of slower stones below 30 degrees may have been an artifact of the observation technique.

The directions of the fast stones were more evenly distributed than the slower stones. The disparity between inward and outward directions did not exist. The stones were broadly distributed around +90 degrees; there was no forward or rearward bias.

9. Effect of Wheel Suspension

Results from Tests IIC1 and IIC2 were compared to judge the effects of wheel suspension. The number of large stones lofted above 75 mm was seven in IIC1 (the T37 wheel) and 21 in IIC2. However, similar numbers of small stones were lofted; 42 in IIC1 and 39 in IIC2. The conclusion is that soft suspension significantly suppresses lofting of large stones, but has little effect on lofting of small stones.

10. Effect of Debris Type

Three tests were conducted with debris other than the standard stones. Data for these tests were only qualitative, since only a few runs were conducted, and the instrumentation could not record some of the high-speed particle motion that resulted.

Tests with 1-inch marbles produced violent results. Marbles were ejected forward at high speed. There was strong circumstantial evidence that the marbles were launched with an intense backspin. In some cases, launch velocity may have exceeded the tire speed. Launch angles were mainly very low.

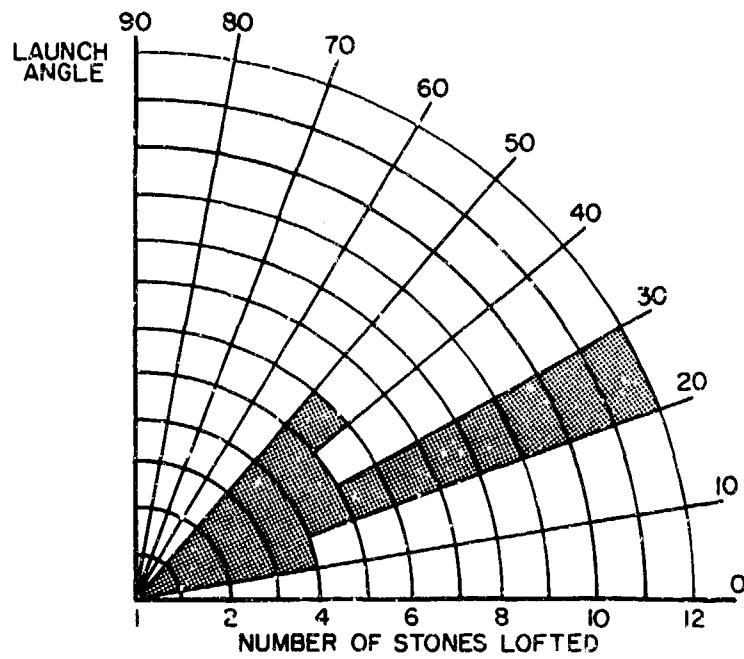


Figure 35. Elevation Angle Distributions for Fast Stones.

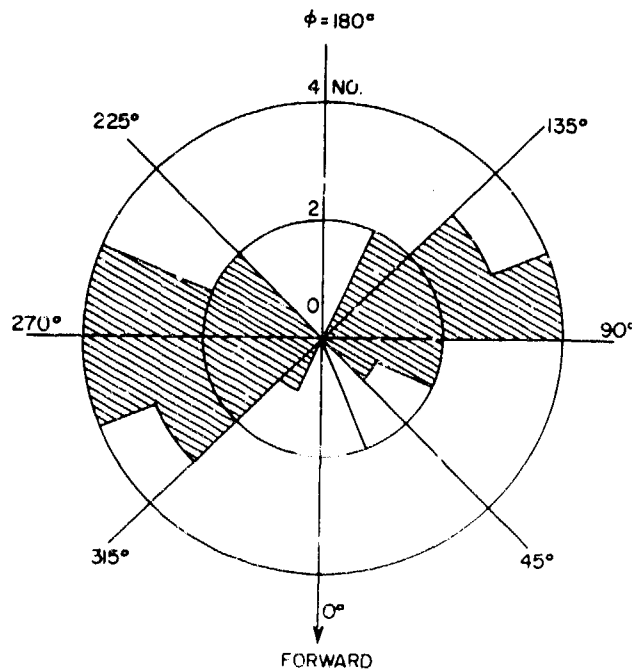


Figure 36. Direction Distribution for Fast Stones.

However, marbles launched from the inside edge of the outside tire characteristically struck the inside tire sidewall, bounced down, and then up off the ground in front of the carriage with a very high angle.

Half-inch marbles were relatively inert. No launchings were observed.

Larger stones, 1.5-inch diameters, were more actively launched than were 1-inch stones. Some of these stones were also thrown forward. The trajectory data were not quantitatively analyzed.

In another test, a miscellaneous collection of "lab junk" was placed on an aggregate test bed. High-speed motion pictures were taken. Objects included nuts and bolts, pencils, small plastic parts, and a rubber ball. Most objects were launched, but at speeds of only a few meters per second. Only the ball launched at high velocity, and the mechanism appeared to be elastic rebound after being squashed by the tire.

SECTION VI THIRD-PHASE TESTS

The third-phase testing was added to the program in an effort to obtain better data for water-covered test beds. A special technique was developed to visualize stones immersed in water spray. The Third Test Matrix is presented in Table 7.

A. STONE VISUALIZATION TECHNIQUE

Tests conducted previously at NASA-Langley had shown significant enhancement of lofting when standing water was present. This observation had not been supported by results from the first phase tests. However, the instrumentation techniques used in those tests had not worked well in wet environments. Conclusions concerning the effect of standing water were only qualitative and tentative. Hence, it was desirable to improve the experimental technique so that more quantitative and definitive results could be obtained for the effect of water on debris lofting.

The principal requirement for improved diagnostics was to improve discrimination. Color photographs taken in the first-phase tests showed that it was possible to distinguish lofted stones from lofted water droplets. However, so many small drops were produced by the splash that many lofted stones were obscured. Lack of identifiable images was due both to screening of the stones by lofted water, and to loss of contrast associated with the dimness of the stone images.

A technique was developed for rendering the water spray invisible to the recording cameras:

- (a) The pebbles themselves were made fluorescent by covering them with a coat of Dayglo[®] paint.
- (b) The illuminating source(s) were covered with filters which allowed only blue and UV light to pass.
- (c) The camera was equipped with a filter which allowed only yellow to red light to pass.

TABLE 7. PART I AND II RUNWAY FOD SUMMARY - PHASE III

Test	Diagnostics	Remarks	V	P	d	cov.	Stones	Runs
1	FC side	scope splash	40→25	200	0.3	10% ^d	LA	4
2	FCf side	test visibility	40→25	200	0.3	10% ^d	LA	4
3	FCf side	test visibility	40→25	200	0.3	10% ^d	SA	4
4	FC front	scope splash	40→25	200	0.3	10% ^d	LA	4
5	FC rear	test visibility	40→25	200	0.3	10% ^c	LA	4
6	Stereo Camera	Base	40	200	0.3	10% ^b	LA ^c	18
7		Velocity	25	200	0.3	10%	LA ^c	19 (No flash on 6)
8		Pressure	40	75	0.3	10%	LA ^c	18
9		Rock Size	40	200	0.3	10% ^d	SA ^c	18
10		Water Depth	40	200	0.6	10% ^b	LA ^c	18
11		Water Depth	40	200	0.1	10% ^b	LA ^c	18
12		Rock Saturation	40	200	0.3	5% ^e	LA ^c	20 (18-20 one run)
13		Rock Saturation	40	200	0.3	15% ^f	LA ^c	18
14		Rock Saturation	40	200	0.3	20% ^g	LA ^c	18
18		Load & Water Velocity	40	200	0.3	5% ^e	LA ^c	9 ^h & 9 ^{h,j}
19		Single Wheel	40	200	0.3	10% ^k	SA ^c	9 ^m
20		Single Wheel	25	200	0.3	10% ^k	SA ^c	9 ⁿ
21		Rock Visibility	40	200	0.3	10% ^k	SA ^c	10
22		Rock Visibility	40	200	0.3	10% ^l	SA ^c	18 ^o
23		Rock Patterns	40	200	0.3	Various	LA ^c	17
24		Rock Size	40	200	0.3	10% ^b	1/2 size	18 ^o
25		Rock Size/Shape	40	200	0.3	10% ^b , 2%	1/2 size, 1" marbles	17 ^p

^b Nom 10% Coverage - Actually 9% (16 rocks per tire).

^c Rocks Have Paint Baked On.

^d Nom 10% Coverage - Actually 9% (16 spots/tire with 6 rocks/spot).

^e Nom 5% Coverage - Actually 4.5% (8 spots/tire, 1 rock/spot).

^f 24 Rocks per side.

^g 34 Rocks per side.

^h 500# load.

^j 1/8 Nylon Balls & Wood Blocks 1/4 x 1/4

^k Nom 10% Coverage - Actually 9% - 2 rocks/spot.

^l Nom 10% Coverage - Actually 9% - 2 rocks/spot - one wheel at a time.

^m Color film, right camera - Filter off, passes 6 to 9.

ⁿ Color film, right camera - Filter off, passes 7 to 9.

^o Rocks under outside wheel only, passes 1 to 9 - Rocks under inside wheel only, passes 10 to 18.

^p 1/2 size rocks, passes 1 to 9 - 1 inch marbles, passes 10 to 17.

In this photographic system, only the pebbles could be detected by the cameras since only the pebbles emit yellow to red light. Non-fluorescent objects such as water, the aircraft tire, etc., were not visible because they could only reflect the blue light from the light source (which the camera filter eliminated).

Trial pictures were made in the University Impact Physics Laboratory to determine the optimum illumination level and apertures for 35 mm stereo and 16 mm movie cameras. Edmund Scientific Corp. No. 82,038 blue acetate filters were used on the lights.

It was found that more light was required than was produced by the Xenon strobe source used previously. Eight Rokinon[®] 26A flash units were connected to a specially constructed sequence box in order to produce consecutive flashes for the 35 mm stereo cameras. Results were satisfactory; see Figure 37.

Six Cinequeen[®] lamps were used for the 16 mm 500 f/s movies. A start/stop unit was constructed so that the University's Photec[®] 16 mm camera and Cinequeen[®] lamps could be remotely turned on and off. The lamps increased to full brilliance in only two frames. With this technique, only about 10 feet of film was used per pass. During the short illumination periods, heat buildup in the blue acetate filters was negligible. The film used was Kodak Video News Film[®].

B. HIGH-SPEED MOVIES

As shown in the test matrix, in the first few tests a 500 fps Photec[®] camera was used with six Cinequeen[®] lamps. Over 35 high-speed movies revealed important details of splash formation, although the films taken of fluorescing stones were badly underexposed. A jet of water was formed in front of the tire. The velocity of this jet exceeded the tire speed. However, no stones were lofted by the forward jet and water rose in sheets behind the tire. The speed of the rising water was similar to the speed of lofted stones. The water sheets were

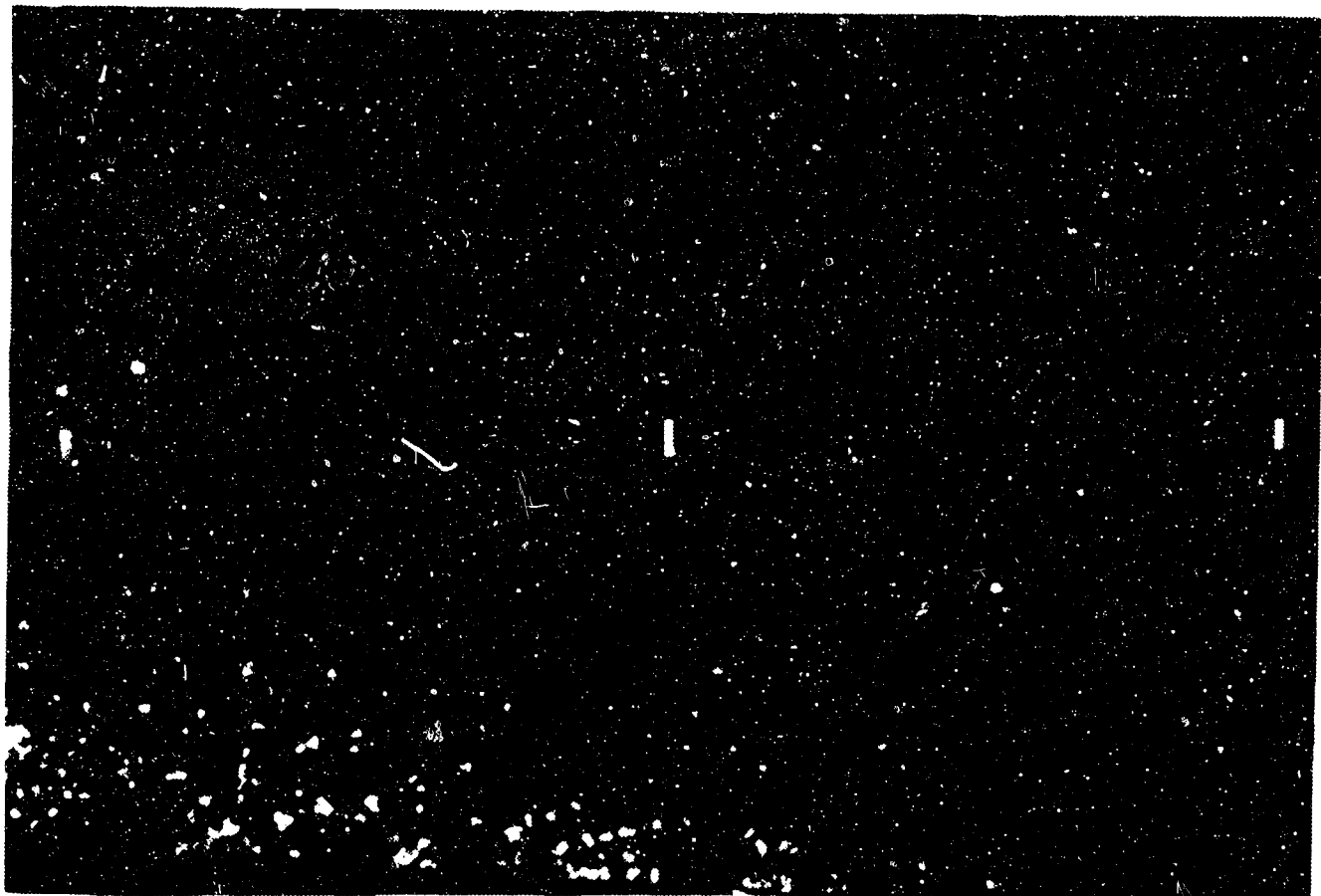


Figure 37. Small Stones Lofted in Test III-9.

opaque, and probably rendered even fluorescent stones invisible. However, the water sheets broke up into droplets after about 50 ms. The painted stones were then plainly visible, even to an unfiltered camera. The loss of information in the previous attempts to photograph through water had probably been caused by film fogging and clutter from the water sheet and subsequent multitude of droplets.

C. STONE TRAJECTORY DATA AND ANALYSIS

The number of rocks launched and visible in the negatives from the 35 mm orthogonal cameras was considerably less than in the two preceding test phases. Test observers also reported less rock activity with the presence of water. However, some lofted rocks were undoubtedly also obscured by the splash.

There were very few passes for which it was worthwhile to analyze prints for detailed trajectory analysis. In most cases, the exposure only served to testify to the absence of lofted stones. A summary of the data from the orthogonal cameras is given in Table 8.

In the following, "number of rocks launched" refers to rocks launched above approximately 50 mm.

1. Baseline Data for Small Rocks

The baseline test for small rocks was IIIWC9. In this test six rocks were placed at 16 different sites under each wheel. So many rocks were launched that it was not feasible to count or digitize them. Test IIIWC21 was added to the matrix. In this test two rocks each were placed at the 16 distinct sites under each wheel. The rocks launched in this test were countable and some were digitizable. Test IIIWC21 was then used as the baseline test for small rocks.

2. Effect of Tire Velocity

Decreasing the tire velocity decreased the number of large rocks launched in the dual wheel test from 12 to 5. This was in agreement with the results on dry pavement.

TABLE 8. SUMMARY OF OBSERVATIONS FROM THIRD TEST MATRIX

Test	Number of Rocks Launched	Number of Rocks Digitized	Launch Velocity		Launch Angle		x, y-Plane Angle		Maximum Height	
			Mean/Std. Dev.	Mean/Std. Dev.	Mean/Std. Dev.	Mean/Std. Dev.	Mean/Std. Dev.	Mean/Std. Dev.		
III-WC6	12									
III-WC7	5									
III-WC8	15									
III-WC10	3									
III-WC11	7									
III-WC12	3									
III-WC13	26	7	2.13/0.33	56.2/7.1	23.9/73.9	160.5/53.1				
III-WC14	11	6	2.91/0.64	41.1/6.7		186.3/76.8				
III-WC19	24	5	3.54/0.64	27.6/4.0	60.5/34.5	142.8/58.6				
III-WC20	25	5	2.32/0.38	26.3/4.4	60.9/22.4	53.6/16.8				
III-WC21	26	12	2.89/0.94	45.7/13.6	73.6/10.0	194.4/92.5				
III-WC22 (Outside)	22									
III-WC22 (Inside)	7									
III-WC23	9									

Using a single wheel, the number of small rocks launched remained constant when the tire speed was decreased. However, the mean velocity of the small rocks observed in the 40 mph test was greater than the velocity of rocks in the 25 mph test: 3.45 m/s to 2.35 m/s. The mean maximum height was also higher in the 40 mph test: 142 mm to 53 mm. The mean launch angles and x,y-plane angles were similar. Thus small rocks were not more likely to be launched with higher tire speed, but if launched, they had a higher speed and reached a greater height.

3. Effect of Tire Pressure

Lowering the tire pressure increased the number of rocks launched from 12 to 15. The data are not complete enough to justify a quantitative correlation.

4. Effect of Rock Size

Three rock sizes were used: Rocks with a nominal principal dimension of 1 inch, 0.5 inch, and 0.25 inch. The relevant tests are: WC6, large rocks; WC25, one-half size rocks; and WC21, small rocks. The comparison was complicated by the difference in number of passes in the tests and the difference in number of rocks per site in the tests. There were 18 passes in WC6, and nine passes in WC25 and WC21. There was one rock per site for tests WC6 and WC25, and two rocks per site for test WC21. For each test the number of rocks launched per encounter was calculated: 0.042, large rocks; 0.076, one-half size rocks; 0.090, small rocks. It appears that the probability of lofting increases with a decrease in rock size.

5. Effect of Load

Decreasing the load decreased the number of rocks launched. In particular, dropping the load from 1000 pounds to 500 pounds decreased the number of rocks launched from 12 to 3. For dry concrete and dry aggregate the decreases were 17 to 13 and 17 to 10 respectively; but with a single wheel in each

case. Thus, they involved a drop in load per wheel from 1000 pounds to 500 pounds. Test Matrix III is a dual-wheel case with a drop in load per wheel from 500 pounds to 250 pounds. The water may cause a greater decrease in launchings with a decrease in load or the greater decrease may be caused by the lower original load.

6. Effect of Coverage (Saturation)

Increasing the coverage increased the number of rocks launched per encounter until a coverage somewhere between 15 and 20 percent was reached. Increasing coverage above this "saturation" point caused a decrease in the number of rocks launched per encounter. This agrees with dry tests from which a "saturation" coverage was predicted between 10 and 20 percent. Figure 38 shows the probability of rock launching per encounter, as a function of coverage.

7. Effect of Water Depth

A distinct decrease in the number of large rocks lofted occurred when the water depth of 0.3 inch was

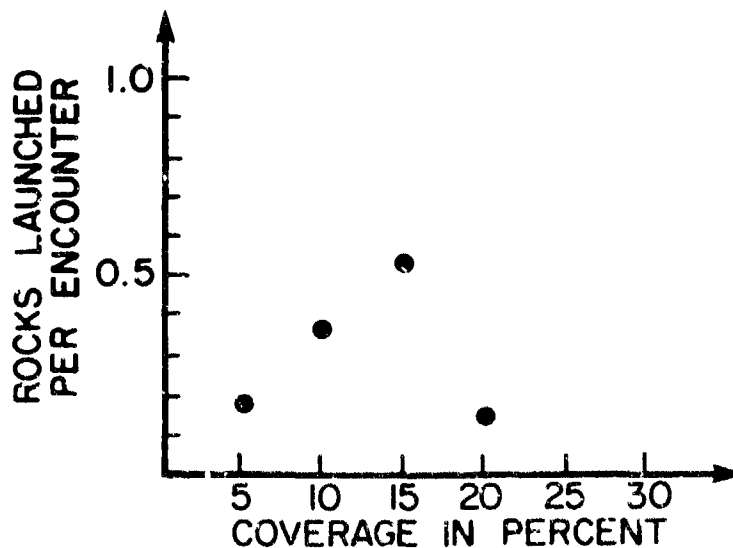


Figure 38. Probability of Lofting versus Coverage.

increased to 0.6 inch: 12 rocks to three rocks. The greater amount of water presents the possibility that the splash is greater and blocks the view of lofted rocks. However, the decrease is so great that this mechanism does not account for it. At 0.6 inch the rocks are almost covered with water. Thus, the change from lying in water to being covered with water may significantly decrease the number of launchings per encounter. On the other hand, there is a drop going to a depth of 0.1 inch from 0.3 inch: 12 rocks to 7 rocks.

8. Effect of Rock Placement Patterns

The normal rock placement patterns were quasi-symmetric with respect to the center line between tires. The standard 10-percent large rock pattern is shown in Figure 39. A special test (IIIWC23) was conducted to see if rock placement

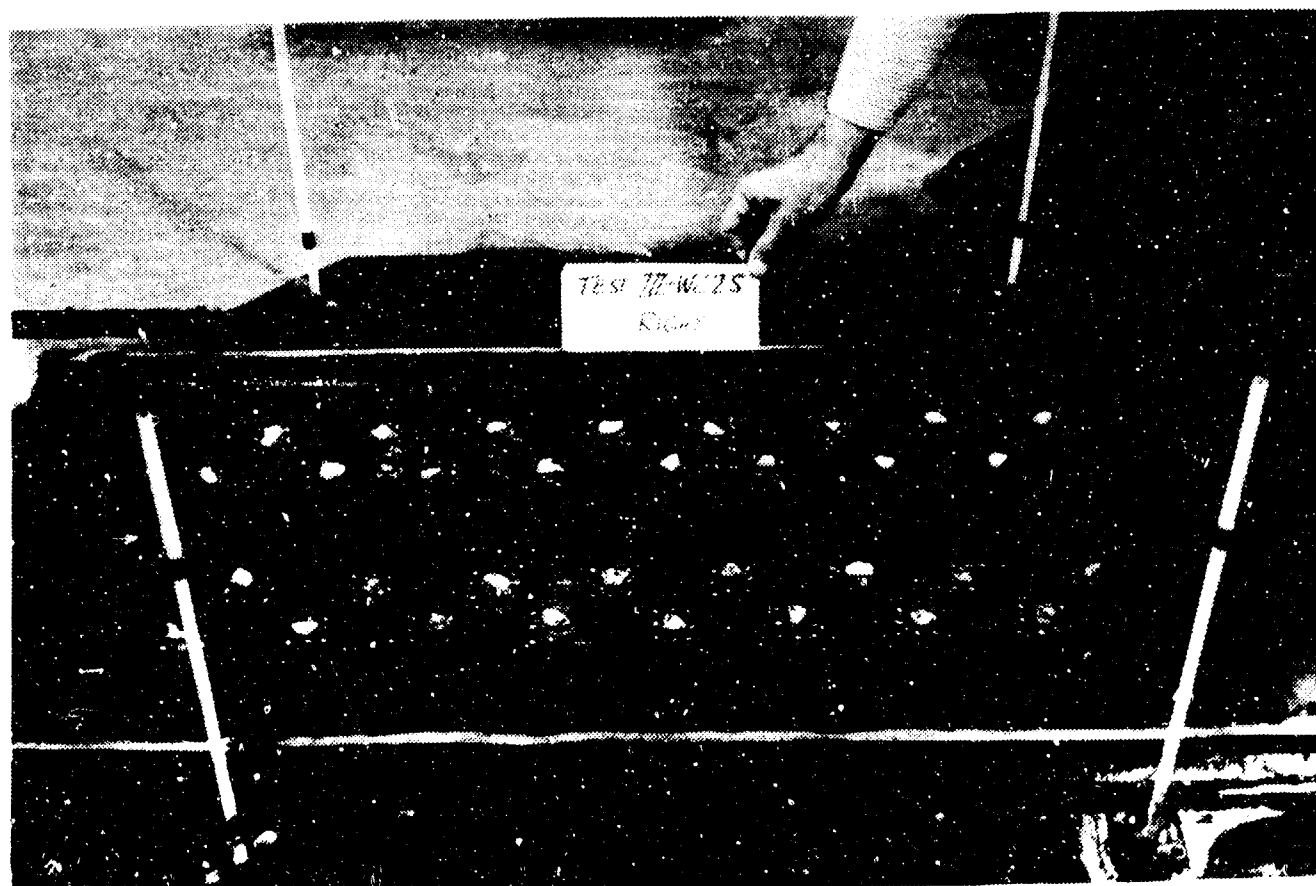


Figure 39. Normal 10-Percent Rock Placement Pattern.

influenced lofting. The same repetitive pattern was placed under both tires, fully symmetric with respect to the center-line between tires. Six rocks were launched. When the pattern under the inside tire was lagged a half-cycle behind the pattern under the outside wheel, only one rock was launched. These patterns are shown in Figure 40. For this particular pattern, symmetry enhanced launching. This result implied that the tires were not independent of one another in their lofting action. Our tentative conclusion from this result and the single-dual-wheel comparisons conducted earlier was that when dual wheels separately encounter stones, lofting is less likely than single wheels encountering stones or dual wheels encountering stones simultaneously.

9. Inside-Outside Bias

In an attempt to determine the ratio of rocks launched by the inside wheel to rocks launched by the outside wheel, tests were run with rocks under only one wheel at a time. Small stones were used.

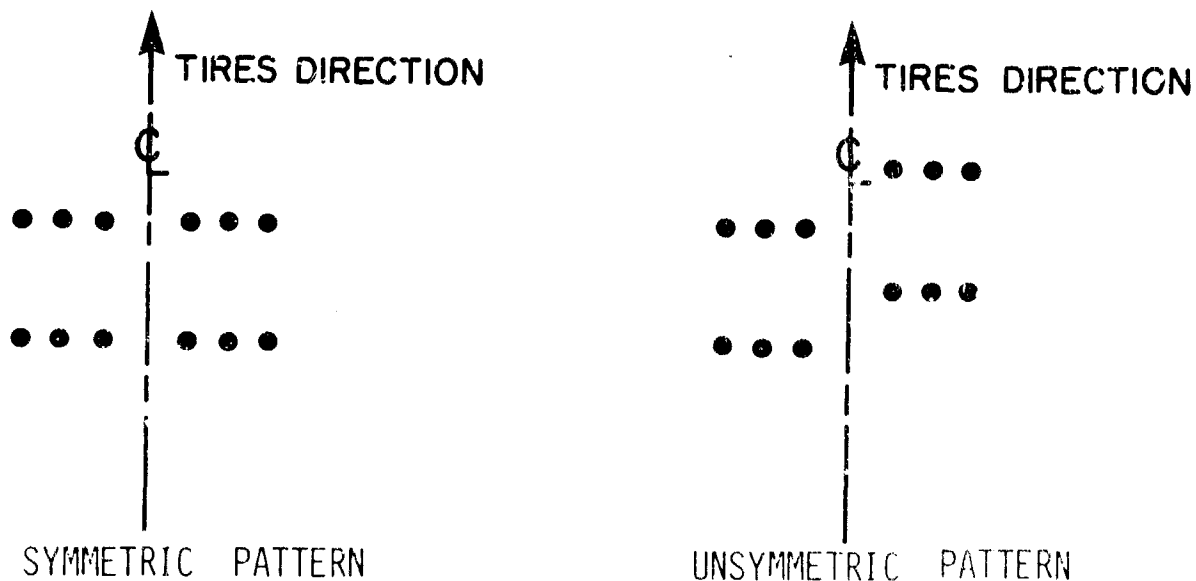


Figure 40. Rock Placement Patterns for Comparison Test.

The number of rocks launched when rocks were placed under both wheels was 26; when rocks were placed under only the outside wheel, 22 were launched; when rocks were placed under only the inside wheel, 7 were launched. The ratio of outside to inside is roughly 3:1. It was interesting that the sum of the number of rocks launched in the outside only case and the number of rocks launched in the inside only case was approximately equal to the number of rocks launched with rocks under both tires. Twelve of the 26 rocks launched with rocks under both wheels appeared clearly enough in black and white prints for trajectory analysis. All 12 came from the outside wheel, reinforcing the conclusion of an outside wheel bias. The bias may have been real or apparent. We believe it was probably apparent, caused by the fact that most of the small stones lofted by the inside tire were obscured by the splash.

Similar tests were conducted with 1/2-inch rocks. For those, the number of rocks launched were: 11 with rocks under both wheels; 2 with rocks under the outside wheel only; 3 with rocks under the inside wheel only. In this case there appears to be no bias. However, the interaction between the two wheels seems to again be manifested in a decrease in launchings per encounter when rocks are placed under only one wheel. Only one rock trace was digitizable so trajectory analysis was not helpful in compiling statistics for which wheel launched the rocks when rocks were under both wheels.

10. Trajectory Statistics

Individual tests did not yield enough trajectory data to support comparison of launch parameters between individual tests. Therefore, all 23 large rocks digitized from this test matrix were lumped together and compared to the rocks digitized in the baseline test of Matrix II. The distribution of launch parameters is given in Table 9. Figure 41 gives a summary of the height distribution. Other data summaries can be found in Appendix B. The mean parameters

TABLE 9. SUMMARY OF TRAJECTORY DATA

	# of Rocks	Launch Velocity		Launch Angle		x, y-plane Angle (+ only)		Maximum Height	
		Mean/Std. Dev.		Mean/Std. Dev.		Mean/Std. Dev.		Mean/Std. Dev.	
All Large Rocks Digitized in III	23	2.34 m/sec		45.9 deg		84.4 deg		137.9 mm	
		0.57 m/sec		10.9 deg		46.4 deg		57.2 mm	
Baseline in III	27	2.57 m/sec		40.8 deg		63.0 deg		144.2 m	
		0.51 m/sec		11.3 deg					

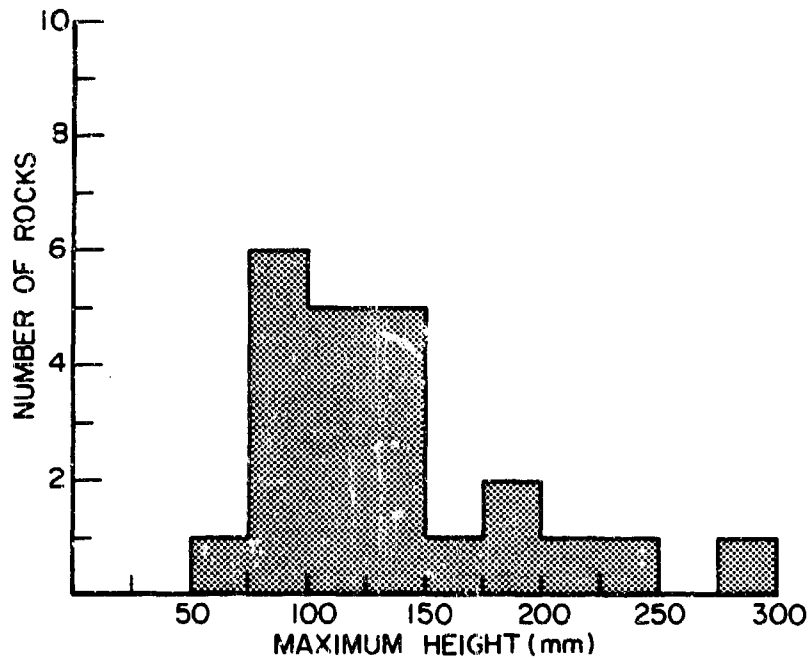


Figure 41. Maximum Height Distribution of All Large Rocks Launched from Wet Pavement in Third Test Matrix.

of a large rock launched from water are similar to those of a large rock launched from dry pavement.

The large rocks digitized from Matrix III came predominantly from the outside half of the outside wheel. This probably reflects the greater visibility of these rocks, rather than a bias for this launch position.

Trajectory analysis showed that most small rocks were not launched from under the tires, but from just to the outside of the outside tire. This suggested that once small stones are launched, they become entrained in the water spray and assume its velocity and direction. To check this, tests were run with small objects with a specific density less than that of water. They floated and were assumed to be launched with the spray. The mean launch velocity of these floaters was 2.98 m/s. This is assumed to be the water velocity, and it is also very nearly the speed of the small stones, indicating that

the small stones were entrained in the spray. A sample photographic print is in Figure 42. Trajectory analysis indicated that launch positions of the floaters were also just outside the outside tire further strengthening the association of small particle trajectories with the water path.

11. Water Suppression of Lofting

Test IIC6 was the dry large rock test which corresponded to the baseline, wet, large rock test, IIIWC6. The analyzed rocks in IIC6 had a ratio of rocks launched outward to rocks launched inward of 16 to 7. The total number of rocks launched was 65. The number of rocks launched on IIIWC6 was six. To estimate the effect of bias, we assumed that the spray blocked the view of rocks launched inward and, thus, that all six rocks were launched outward. Then there could have been $6 \times 7/16 = 2.625$ rocks launched inward. Supposing there were actually $6 + 3 = 9$ rocks launched in Test IIIWC6, then the presence of water reduced the number of rocks launched per encounter by $\frac{65 - 9}{65} \times 100 = 86$ percent. Most other plausible assumptions about bias resulted in even greater suppression factors.

12. General Review of Water Effects

Water inhibited lofting of 1-inch and 1/2-inch stones. The effect was chiefly to limit the total number of lofted stones; the distribution of lofting parameters was not significantly affected. In particular, saturation effects were similar in wet and dry tests. The lofting of 1/4-inch stones was greatly affected by water; the stones were entrained in the splash. The data obtained from water events were less precise than those obtained previously because fewer stones were lofted and some were obscured by the splash. The data indicated, however, that the number of rocks launched per encounter was decreased for large rocks in the presence of a layer of water. Launch parameters were not noticeably affected. For small

stones, probability of launch per encounter was not affected by water. However, the trajectories of small stones were greatly affected, due to entrainment in the splash.

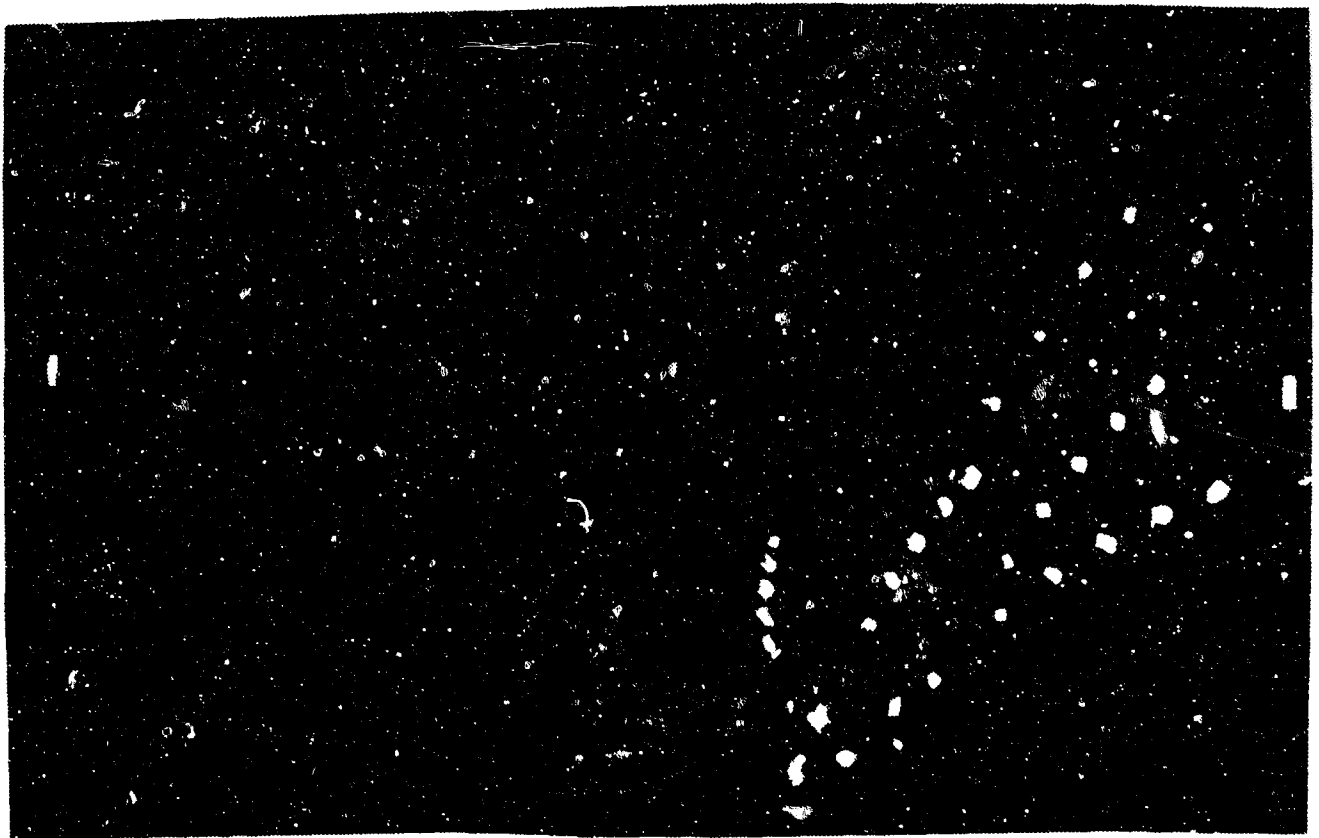


Figure 42. Floating Objects After Launch.

SECTION VII
ANALYTICAL MODELLING OF LOFTING
FROM AIRCRAFT RUNWAYS

The analytical modelling of lofting of runway debris was approached by both inductive and deductive analyses. Many, but not all, features of the observed phenomena were explained, and predictions for runway operation were made. Some of the source material for this section is developed in Appendix A, which was prepared under subcontract to the University of Dayton by H.F. Swift of Physics Applications, Inc.

A. INFERENCES FROM THE DATA

Section VIII contains a recitation of the observed variations in lofting characteristics with encounter parameters. Those observations provide insight into the physical mechanisms responsible for debris lofting.

Debris that constituted a significant obstruction to the tire was more likely to be lofted. There are two lines of evidence supporting this statement. First, when two stones simultaneously occupied a tire-contact patch, the probability of lofting either one was greatly reduced. Second, (within the limited range of stone sizes investigated), larger stones were more likely to be lofted than smaller ones. It is inferred that the loft mechanism involves displacing a stone from the path of the tire, from which it follows that the higher the tire speed, the more violent the lofting action.

Different launch mechanisms were responsible for slow and fast stones. Slow stones had speeds less than about 2.5 m/s, and constituted about 90 percent of launches. The principal evidence for different mechanisms came from the direction distributions. Fast stones were much more likely to emerge nearly normal to the tire plane at 30-degree elevation, and unlike slower stones, they were equally likely to be launched to the inside or outside of the curved test track.

The launch mechanisms involved the sides of the contact patch. There is no evidence to support "tread envelopment" or "tread gripping," These had been proposed earlier as possible launch mechanism (Reference 1). However, that would lead to rearward launch of debris, and this was almost entirely absent. Since neither tire pressure nor weight exerted great influence on lofting parameters, the precise angle at which the tire sidewall meets the ground is inferred to be of minor importance. From these observations, the existence of an "active zone" is hypothesized. Stones in this zone are subject to expulsion leading to lofting. It follows that the location of a stone relative to the tire path is probably one of the important encounter parameters that determines whether or not a given stone is lofted.

The available evidence supports the hypothesis that the outward bias of the launch directions of slow stones is not due to shifting load, since load and pressure are relatively unimportant encounter parameters. Rather, the outward bias is probably due to "scrubbing"; as the tire rolls onto a stone and loses traction, it will tend to rotate so as to be more nearly aligned with the local track tangent. The effect is probably to suppress inward lofting, although that cannot be definitively supported by the data. A consequence of this hypothesis is that the number of slow stones lofted by a tire rolling in a straight line would be greater than reported here by almost a factor of two.

Hypothetical launch mechanisms should explain why angular stones are much more likely to be lofted to low speeds than smooth stones. (It is not clear if angular stones are preferentially launched to high speeds.) The forward tumble* of most angular stones also requires an explanation. The importance of angularity and tumbling leads to the hypothesis that angular

* (e.g., they tumble in the same direction as if they were rolling on the ground.)

stones are first launched spinning and along the ground. They become airborne when asperities strike the ground plane.

The data and hypothesized physical processes are generally consistent with linear size scaling (Equation 5). Scaling was not rigorously checked because only one tire size was employed. However, all of the physical models proposed to explain various aspects of lofting from dry pavement should obey this scaling rule. Only lofting of small stones from wet pavement was influenced by viscous forces, for which Equation 9 is expected to apply.

B. ENGINE CAPTURE CRITERIA

Capture of lofted debris by engine inlet ducts is assumed to be the major FOD mechanism for aircraft operation on damaged runways. The trajectories of lofted particles will be influenced by the ambient air flow. At least for slowly moving aircraft, the trajectories may be quite different from the ballistic arcs assumed here. However, consideration of perturbations on trajectories due to inlet air flow is beyond the scope of the present investigations. Such effects are not considered in the following analysis. Consequently, although the analysis undoubtedly is correct for aircraft speeds high enough that there is no stagnation point beneath the inlet duct, it may be only approximate for low aircraft speeds.

Given this caveat, evidently only stones that are lofted into rather narrow direction cones can enter the engine inlets of aircraft. The critical directions are functions of aircraft speed and stone speed. Figures 43 through 46 give criteria for stone ingestion by F-4E and F-15 aircraft. Ingestion by F-16 aircraft was deemed impossible.

C. PINCH STONE-LOFTING MODELS

Several stone lofting models are considered in detail in Appendix A. Attention there is limited to candidate techniques

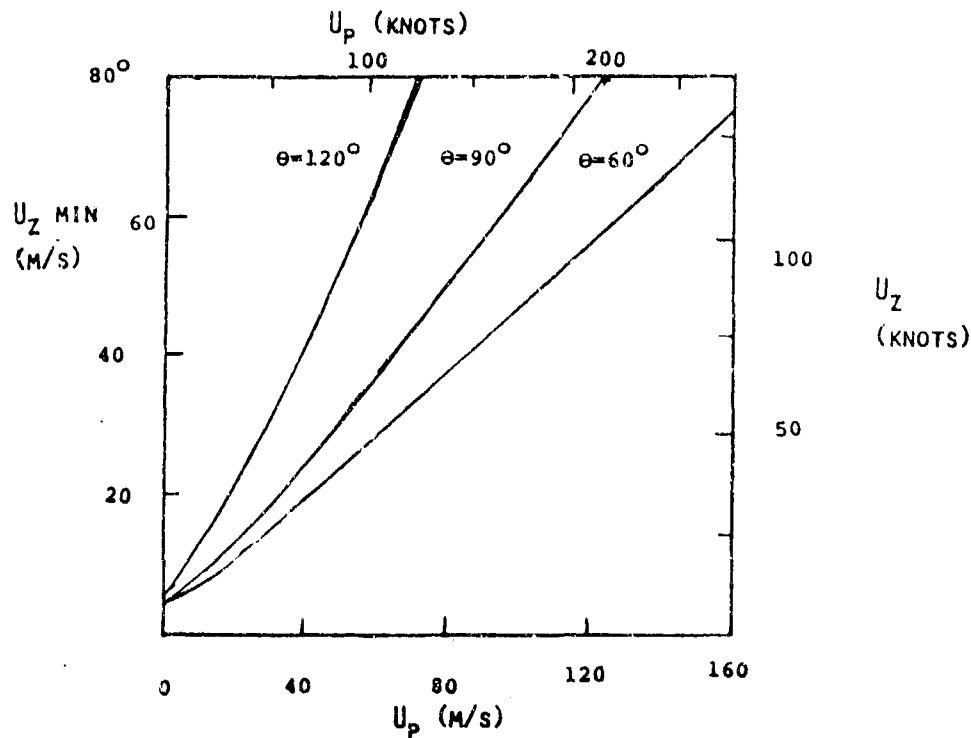


Figure 43. Minimum Vertical Velocity, U_z , vs. Aircraft Speed, U_p , for Ingestion of Debris Lofted by the Nosewheel of an F-4E Aircraft. (θ is the launch direction angle; $\theta = 0$ is forward).

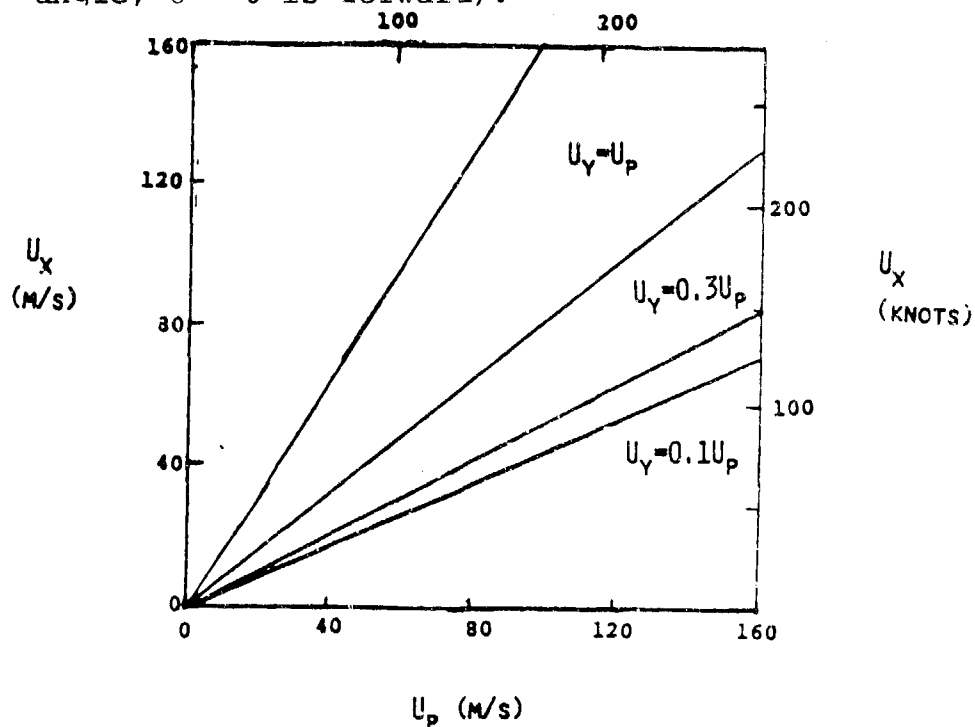


Figure 44. Minimum Outward Velocity, U_x , vs. Aircraft Velocity, U_p , for Ingestion of Debris Lofted by the Nosewheel of an F-4E Aircraft. (U_y is the stone velocity component parallel to U_p .)

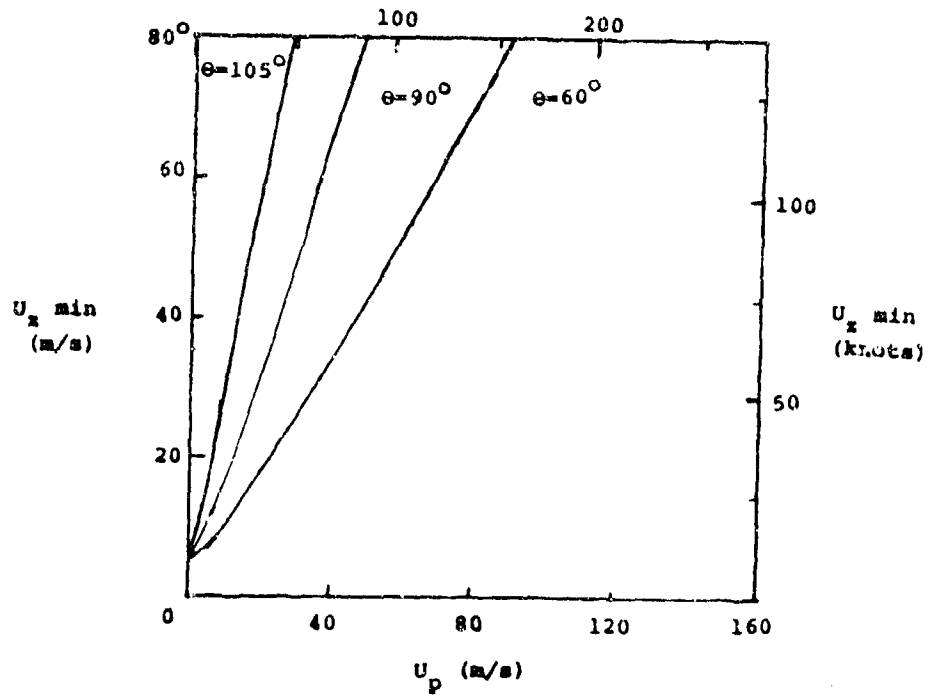


Figure 45. Minimum Vertical Velocity, U_z , vs. Aircraft Speed, U_p , For Capture of Stone Lofted by the Nosewheel of an F-15 Aircraft.

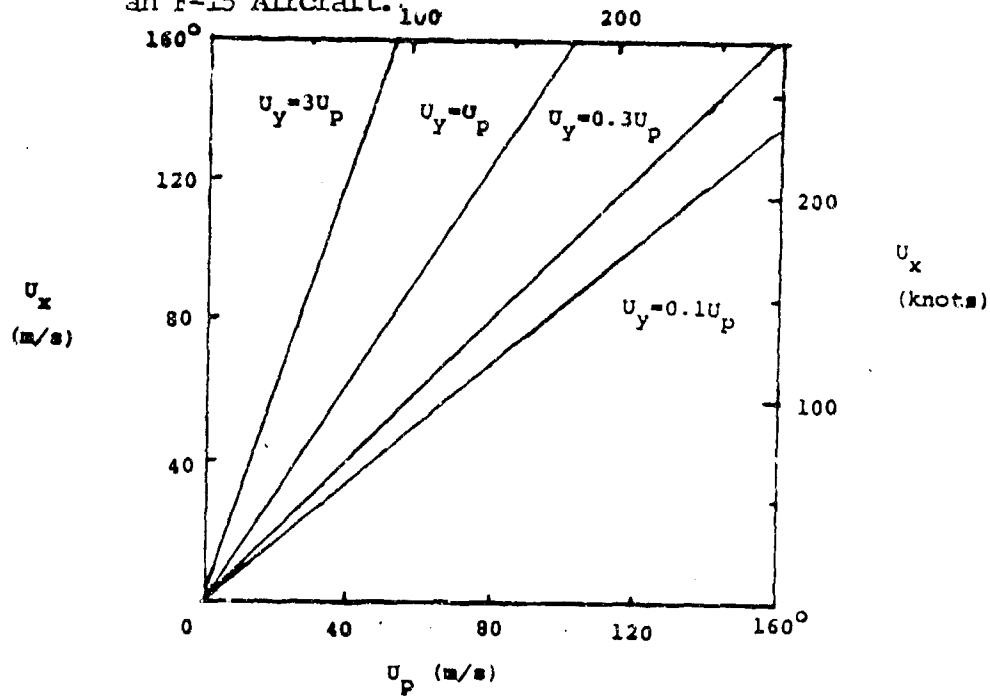


Figure 46. Minimum Outward Velocity Component vs. Aircraft Velocity for Ingestion of Stone Lofted by the Nosewheel of an F-15 Aircraft.

for launch of fast stones, defined as having speeds higher than 4 m/s.

Appendix A concludes that the most probable launch mechanism is pinching out of stones caught under the side of the tread. Rocks rolled over by the tire experience both a net outward force and (if slippage on the ground or tire takes place) a torque. It is shown that the maximum velocity that may be achieved is proportional to the square root of the tire pressure. There is also a weak dependence on stone size.

Vertical velocity components arise as a consequence of stone spin. When nonspherical stones spin near the ground, they can launch themselves when a protuberance comes in contact with the ground plane, thereby raising the stone center of mass.

This model unfortunately fails to account for most detailed observations of lofted rocks. It predicts velocities significantly higher than observed, it does not explain why higher tire speeds loft more efficiently, and it overestimates the effect of pressure. Therefore, it has been concluded that the model represents a hypothesis for launch of very high speed stones that were not, in fact, observed in these tests, but may occur under some other conditions.

D. HAMMER-LOFTING MODEL

An alternate hypotheses for lofting can be based on a hammer analogy. The tire is regarded as a hammer that descends on the rock at a speed given by:

$$u = \frac{2V_T}{d} \sqrt{y^2 \tan^2 \phi - dy \tan \phi + dh - h^2}, \quad (26)$$

where ϕ is the contact angle of the tire, y and h are the horizontal and vertical distances from the footprint edge to the point where the stone of diameter d is struck. At 40 mph for 1-inch stones and the tire profile used in these tests, $u = 6.9$ m/s.

A rock near the edge of the tire may be struck a glancing blow that will cause it to turn out and rotate. High-speed movies of rocks struck by rubber mallets verified this mechanism. The velocity of the stone will be proportional to the tire velocity, since the faster the blow falls, the faster the stone must move out of the way. However, the probability of lofting will be roughly proportional to the difference between the stone diameter and the equilibrium height of the tire from the pavement at the stone position. (This distance is about 6 mm for 1-inch stones at the edge of the tires used in this program.) This critical distance will increase with increasing load; the rate of increase will depend upon tire design.

The hammer model predicts that at higher tire speeds stone velocity will increase, but direction and lofting probability will not. The model also predicts that the number of stones lofted will be approximately proportional to the square root of the tire load and the first power of the stone diameter. Lofting probability also depends greatly on stone shape and tire contour. According to this theory, no stone may be lofted at a speed exceeding that given by Equation (26). For empirical studies conducted with rubber mallets, no stones were launched above 45-degree elevation angles.

The hammer model is in fairly good agreement with observations of high velocity stones. The maximum velocity and preferred directions are explained. The effects of pressure and tire speed are not well enough resolved for high speed launches to evaluate the model. The model does not fit the low-velocity stone observations. It fails to explain the enhanced number of stones lofted by higher tire speeds and it can not explain the forward tumble of most low speed stones.

E. APPLICATION TO RUNWAY SCENARIOS

In Appendix A, equations are developed for the number of stones ingested, N_1 , by an aircraft per maneuver. The principal equation is:

$$N_i = \frac{8L_s}{\pi} \sum \frac{Q_d S_d C}{d_s} \quad (27)$$

In this equation,

L_s = length of roll

Q_s = the probability of launching a stone to a critical velocity high enough to reach the inlet duct, given that the stone is partially overrolled by the tire. Q_d is a function of stone shape, stone size, tire design, and aircraft speed. Q_d is related to the probability that a stone encountered will be lofted, P , by:

$$2Q_d = P \times (\text{tire width}) \quad (28)$$

S_d = the probability that a stone launched above the critical speed will actually intercept an inlet duct. S_d only depends on the aircraft geometry.

The other parameters have their usual definitions, namely C is the areal coverage fraction and d is the stone diameter. The sum is over all the stone diameters represented in the debris field.

If we assume (as in the hammer model) that the launch speed is proportional to the tire speed, that linear size scaling holds, and that (as found empirically) the launch speed does not significantly depend on load, then it follows that the probability for ingestion does not depend on aircraft speed. Empirically, it has been observed that most nosewheel spray appears to lie in a rather narrow band directly behind the wheel (referenced to the moving aircraft). This is consistent with the behavior of the 90-percent majority of low speed stones, whose speed does not change with encounter parameters. However, we proceed here on the more severe assumption that the launch speed of the high-speed stones is proportional to tire velocity.

Even with this assumption there were no stones that would ballistically reach the inlet duct of an F-4E aircraft observed in this program. Thus, in the absence of air inlet flow effects, we can set an upper limit on Q_d of 0.001. For the F-15 aircraft, the probability of ingestion due to a ballistic trajectory is so remote that Q_d should be regarded as vanishingly small.

In Appendix A, a 10-percent coverage debris field judged as representative of a postattack runway is defined. Using $Q_d \leq 0.001$ and S_d for the F-4E, it is derived that on the average less than 0.16 stones will be ingested per kilometer. If $Q_d = 10^{-4}$, only 0.08 stones are ingested per kilometer at 50 percent coverage. It follows that, in the absence of flow-field effects, stones of the type considered in this report pose a minimal threat to operating aircraft. In particular, the hazard caused by elimination of FOD suppression mats is insignificant.

SECTION VIII
SUMMARY AND CONCLUSIONS

An experimental technique has been developed and applied to study of lofting of debris by overrolling tires. The debris was mainly stones, either 1-inch or 1/4-inch in diameter. Tire speeds were between 11 and 18 m/s. The data have important implications for operation of aircraft on dirty runways.

A. TECHNIQUES

1. The MDL provides an ideal environment for study of debris lofting by tires.

2. The orthogonal camera setup and data analysis algorithms developed for this program are adequate to measure the trajectories of tire-launched debris.

3. The fluorescent technique developed for use on water-covered surfaces was useful but not totally successful for study of trajectories.

B. GENERAL CHARACTERISTICS OF LOFTED DEBRIS

1. Lofting is a strong function of coverage. Maximum lofting occurs at an areal coverage of about 15 percent.

2. Saturation occurs when there is more than one stone per footprint area. Above saturation, the probability of launching debris declines.

3. Typical probabilities for lofting 1-inch size objects to heights of several inches are 10 to 20 percent per encounter for unsaturated surfaces.

4. Approximately 90 percent of all lofted stones had speeds of less than 2.5 m/s. None of the stones had speeds greater than one-half the tire speed.

5. The probability per encounter of a high-speed launch (over 4 m/s) is approximately 0.03.

6. Most stones are launched within 40 degrees of the normal to the tire plane. Translated to the tire frame of reference, the launch angles are rearward \pm about 8 degrees.

7. The presence of standing water suppresses lofting of 1-inch stones.

8. Angular stones are at least three times more likely to be lofted than smooth stones.

9. Most stones are launched with forward spins.

10. There was no important synergism between wheels in dual-wheel configurations.

11. For dry conditions, below saturation, and low launch velocities, there was a bias of approximately 2:1 for stones to be thrown to the outside of the curved test track.

12. Large stones are more likely to be lofted than small stones.

13. Launch probability increases with tire speed; $(\Delta N/N)/(\Delta v/v)$ is at least 1.5.

14. Average launch velocity does not increase with tire speed.

15. The highest velocity stones are mainly ejected normal to the tire plane at 30 degrees of elevation, symmetric about the roll direction.

16. Lofting depends little on tire pressure or load.

17. Large marbles are launched at very high speed in the forward direction. This effect depends critically on marble size, however. The launch mechanism is different than for rocks, and synergism between dual wheels is important.

18. Aggregate beds do not erode after 10 passes with a scaled version of an F-4 nosewheel.

19. Soft suspension suppresses lofting of large stones but not small stones.

20. Large marbles are launched by a different mechanism than stones that produces significant forward velocity components.

21. Small debris can be entrained in water splashes. However, principal splash velocities are less than 20 percent of the tire speed.

C. CONCLUSIONS FOR LOFTING MECHANISMS

1. Different mechanisms are responsible for lofting of low velocity ($V < V_{CO}$) and high velocity ($V > V_{CO}$) debris. V_{CO} is about 2.5 m/s.

2. No comprehensive model to account for all features of lofted debris was developed. The models best describe the data for debris launched above V_{CO} . The lofting models predict that size scaling applies, loft directions are not changed by scaling, and that launch velocities are proportional to the tire velocity.

3. The loft mechanism for $V > V_{CO}$ probably involves a hammer-like blow that debris receives from overrolling tires. This results in sideways expulsion of the debris from the tire footprint.

4. The outward-inward bias observed in launches at $V < V_{CO}$ is probably due to scrubbing. On a straight track, launch frequency to either side would probably resemble that characteristic of the outward direction.

D. CONCLUSIONS FOR AIRFIELD OPERATIONS

1. Airfield predictions require extrapolations of present results. The extrapolations are based on physical models for lofting.

2. The probability of a stone being ingested by an engine inlet duct, independent of inlet flow-field effects, is proportional to the product of (a) the probability of a stone being partially rolled over, (b) the probability that a rolled-over stone achieves a critical velocity, and (c) the probability

that a launched stone is within a critical direction cone. Critical velocities and direction cones depend on aircraft speed and geometry.

3. The probability of partially rolling over a stone is proportional to stone diameter and number of stones per unit area.

4. The probability of launching a stone above the critical velocity for an F-4E is less than 10^{-3} for the stones and test parameters investigated in this program.

5. For the F-15, the probability of launching stones above the critical velocity is extremely small.

6. For the F-16, there is no possibility that a ballistically moving stone can enter an inlet duct.

7. For ballistic capture (e.g., ignoring air drag effects due to inlet flow), the probability that an F-4E will ingest a stone launched above the critical velocity is 2 percent, assuming stone launch direction is random.

8. There exists debris (such as large marbles) that can be lofted by different mechanisms than those that loft the stones studied in this effort. Predictions for ingestion of such particles are not possible at this time.

9. Assuming the inlet flow-field effects are negligible, the frequency of inlet ingestion of stones for the F-4E aircraft on a 10-percent cluttered runway is predicted to be 0.165/km. F-15 and F-16 aircraft face no danger. Therefore, FOD suppression mats are not necessary.

10. If inlet flow-field effects are found to be significant, then additional measures should be taken to reduce lofting of debris. Such measures could include: use of small smooth stones for repairs, avoiding high speeds on uncleaned sections of pavement, and use of soft suspensions. Operation on wet or unpaved runways poses no additional FOD hazard. Operation

on runways covered to greater than saturation (about 15 percent) poses no additional hazard.

E. RECOMMENDATIONS

1. Conduct larger scale tests. Instrument to measure particle trajectories. Include all relevant debris types.

2. Determine if particle trajectories may be significantly affected by inlet air flow.

If the results of 1 or 2 indicate that the danger of ingestion is significant, then also do the following.

3. Conduct additional laboratory scale tests to elucidate the mechanisms for high-speed lofting.

4. Determine the relationship between particle size and engine vulnerability.

SECTION IX
REFERENCES

1. S. Bless, H.F. Swift, and R.S. Bertke, FOD Hazard from Operation on Unconventional Runways, UDR-TR-80-124, prepared for BDM Corporation, December 1980.
2. K. Terzaghi and R.B. Peck, Soil Mechanics in Engineering Practice, pp. 440-443, John Wiley & Sons, Inc., New York, 1967.

APPENDIX A

MODELLING SUPPORT FOR THE UDRI/USAF FDL STONE LOFTING PROGRAM

The report contained in this appendix was prepared by H.F. Swift of Physics Applications, Inc., in response to P.O. No. RI-20447 of Contract Number F08635-82-K-0102. This portion was reprinted in their format.

TABLE OF CONTENTS

TABLE OF CONTENTS.....	98
LIST OF SYMBOLS.....	100
LIST OF FIGURES.....	102
LIST OF TABLES.....	103
1. STONE LOFTING REQUIREMENTS TO ACHIEVE INGESTION....	105
1.1 COORDINATE SYSTEM.....	105
1.2 GEOMETRIES OF THE AIRCRAFT UNDER CONSIDERATION	107
1.3 RELATIONSHIPS FOR DEFINING STONE VELOCITIES TO ACHIEVE AIR INLET CAPTURE.....	110
1.3.1 <u>Minimum Vertical Velocity For Capture..</u>	110
1.3.2 <u>Rearward Velocity Requirements for Capture by a Very Slow Moving Aircraft.</u>	111
1.3.3 <u>Stone Capture by Moving Aircraft.....</u>	112
1.3.4 <u>Outward Stone Velocities Needed For Capture.....</u>	113
1.4 STONE LOFTING REQUIREMENTS FOR CAPTURE BY MOVING F-4E and F-15 AIRCRAFT.....	113
2. STONE LOFTING MODELS.....	117
2.1 STONE LAUNCHING PARAMETERS.....	117
2.2 QUALITATIVE MODELS FOR STONE LOFTING BY TIRE OVERROLL.....	118
2.2.1 <u>Mechanisms for Producing Horizontal Stone Motion.....</u>	118
2.2.2 <u>Mechanisms for Producing Vertical Velocity Components.....</u>	120
2.3 QUANTITATIVE STONE LOFTING MODELS.....	122
2.3.1 <u>Tire Tread Motion W.S.T.-Lofted Stones.</u>	122
2.3.2 <u>Stone Loading by Tire Treads.....</u>	124
2.3.3 <u>Horizontal Slide Launching of Stones...</u>	128
2.3.4 <u>Horizontal Spin Launching of Stones....</u>	131

TABLE OF CONTENTS (continued)

2.3.5	<u>Vertical Launching of Sliding Stones</u>	135
2.3.6	<u>Vertical Launching of Spinning Stones</u>	137
2.3.7	<u>Elastic Launch of Stones</u>	138
2.3.8	<u>Discussion of Stone-Lofting Mechanisms</u> ..	142
3.	APPLICATION OF ANALYSIS AND EXPERIMENTAL RESULTS TO ENGINEERING EXPERIMENTS AND AIRCRAFT OPERATIONS.....	147
3.1	LIKELIHOOD OF OPERATIONAL AIRCRAFT INGESTING DANGEROUS STONES.....	147
3.2	EVALUATING PARAMETERS CRITICAL TO STONE INGESTION ANALYSIS.....	151
3.2.1	<u>Percentage Runway Coverage</u>	151
3.2.2	<u>Lofting Probability For Encountered Stones</u>	152
3.2.3	<u>Probability That Dangerous Stones Launched To Dangerous Velocities Are Actually Ingested</u>	154
3.2.4	<u>Numerical Example</u>	156
3.3	SUGGESTED MEANS FOR REDUCING STONE INGESTION PROBABILITIES.....	158
3.4	RECOMMENDATIONS.....	159

LIST OF SYMBOLS

a_o	=	Sound speed
A_{run}	=	Surface area containing stone candidates for launching
A_s	=	Cross sectional area of stone
d_s	=	Stone diameter
d_{sc}	=	Critical stone diameter that transfers all tire load during overroll
d_t	=	Tire tread thickness
E_{el}	=	Elastically stored energy
E_{sr}	=	Rotational kinetic energy of a rotating rock
E_{st}	=	Translational kinetic energy of a stone
F_{acc}	=	Acceleration reaction force produced by a "bounding" wheel
F_l	=	Tire loading force
g	=	Acceleration of gravity: $g = 9.80 \text{ m/s}^2$
I_s	=	Moment of inertia of rotating stone
L_f	=	Tire footprint length
L_s	=	Length of aircraft maneuver along taxiway/runway
M	=	Young's Modulus
M_w	=	Mass of wheel assembly back to the springs
N	=	Number of partially overrolled stones per aircraft maneuver
N_a	=	Number of stones per unit surface area partially overrolled
N_L	=	Number of stones per maneuver launched to dangerous velocities
P_i	=	Tire inflation pressure
P_d	=	Fraction of runway surface covered with stones near size, d_s

- Q_d = Probability of a partially overrolled stone being lofted to dangerous velocity
 R_t = Tire radius
 S_d = Fraction of dangerously launched stones actually inquested
 $U_{y \text{ min}}$ = Min Y component of stone velocity for capture
 U_p = Aircraft forward velocity
 U_{pz} = Local downward velocity of the rotating tire tread
 $U_{x \text{ max}}$ = Maximum horizontal stone velocity
 Note: The message near the base of the vertical line describes the computed situation.
 $U_{x \text{ min}}$ = Min. X component of stone velocity for capture
 $U_{z \text{ min}}$ = Min. vertical stone velocity component for capture
 Y_{i3} = Y coordinate of the #3 corner of the exhaust manifold
 Z = $\Delta d/ds$
 Z_{i3} = Z coordinate of the #3 corner of the exhaust manifold
 Z_t = Tire tread deflection (flattening) produced by loading
 θ_r = Stone trajectory loft angle
 ϕ_{i3} = Declination angle coordinate of #3 coordinate of the air intake
 μ_r = Running friction
 μ_s = Starting friction
 Δd = Height of "bump" on nearly spherical stone
 δ_d = Stone deflection under compressive load
 Δd_s = Height of "bump" on nominally - spherical stone
 ρ_s = Stone material density

LIST OF FIGURES

Figure A1.	Coordinate System Used for the Stone-Lofting Analysis	Page 106
Figure A2.	Relative Positions of the Nosewheel Contact Point and Air Inlets for the F-4E Aircraft .	Page 107
Figure A3.	Polar Plot of Loft and Declination Angles of Air Intakes of the F-4E and F-15 Aircraft with Respect to Nosewheel Contact Point ...	Page 108
Figure A4.	Relative Positions of the Nosewheel Contact Point and Air Inlet Corners of the F-15 Aircraft	Page 109
Figure A5.	Minimum Vertical Velocities for Stone Capture by F-4E Aircraft vs. Roll Speed for Several Declination Angles	Page 115
Figure A6.	Minimum Outward Velocity Components for Stones Captured by F-4E Aircraft vs. Roll Speed for Several Declination Angles	Page 115
Figure A7.	Minimum Vertical Velocities for Stone Capture by F-15 Aircraft vs. Roll Speed for Several Declination Angles	Page 116
Figure A8.	Minimum Outward Velocity Components for Stone Capture by F-15 Aircraft vs. Roll Speed for Several Declination Angles	Page 116
Figure A9.	Downward Component of Tire Tread Velocity vs. G, Ratio of Stone Height to Tire Radius ...	Page 123
Figure A10.	Vertical Stone Load vs. Stone Height for Conditions Typical of UDRI/USAF FDL Test Program	Page 125
Figure A11.	Maximum Lateral Velocity Imparted to Stones Through "Slide-Launching"	Page 130
Figure A12.	Maximum Lateral Velocity Imparted to Stones Through "Spin-Launching"	Page 133
Figure A13.	Vertical Velocity Normalized to Horizontal Velocity vs. "Bump" Height Normalized to Stone Diameters for "Spin-Launching" of Stones	Page 137
Figure A14.	Maximum Vertical Velocity That Can Be Imparted to a Stone Lofted by Stored Elastic Energy .	Page 141
Figure A15.	Elevation Angle, θ_r , and Declination Angle ϕ_r Distribution for Stones Launched to More Than 4.0 m/sec. During UDRI/USAF FDL Test Program	Page 153

LIST OF TABLES

Table A1. Coordinates of Corners of the Air Intake Manifolds of the F-4E and F-15 Aircraft	...	Page 108
Table A2. Hypothetical Stone Distribution Covering 10% of an Airport Operational Surface	...	Page 152

1. STONE LOFTING REQUIREMENTS TO ACHIEVE INGESTION

Section 1 treats the kinematics of the stones launched by aircraft nosewheels encountering them on runways and taxiways. The speeds and launch angles required for stones projected from the nosewheel/runway contact area to be ingested by the engine air intake manifold(s) are determined. Three tactical aircraft are considered, the F-4E, the F-15 and the F-16. Two basic assumptions are made for conducting this part of the analysis: (1) all debris of interest is projected from the nominal contact point at the center of the contact area between the nosewheel and the runway surface; (2) projected stones fly ballistically, i.e., they fly under the sole influence of gravity. We have chosen here to ignore effects both of air drag created by the stones flying through quiescent atmosphere and of trajectory perturbations caused by the stones interacting with intake airflow of operating engines. Stones of sizes interesting to this study (5 mm to 50 mm diameter) are not affected strongly by air resistance while traveling through the very few meters of quiescent air between launch point and air intake. The possibly major effects caused by airflow around the intakes of operating engines may cause significant perturbations to stone flight paths, but evaluation of such perturbations is the subject of another related research effort.

1.1 COORDINATE SYSTEM

We have chosen to fix the origin of the coordinate system used for this study at the nominal contact point between the aircraft nosewheel and the runway surface. Strictly speaking this point is an area of, perhaps, 100 cm^2 . The dimensions of the stones' flight paths are large with respect to the linear dimensions of this area and these dimensions are ignored here. A Cartesian coordinate system has been established with the Y axis along the runway surface and the positive X axis along the runway surface perpendicular to the right (when looking down on the contact point). The positive Z axis points

points vertically upward. Two angles have also been defined for both stone trajectories and for locating critical points on the airframe. The loft angle, θ , is measured upward from the runway surface (X-Y Plane). The declination angle, ϕ , is measured in the horizontal X - Y plane with $\phi = 0$ corresponding to the positive Y axis, $\phi = 90^\circ$ corresponding to the positive X axis, $\phi = 180^\circ$ along the negative Y axis, and $\phi = 270^\circ$ along the negative X axis. A diagram showing the coordinate system is presented in Figure A1.

Subscripts attached to variables are used to denote the item specified. The subscript "r" refers to lofted stones (or rocks), and "i" refers to the coordinates of the air intake manifolds.

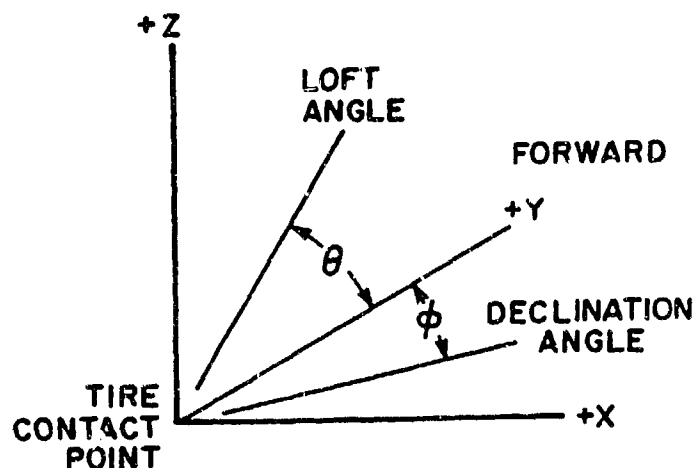


Figure A1. Coordinate System Used for the Stone-Lofting Analysis.

1.2 GEOMETRIES OF THE AIRCRAFT UNDER CONSIDERATION

The F-4E aircraft employs a dual nosewheel-mounted well forward along the fuselage. Two air intakes are mounted on either side of the fuselage some distance behind the nosewheel assembly. The intakes follow the contour of the fuselage and extend over about two thirds of its vertical projection. The intake manifold entrance is canted approximately 16.5° forward of vertical. The aspect ratio (vertical to horizontal dimension) for each air inlet is somewhat greater than 3 to 1. A dimensioned sketch showing the relative positions of the inlet and the nosewheel/runway contact point is presented in Figure A2. The approximate positions of the four corners of the inlet are presented in Table A1 with the dimensional system described in Paragraph 1.1. A rather interesting polar plot of loft angle versus declination angle for the air inlets as viewed from the nosewheel/runway contact point, is presented in Figure A3.

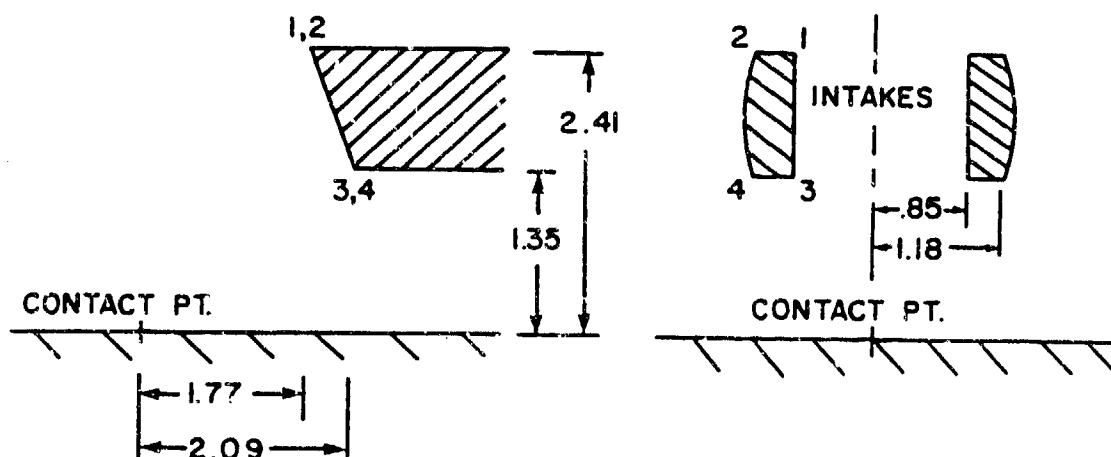


Figure A2. Relative Positions of the Nosewheel Contact Point and Air Intakes for the F-4E Aircraft.

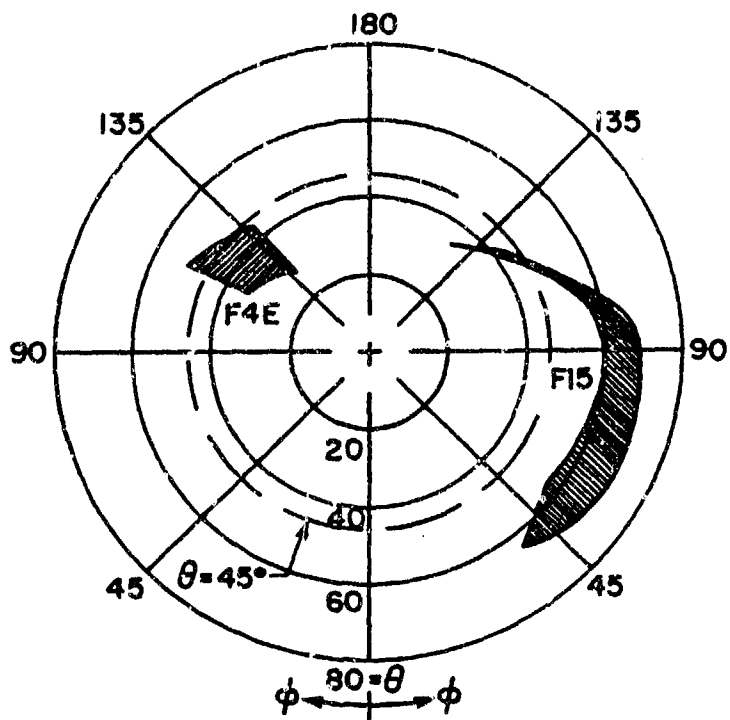


Figure A3. Polar Plot of Loft and Declination Angles of Air Intakes of the F-4E and F-15 Aircraft With Respect to Nosewheel Contact Point.

TABLE A1. Coordinates of Corners of the Air Intake Manifolds of the F-4E and F-15 Aircraft.

COORDINATES	F-4				F-15			
	1	2	3	4	1	2	3	4
X_i (m)	+0.85	+1.18	+0.85	+1.18	+0.79	+1.42	+0.79	+1.42
Y_i (m)	-1.77	-2.09	-2.09	-1.77	+1.02	+1.02	-1.02	-1.02
z_i (m)	+2.41	+2.41	+1.35	+1.35	+2.67	+2.67	+1.73	+1.73
θ_i	50.82°	45.11°	30.5°	32.4°	64.21°	55.78°	53.2°	44.69°
ϕ_i	115.65°	138.0°	157.9°	146.3°	37.80°	54.31°	127.8°	144.3°

The F-15 aircraft has a pair of steeply canted (tipped 65° forward), nearly rectangular air inlet ducts mounted directly over a single nosewheel so that the upper edge of the inlet duct extends nearly as far in front of the nosewheel as the lower edge extends behind it. A dimensioned sketch showing the position of these ducts in relation to the contact point is presented in Figure A4. The coordinates of the duct corners are presented in Table A1, and the polar plot of loft angle versus declination angle for the ducts is presented in Figure A3.

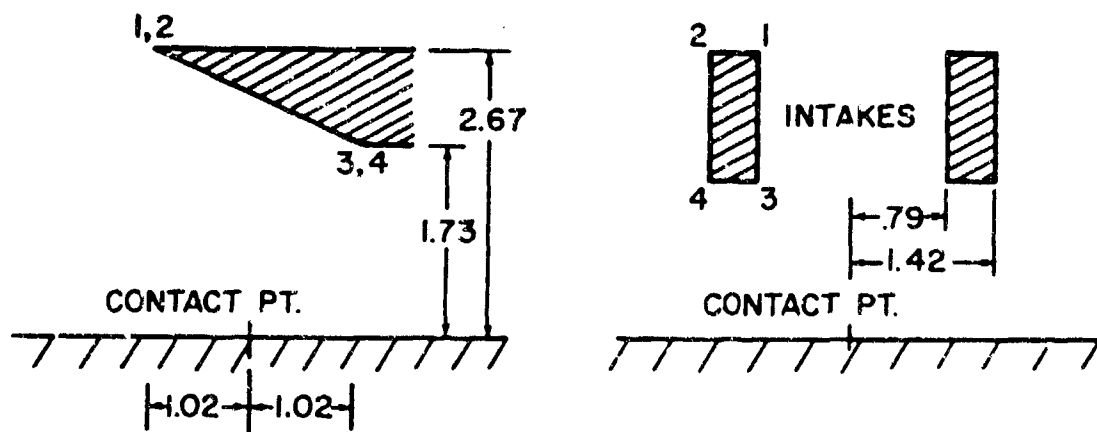


Figure A4. Relative Positions of the Nosewheel Contact Point and Air Inlet Corners of the F-15 Aircraft.

The F-16 aircraft has a centrally located air intake manifold under the fuselage well ahead of the nosewheel. We understand that considerable problems have been experienced by this aircraft "vacuuming up" finely divided debris from runways. The duct is shielded entirely from the nosewheel so that no stone meeting the analysis criterion may enter it. We have, therefore, eliminated the F-16 from further considerations in this analysis.

1.3 RELATIONSHIPS FOR DEFINING STONE VELOCITIES TO ACHIEVE AIR INLET CAPTURE

The first step in our analysis is to evaluate the minimum vertical velocity component a launched stone must achieve if it is to reach the bottom of the air intake manifold. We may then evaluate the rearward velocity component (negative U_y) relative to the airframe which is needed to propel the rock rearward far enough to reach the intake manifold during the time needed for it to climb to maximum height. We then generalize the analysis by considering forward velocity of the aircraft and develop a relationship for the minimum vertical velocity component, U_{zmin} , to allow capture of a lofted stone. Finally, we consider the stone's velocity component in the + X direction needed to propel it far enough from the centerline of the aircraft to allow capture by the time it is overrun by the entrance of the air intake.

1.3.1 Minimum Vertical Velocity For Capture

The minimum vertical velocity component required to loft a stone high enough to reach the bottom lip of the air intake manifold, U_{zmin} , is evaluated by the very simple expression presented as:

$$U_{zmin} = \sqrt{2g Z_{i3}} \quad (A1)$$

where the acceleration of gravity, $g = 9.80$ m/sec and Z_{i3min} is height of the lower lip of the air intake manifold. The F-4E aircraft has a minimum lip height of the air intake manifold of 1.35m as presented in Table A1 which infers a value for $U_{zmin} = 5.14$ m/sec. The F15 aircraft has a slightly higher lip height for the intake manifold of 1.73 meters which yields a value for the U_{zmin} of 5.82m/sec.

We can, for the purposes of this analysis, eliminate consideration of all stones launched during the UDRI/AF FDL test program with velocities below 3.75 to 4m/sec because they cannot rise high enough to be captured even after allowances are made through replica scaling for increases in loft velocities caused by changes in operational parameters.

1.3.2 Rearward Velocity Requirements for Capture by a Very Slow Moving Aircraft

The time required for the stone evaluated in Paragraph 1.3.1 to reach its maximum height has been evaluated and equated to the time available for the stone to move rearward from the nosewheel/surface contact point to the lower lip of the air intake manifold. The resulting equation is solved for the maximum stone velocity component in the negative Y direction for capture U_{ymin} , in Equation A2.

$$U_{ymin} = Y_{i3} \sqrt{\frac{g}{2Z_{i3}}} \quad (A2)$$

where Y_{i3} is the Y coordinate of the #3 corner of the intake manifold (as shown in Figures A1 and A3) and Z_{i3} is Z component of this corner. The value for the F-4E aircraft is $U_{y\max} = -3.98\text{m/sec}$, and for the F-15 aircraft, $U_{y\max} = -1.72\text{m/sec}$.

1.3.3 Stone Capture by Moving Aircraft

By far the most interesting capture situations occur when the aircraft is moving forward at finite speeds (up to takeoff speed). Under these circumstances the time available for a stone to rise from the runway level to the bottom of the air intake manifold is limited by the time required for the lower lip of the manifold to pass over the stone launch point. This time is, simply, the forward velocity of the aircraft, V_p divided by Y_{i3} if the stone is launched perpendicular to the plane of the nosewheel (along the positive or negative X-axis) and, therefore, has no velocity component in the direction of aircraft motion. The more general situation occurs when a stone has both a Y and a Z velocity component, U_y and U_z . U_y is added algebraically to the aircraft velocity to determine the intake manifold overrun time. Finally U_y may be expressed in terms of U_z and U_x through the lofting angle of the stone θ_r . The relationship resulting from this derivation cannot be solved in closed form for the vertical component of stone velocity, $U_{z\min}$ in terms of the aircraft velocity and geometric factors. The expression has been solved for the aircraft's velocity U_p , however, and the result is presented as Equation A3.

$$U_p = \frac{gY_{i3}}{U_{z\min} - \sqrt{U_{z\min}^2 - 2gZ_{i3}}} + \frac{U_{z\min}}{\tan\theta_r \sqrt{1 + \tan^2\phi_r}} \quad (\text{A3})$$

A simple logic program can be used to extract values of U_{zmin} from Equation A3 for preselected values of U_p ... or the equation can be plotted and individual data extracted graphically.

1.3.4 Outward Stone Velocities Needed For Capture

The time for the lower lip of the air intake assembly to overrun the launch point is available for a launched stone to move outward (along the + X-axis) from near the centerline of the aircraft to the inward edge of the manifold if capture is to occur. In this case the expression for the minimum outward velocity component U_{xmin} can be expressed in closed form. An expression for the velocity required to achieve this capture, U_{xmin} , is presented in terms of the aircraft velocity, the vertical stone projection velocity, the stone loft angle, and the aircraft geometry in Equation A4.

$$U_{xmin} = - \tan \phi_{i3} (U_p + U_y) \quad (A4)$$

Equations A3 and A4 taken together effectively express the minimum stone projection conditions for capture by a moving aircraft in terms of the aircraft velocity and its geometry. Remember that the constraints upon stone movement are solely that the stones obey simple ballistic relationships.

1.4 STONE LOFTING REQUIREMENTS FOR CAPTURE BY MOVING F-4E AND F-15 AIRCRAFT

Equations A3 and A4 have been evaluated for the F-4E and F-15 aircraft moving at speeds between 0 and 68m/sec (0 to 120 knots). The graphs show results as continuous functions of U_p . Lofting angle of the stone trajectories of $\theta_r = 60^\circ, 90^\circ$ are considered. Plots

of the resultant data are presented in Figures A5 and A6 for the F-4E aircraft and A7 and A8 for the F-15.

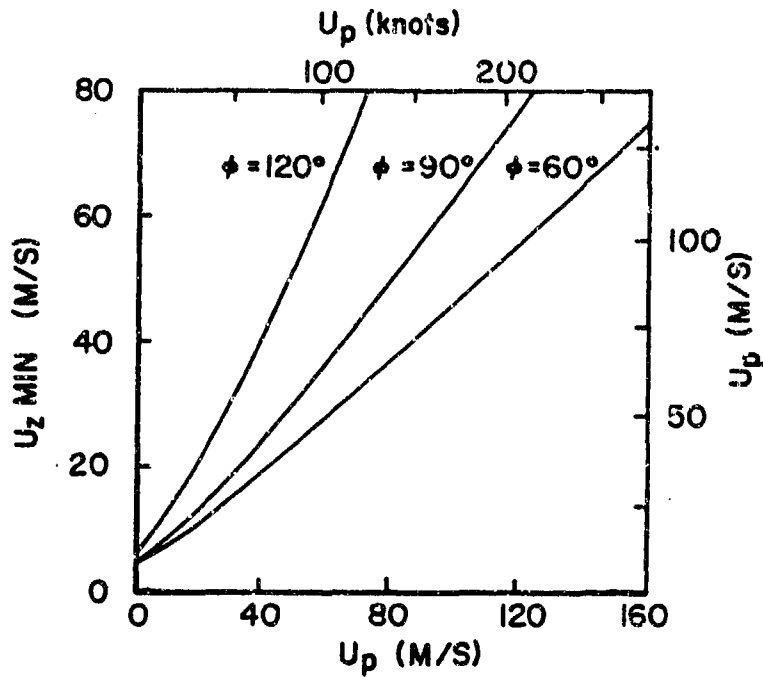


Figure A5. Minimum Vertical Velocities for Stone Capture by F-4E Aircraft vs. Roll Speed for Several Loft Angles.

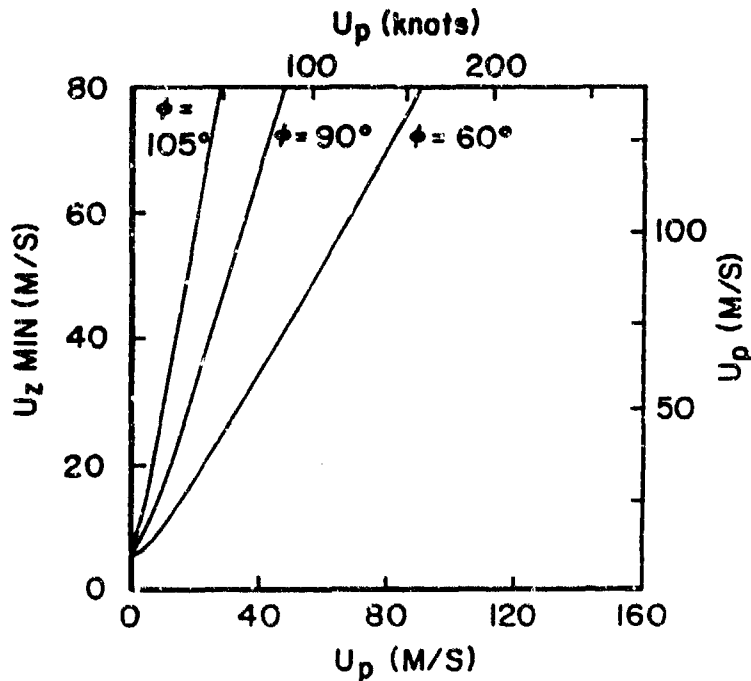


Figure A6. Minimum Outward Velocity Components for Stones Captured by F-4E Aircraft vs. Roll Speed for Several Declination Angles.

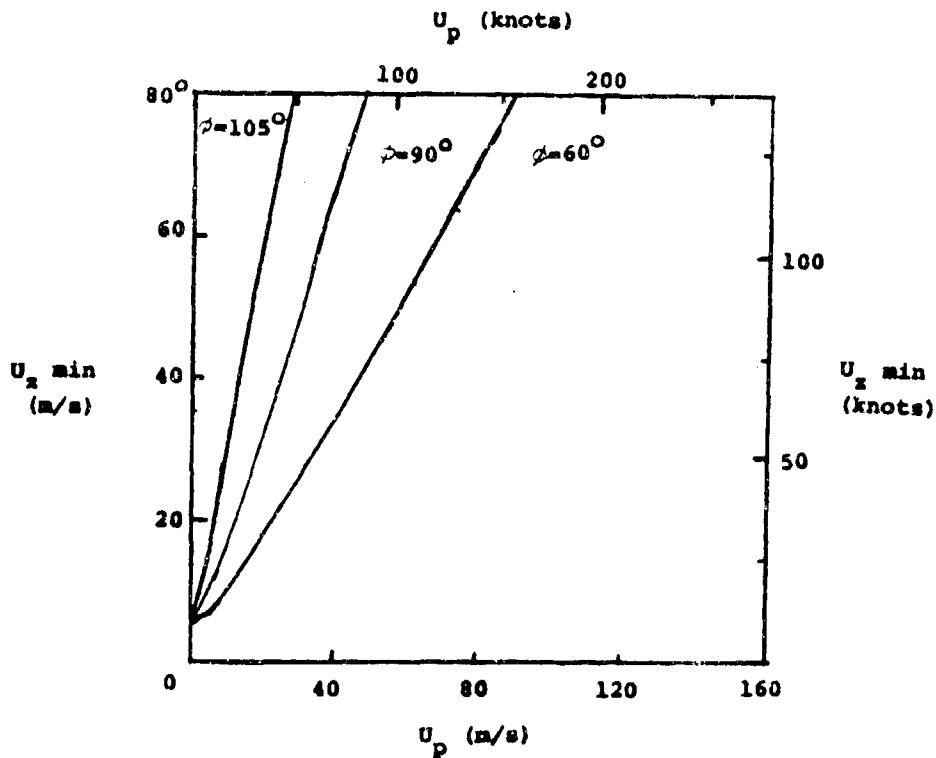


Figure A7. Minimum Vertical Velocities for Stone Capture by F-15 Aircraft vs. Roll Speed for Several Loft Angles.

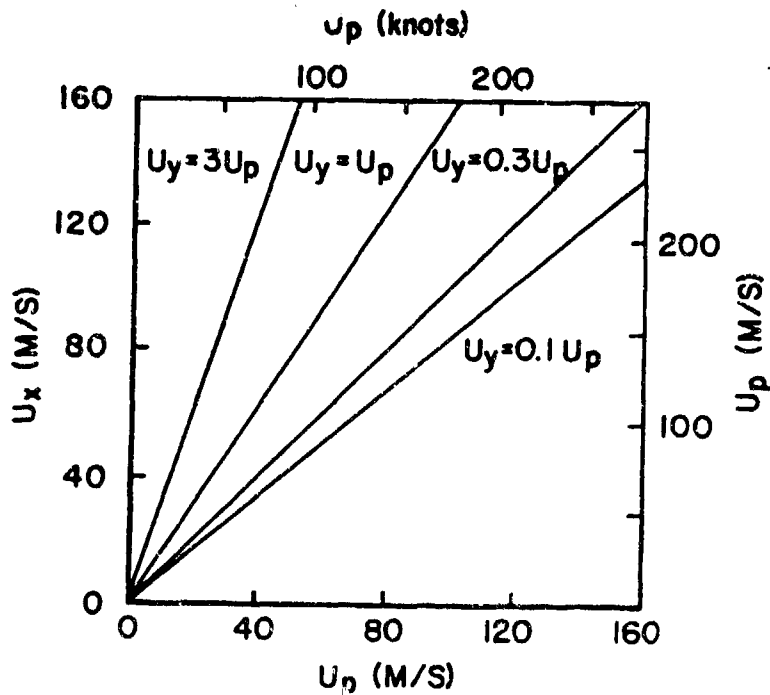


Figure A8. Minimum Outward Velocity Components for Stone Capture by F-15 Aircraft vs. Roll Speed for Several Declination Angles.

2. STONE-LOFTING MODELS

Section 2 presents qualitative and quantitative models of candidate stone-lofting phenomena produced by the nosewheels of an overrolling aircraft. Since the sizes and especially the shapes of stones vary widely from individual to individual, both during engineering simulations and actual aircraft operations, no specific model can be developed which has universal applicability. We chose, therefore, to seek the principles underlying stone lofting by overrolling tires and to apply these models statistically to both results from engineering experiments and experience from actual flight operations.

2.1 STONE-LAUNCHING PARAMETERS

The test sequence conducted jointly by the University of Dayton and the USAF FDL at the Mobility Laboratory, produced a mass of stone-lofting data under accurately controlled laboratory conditions. The majority of stones lofted attained vertical velocity components, U_z , far below those necessary to achieve ballistic capture by the air inlet ports of F-4E, and F-15 engines. A relatively small population (of some 28 stones) achieved launch velocities in excess of 4m/sec. While 4m/sec is significantly below the capture velocity criterion for the aircraft considered, it is close enough to extrapolate to adequate velocities when actual overroll conditions are extrapolated to true flight conditions.

Thus, these experiments indicate that only an extremely small proportion of the stones encountered by simulations of overrolling nosewheels were launched with dangerous velocities. The question is still open at this point as to whether or not this result is some subtle artifact of the UDRI/USAF FDL test program or reflects engineering reality.

2.2 QUALITATIVE MODELS FOR STONE LOFTING BY TIRE OVERROLL

2.2.1 Mechanisms for Producing Horizontal Stone Motion

Two distinct mechanisms have been identified for producing stone velocity components parallel to the runway surface (U_x and U_y) by tire overroll. In the simplest case, an oncoming tire pushes a stone aside and/or in the direction of tire motion. Push-aside launching occurs when a stone is not overrolled by the tire but is simply pushed aside. The propensity for tires to push aside stones rather than overroll them is governed by a number of factors involving ease with which the stone may move across the runway surface, rigidity of the tire tread and the relative height of the stone surface engaged by the tread with respect to the tire radius (which controls push-aside vs. overroll). This last parameter indicates that no stones of interest to this study will be pushed aside with very high velocities (since the stones of interest have characteristic sizes small respect tire radius).

The second mechanism involves a stone being partially overrolled by the aircraft tire when its center-of-mass (c.g.) is close to but not quite under the edge of the tire footprint. The tire tread is deformed during such an encounter and lateral stone motion is produced as the stone "squirts" out from under the tire with a direction more or less perpendicular to the direction of tire motion.

The "squirting" process occurs when the outward-directed force on the top of the stone exceeds the friction forces produced between the stone and the runway and tire tread surfaces. Two types of stone propulsion may be visualized. In the first case, the stone slides both against the runway surface and the tire surface and is launched with a sideward velocity component, U_x , without undergoing rotation. The second mechanism occurs when the stone being launched slides along the runway but rolls along the tire tread surface. Under these conditions, the stone is both launched sideways in the X direction and rotated with its rotational axis aligned roughly with the

aircraft velocity vector. The rotational direction produces a velocity component on the stone surface in contact with the runway in the opposite direction to that of the stone travel (i.e., a stone launched in the positive X direction will turn counter-clockwise when viewed along the aircraft velocity axis and its surface velocity along the runway is well above its projection velocity, U_x).

The simple sliding launch mechanism is the only one available to stones whose shape deviates significantly from spherical (or cylindrical with the axis oriented along the aircraft velocity vector). Stones with large aspect ratios cannot rotate effectively through the large angles required for spin launches while being forced against the runway surface.

The kinetic energy associated with both of these "squirting" launch mechanisms is derived from tire tread deflection. We may conclude from this observation that stones may only be launched to high velocities via "squirting" when the tire tread stores significant energy by deflection prior to stone launch. Since the launch process must, of necessity, take up far less time than the stone overroll process if high velocities are to be achieved, the relative position between the stone and the edge of the tire tread must be a very critical parameter for the launch process. If the relative position between the tread edge and the stone deviates slightly from this critical value in one direction, the tire simply will overroll the stone without producing any significant stone movement. If the stone/tire edge position deviates in the other direction, the squirting process will begin almost immediately upon stone contact with the tire tread. Little energy will be stored in the tire tread, and the stone will be propelled sideward at a low velocity. This situation approaches in the limit the simple push-aside case. Thus, the width of the zone which produces high "squirting" efficiency is expected to be much narrower than the width of the stone itself. The area produced by considering the stone dimension along the aircraft velocity vector times the critical width becomes the equivalent stone area to be considered statistically when

establishing whether a stone located at random on a runway or a taxiway will be launched by tire encounter via "squirting."

2.2.2 Mechanisms for Producing Vertical Velocity Components

The majority of the mechanisms proposed originally as candidates for lofting stones above the runway surface during encounters with aircraft tires were not detected during the UDRI/USAF FDL testing program. These undetected mechanisms included tire surface envelopment, gripping with tire tread grooves, etc. The only mechanisms observed with substantial vertical velocity components involved stones being launched laterally from the edges of tire treads. A search was initiated to discover mechanisms for producing these vertical velocity components. This search revealed two mechanisms where vertical velocity components are produced via indirect tire tread/stone interactions. Part of the horizontal velocity components produced by "squirting" are transferred into rotational kinetic energy and thence into vertical velocity. A third potential lofting mechanism involves elastic rebound of stones after they have undergone compressive loading.

The simplest mechanism is a direct consequence of a spin launch when stones projected from the edge of tire treads are propelled sideward with counter-rotational surface velocities approaching their linear velocities. If such a stone possesses a projection from the surface, "a bump," which encounters the runway surface during rotation, the c.g. of the stone must be elevated to allow the bump to pass under the stone. Rapid elevation of the c.g. introduces a vertical velocity to the stone which is retained after the bump passes under it thus producing a vertical velocity component. This mechanism can be operative only with stones with roughly spherical or cylindrical shapes which meet the spin launch criterion discussed in Paragraph 2.2.1.

A similar phenomenon can produce vertical motion for slide-launched stones. Here a stone sliding across the runway surface encounters a relatively tiny imperfection in the surface which causes the lower leading edge to "dig in." The stone is then obliged to pivot around its lower leading edge. Deviation of the stone from spherical (or cylindrical) symmetry requires elevation of its c.g. to accommodate the rotation thus imparting a vertical velocity component to the stone.

Both of these mechanisms are relatively unlikely to occur at least to the point where significant fractions of the horizontal velocity are converted to vertical velocity (to produce significant loft angles, θ_r). Thus, we have a situation where stones must be launched to high velocities in the plane of the runway via mechanisms that have inherently low probabilities for occurrence, and vertical velocities are imparted to these stones via other mechanisms which are also relatively improbable. The result is that the probability for lofting stones with high vertical velocity components may be expected to have inherently low probability for occurrence. This tentative conclusion is supported by the results from the UDRI/USAF FDL test program.

A third potential mechanism identified for lofting stones involves the stone being compressed elastically by the tire load and then releasing this elastic energy as it rebounds from the runway surface. The kinetic energy for the stone's launch is limited in this case to the potential elastic energy stored within the stone by the loading procedure. An additional limitation placed upon this launch mechanism involves release of stone loading as the stone passes under the tire tread. This release must be fast enough for the stone to couple its elastic potential energy into upward-directed kinetic energy rather than simply "giving back" the elastic energy to the tire tread. In addition, the tire tread must recede away from above the stone at a speed which allows the stone to move upward without impacting the tire and being deflected by it. One interesting possibility to be explored is that of a heavily loaded

stone being "squirted" sideways from under an overrolling tire at high speed so that it clears the tread during a short time with respect to the period required to produce elastic lofting.

2.3 QUANTITATIVE STONE LOFTING MODELS

The procedure we followed to evaluate the lofting models described quantitatively in Paragraph 2.2 involved calculating some basic parameters of tire/stone interaction processes and then developing mathematically tractable models for each of the lofting processes. These models were exercised using parameters from the UDRI/USAF FDL test program to determine model viability and provide inputs for the analysis in Section 3 where predictions are made concerning results of subsequent testing programs and actual flight operations.

2.3.1 Tire Tread Motion W.R.T. Lofted Stones

We start the analysis by calculating the local downward velocity of the tire tread as it encounters a stone lying on a surface. The expression may be derived using simple geometry as presented in Figure A9. The equation for the downward velocity of the tire, U_{pz} , normalized to the aircraft velocity, U_p , in terms of a parameter, G , which is the ratio of the stone diameter to the tire radius is presented in Equation A5 and is plotted in Figure A9.

$$\frac{U_{pz}}{U_p} = \sqrt{2G - G^2} ; G = d_s / R_t \quad (A5)$$

Note that Equation A5 assumes that the undeformed tire rides tangent to the runaway surface, i.e., has zero-load deformation. Tread deformation from a finite load may be modeled as a simple extension of the stone's height if we assume that the tire tread not

in contact with the runway is not distorted. The analysis becomes slightly more complex if we account for the finite deflection of the tire surface caused by tire loading. This deflection may be expressed in terms of the easily measured footprint length of the tire using Equation A5A.

$$Z_t = R_t - \sqrt{R_t^2 - L_f^2/4} \quad (A5A)$$

If the assumption is made that the tire surface clear of the runway is undistorted by runway contact, the tire deflection, (Z_t from Equation A5A) may be simply added to the height of the stone when calculating the parameter G , for use in Equation A5. Thus, the two Equations, A5 and A5A, provide a simple, complete, and relatively accurate computation for the downward-directed velocity of a tire tread as it contacts a surface stone as a function of stone height, tire geometry, and aircraft forward velocity.

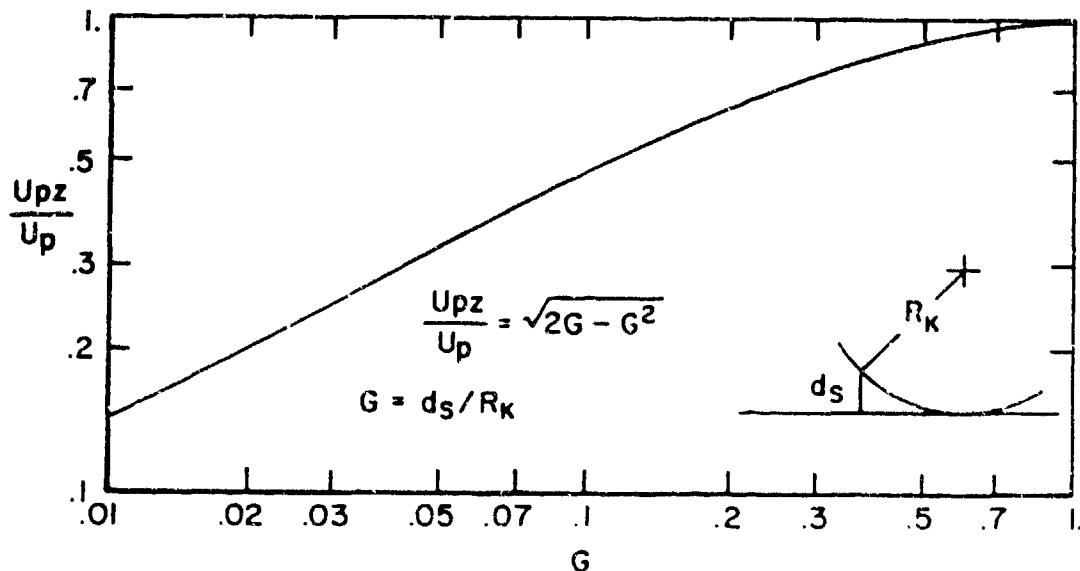


Figure A9. Downward Component of Tire Tread Velocity vs. G , Ratio of Stone Height to Tire Radius.

2.3.2 Stone Loading by Tire Treads

A fully loaded tire supports its load by exerting its inflation pressure over its footprint area. When the tire contains a separate tread, as is the case for the aircraft nosewheels under consideration, the footprint is essentially a rectangle whose area times the inflation pressure equals the tire load. When the tire overrolls a stone on a runway, the tread immediately above the stone is lifted off of the runway surface. Sample measurements made during the UDRI/USAF FDL tests indicate that an area surrounding the stone with a radius of two stone diameters is lifted free of the surface. The stone must bear the load normally supported by this lifted surface. In addition, the local pressure exerted by the tire tread at the periphery of the lift zone is near zero. This pressure builds monotonically to that of the undisturbed tread (the inflation pressure as one moves outward away from the stones center a distance equal to approximately one tread thickness). Data concerning the rate at which this pressure buildup increases as one proceeds away from the edge of the tread lift are not available so we have chosen to assume linearity. The overall analysis is not particularly sensitive to this pressure buildup around tread lift assumption which is probably at least approximately correct. We anticipate no serious difficulty with the model predictions arising from the assumption of linear pressure increase. The stone must also bear the load reduction caused by this pressure reduction, of course.

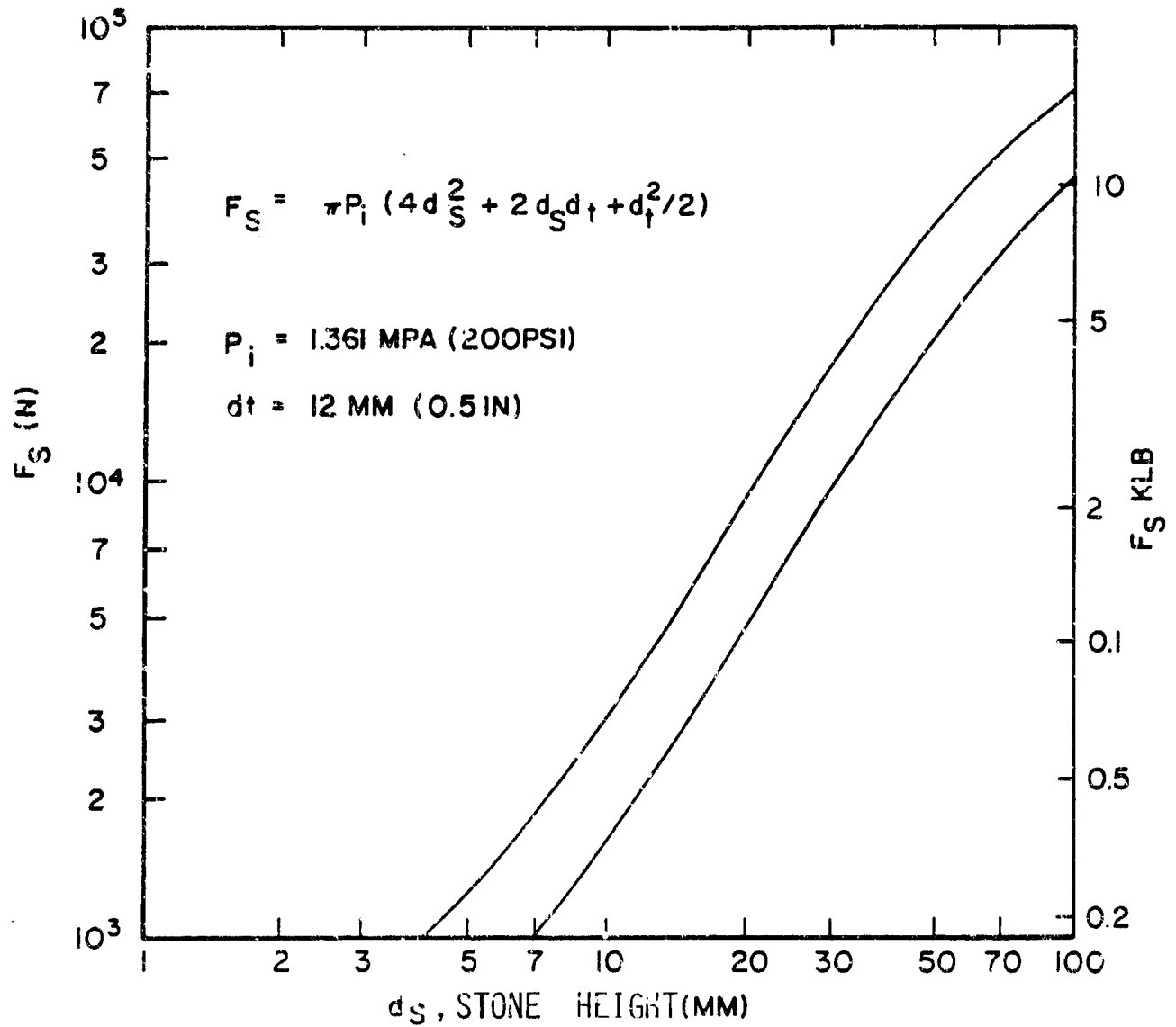


Figure A10. Vertical Stone Load vs. Stone Height for Conditions Typical of UDRI/USAF FDI Test Program.

We may now develop an expression for load placed upon a stone, F_c , in terms of the stone diameter, d_s , the tread thickness, d_t , and the inflation pressure, P_i , as is presented in Equation A6. Note that the interesting case where the edge of the tire rolls over a stone produces a loading of just half the load calculated by Equation A6 since only a semi-circle of the tire tread is displaced. A plot of F_e versus d_s for parameters typical of the UDRI/USAF FDL test program is presented in Figure A10.

$$F_s = \pi P_i (4d_s^2 + 2d_s d_t + d_t^2/2) \quad (A6)$$

The model is produced under the assumption that the load on the tire is sufficient to hold at least part of the tire on the runway surface when stone overroll occurs. Should the upward-directed force exceed tire loading, the tire might be expected to clear the runway surface thereby transferring its load to the stone over which it is rolling. Conversely, the load applied to the stone is limited to the tire load once the stone size has reached the critical value where tire liftoff is predicted.

This situation is only true, strictly, when the aircraft speed is very near zero. Tire liftoff produces a vertical acceleration of the unsprung mass (the mass of the tire, wheel assembly, etc., up to the springs). Upward acceleration of this mass produces an additional load which must be borne by the stone. This load may be evaluated by computing the critical stone size, d_{sc} , which just produces tire liftoff in terms of the applied tire load, F_l , the tread thickness, d_t , and the inflation pressure, P_i , using Equation A7.

$$d_{sc} = \frac{3}{2} \sqrt{\frac{F_1}{4\pi P_i} - \frac{d_t}{4}} \quad (A7)$$

This critical height, d_{sc} , is subtracted from the height of the actual stone, d_s , to determine the height through which the unsprung tire assembly will be lifted. This height, $d_s - d_{sc}$, is used to establish the peak acceleration transmitted to the unsprung mass associated with the wheel. This peak acceleration is used with the unsprung mass associated with the wheel to determine the force produced by the upward acceleration of the wheel assembly, F_{acc} . A basic expression for F_{acc} is presented in Equation A8.

$$F_{acc} = \frac{2M_w U_p^2}{\sqrt{(d_s - d_{sc})(2R_t - d_s + d_{sc})}} \quad (A8)$$

It is important to remember that the upward acceleration force described in Equation A8 is produced only when a wheel encounters a stone whose height exceeds the critical height, d_{sc} , which is sufficient to lift the tire assembly off the runway under static conditions.

Let us evaluate the critical stone size for a typical experimental situation from the UDRI/USAF FDL test program. The critical parameters are as follows:

$$\begin{aligned} F_1 &= 4,440 \text{ N} \quad (1000 \text{ lbs.}) \\ P_i &= 1.361 \text{ Mpa} \quad (200 \text{ psi}) \\ d_t &= 0.012 \text{ m.} \quad (0.5 \text{ inches}) \\ d_{sc} &= 14.95 \text{ mm} \quad (0.588 \text{ inches}) \\ M_w &= 454. \text{ Kg} \quad (31.25 \text{ slugs}) \end{aligned}$$

$$\begin{aligned}
 U_p &= 17.88 \text{ m/sec. (58.7 ft/sec)} \\
 d_s &= 0.0254 \text{ m (1 inch)} \\
 R_t &= 0.127 \text{ m (0.5 inches)} \\
 F_{acc} &= 6.01 \times 10^5 \text{ M (135,000 lbs.)}
 \end{aligned}$$

The value for the force, F_{acc} , predicted by Equation A8 is clearly unrealistic. This result demonstrates that the dynamic tire-loading process is considerably more complicated than the analysis shows. In actuality, a stone of larger height than the critical height, d_{gc} , is loaded according to Equation A6 even though the total load exceeds the dead-weight load on the wheel by a large margin.

2.3.3 Horizontal Slide Launching of Stones

Lateral slide launching of stones is a complex process involving the tire tread being deflected as the stone to be launched is overrolled. The c.g. of the stone must, of course, lie almost directly under the edge of the tire so that it may escape by moving sideways. High stone velocities can only be achieved when this motion is delayed until the tire deflection is near maximum and the axis of the wheel is almost directly above the stone. The stone then starts accelerating sideways as the tire tread deflection is relieved. The energy absorbed by the stone launch process may approach closely the work done by the tire tread as it relaxes, since the tire tread need not achieve a significant velocity during the launch process. The energy associated with the stone launch consists of the kinetic energy imparted to the stone plus the work done overcoming friction as the stone slides along the runway and the tire tread surface. Division of the available energy between frictional work and stone kinetic energy is a crucial factor in determining whether the slide launch mechanism is capable of producing substantial stone velocities.

Let us consider first the total energy available to determine whether it is sufficient to produce dangerous stone velocities and then consider what fraction of this energy may actually be transferred to kinetic energy of the launched stone. Equation A6 describes the vertical force on a stone deep under the tire tread in terms of tire/wheel parameters and stone height, d_s . As stated earlier, half this vertical force is exerted upon a stone under the edge of the tire tread (which is a requirement for slide launching). Integration of Equation A6 over vertical deflection from zero to the stone height under consideration yields a measure of the work done by the tire tread as it relaxes during stone acceleration. This work, E_{st} , approximates the total energy available for the acceleration process. An expression for E_{st} is presented as Equation A9.

$$E_{st} = \pi P_i (4d_s^3 + d_s^2 d_t + d_s d_t^2 / 2) \quad (A9)$$

Equating E_{st} to the kinetic energy of the stone, yields a measure of the maximum possible velocity to which a stone may be launched, U_{smax} , which is presented in Equation A10 and is plotted in Figure A11 for typical values of relevant parameters from the UDRI/USAF FDL test program.

$$U_{xmax} = \sqrt{\frac{12 P_i}{\rho_s} (4/3 + d_t/d_s + d_t^2/2d_s^2)} \quad (A10)$$

The plot in Figure A11 indicates strongly that sufficient kinetic energy is available to produce velocities far in excess of those observed during the UDRI/USAF FDL test program.

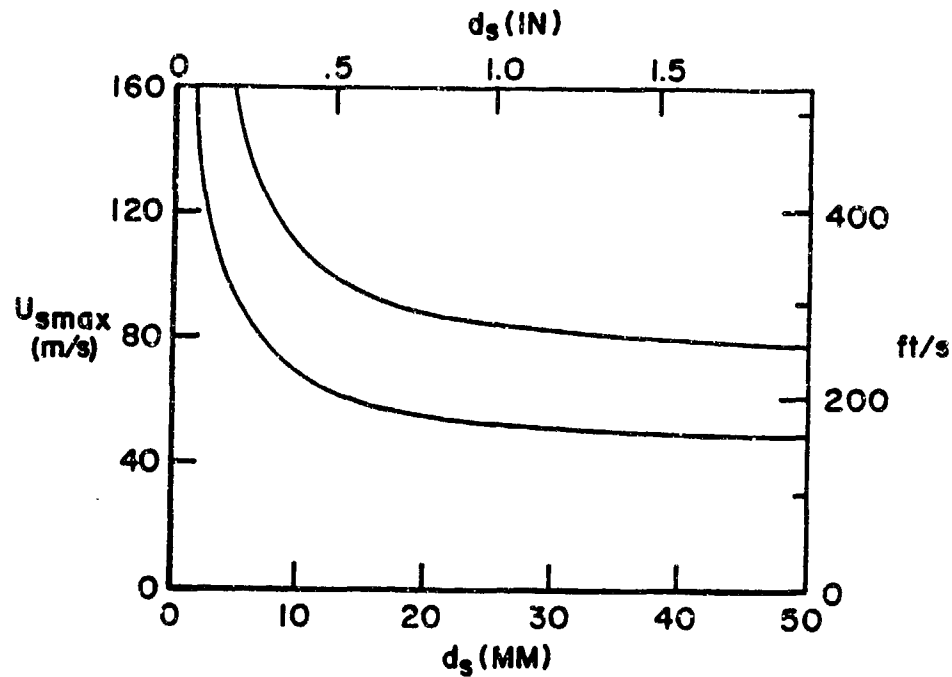


Figure All. Maximum Lateral Velocity Imparted to Stones Through "Slide-Launching"

One reason for this disparity becomes apparent when one considers the frictional problem carefully. High velocities are achieved only when the wheel axle has a chance to move almost directly above the stone before stone launch occurs. The mechanism which prevents the stone from moving earlier is that the frictional forces holding the stone in position exceed the forces attempting to accelerate it sideways until some critical parameter is exceeded. Since this critical parameter must have a near maximum value when the wheel axle is directly overhead, the starting friction associated with stone movement (the sum of the frictional forces between the stone/runway and the stone/tire tread interfaces), must balance the acceleration force. Should this situation be maintained as the stone moves, all of the energy associated with the launch process would go into work done against friction and the stone would be left with

negligible kinetic energy. The kinetic energy transferred to the stone occurs because of the disparity between starting friction and sliding friction. The sliding friction forces are always lower than the starting friction forces and the reduction of energy required by them is available for stone acceleration. The relationships between sliding and starting friction varies strongly with the nature of the interacting surfaces but it is generally bounded by a ratio of sliding to starting friction of .5 to .75. One minus this ratio is the fraction of kinetic energy evaluated in Equation A9 which is available for projectile launch. Equation A11 is, simply, Equation A10 with the starting versus sliding friction parameter added to produce a realistic value for peak stone launch velocity, U_x . This curve is also plotted in Figure A11.

$$U_s = \sqrt{\frac{12 P_i (1 - \mu_r / \mu_s)}{\rho_s} (4/3 + d_t / d_s + d_t^2 / 2 d_f^2)} \quad (\text{A11})$$

The velocities estimated as realistic upper limits, U_s , are still well in excess of the vast majority of those actually observed which indicates strongly that an absolutely ideal launch of a stone via the sliding process is a very unusual occurrence. More typically, stones are launched somewhat prematurely or postmaturely, i.e., when the axle is not directly overhead and considerably less than optimum energy is stored in tread deflection.

2.3.4 Horizontal Spin Launching of Stones

Spin launching of stones occurs through a mechanism notably similar to slide launching described in Paragraph 2.3.3. In the case of spin launching, a stone under the edge of an oncoming tire is propelled sideward while it slides with respect to the runway surface but rolls with respect to the tire tread surface. Thus, the stone is propelled sideways and simultaneously given an intense back spin.

The ratio of rotational surface velocity to sideward velocity may vary over reasonably narrow limits depending upon stone shape and the peak speed achievable by the tire tread rubber during relaxation. These parameters combine to determine the stone position when contact between the tread and the stone is lost. We may assume that, on the average, the surface tangential velocity associated with stone rotation equals the outward-directed velocity of the stone. The energy available for stone launching is just that calculated using Equation A9 (the same as is available for slide launching). The maximum energy available for launching must be divided between the energy of translation and the energy of rotation.

If we assume that the relatively round stone required for spin launching is spherical with homogeneous material density, its moment of inertia, I_s , may be calculated using Equation A12.

$$I_s = \frac{\pi \rho_s d_s^3}{60} \quad (\text{A12})$$

Combining Equation A12 with the basic formula for evaluating rotational kinetic energy and applying the assumption that the surface tangential velocity of the launch stone equals its translational velocity yields an expression for the kinetic energy associated with rotation E_{sr} presented in Equation A13.

$$E_{sr} = \frac{\pi \rho_s U_s^2 d_s^3}{30} \quad (\text{A13})$$

The energy associated with translational motion of a spherical homogeneous stone, E_{st} , is evaluated in Equation A14.

$$E_{st} = \frac{\pi \rho_s U_s^2 d_s^3}{12} \quad (A14)$$

The ratio of the two energies for a spin-launched spherical stone is $(E_{st}/E_{sr}) = 30/12 = 2.5$. Thus, 60% of kinetic energy associated with a spin-launched stone may be expected to appear as kinetic energy and the remaining 40% should appear as rotational energy. The expression for the maximum possible translational velocity for a spin launch stone U_{smax} , thus, becomes a simple modification of Equation A10 which is presented as Equation A15.

$$U_{smax} = \left[\frac{7.2 \text{ Pi}}{\rho_s} \left(\frac{4}{3} + d_t/d_s + \frac{d_t^2}{2d_f^2} \right) \right]^{1/2} \quad (A15)$$

Equation A15 serves as the basis of the upper curve of Figure A12, where U_{smax} for an idealized spin launch is plotted versus the stone diameter, d_s . Using the same set of test parameters typical of experience with the UDRI/USAF FDL test program.

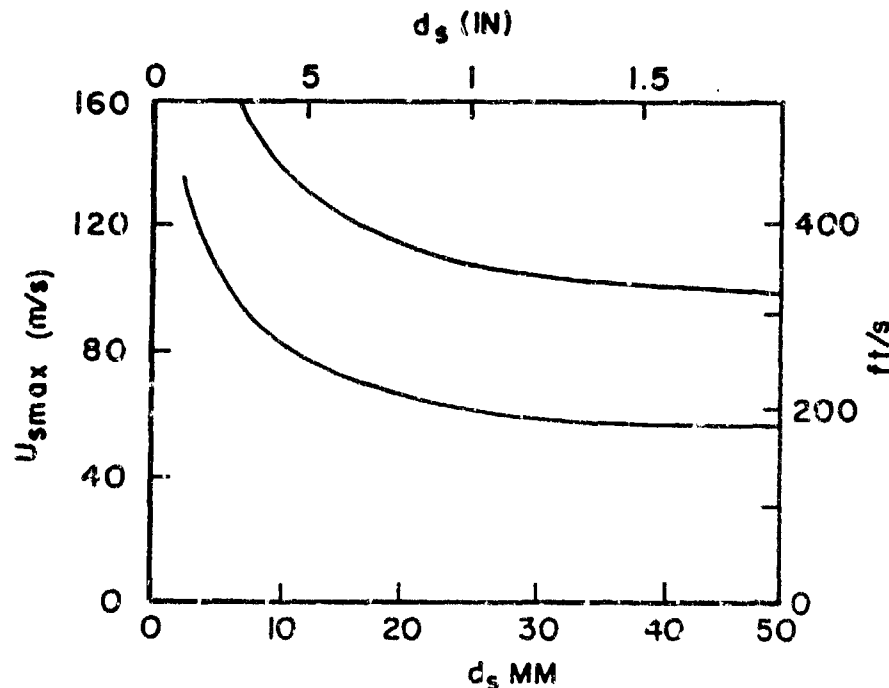


Figure A12. Maximum Lateral Velocity Imparted to Stones Through "Spin-Launching"

The question of launch process energy dissipation as work against friction is somewhat different for a spin launch than for a slide launch because the frictional work done by the stone rolling across the rubber surface is much smaller than when the stone slides across the rubber surface. The stone's velocity across the runway/taxiway surface is double that associated with a slide launch (being caused by both translational and tangential rotation velocities being added). Thus, the work done overcoming friction is, simply, twice the work done during a slide launch. The two friction correction values would be identical for slide and spin launch if the coefficients of friction between the stone and runway and stone and tire tread were equal. The entire concept of spin launching is founded upon the implicit assumption that the frictional coefficient between the stone and the tire tread is inherently larger than that between the stone and the runway, which leads us to the prediction that a smaller percentage of the available energy is dissipated overcoming friction for a spin launch than for a slide launch. We have chosen somewhat arbitrarily to reduce the energy dissipated by one-third for spin launches which leads to Equation A16 and the second plot in Figure All.

$$U_s = \left[\frac{9.6 P_i (1 - \mu_r/\mu_s)}{\rho_s} \left(4/3 + d_t/d_s + d_t^2/2d_s^2 \right) \right]^{1/2} \quad (A16)$$

As with slide launching, the predicted spin launching velocities are well above those that have been observed experimentally during the UDRI/USAF FDL test program. We must assume, therefore, that an idealized launch is extremely rare and that most launches occur prematurely before or after the tire tread has been deformed to the maximum extent possible.

The remaining launch mechanisms described in Paragraphs 2.3.5, 2.3.6 and 2.3.7 treat mechanisms for producing vertical velocity components, either secondarily from horizontal ones or from other phenomenology associated with the stone loading process.

2.3.5 Vertical Launching of Sliding Stones

The mechanism by which a sliding stone may achieve a vertical velocity component involves the lower leading edge of the stone "digging into" the runway surface for one reason or another. In the extreme situation where a stone is converted completely from a slider to a roller, the kinetic energies associated with sliding motion and rolling motion are partitioned under the constraint that tangential surface rotational velocity must equal translational velocity. The actual value of this ratio is dependent upon the shape of the rock. As developed in Paragraph 2.3.4, this partition of the total energy is 40% for a sphere. This ratio increases to 45% for a cube and is 44.2% for a right circular cylinder spinning about its axis of symmetry. We feel safe assuming that up to 50% of the original kinetic energy of a sliding stone can be translated into rotational kinetic energy in the spin-up process. The original translational velocity of the stone is reduced to 70.7% of its original value under these extreme conditions. Continuing with this line of argument, we may make the tentative assumption that up to all the rotational kinetic energy imparted to the stone is converted to vertical translational energy. This vertically-directed energy yields a velocity up to 70.7% of the original sliding velocity. The ratio of these two velocities (the horizontal translational velocity and the vertical translational velocity) is simply the tangent of the loft angle, θ_r . The maximum value of θ_r produced by this mechanism is $\tan^{-1}(U_z/U_x) = 45.0^\circ$. Stones have been observed that were lofted at considerable higher angles, but a large number of the lofted stones have loft angles at or below this value.

Let us now examine this rotational lofting assumption in more detail. The crucial phenomenon is clearly conversion of up to 40% of the translational energy to rotational energy. Let us consider, however, the mechanism by which the rotational kinetic energy is converted to vertically-directed translational energy. An appendage projecting from the surface of the stone engages the runway/taxiway surface. The c.g. of the stone must rise upward to allow the appendage to pass under it. The fractional height of the appendage with respect to the average diameter of the stone may be used for calculating the upward rise of the c.g. during time required for the appendage to move from original contact with surface to a point directly below the c.g. The functional relationship is presented as Equation A17 in terms of $\Delta d/d_s$, the ratio of bump height to stone diameter.

$$U_z / U_x = \frac{2Z}{\cos^{-1}\left(\frac{1}{1+Z}\right)} \quad ; \quad Z = \Delta d / d_s \quad (\text{A17})$$

A plot of Equation A17 is presented in Figure A13.

The horizontal dashed line represents the maximum vertical velocity calculated on the basis of energy conservation. Note that the corresponding value for Z is small enough to make the entire analysis creditable.

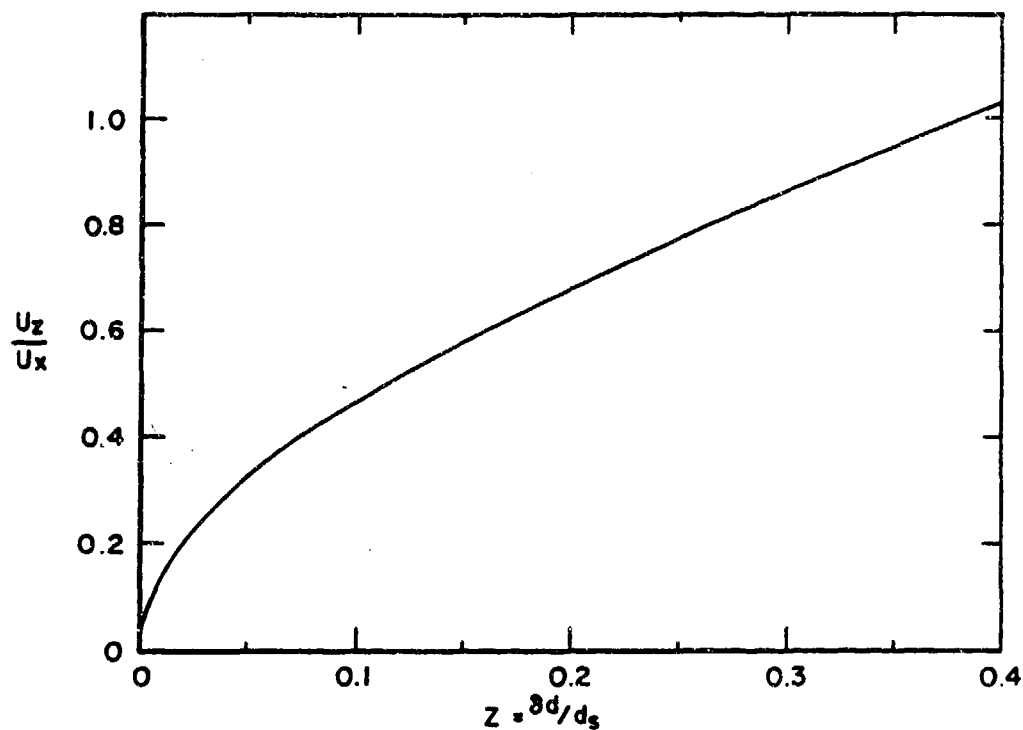


Figure A13. Vertical Velocity Normalized to Horizontal Velocity vs. "Bump" Height Normalized to Stone Diameters for "Spin Lofting" of Stones.

2.3.6 Vertical Launching of Spinning Stones

The problem of converting translational to rotational velocity has been solved automatically for the case of a spinning launch of a stone. The problem for this paragraph reduces to estimating the maximum vertical velocity that can be achieved by a projectile. The "reverse spin" orientation of rock rotation effectively precludes transfer of translational kinetic energy from horizontal motion to kinetic energy of vertical flight. However, up to all of the rotational energy may be converted to vertical translational energy by interaction of a "bump" with a hard surface. Numerically, this situation matches the situation described in Paragraph 2.3.5 for the

case of sliding stones that become rollers. Thus, the Equations A15, A16, and A17 hold as does the plot presented in Figure A13. The somewhat disturbing conclusion to be drawn here is that neither mechanism otherwise credible produces predictions of loft angles above 45° from the plane of the runway.

2.3.7 Elastic Launch of Stones

The final mechanism identified for producing vertical stone velocity components is basically unrelated to the two preceding ones which involve stone rotation. In this case, we postulate that the stone deforms elastically under load from the tire tread and then releases this energy upon removal of the load to produce a vertical velocity component. In principle, elastic energy stored by the stone loading the ground surface may be made available for providing additional vertical velocity. We have rejected further consideration of this possibility for two reasons which depend upon surface characteristics. If the surface is hard, its structural rigidity may be expected to be many times that of the relatively small stone. Under these conditions, its deflection under influence of the stone load must be very small compared to that of the stone as is the energy stored in elastic deformation. The ground deformation may grow to equal or exceed that of the stone if the surface is compacted gravel. This material is highly inelastic, when its condition allows large deformations to develop. Most of the energy entering the surface during the deformation process is not available for return to the stone. Thus, we are left with the assumption that only energy stored elastically in the stone by the loading process is available for stone lofting.

Release of elastically stored energy in the stone upon load removal is available both to propel the stone upward and to be returned to the loading mechanism (the tire tread). The relative efficiencies of these processes depend upon the rate at which the load is removed.

Let us continue the analysis by evaluating the energy stored elastically in a loaded stone. For computational simplicity, we assume that the stone is a right circular cylinder with a load applied axially to each end (the cylinder stands on one end and the load is applied to the other). The first step to carrying out this analysis is to establish Young's Modulus for the stone material. This may best be accomplished by using the relationship that the compressional wave speed in the stone is related to stone material density and sonic speed as presented in Equation A18.

$$M = a_0^2 \rho_s \quad (A18)$$

The compressive deformation of the stone, d , may now be evaluated from Hook's Law as is presented in Equation A19 where F_s is the applied load and A_s is the horizontal cross-sectional area of the stone.

$$\Delta d = d_s F_s / A_s M \quad (A19)$$

A working relationship for the deformation may now be developed by substituting into Equation A19 the expression for the load on the stone (Equation A6), the stone modulus from Equation A18, and the formula for the cross-sectional area as is presented in Equation A20).

$$\Delta d = \frac{4P_i}{a_0^2 \rho_s d_s} (4d_s^2 + 2d_s d_t + d_t^2 / 2) \quad (A20)$$

The energy stored in the stone through elastic deformation, E_{el} , may now be computed using the basic relationship presented in Equation A21.

$$E_{el} = \frac{F_S \Delta d}{2} \quad (A21)$$

Substituting Equation A6 and Equation A20 into Equation A21 provides a working relationship for the energy stored elastically in the stone as presented in Equation A22.

$$E_{el} = \frac{2 \pi P_i^2}{\rho_S a_0^2 d_S} (4 d_S^2 + 2 d_S d_t + d_t^2 / 2)^2 \quad (A22)$$

If we assume that all of the stored elastic energy is transferred to vertically directed kinetic energy, an expression for U_{zmax} , may be derived. (Equation A23).

$$U_{zmax} = \frac{4.9 P_i}{\rho_S a_0 d_S^2} (4 d_S^2 + 2 d_S d_t + d_t^2 / 2) \quad (A23)$$

A plot of U_{zmax} vs. d_S as evaluated in Equation A23 is presented as Figure A14.

Note that the velocities from elastic rebound are strikingly low even under the assumption that all the elastic energy is transformed to upward-directed kinetic energy; we find that speeds for the smallest particles of interest are less than 8 m/sec. and that these speeds sink to less than 3.5 m/sec. at the upper end of the size range of interest.

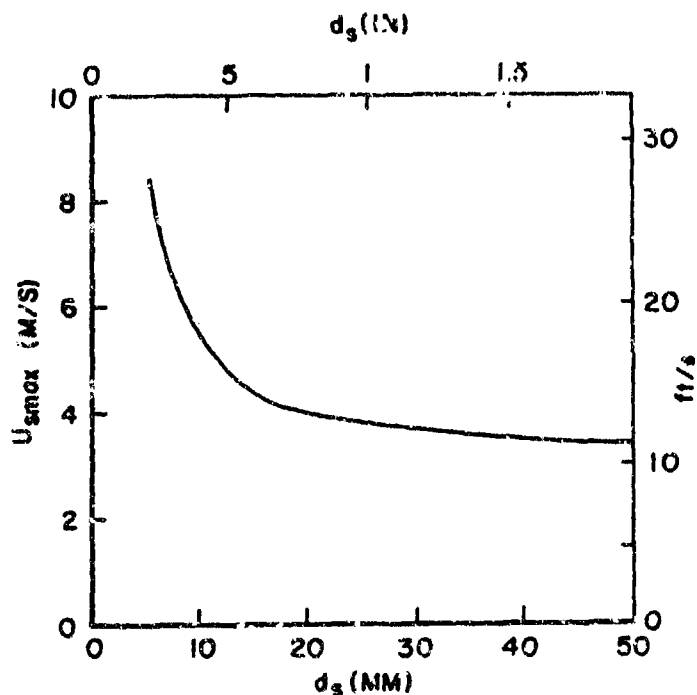


Figure A14. Maximum Vertical Velocity That Can Be Imparted to a Stone Lofted by Stored Elastic Energy.

Let us now consider the question of energy distribution between kinetic energy of the stone and "giveback" to the tire tread. Basically, release waves which travel at sonic velocity emanate from the upper surface of the stone as load removal begins. These waves propagate downward to the bottom surface of the stone causing the stone to lift off the runway and travel upward. They also reflect and propagate back to the upper stone surface. Should the tire still be in place at this time above the stone, the upper surface of the stone will simply expand into the tire yielding up the vast majority of its elastically released energy to the tread and experience no net lofting.

The sonic velocity for crushed limestone is near 3.2 km/sec. which implies a dual transit time through a 25 mm high stone of 14.28 microseconds. This time is extremely short in relation to the times associated with conventional loading and unloading of stones

overrolled by tires. Such times for either experimental or operational conditions extend to tens of milliseconds.

The most rapid removal of tire load from a stone occurs during slide launching or spin launching of stones from the sides of tires. A clear launch of the stone from under a tire in 14 microseconds infers an average velocity during the stone removal process of 0.90 km/sec.. The peak velocity which the stone must achieve in order to meet this average velocity requirement is well above 0.90 km/sec. It may be as high as twice that value or 1.80 km/sec. These velocities are clearly unrealistic since they defy limitations imposed by energy conservation requirements.

We conclude on the basis of these results that energetic stone launching from tire overrolling (velocities over 4 m/sec.) is not the result of elastic energy being stored in stones under compression although elastic launching may produce lower stone velocities.

2.3.8 Discussion of Stone Lofting Mechanisms

We started this model development exercise with the realization that launches of large stones at high velocities by nosewheel/surface interactions are relatively rare occurrences. A variety of mechanisms is available for explaining stone projections in the plane of the surface. Stones may be pushed aside more or less violently by tire treads which remain essentially rigid during the interaction process. Stone velocities up to the forward velocity of the aircraft can, in principle, be generated either in the direction of aircraft movement or perpendicular to it. Rigid tread propulsion of stones, however, does not account for the stones developing velocity components upward away from the runway surface. They are also inhibited by the tendency of the tires to overroll the stones.

Tires store considerable amounts of elastic energy when they overroll stones. This energy storage is sufficient to provide more than ample stone velocities to cover all stone lofting observations. Two mechanisms are available for coupling this energy to stone movement efficiently. The first involves the dual sliding of a stone sideward when the stone is half overrolled by an oncoming tire. Allowing the stone to slide, both with respect to the surface and the tire tread, propels the stone without requiring rotation. Normally stones with flat lower surfaces would be propelled by such a mechanism since causing these stones to tumble while under influence of the tire tread is awkward. The inverse situation occurs when stones are "spin launched." Here the stone slides along the runway surface but rolls along the tire tread surface. The resulting backspin on the stone will, on the average, produce a surface speed equal to the forward velocity of the stone, but in the opposite direction at the stone/surface interface.

Both of these launch mechanisms depend heavily upon the frictional coefficients between the stones and the surfaces engaging them. The starting friction levels determine largely when during the loading process stone movement begins. The stones cannot, in general, achieve the finite kinetic energies if movement occurs under starting friction resistive conditions. Kinetic energy is imparted to the stones when sliding friction falls well below starting friction. However, frictional energy loss remains an important mechanism limiting the kinetic energy available to launched stones.

Three mechanisms have been considered for producing stone lofting. The first two, which are closely related, involve an irregular stone developing a high rotational velocity and an appendage (or bump) on the stone engaging the runway as the stone rolls between the c.g. of the stone and the runway forcing the c.g. upward, thus producing lofting. This lofting mechanism can use up virtually all of the rotational kinetic energy available.

Slide-launched stones do not initially possess significant amounts of rotational kinetic energy. Part of their translational energy may be transferred to rotational energy if the front lower edge of the stone "digs into" the runway surface, thereby forcing the stone to start rolling. Such a "dig in" can cause a combination of stone sliding and rolling up to a complete forward roll of the stone when the surface velocity associated with rotation equals the translational velocity. Stone lofting under these conditions should be expected to leave a residual forward roll rate which has been observed during high speed photographic studies of selected runs from the UDRI/USAF FDL test program. Spin-launched stones have reverse roll rates whose surface velocities are comparable to their translational velocities. Under either circumstance, (forward or reverse roll rates), a series of energetics arguments can be made to show that the maximum loft angle for the stones above the runway surface is limited to approximately $\theta_r = 45^\circ$.

We feel strongly that energetic stone launches are produced almost exclusively by stone-spin launches from the edges of tires.

The final mechanism considered for stone lofting above the runway surface involves release of elastic energy stored in the stone by vertical loading. We have examined this process in some detail and find that insufficient energy is available to produce more than marginal stone lofting for the stone size ranges of interest to this investigation. In addition, we find that coupling of elastic energy to upward-directed kinetic energy is, at best, an inefficient process which further curtails the upward velocities that can be produced.

Taken in their pure forms, the mechanisms we have proposed for projecting stones away from nosewheel/surface contact points emphasize movement perpendicular to the direction of the aircraft when viewed in a coordinate system fixed to the runway, along the +X axis. Stones are observed to move in almost all directions, although distinct minima are observed along the direction of wheel movement and opposite to it (+Y axis). Fairly substantial positive lobes are observed in multiple-stone trajectory plots along the directions

perpendicular to tire translational velocity (+X axis). We feel that the components along the +Y axis are most plausibly explained as arising from asymmetries in the four primary launch mechanisms (slide launch and spin launch of stones along the runway surface and forward and rearward spin launches of the stones upward away from the runway surface).

Section 3 of this report proposes a means for applying the models developed in Section 2 and the launch criteria for air intake ingestion developed in Section 1 to the development of engineering experiments to evaluate aircraft vulnerability to lofted stones and to estimate critical runway debris conditions which may lead to catastrophic aircraft failure during airport operations.

3. APPLICATION OF ANALYSIS AND EXPERIMENTAL RESULTS TO ENGINEERING EXPERIMENTS AND AIRCRAFT OPERATIONS

This third and last section provides a formalized system for describing the probability of a stone of a minimum critical size being ingested by an aircraft engine during a specified ground maneuver. The analysis contains several parameters, few of which can be identified with much precision and/or reliability on the basis of currently available data. One paragraph describes means for continuing the search for appropriate data to support the probability analysis. Another discusses procedures for operating airports (and possibly aircraft) that are expected to minimize the probability of operating aircraft ingesting stones large enough to cause significant individual damage. The section concludes with recommendations for further study.

3.1 LIKELIHOOD OF OPERATIONAL AIRCRAFT INGESTING DANGEROUS STONES

Let us start this phase of the analysis by considering conditions that may produce dangerous stone-lofting events. All of the mechanisms for producing dangerous launchings that have been observed to date involve aircraft tires partially overrolling stones. Thus, a band one stone-width wide on each side of the footprint of a single overrolling tire must contain all candidate stones for dangerous launching. The areas of these bands are nominally doubled for aircraft such as the F-4E which employ dual nosewheels. The question of whether the two bands involving the inner edges of the tires produce dangerous stone launches depends upon whether or not we consider the possibility of stones lofted from one wheel bouncing off the other before being projected upward and outward. We may eliminate inner bands from further consideration if we do not consider the bouncing situation to be dangerous because stones launched from the interior edge of one wheel are effectively shielded by its neighbor (dangerous stone trajectories must have substantial

loft angles, θ_r , which effectively preclude their being launched without encountering the second wheel in any direction except nearly forward and rearward, near the $\pm Y$ axis).

The remainder of the analysis in this paragraph assumes only two tire edges may produce significant stone lofting. The resulting probabilities should all be multiplied by a factor between 1 and 2 to treat the dual-wheel launch situation. A factor of 2 should be employed if bouncing of stones lofted by the inner edge of one tire are assumed to retain their danger fully after bouncing off the other tire. A factor of 1 should be used if bounce launches are considered nondangerous. An intermediate value should be used if stone bouncing is considered to reduce but not eliminate danger of stone ingestion.

The area on the runway surface A_{run} occupied by stones which are partially overrolled during an aircraft maneuver requiring a runway length, L_s , is given by Equation A24.

$$A_{run} = 2 L_s d_s \quad (A24)$$

The number of stones per unit surface area lying within area A_{run} , N_a , is evaluated using Equation A25.

$$N_a = \frac{4}{\pi} \sum_{d_s} \frac{P_d}{d_s^2} \quad (A25)$$

The term P_d is the fraction of the runway surface covered by stones with characteristic dimensions in a range of d_s . This percentage divided by the stones' cross-sectional areas is summed over all of the stone size ranges which represent ingestion danger to aircraft engines and are common enough on the runway/taxiway surface to make aircraft encounter a finite possibility.

The number of stones of dangerous size encountered in a maneuver, N , is simply the product of Equations A24 and A25 as presented in Equation A26.

$$N = \frac{8L_s}{\pi} \sum_{d_s} \frac{P_d}{d_s} \quad (A26)$$

The number of stones per aircraft maneuver lofted with potentially dangerous velocities N_1 is, simply, the sum over dangerous stone sizes of the stones encountered times the probability of stones these sizes being lofted by the encounter, Q_d , as presented in Equation A27.

$$N_1 = \frac{8L_s}{\pi} \sum_{d_s} \frac{Q_d P_d}{d_s} \quad (A27)$$

We must now consider the probability of a stone launched to dangerous velocity (speed and direction) being ingested by the engine(s) of an operating aircraft. For any aircraft roll situation, a particular "window" of launch velocity (speed, direction, aircraft roll speed) effectively ensures capture. The size and location of this "window" is a function of airframe geometry, (the size and location of the air intake(s) relative to the nosewheel/runway contact area and the velocity of the aircraft along the runway). The aircraft velocity term may be eliminated from establishing this window if the stone loft trajectories are specified in a coordinate system fixed to the airframe.

We choose to define a term, S_d , which evaluates the fraction of stones launched in the dangerous velocity regime that pass through the critical launch window for ingestion. This term is obviously affected by both the size of the critical launch window and the relationship of its direction to the velocity distribution function

for lofted stones. The term is included in the general analysis as presented in Equation A28 where the number of stones ingested per aircraft maneuver, N_i , is evaluated.

$$N_i = \frac{8L_s}{\pi} \sum_{d_s} \frac{Q_d S_d P_d}{d_s} \quad (A28)$$

Equation A28 may, in principle, be used to evaluate stone ingestion dangers associated with a wide variety of airport operational scenarios. The value of N_i calculated from any individual application of Equation A28 should be far less than unity. These values of N_i may be considered as 1% of the probability of an aircraft experiencing a damaging stone ingestion during an individual maneuver involving a roll of distance, L_s . These probabilities may be summed over an entire aircraft maneuver (such as engine startup through aircraft liftoff) by summing individual values of N_i from segments of the maneuver which are chosen small enough so that all of the variables may be treated as constants (or functions of an individual launch parameter such as aircraft roll speed).

Probability of any aircraft involved in a major airport operation ingesting a damaging stone may be established by summing values of N_i from Equation A28 over an entire operational scenario. Under airport operational conditions, the value of N_i may approach or exceed unity. Under these conditions, N_i may be considered as an estimate of the number of aircraft engines sustaining damage during a particular operational scenario.

Application of Equation A28 is straightforward once values have been established for P_d (runway coverage with stones of given size), Q_d (fraction of stones encountered that are launched to dangerous velocities), and S_d (fraction of dangerously launched stones which are actually ingested).

Means for specifying or at least estimating these parameters are discussed in the next paragraph.

3.2 EVALUATING PARAMETERS CRITICAL TO STONE INGESTION ANALYSIS

3.2.1 Percentage Runway Coverage

Normally, the amount of debris covering a surface for either a test or an airport operation is reported as total percentage coverage although the particle size of the material on the surface is partitioned over a wide range. The lethality of the material, and almost certainly its lofting probability, is determined by stone size. We need, therefore, to acquire information about covering percentages for individual ranges of stone sizes.

This information may be obtained experimentally by sweeping up a predetermined area established as typical of the overall coverage and determining the percentage areal coverage of stones in each size range of interest. This data may be expressed separately or it may be expressed in terms of percentage of total debris coverage on operational surfaces to develop a coverage spectrum from each stone size. Use of this latter technique allows percentage coverages of individual stone sizes to be extracted from total coverage percentage information under the assumption that all of the material covering a runway/taxiway has the same spectrum of relative stone sizes.

For the purpose of further analysis, we have devised a stone coverage spectrum that may be typical of ones encountered during attacks upon airports. Table A2 treats debris from this spectrum covering 10% of the operational surface at an airport.

TABLE A2 Hypothetical Stone Distribution Covering
10% of an Airport Operational Surface.

d_s mm	% Cover of Population	P_d (10% d_s Cover)	P_d/d_s i./m
0-5	21	.021	
5-10	25	.025	
10-15	20	.020	1.6
15-20	15	.015	.86
20-25	10	.010	.44
25-30	7	.007	.26
30-35	2	.002	.06
35	0.2	----	

$$\sum_{d_s} P_d/d_s = 3.22/m$$

3.2.2 Lofting Probability For Encountered Stones

One of the core issues for all tire-lofting experiments is to establish the probabilities that specific stone/tire encounter situations may produce dangerous stone lofting. The basic method for establishing these lofting data is to observe the tire/runway contact area during tests and monitor the velocities of stones projected from it. This monitoring may occur in either the laboratory or the tire frame of reference. Differences between these two reference frames are of crucial importance for determining which stone trajectories represent dangers to a specific aircraft rolling at a specific velocity.

Figure A15 is a graphical presentation of the energetic stone data from the UDRI/USAF FDL tire test program. The upper left diagram is a polar plot of the declination angle versus numbers of lofted stones. Note that the stones are lofted in two lobes centered

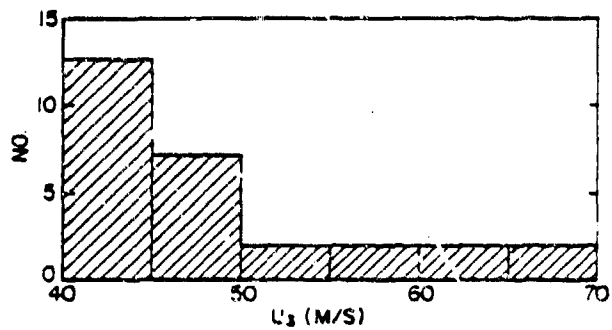
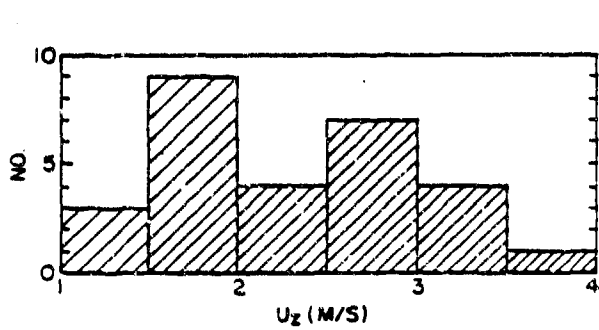
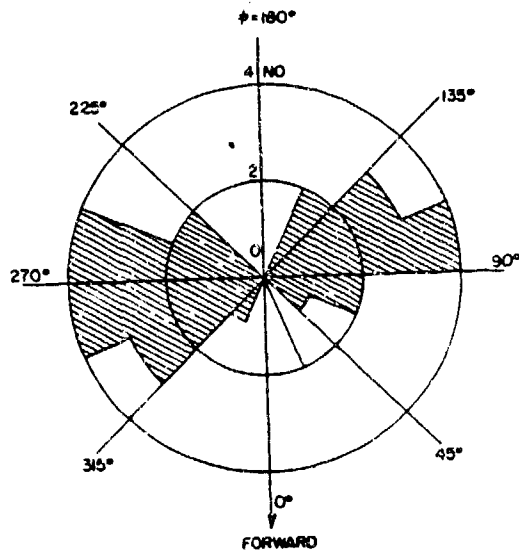
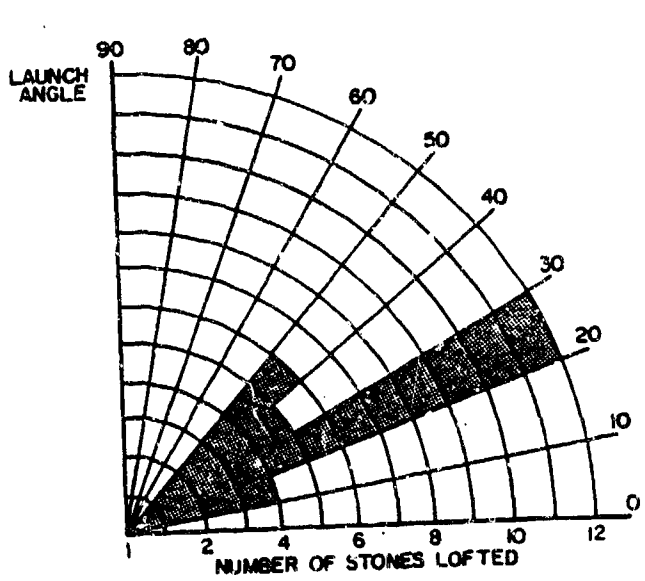


Figure A15. Elevation Angle θ_r , Declination Angle, θ_r , Launch Speeds, U_s and Vertical Components of Launch Velocity U_z vs. Number Stones Launched for Energetic Stones Observed During the UDRI/USAF FDL Tire Test Program.

around perpendiculars to tire motion (90° , 270°). A similar plot in the aircraft frame-of-reference would produce two narrow lobes centered near $\phi = 20^\circ$, 340° if an aircraft roll speed of 15 m/sec is considered (typical of the experimental test program).

The diagram in the upper right quadrant of Figure A15 is a polar plot. The same energetic stone data in numbers versus loft angle, θ_r . Note that some 86% of the stones are lofted with angles below $\theta_r = 45^\circ$ (the maximum angle permitted by the spin-launch model) in the laboratory reference frame. This distribution shrinks to a narrower lobe with a central angle of $\theta_r = 10^\circ$ when the data are considered in the reference plane of an aircraft rolling forward at 15 m/sec.

The bar charts in the lower two quadrants of Figure A15 describe stone velocities in the laboratory reference frame. U_s represents the total speed of the stones and U_z represents the vertical components of the stone velocities. The values of U_z would be unaffected by considering stone velocities in the aircraft reference frame, but the values of U_s would "bunch up" closely around 15.25 m/sec if the data were considered in the reference frame of an aircraft rolling at 15 m/sec.

3.2.3 Probability That Dangerous Stones Launched To Dangerous Velocities Are Actually Ingested

The problem of determining whether or not stones lofted from the nosewheels of rolling aircraft actually intercept the engine air intake(s) is essentially geometrical in nature. A first approximation for establishing a value of the capture probability, S_c , is to compute the ratio of the area of the solid angle subtended by the air intakes (or the fraction of them whose loft angles are below critical values) to the solid angle into which all realistic stone trajectories must fall. This computation infers the assumption that stones are lofted by tires at random angles in the aircraft reference frame. Note that the solid angle for realistic stone

total solid angle of a sphere is 4π steradians. We may immediately eliminate half of this solid angle as being below the operational surface (2π sr.). We may subdivide the remainder by two to reflect the fact that launch probabilities across the symmetry plane of the aircraft are very unlikely (π sr.). Finally we may divide the permissible solid angle yet again by two by observing that stones launched with forward velocities in the aircraft reference frame are extremely unlikely. Thus, we are left with a solid angle into which stone lofting is likely of $\pi/2$ sr.

We may now refine the estimation of S_d by realizing that the probabilities of stones being launched at particular directions within the permitted solid angle are nonuniform. Observed stone-launch directions (in the aircraft reference frame) may be used to establish relative probabilities versus direction. The direction of the engine air inlets from the wheel/surface contact area may then be used to determine the relative probability of launched stones being ingested. Mathematically, this relative probability factor, K , is related to the overall capture probability, S_d , as presented in Equation A29.

$$S_d = \frac{2KA_{in}}{\pi R_{ct}^2} \quad (A29)$$

where: A_{in} is aircraft engine intake area (with loft angles below a critical value) and R_{ct} is the distance from tire/surface contact area to the centroid of A_{in} .

3.2.4 Numerical Example

Let us complete this section of the analysis by developing hypothetical data concerning stone lofting under an actual combat situation at an airport and apply this data to one typical operating maneuver of an F-4E, an F-15, and an F-16 aircraft. Inspection of Figure A15 indicates that no stones dangerous to the operation of any of the aircraft considered were observed during the UDRI/USAF FDL tire test program since the highest vertical component of launch velocity was only 4m/sec which cannot loft the stone high enough to reach the engine air intakes of the F-4E and F-15 aircraft and no stone lofted from the nosewheel contact area may enter the air inlet of the F-16 aircraft if it travels along a ballistic trajectory.

We may use this experimental information to provide an upper bound on the launch probability, Q_d , from Equation A27, if we choose the aircraft maneuver to be a straight roll at 15 m/sec. Since approximately 1000 stones were encountered during the experimental program, we can provide, as a best current estimate, an upper bound of $Q_d = 10^{-3}$. We have chosen to employ the debris size distribution data presented in Table A2 to establish P_d , size distribution, as a function of aerial coverage. Finally, we have evaluated the air inlet capture probability, S_d , for the F-4E by determining the ratio of the air inlet area (whose loft angle relative to the surface at the nosewheel contact point is less than $\theta_i = 45^\circ$) to the area of 1/8th of a sphere whose radius is the distance from the nosewheel contact point to the centroid of the engine air inlet area being considered as is expressed in Equation A29. This value (for the F-4E aircraft is $S_d = 0.02$. We have no way of knowing at this point the preferred directions of energetic stones projected from the nosewheel of an operating F-4E aircraft so we cannot evaluate the relative direction probability, K , in Equation A29. We have chosen, somewhat arbitrarily, to set K equal to unity, thereby allowing the value of S_d to remain $S_d = 0.02$. Table A2 contains individual tabulations of P_d/d_s which appears in Equation A28 summed over the values of d_s of

interest. We have chosen values in Table 2 of stone diameters, d_s , between 10 mm and 35 mm for our computations. Stones smaller than 10 mm will probably not produce catastrophic damage during individual ingestions by an operating aircraft engine. Stones with diameters above 35 mm are so rare that their inclusion is not worth considering. The sum over interesting values of d_s of P_d/d_s is 3.22/M. Applying the combination of this information for the F-4E aircraft moving at 16 m/sec. to Equation A28 provides a number of ingested stones, N_i vs. the length of the specified maneuver, L_s , presented in Figure A16. Figure A16 is specific to the F-4E aircraft rolling over a surface 10% of whose area is covered by debris with a size distribution specified in Table A2. The roll velocity is such that the lofting probability of stones with dangerous sizes to dangerous velocities is $Q_d = 10^{-3}$. The upper curve of Figure A16 is a graphical representation of this situation.

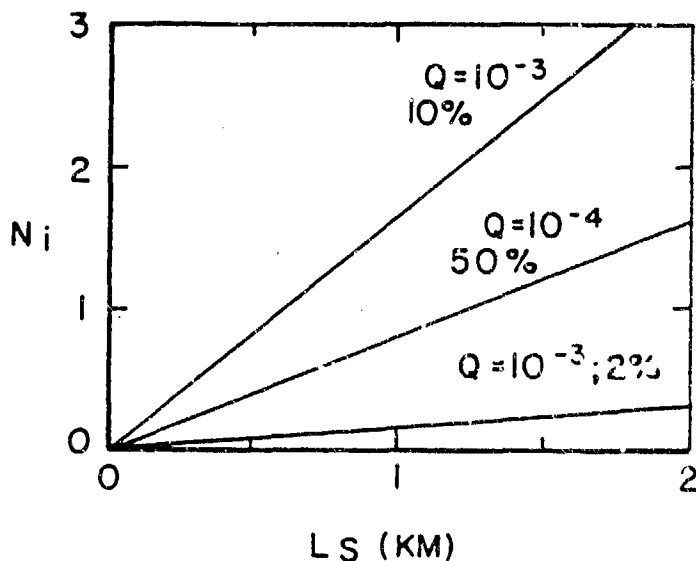


Figure A16. No. of Stones Ingested for Various Aircraft Rollout Scenarios

It indicates that an aircraft rolling 1 km under the specified conditions will have a probability of ingesting a damaging stone of 16.3%. This probability is expected to fall to 1.2%/km of roll distance if total debris coverage is reduced to 2%, as shown in the lower curve of Figure A16. Should the actual loft probability be reduced to $Q_d = 10^{-4}$, the middle curve from Figure A16 indicates an ingestion probability of 8.4% when the total debris coverage factor is as high as 50% of the overrolled surface.

A similar analysis for the F-15 aircraft was not conducted because only a small fraction of the air inlets fall below loft angles of 45° (as tabulated in Table A1 and shown graphically in Figure A3, the probabilities of an F-15 aircraft ingesting a stone are far lower than those of the F-4E.

3.3 SUGGESTED MEANS FOR REDUCING STONE-INGESTION PROBABILITIES

Clearly, the most obvious method for reducing stone-ingestion probabilities during aircraft operations is to keep the runways and taxiways clean. This truism is hardly worth mentioning except for the fact that potential exists for grossly improving the rate at which runways soiled by shrapnel, bomb-crater debris, and debris from degrading runway/taxiway patches may be cleaned through development of specialized equipment.

The stone-lofting analysis from Section 2 indicates strongly that "chunky" stones are more likely to be lofted by aircraft tires than are disc-shaped stones (where two orthogonal linear dimensions are notably larger than the third). The choice of stone fill materials for patches which naturally crush into disc-like shapes might significantly reduce the likelihood that stones encountered by aircraft nosewheels will be lofted into air intake manifolds.

Another means apparent for protecting aircraft from stone launching is to control the sizes of stones used for aircraft runway/taxiway patches. Large stones (such as 100 mm diameter and up) probably cannot be lofted. Individually ingested stones smaller

than, perhaps, 10 mm diameter probably cause little serious damage. Thus, the possibility exists for forming runway patches with a combination of large and small stones only, thereby eliminating members of the population of intermediate size which represent a danger from individual ingestion.

3.4 RECOMMENDATIONS

Our understanding of stone lofting is incomplete at present. Predictions indicate strongly that spin-induced lofting can produce loft angles, θ_r , limited to approximately 45° . Data from the UDRI/USAF FDL test program indicate that approximately 14% of large stones launched to potentially dangerous velocities have loft angles in excess of 45° . A number of possibilities exist for resolving this question, including ricochet of stones lofted at low angles against other stones lying nearby to produce substantial loft angles. We recommend that this, and other possibilities, be examined carefully using high-speed cameras at the AFFDL Mobility Laboratory facility.

If our estimate of $Q_d = 2.8\%$ is accurate, a total of 250 partially overrolled stones (observed during 25 runs) should provide a 50% probability of observing seven launches at speeds above 4m/sec. The observation of at least one or two high velocity launches is a virtual certainty. An experiment of this sort is probably required to establish with high certainty launch mechanisms responsible for lofting a significant fraction of stones which represent dangers to operating aircraft.

Our second recommendation is to continue the stone lofting research program by conducting engineering tests where actual airport operations are simulated more and more closely. We understand that each advance in airport operational simulation increases the cost of the tests significantly. For this reason, we recommend that sufficient stone lofting data be acquired for each test sequence so that its analysis will reveal discrepancies between current and past data. In this way, new launching phenomena triggered by progressive

application of more realistic launch conditions may be detected and investigated efficiently so that they may be separated from other phenomena triggered by yet more realistic tests. A corollary to this approach is that accurate predictions of experimental observations should be made before each experiment is conducted so that actual results may be compared with prediction quickly to detect onset of any new and unpredicted stone-launch characteristic.

APPENDIX B
TEST DATA FOR STONE-LOFTING PROGRAM

FIRST TEST MATRIX

Test Number	Remarks	CRR	V (mph)	P (psi)	Load (lbs)	Water Level (in)	Loose Stones (1)
IC1A	baseline, dry	∞	40	200	1000	0	LR, LA, SR, SA
IC2A	effect of stone size	∞	40	200	1000	0	$\frac{1}{2}$ LR, $\frac{1}{2}$ LA, $\frac{1}{2}$ SR, $\frac{1}{2}$ SA
IC4A	effect of velocity	∞	25	200	1000	0	LR, LA, SR, SA
IC5	effect of weight	∞	40	200	500	0	LR, LA, SR, SA
IC6	effect of pressure	∞	40	150	1000	0	LR, LA, SR, SA
IC7	pressure, patch scale	∞	40	70	1000	0	LR, LA, SR, SA
IC8	baseline, wet	∞	40	200	1000	0.36	$\frac{1}{2}$ LA, $\frac{1}{2}$ LR, LA, LR*
IC9	effect of pressure	∞	25	70	1000	0.36	LA, LR*
IC11	effect of velocity	∞	25	200	1000	0.36	$\frac{1}{2}$ LA, $\frac{1}{2}$ LR, LA, LR*
IC12	pressure, patch scale	∞	40	70	1000	0.36	$\frac{1}{2}$ LA, $\frac{1}{2}$ LR, LA, LR*
IA13	baseline, bed	100	40	200	1000	0	LA, LR, $\frac{1}{2}$ LA, $\frac{1}{2}$ LR*
IA14	effect of velocity	100	25	200	1000	0	LA, LR, $\frac{1}{2}$ LA, $\frac{1}{2}$ LR*
IA15	effect of weight	100	40	200	500	0	LA, LR, $\frac{1}{2}$ LA, $\frac{1}{2}$ LR*
IA16/SM	effect of stone size	100	40	200	1000	0	SA
IA16	effect of velocity	100	30	200	1000	0	LA, LR, $\frac{1}{2}$ LA, $\frac{1}{2}$ LR*
IA17	effect of pressure	100	40	150	1000	0	LA, LR, $\frac{1}{2}$ LA, $\frac{1}{2}$ LR*
IA18	pressure, patch scale	100	40	70	1000	0	LA, LR, $\frac{1}{2}$ LA, $\frac{1}{2}$ LR*
ISA1	effect of stone size	100	40	200	1000	0	SA, SR, $\frac{1}{2}$ SA, $\frac{1}{2}$ SR
ISA2	effect of stone size*	100	40	200	1000	0	SA, SR, $\frac{1}{2}$ SA, $\frac{1}{2}$ SR
IC41	calibration*	100	40	200	1000	0	$\frac{1}{2}$ LA, $\frac{1}{2}$ LR
IC41	baseline, wet bed*	100	40	200	1000	0.36	$\frac{1}{2}$ LA, $\frac{1}{2}$ LR

* 1/2 refers to large (approximately 1 inch) or small (tread size). A or R refers to angular (tumbled lim-stone) or smooth (gravel). 1/2 refers to half-size.

* Size segregated by size.

* Trough catcher used instead of orthogonal cameras.

SECOND TEST MATRIX

Test	Remarks	Wheel	CBR	V (mph)	P (psi)	L (lbs)	Cov. (%)	Stones
II1	effect of tire shape	T37	∞	40	nom	nom	2	LA, SA
II2	baseline	Falcon	∞	40	200	1000	2	LA, SA
II3	dual baseline	dual	∞	40	200	1000	2	LA
II4	dual baseline	dual	∞	40	200	1000	2	SA
II5	saturation	dual	∞	40	200	1000	20	LA
II6	saturation	dual	∞	40	200	1000	10	LA
II7	saturation	dual	∞	40	200	1000	5	LA
II8	saturation	dual	∞	40	200	1000	1	LA
II9	shape effect	dual	∞	40	200	1000	2	MARBLES
II10	velocity effect	dual	∞	30	200	1000	2	LA
III1	pressure effect	dual	∞	40	75	1000	2	LA
III2	aggregate	dual	100	40	200	1000	2	LA
III3	pressure effect	dual	100	40	75	1000	2	LA
III4	hi-speed photo	dual	100	40	200	1000	20	LA
III5	hi-speed photo	dual	100	40	200	1000	2	LA

THIRD TEST MATRIX

Test	Diagnostics	Remarks	V	P	d	cov.	Stones	Runs
1	FC side	scope splash	40+25	200	0.3	10% ^d	IA	4
2	FCf side	test visibility	40+25	200	0.3	10% ^d	LA	4
3	FCf side	test visibility	40+25	200	0.3	10% ^d	SA	4
4	FC front	scope splash	40+25	200	0.3	10% ^d	IA	4
5	FC rear	test visibility	40+25	200	0.3	10% ^d	LA	4
6	Starco Camera ↓	Base	40	200	0.3	10% ^b	LA ^c	18
7		Velocity	25	200	0.3	10%	LA ^c	19 (No flash on 6)
8		Pressure	40	75	0.3	10%	LA ^c	18
9		Rock Size	40	200	0.3	10% ^d	SA ^c	18
10		Water Depth	40	200	0.6	10% ^b	LA ^c	18
11		Water Depth	40	200	0.1	10% ^b	LA ^c	18
12		Rock Saturation	40	200	0.3	5% ^e	LA ^c	20 (18-20 one run)
13		Rock Saturation	40	200	0.3	15% ^f	LA ^c	18
14		Rock Saturation	40	200	0.3	20% ^g	LA ^c	18
18		Load & Water Velocity	40	200	0.3	5% ^e	LA ^c	9 ^h & 9 ^{h,j}
19		Single Wheel	40	200	0.3	10% ^k	SA ^c	9 ^m
20		Single Wheel	25	200	0.3	10% ^k	SA ^c	9 ⁿ
21		Rock Visibility	40	200	0.3	10% ^k	SA ^c	10
22		Rock Visibility	40	200	0.3	10% ^l	SA ^c	18 ^o
23		Rock Patterns	40	200	0.3	Various	LA ^c	17
24		Rock Size	40	200	0.3	10% ^b	1/2 size	18 ^o
25		Rock Size/Shape	40	200	0.3	10% ^b , 2%	1/2 size, 1" marbles	17 ^p

^b Nom 10% Coverage - Actually 9% (16 rocks per tire).

^c Rocks Have Paint Baked On.

^d Nom 10% Coverage - Actually 9% (16 spots/tire with 6 rocks/spot).

^e Nom 5% Coverage - Actually 4.5% (8 spots/tire, 1 rock/spot).

^f 24 Rocks per side.

^g 34 Rocks per side.

^h 500# load.

^j 1/8 Nylon Balls & Wood Blocks - 1/4 x 1/4

^k Nom 10% Coverage - Actually 9% - 2 rocks/spot.

^l Nom 10% Coverage - Actually 9% - 2 rocks/spot - one wheel at a time.

^m Color film, right camera - Filter off, passes 6 to 9.

ⁿ Color film, right camera - Filter off, passes 7 to 9.

^o Rocks under outside wheel only, passes 1 to 9 - Rocks under inside wheel only, passes 10 to 18.

^p 1/2 size rocks, passes 1 to 9 - 1 inch marbles, passes 10 to 17.

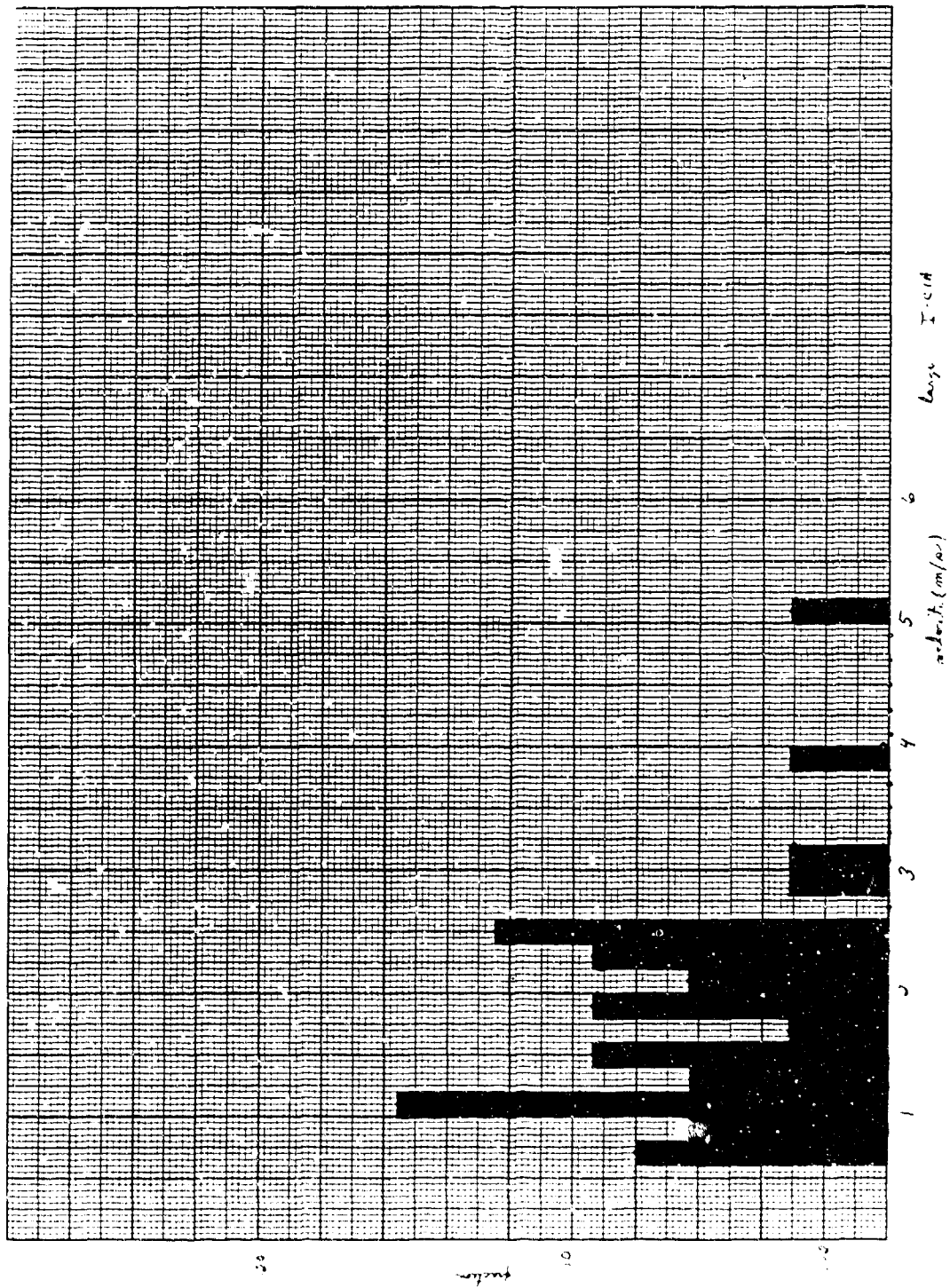


Figure B1. Test ICLA, Single-Wheel Baseline, Large Stones, Velocity Distribution.

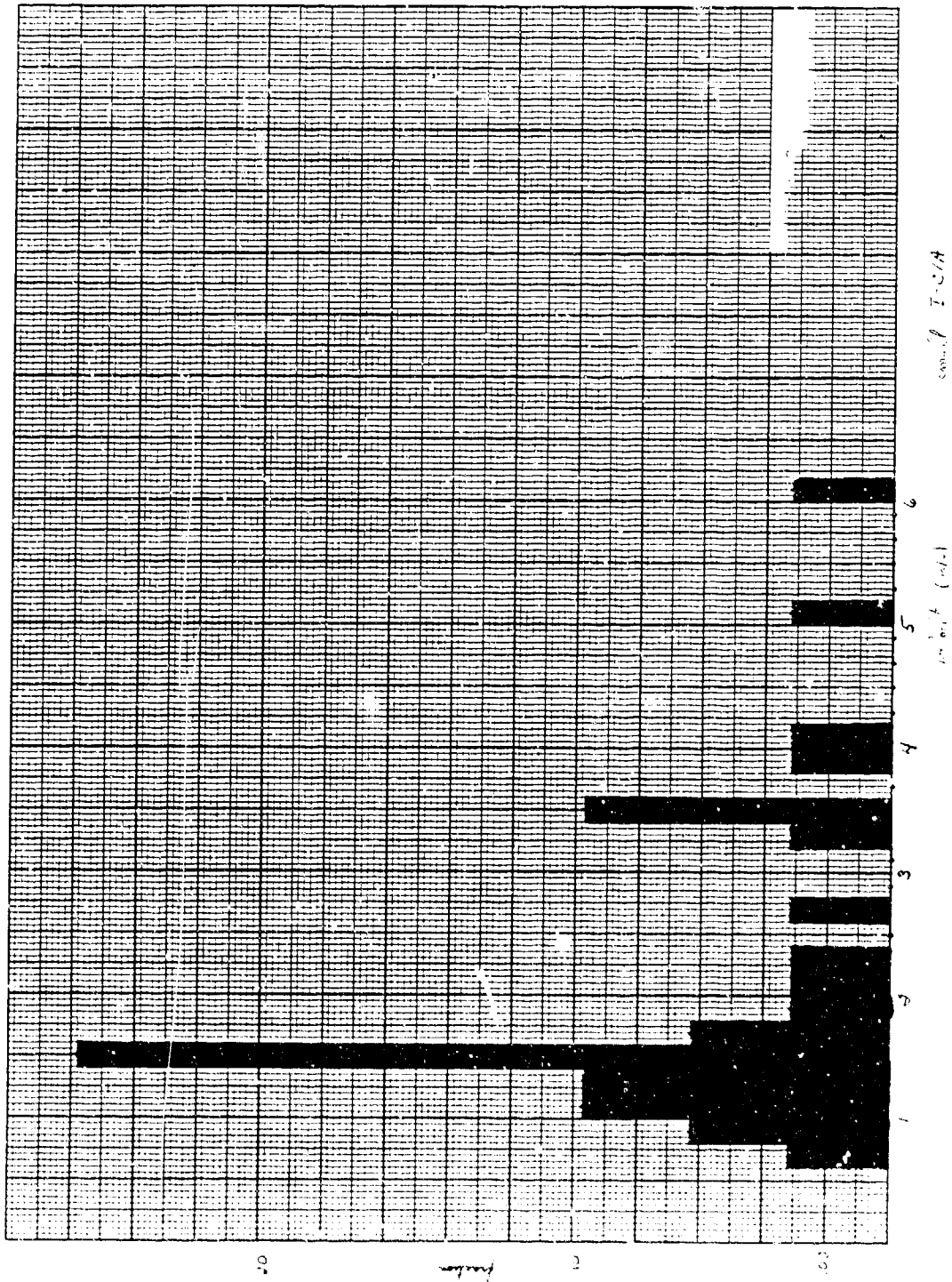


Figure B2. Test 1C1A, Single-Wheel Baseline Small Stones, Velocity Distribution.

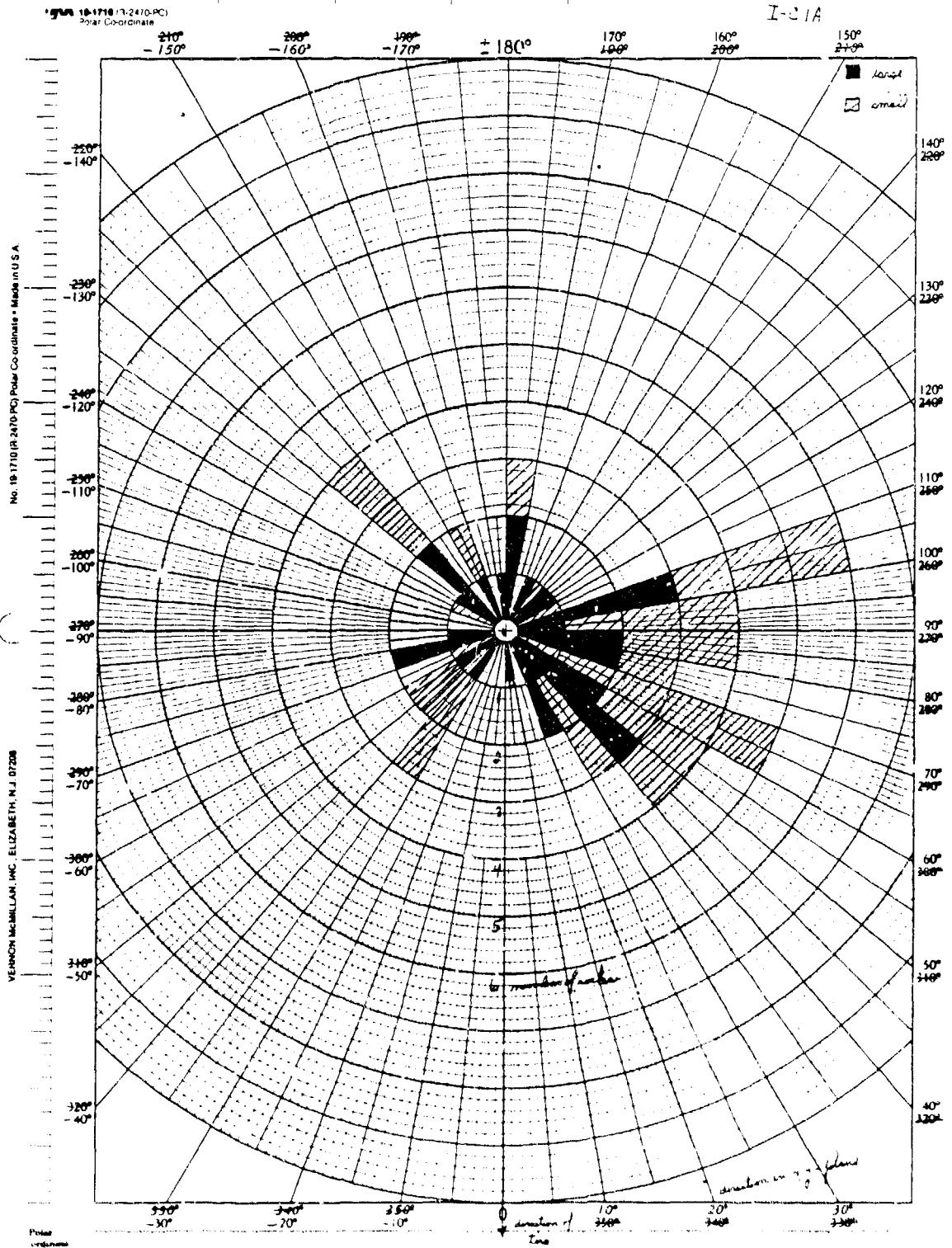


Figure 33. Test I-C1A, Single-Wheel Baseline, All Stones, Direction Distribution.

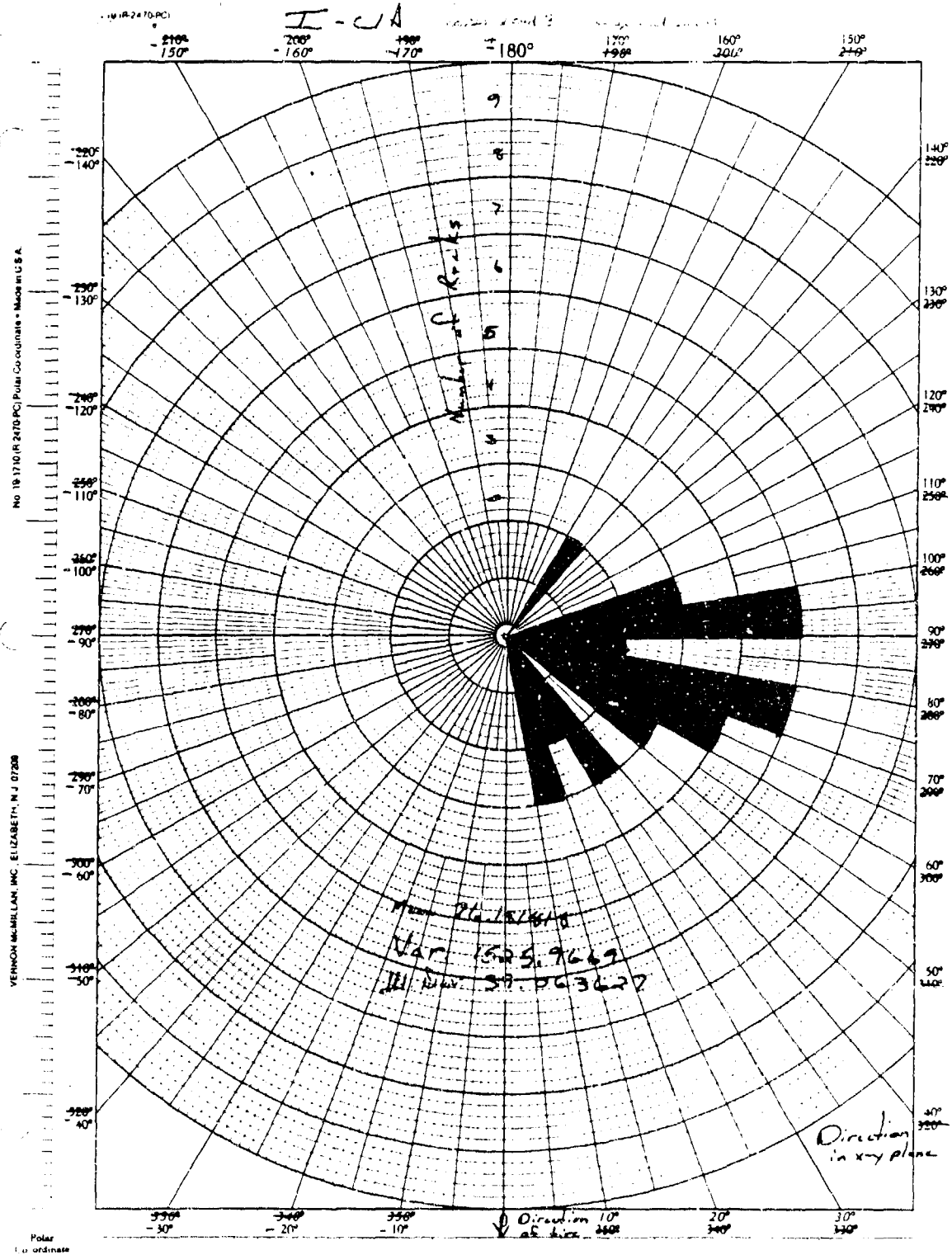


Figure B4. Test 1C1A, Single-Wheel Baseline, All Stones, Passes 2 and 3, Direction Distribution.

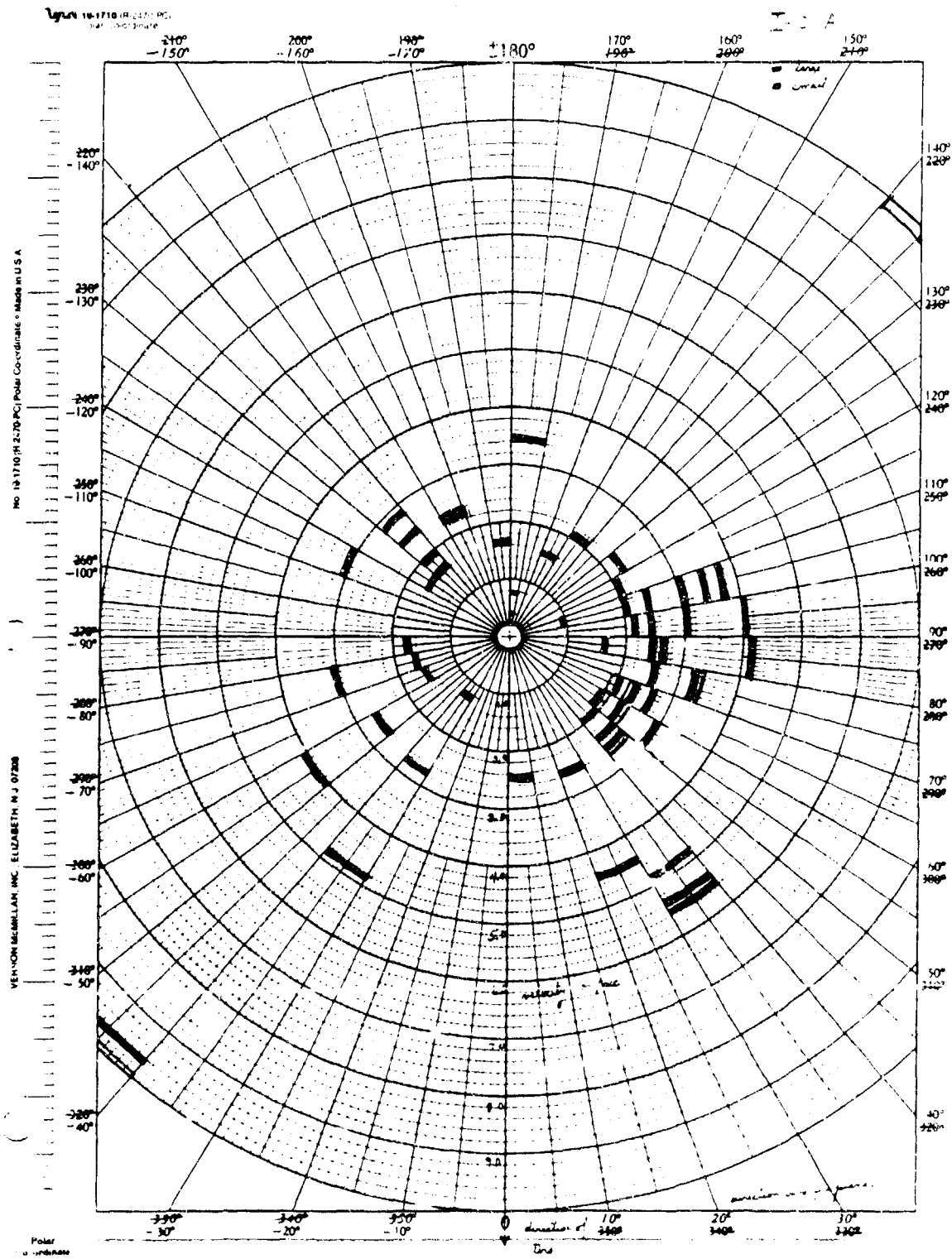


Figure B5. Test 1CLA, Single-Wheel baseline, All Stores, Distribution of Velocity Direction.

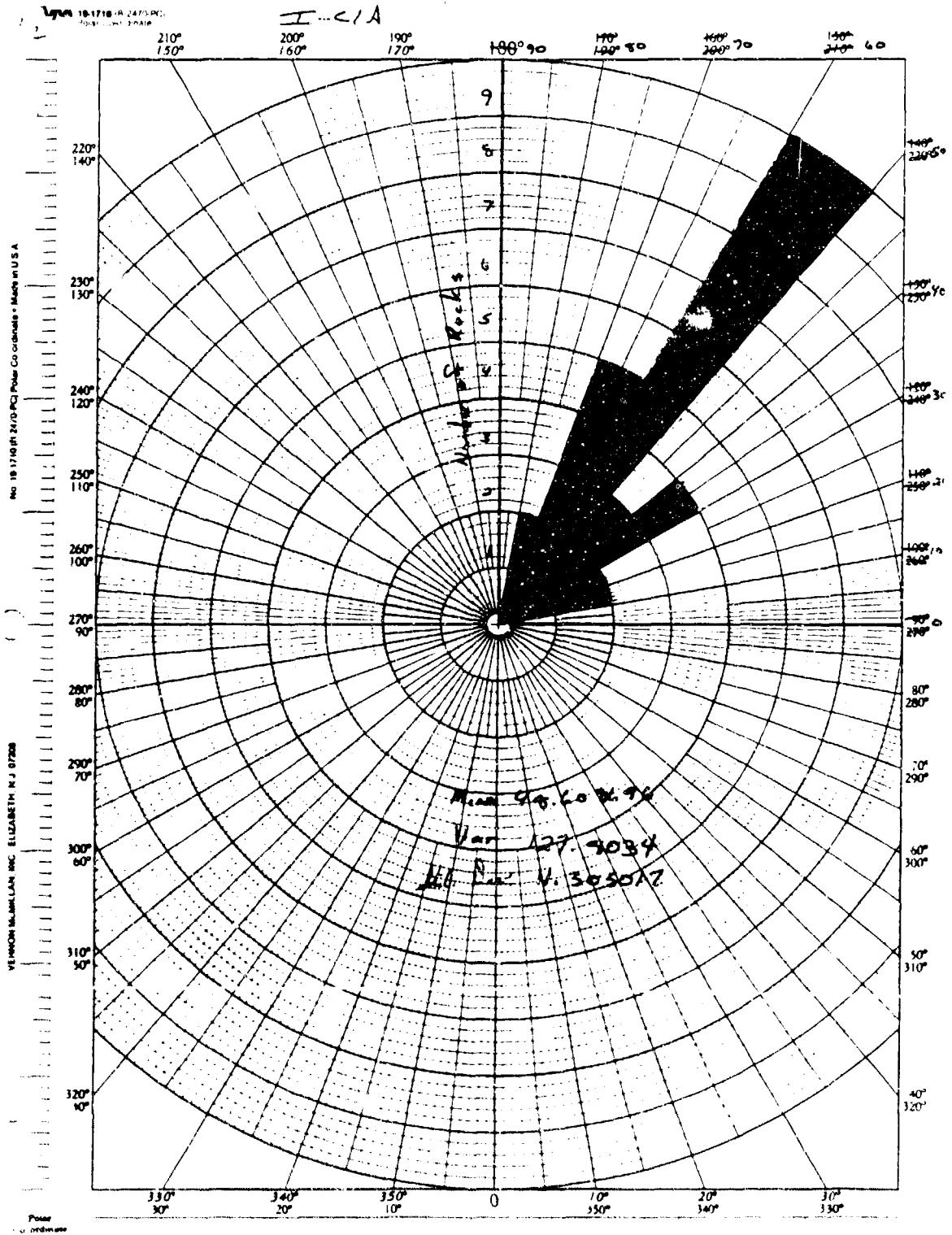


Figure B6. Test 1CIA, Single-Wheel Baseline, Large Stones, Elevation Angle Distribution.

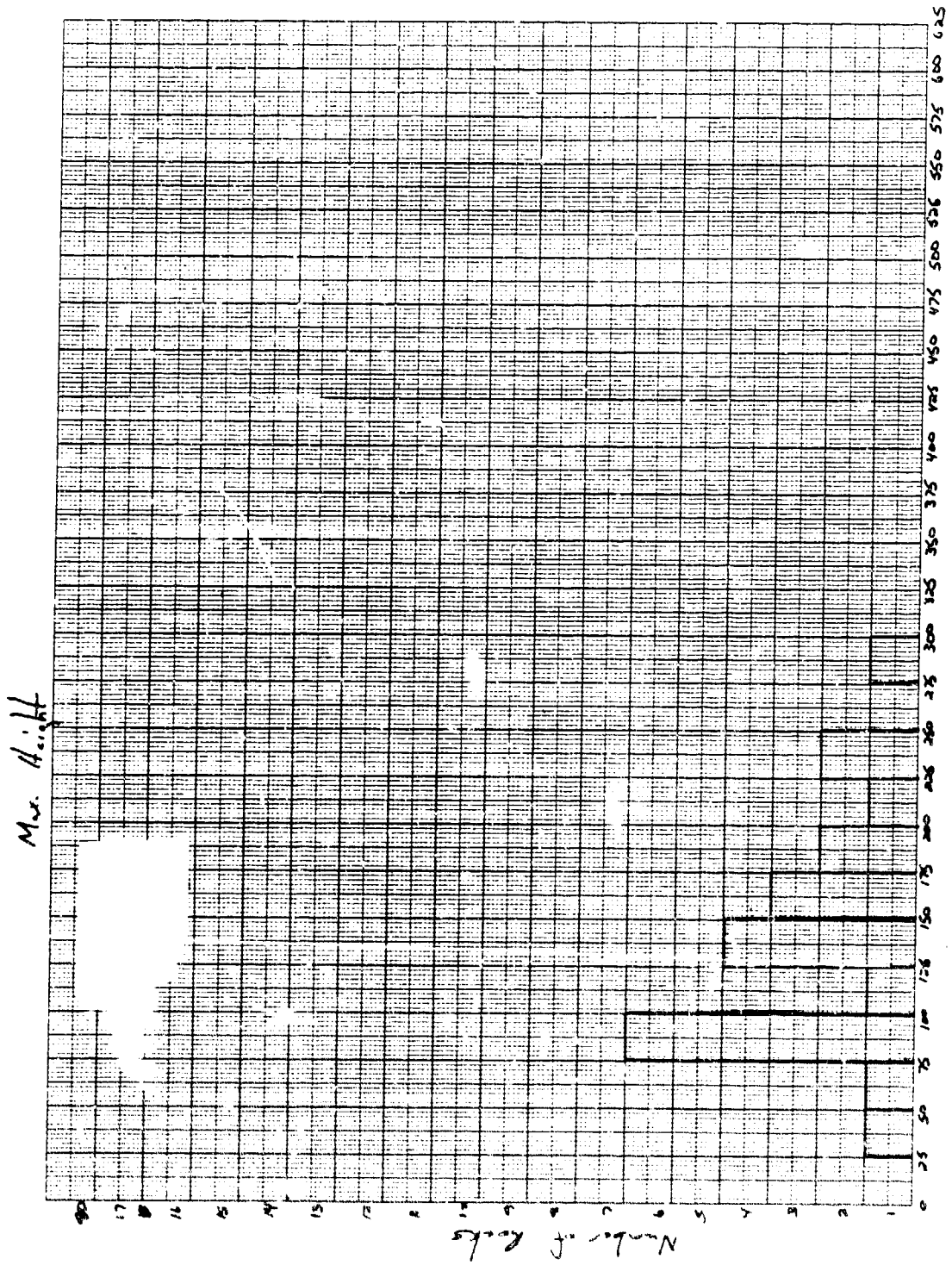


Figure B7. Test 1CiA, Single Wheel Baseline, Large Stones, Maximum Height Distribution.

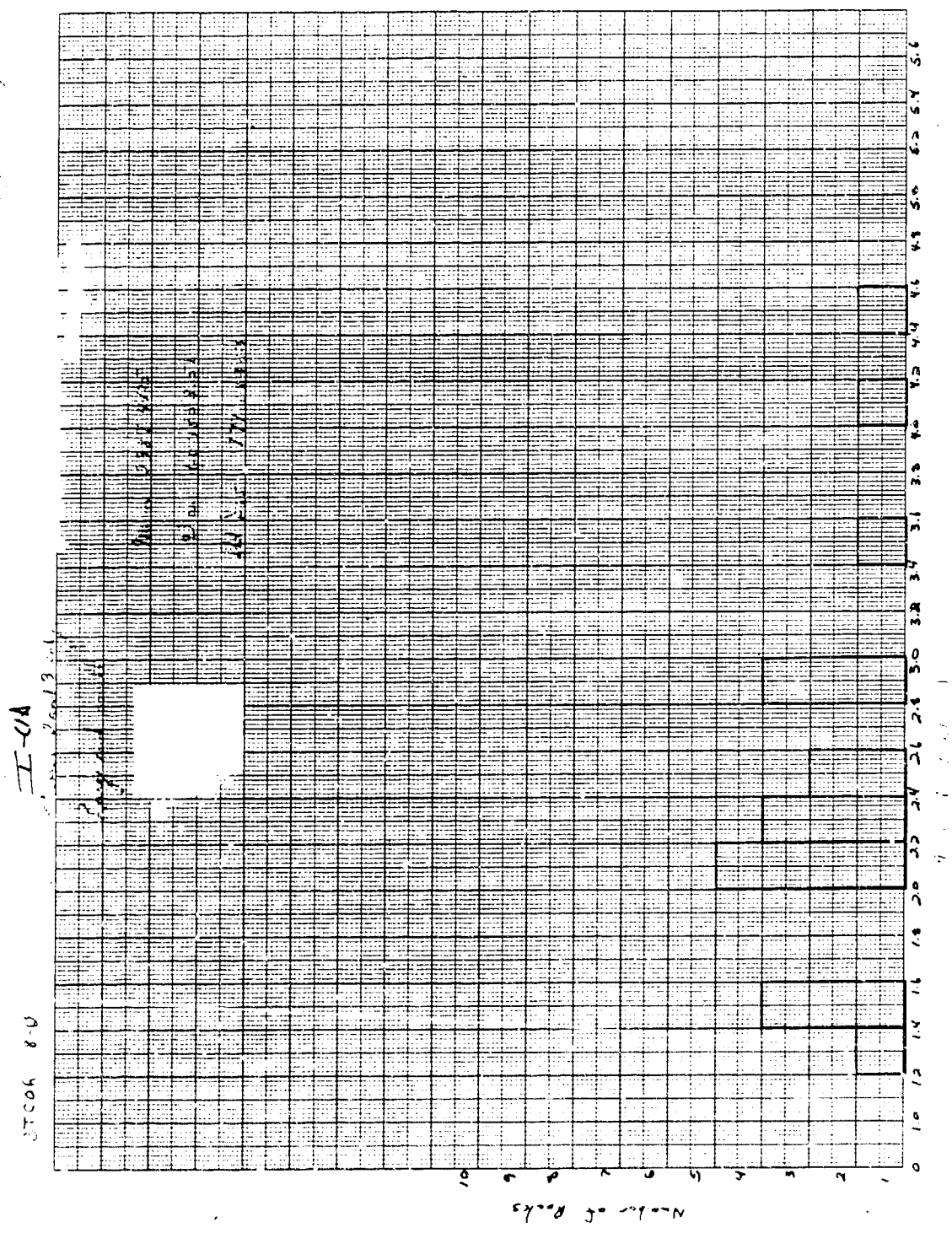


Figure B8. Test 1CLA, Single-Wheel Baseline, All Stones, Passes 2 and 3 Only, Velocity Distribution.

I-241

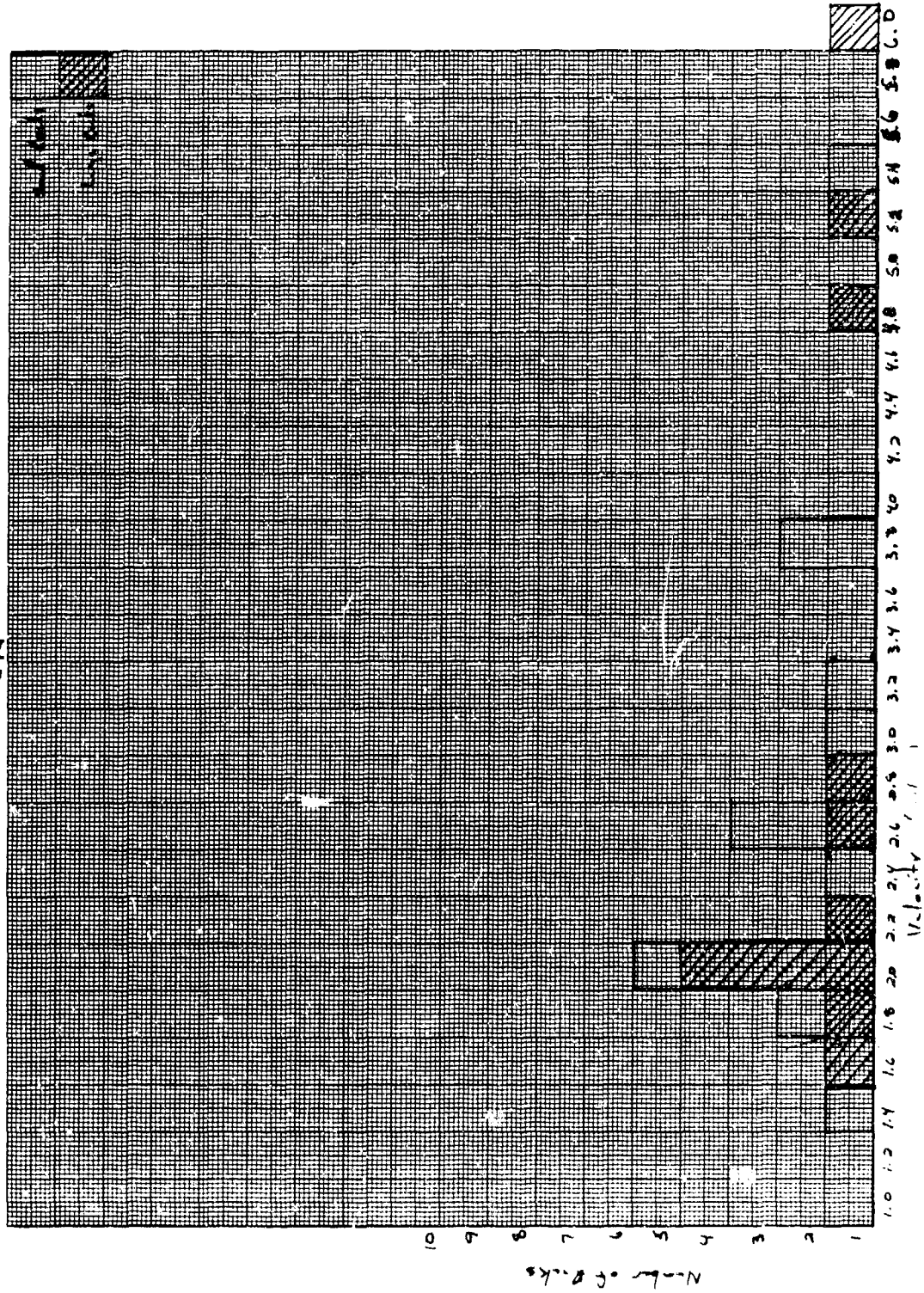


Figure B9. Test 1C4A, Single-Wheel, Low-Velocity, All Stones, Velocity Distribution.

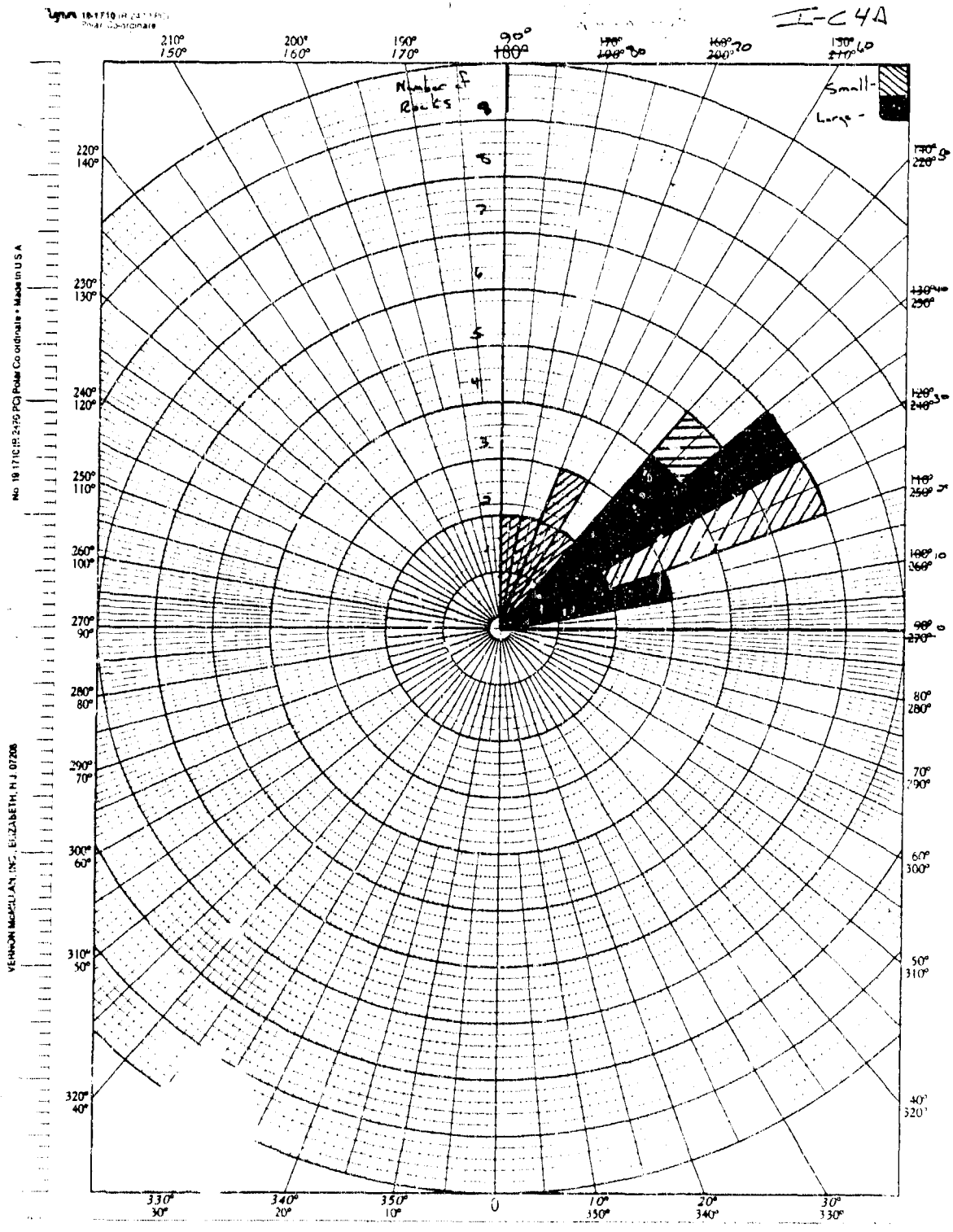


Figure B10. Test IC4A, Single-Wheel, Low-Velocity, All Stones, Elevator Angle Distribution.

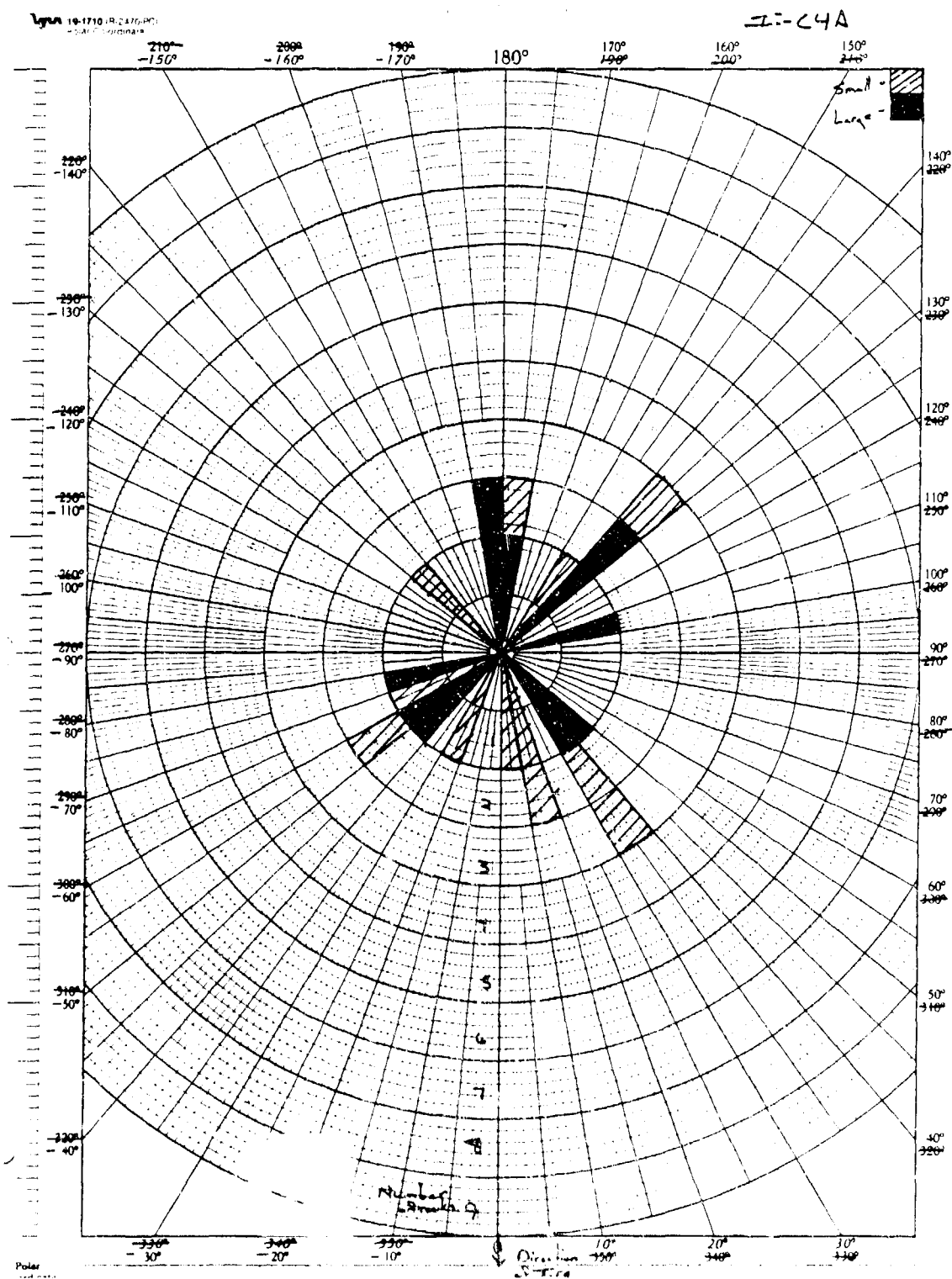


Figure B11. Test 1C4A, Single-Wheel, Low Velocity, All Stones, Direction Distribution.

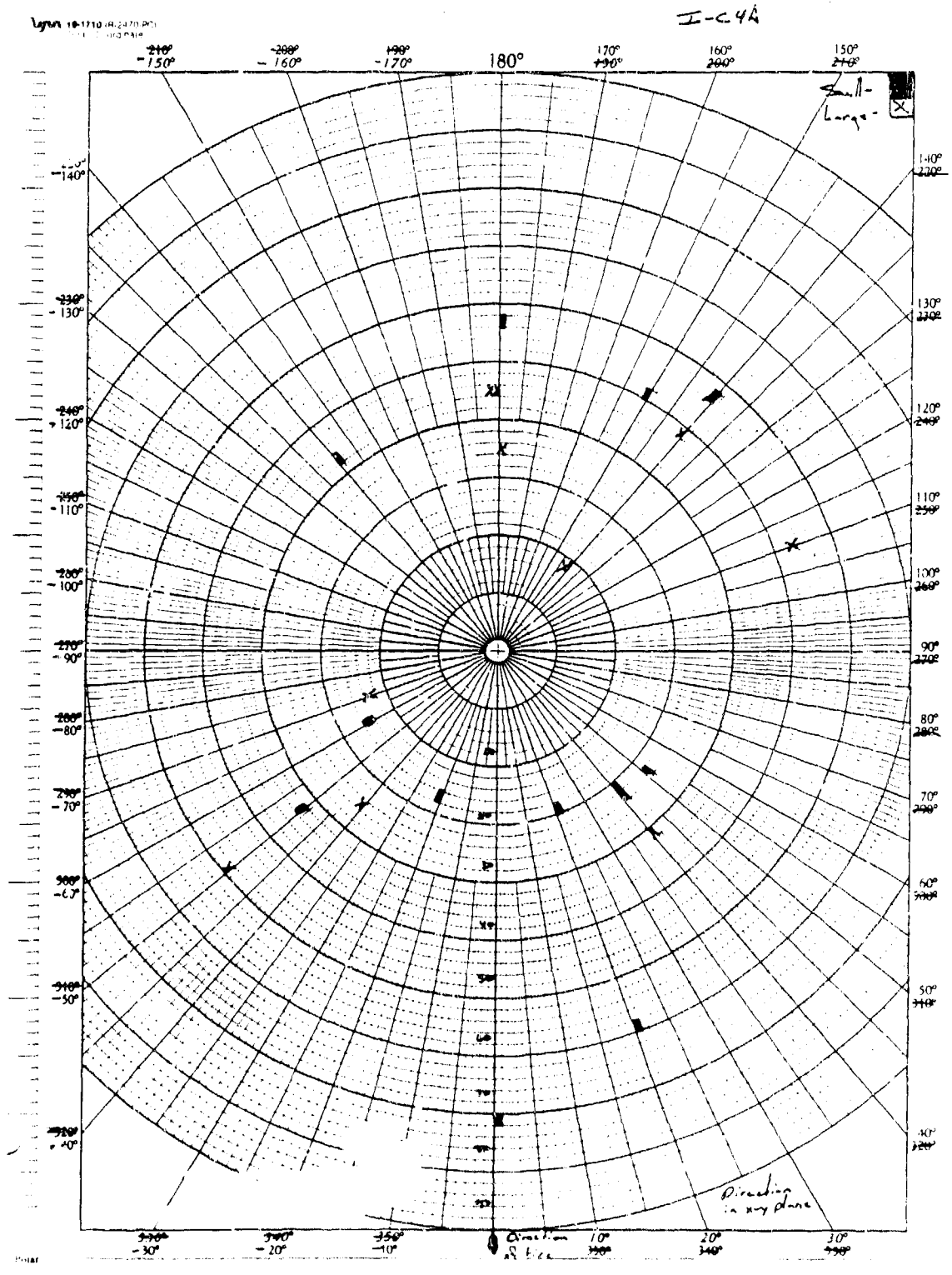


Figure B12. Test IC4A, Single-Wheel, Low-Velocity, All Stones, Direction and Elevation Distribution.

I-26

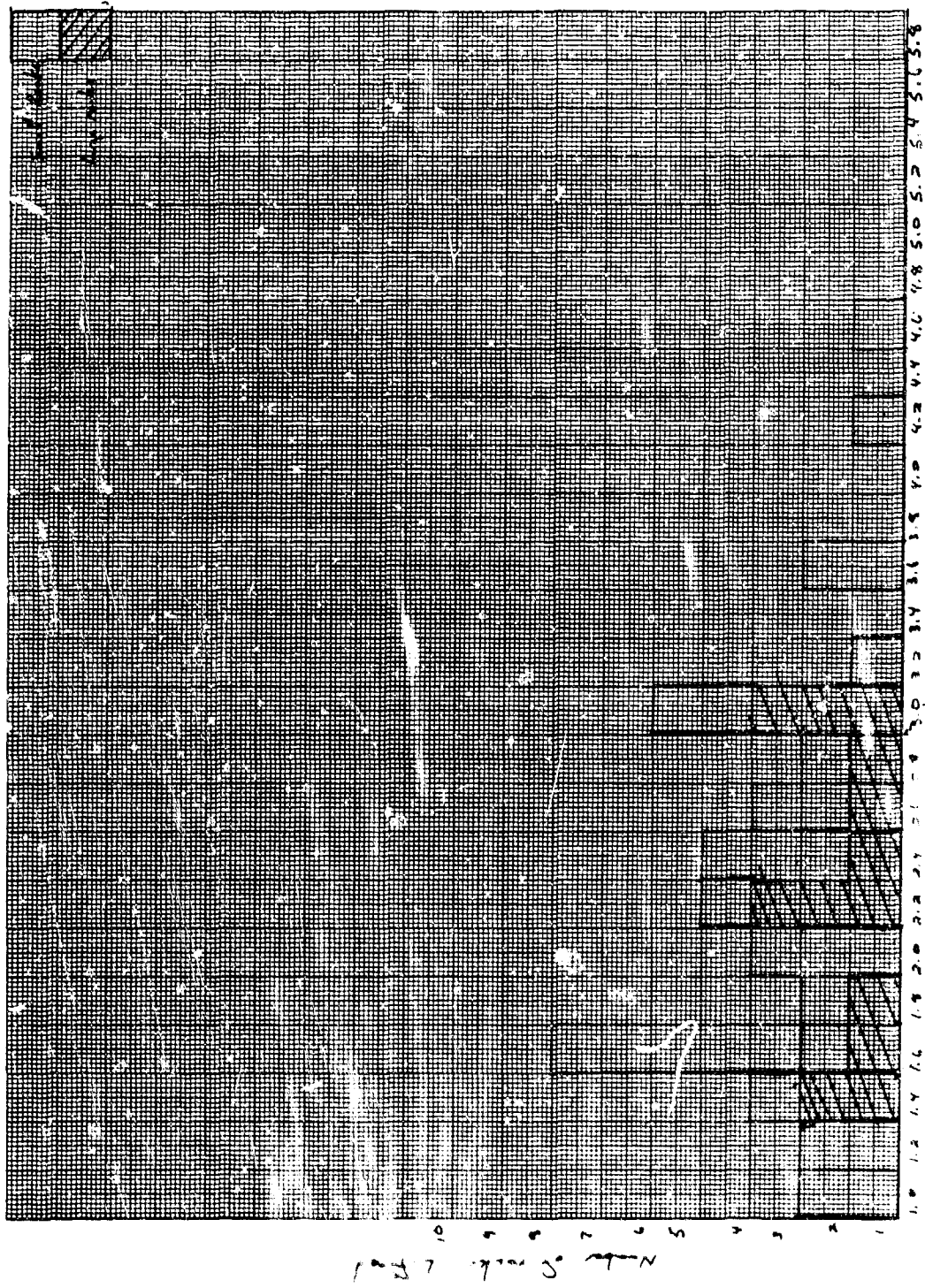


Figure B13. Test 1C6, Single wheel, low pressure, All Stones, Velocity Distribution.

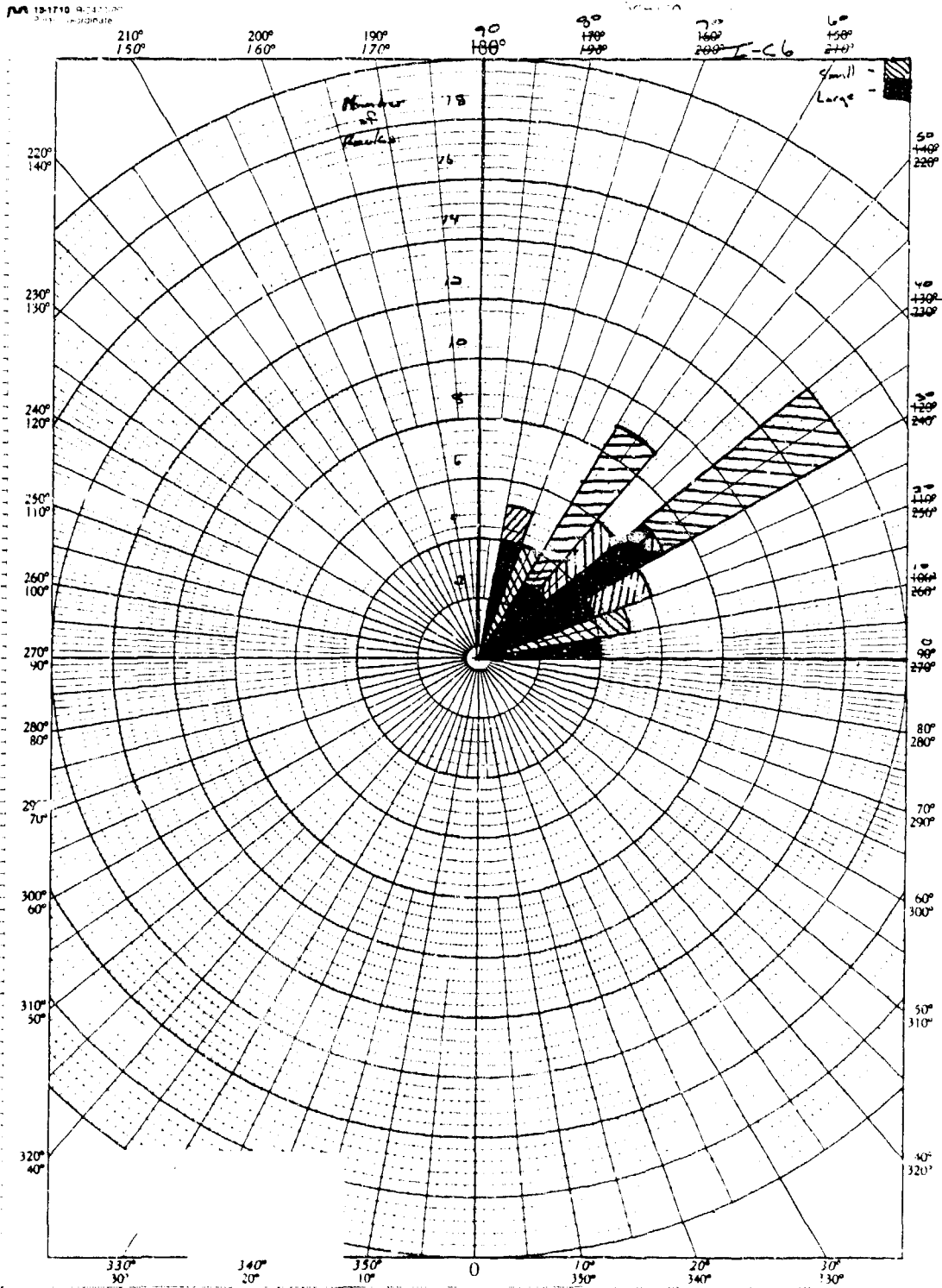


Figure B14. Test 1C6, Single Wheel, Low-Pressure, All Stones, Elevation Angled Distribution.

Lynn 10-1710 (R2470 PC)
Polar Coordinate

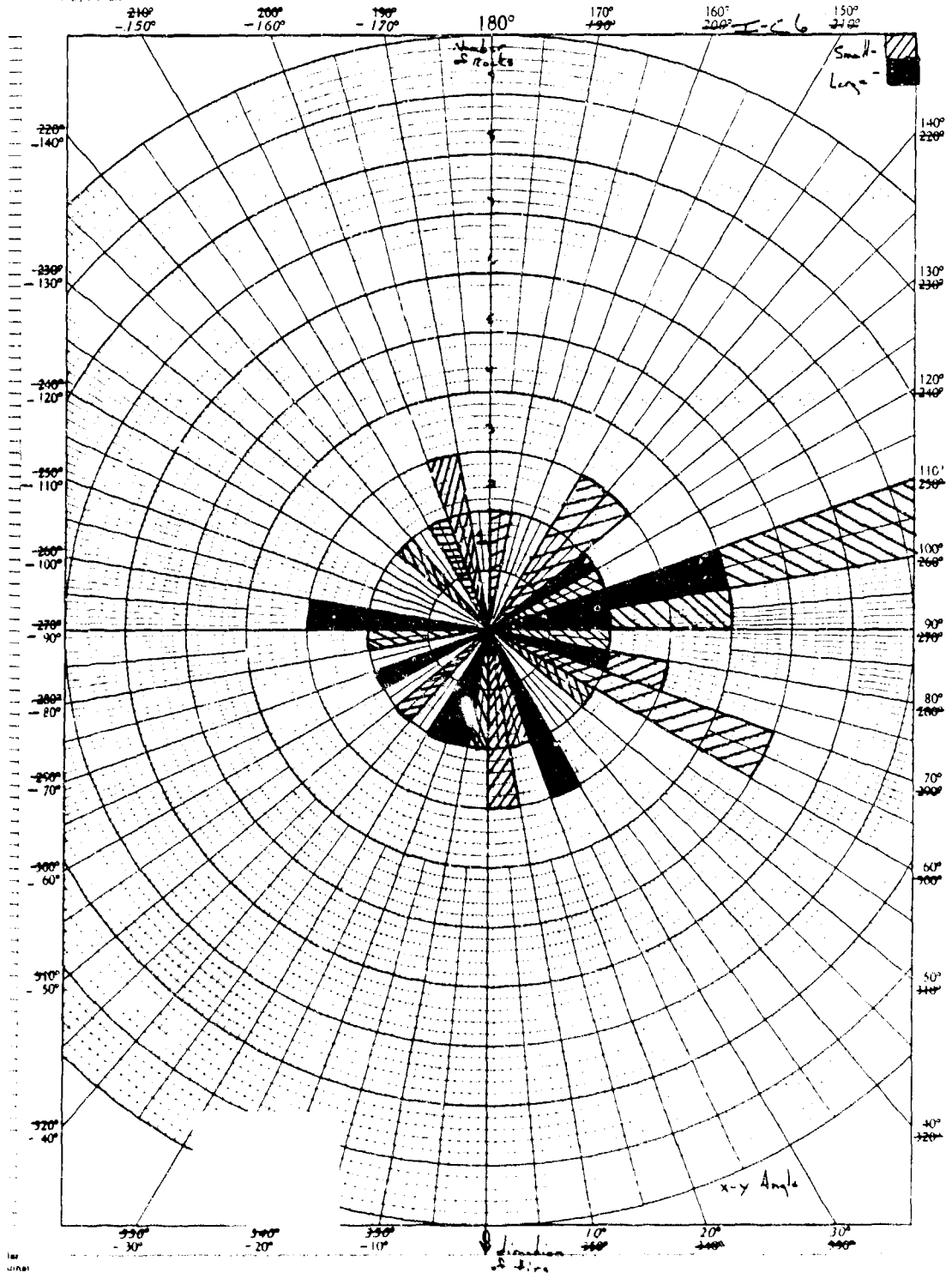


Figure B15. Test 1C6, Single-Wheel, Low-Pressure, All Stones, Direction Distribution.

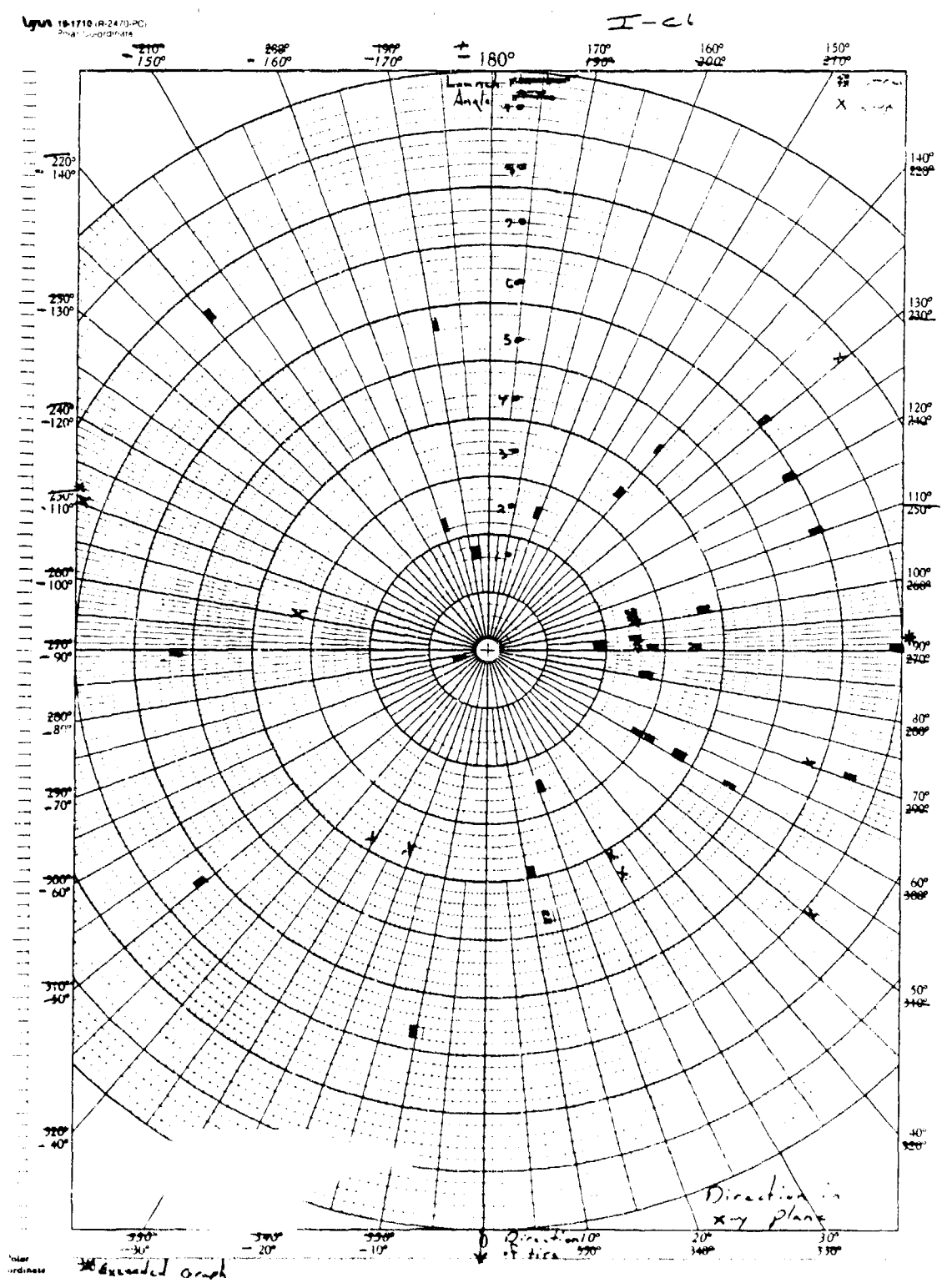


Figure B16. Test 106, Single-Wheel, Low Pressure, All Stones, Direction and Elevation Distribution.

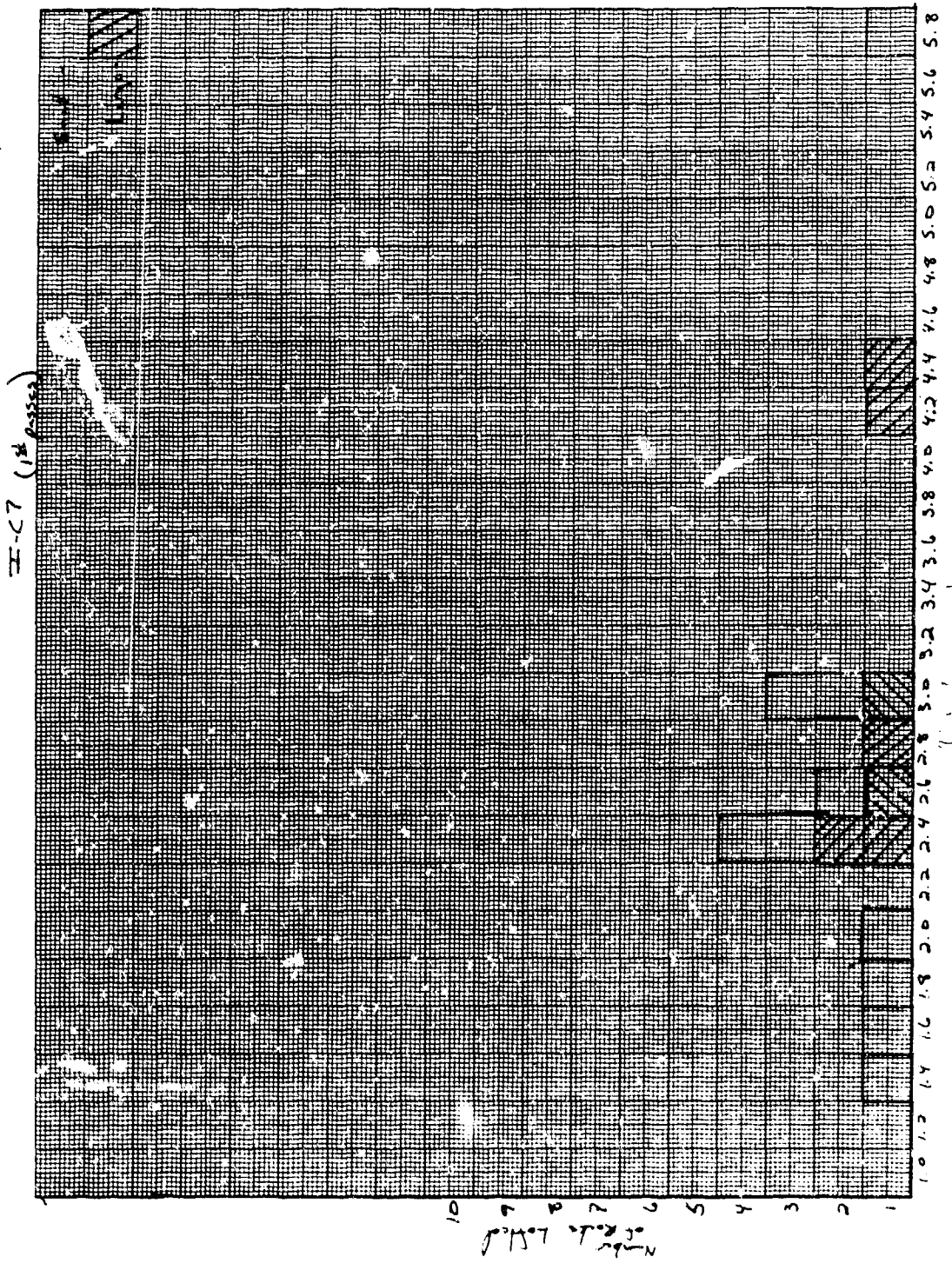


Figure B17. Test IC7, Single Wheel, Very Low-Pressure, All Stones, Velocity Distribution.

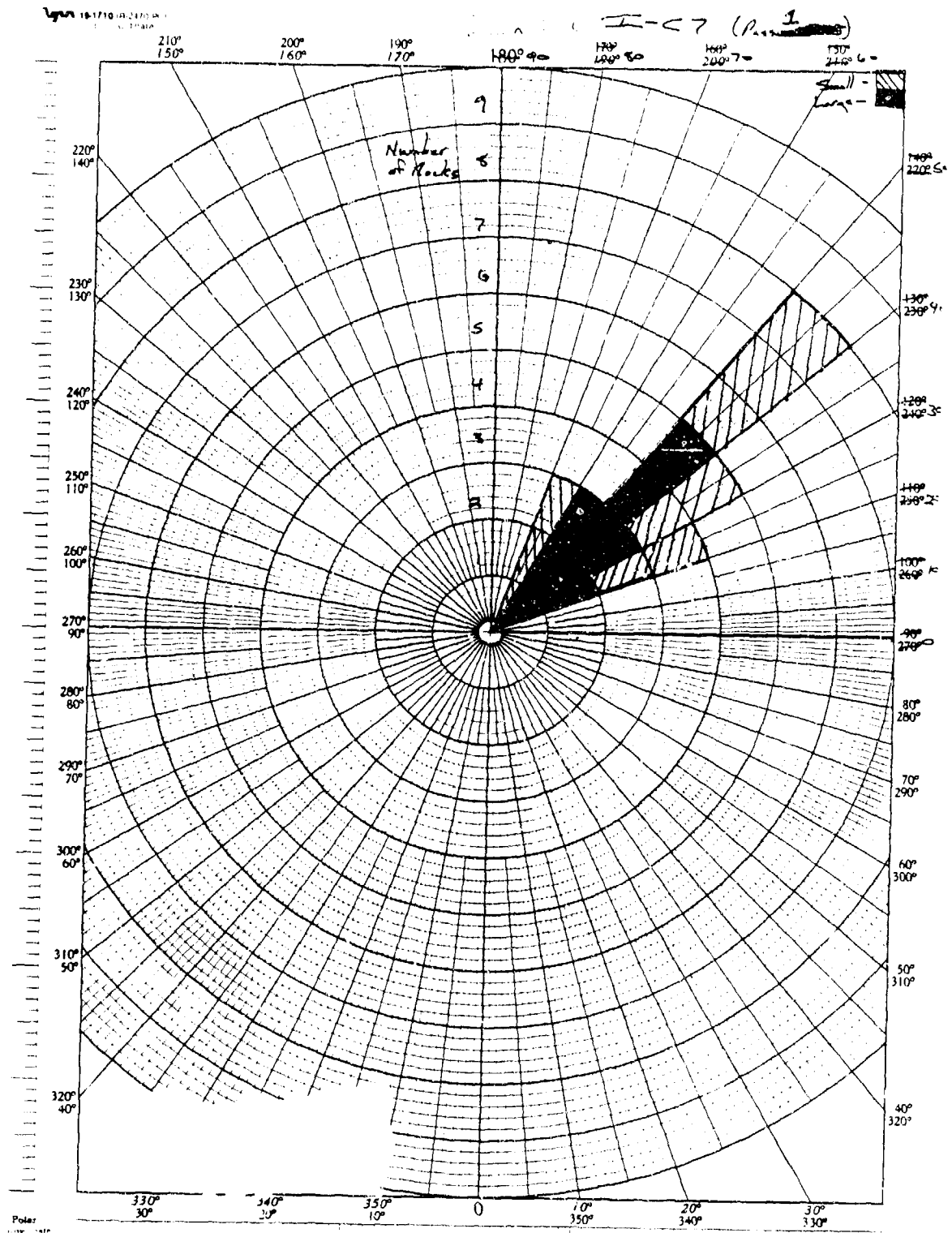


Figure B18. Test IC7, Single-Wheel, Very Low-Pressure, All Stones, 1 Pass Only, Elevation Angle Distribution.

I-17 (Passes 2+3)

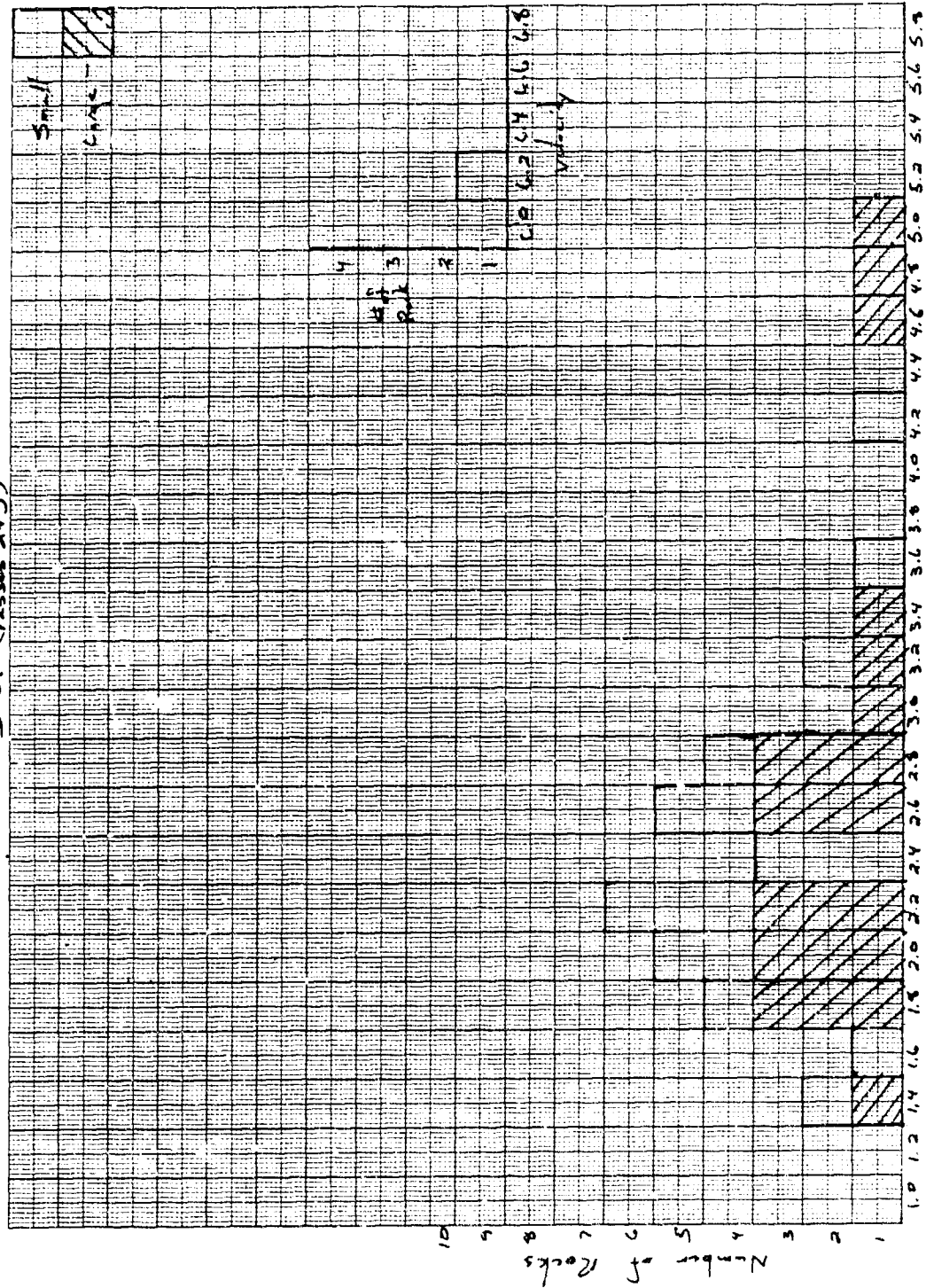


Figure B20. Test 1C7, Single Wheel, Very Low Pressure, All Stones, Velocity Distribution.

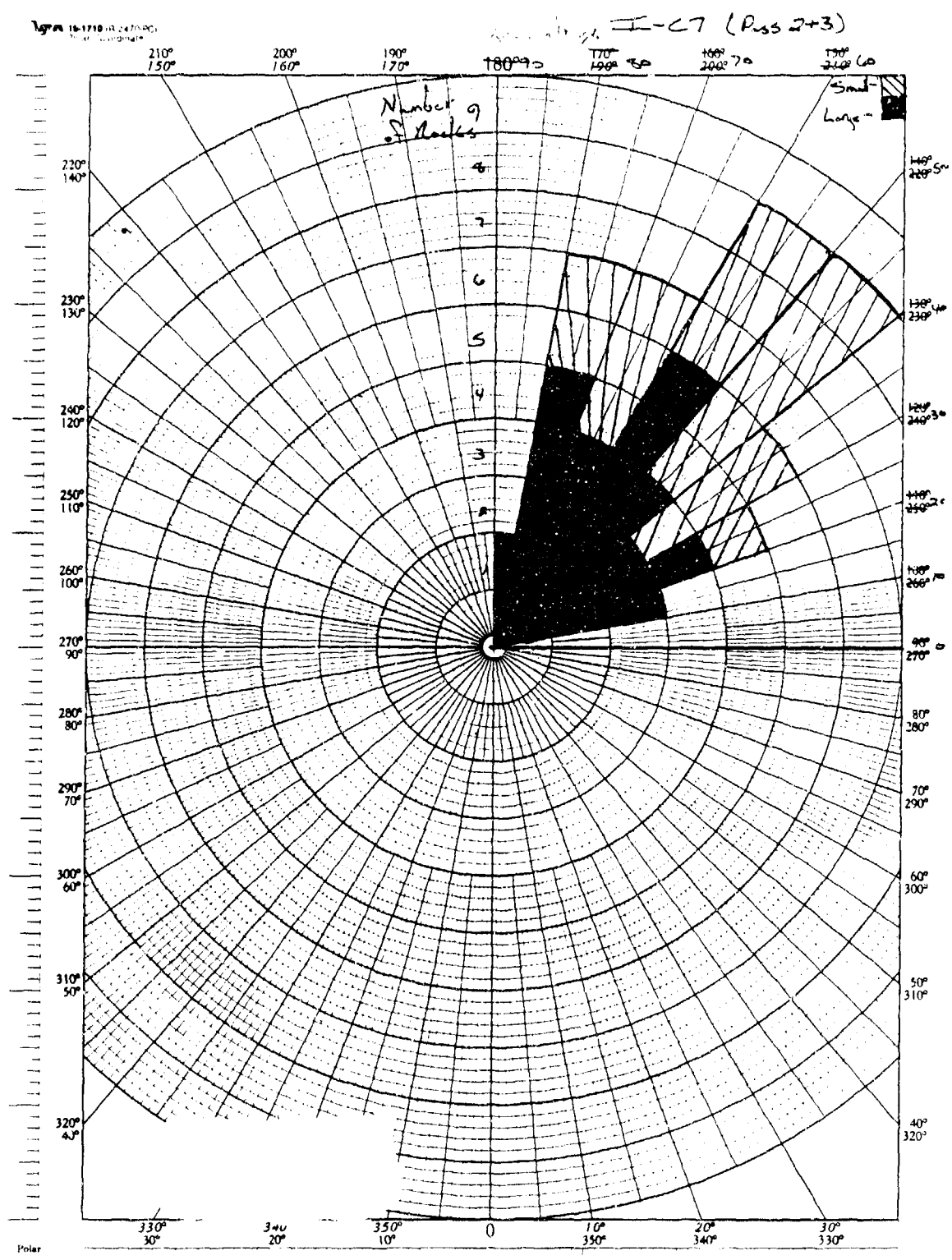


Figure B21. Test I-27, Single Wheel, Very Low Pressure, All Stones, Passes 2 & 3, Elevation Angle Distribution.

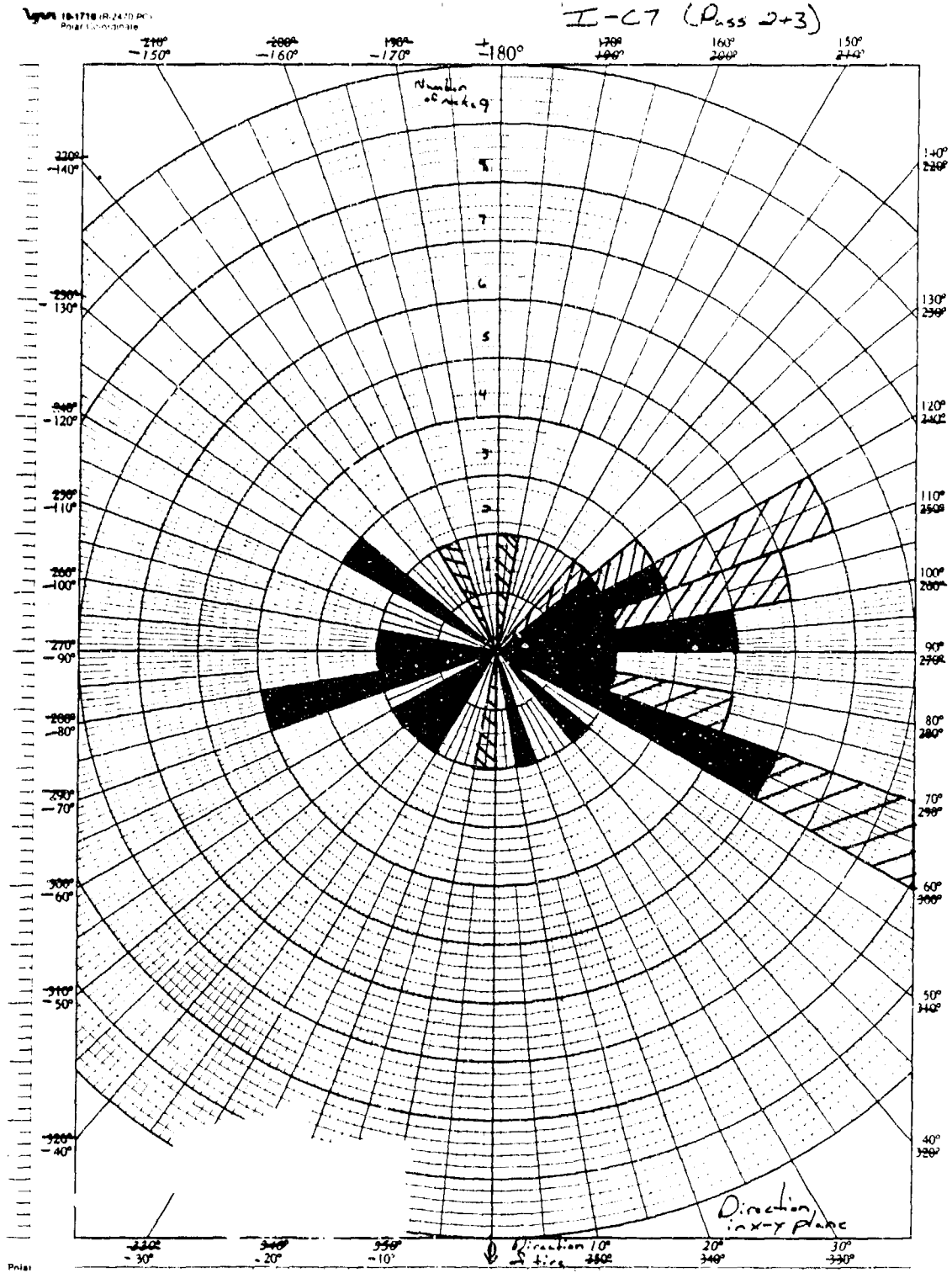


Figure B22. Test IC7, Single-Wheel, Very Low-Pressure, All Stones, Passes 2 & 3, Direction Distribution.

EE-67 (1/2 page)

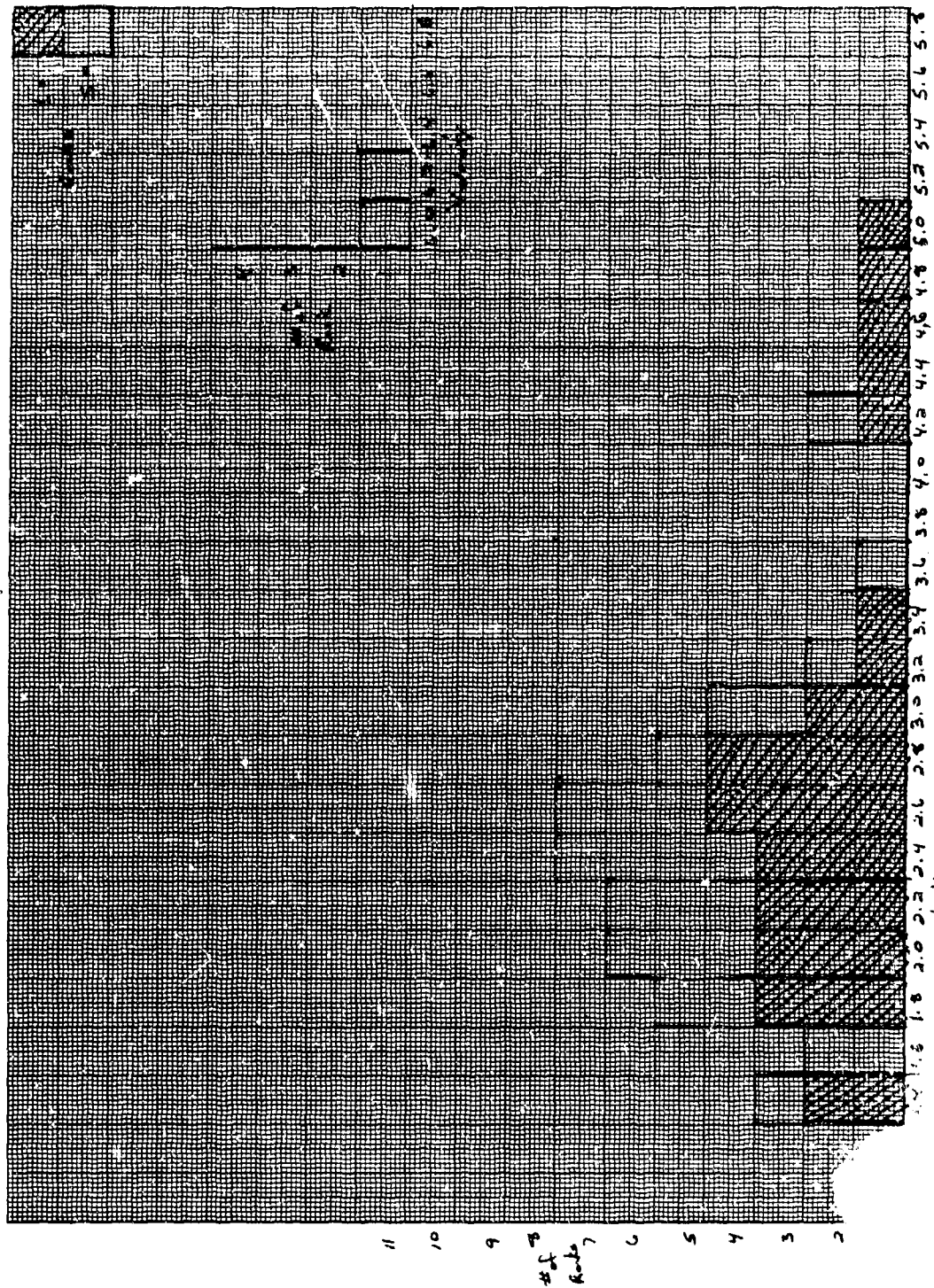


Fig. 107, Single Wheel, Very Low-Pressure, All Stones, Velocity Distribution.

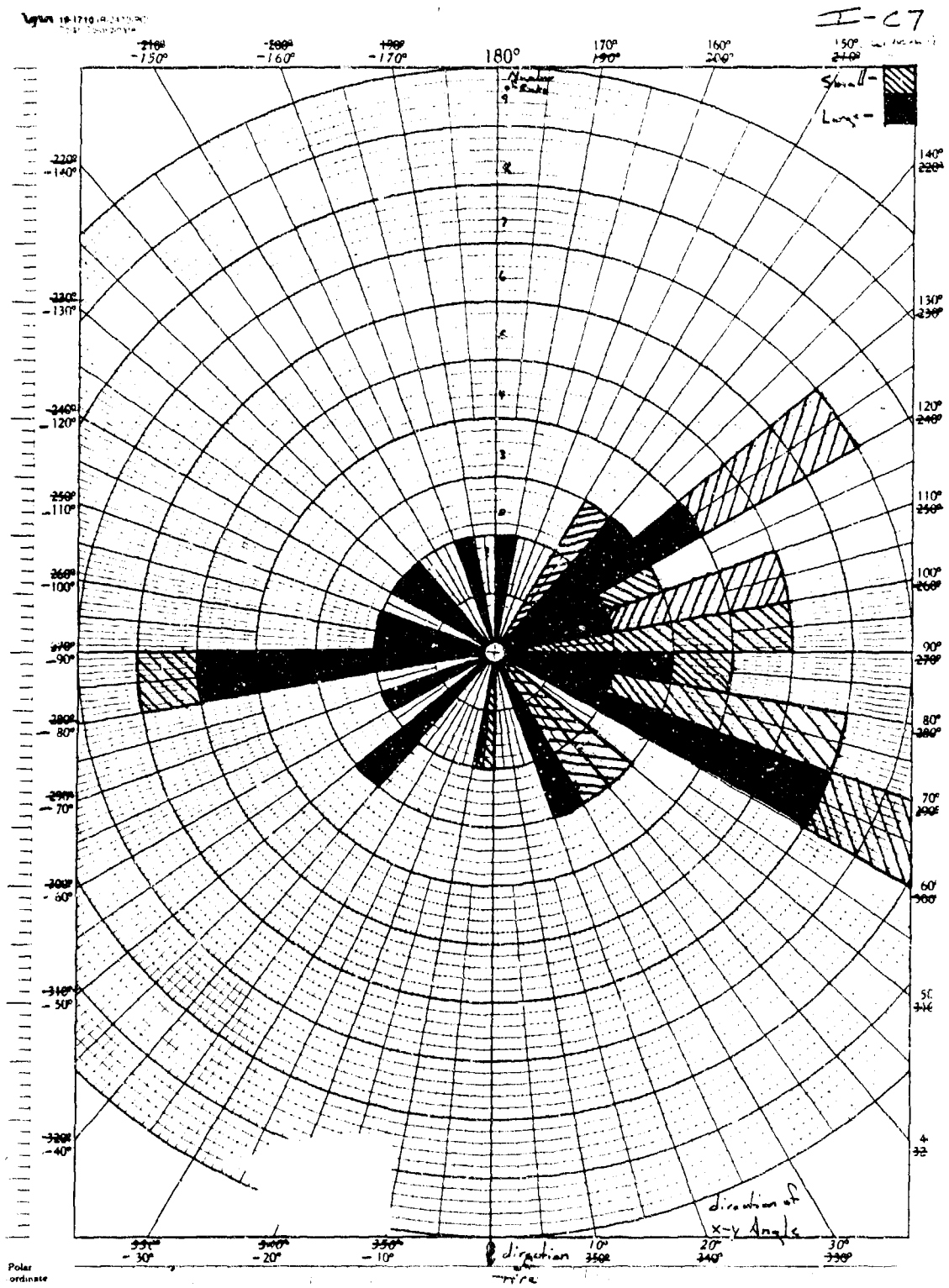


Figure B25. Test IC7, Single Wheel, Very Low-Pressure, All Stones, Direction Distribution.

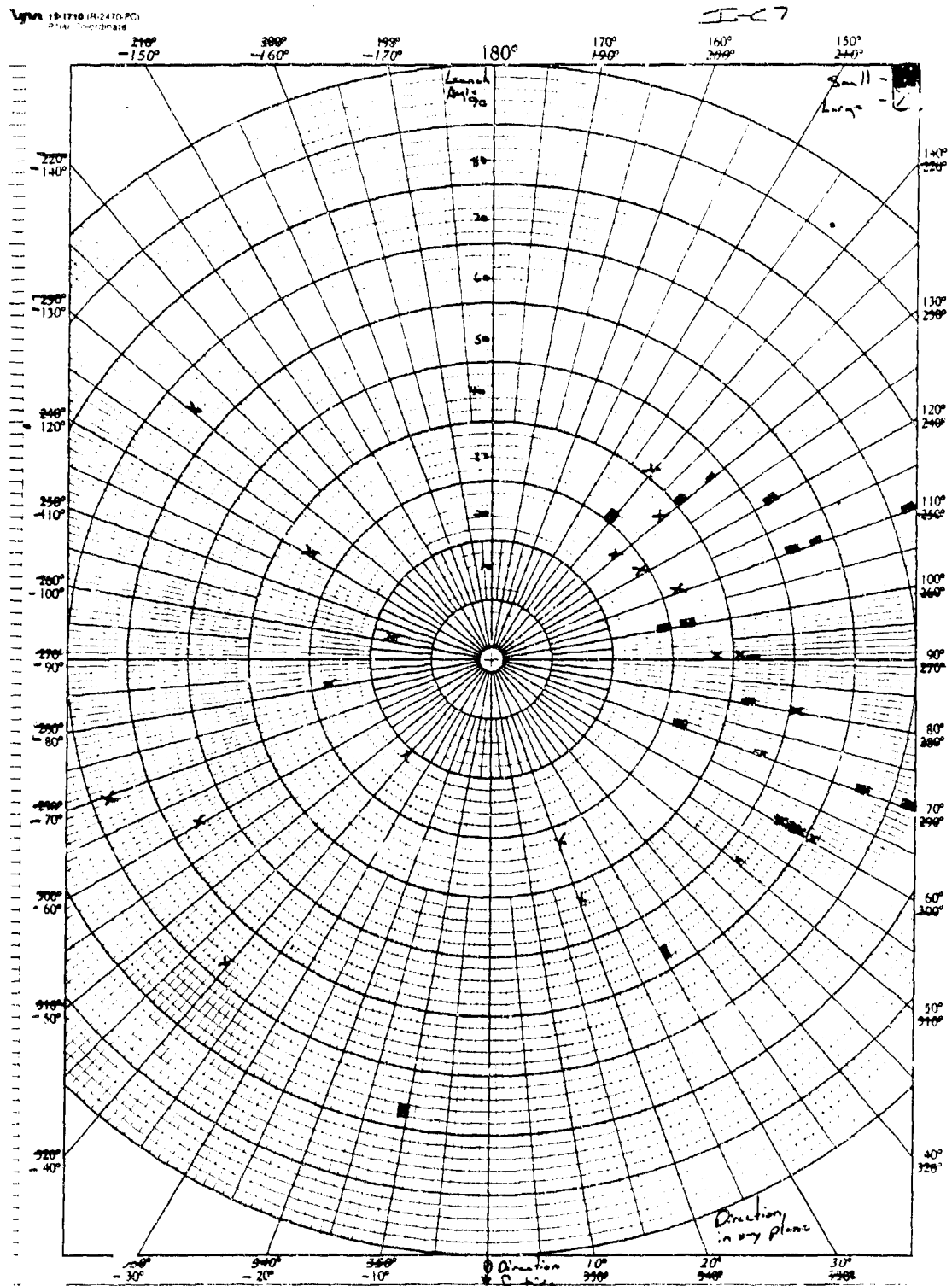


Figure B26. Test 1C7, Single-Wheel, Very Low Pressure, All Stones, Direction and Elevation Distribution.

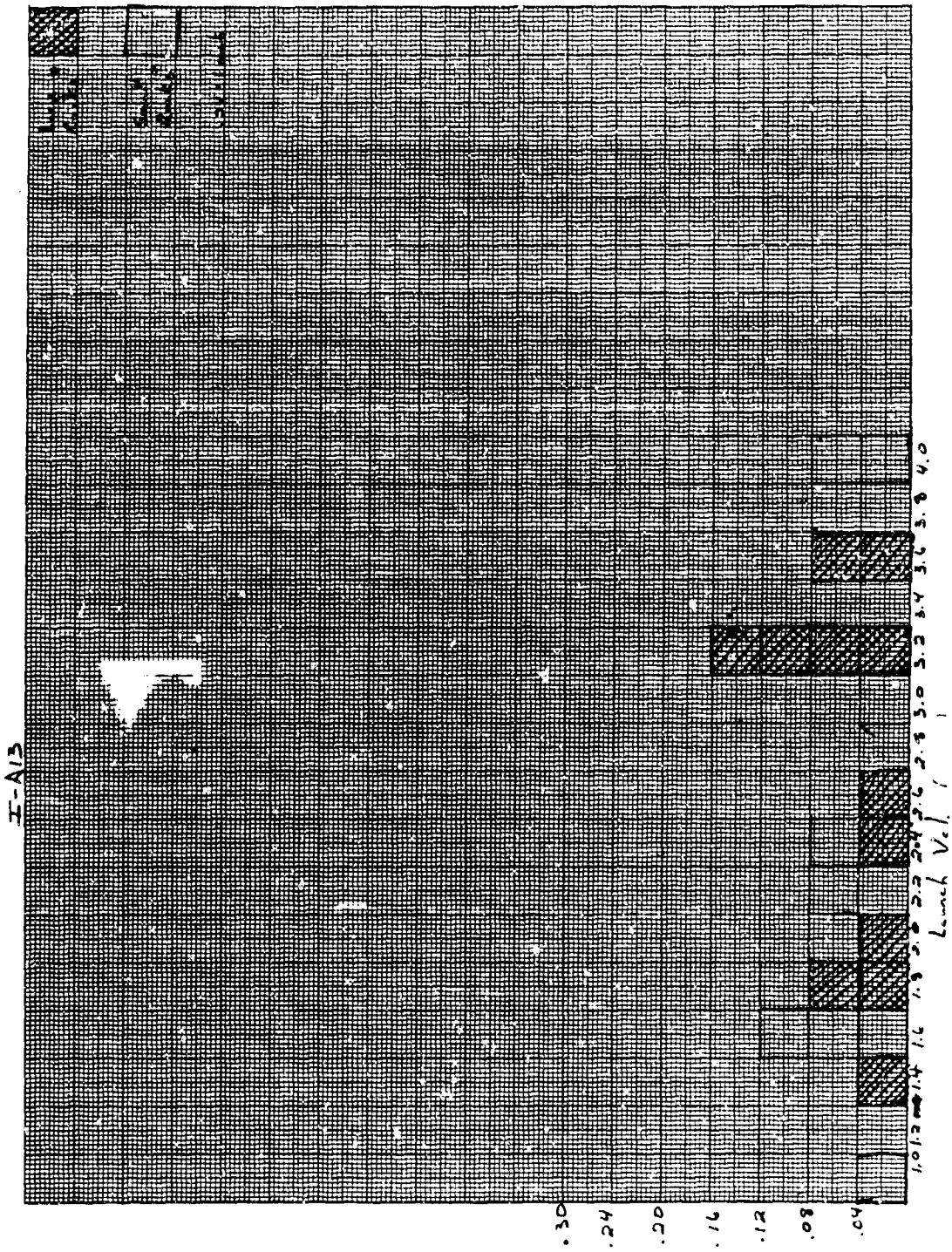


Figure B27. Test I-A13, Baseline, Single-Wheel, Aggregate Bed, All Stones, Velocity Distribution.

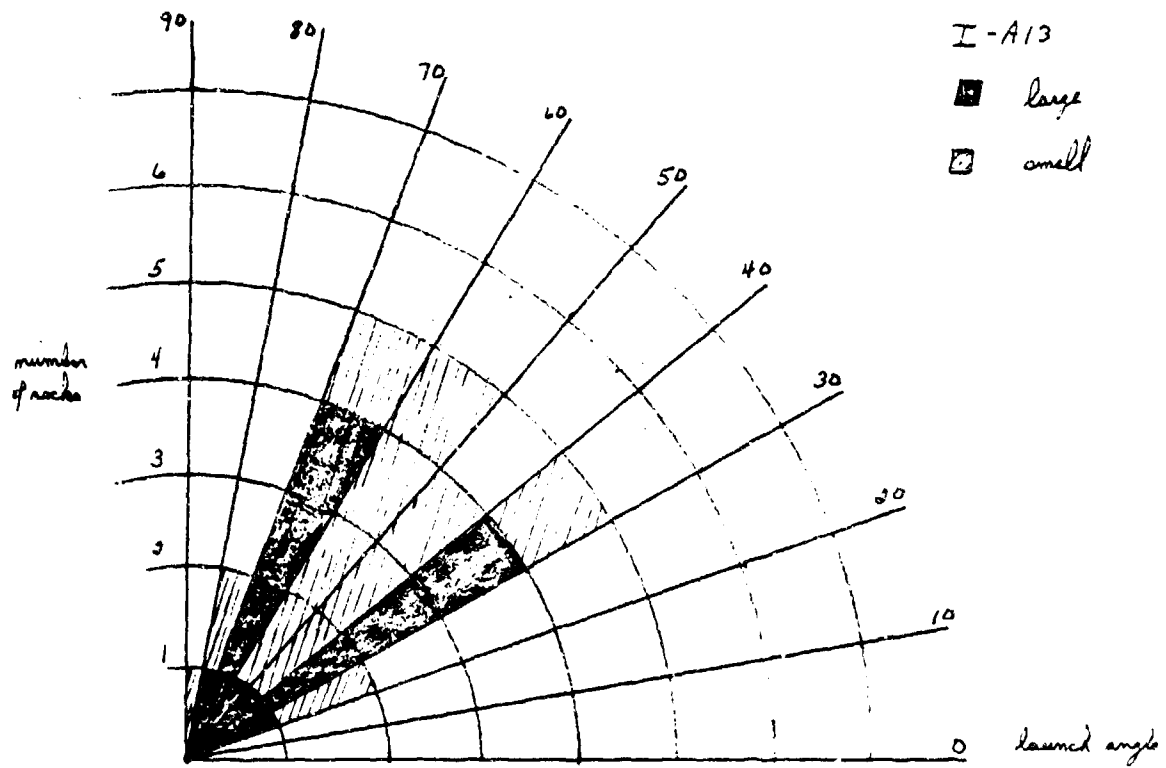


Figure B28. Test 1A13, Baseline, Single-Wheel, Aggregate Bed, All Stones, Elevation Angle Distribution.

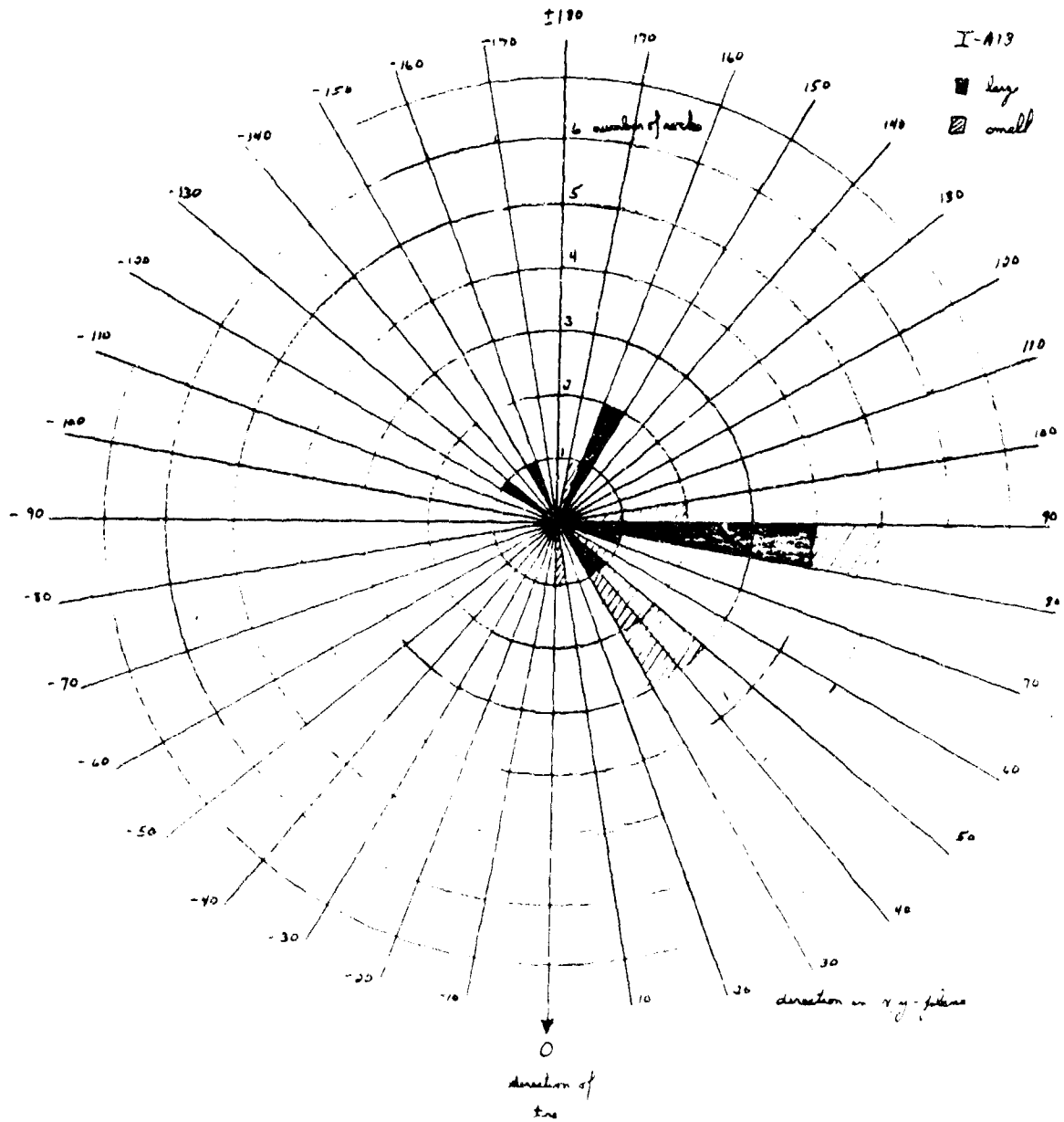


Figure B29. Test 1A13, Baseline, Single-Wheel, Aggregate Bed, All Stones, Elevation Angle Distribution.

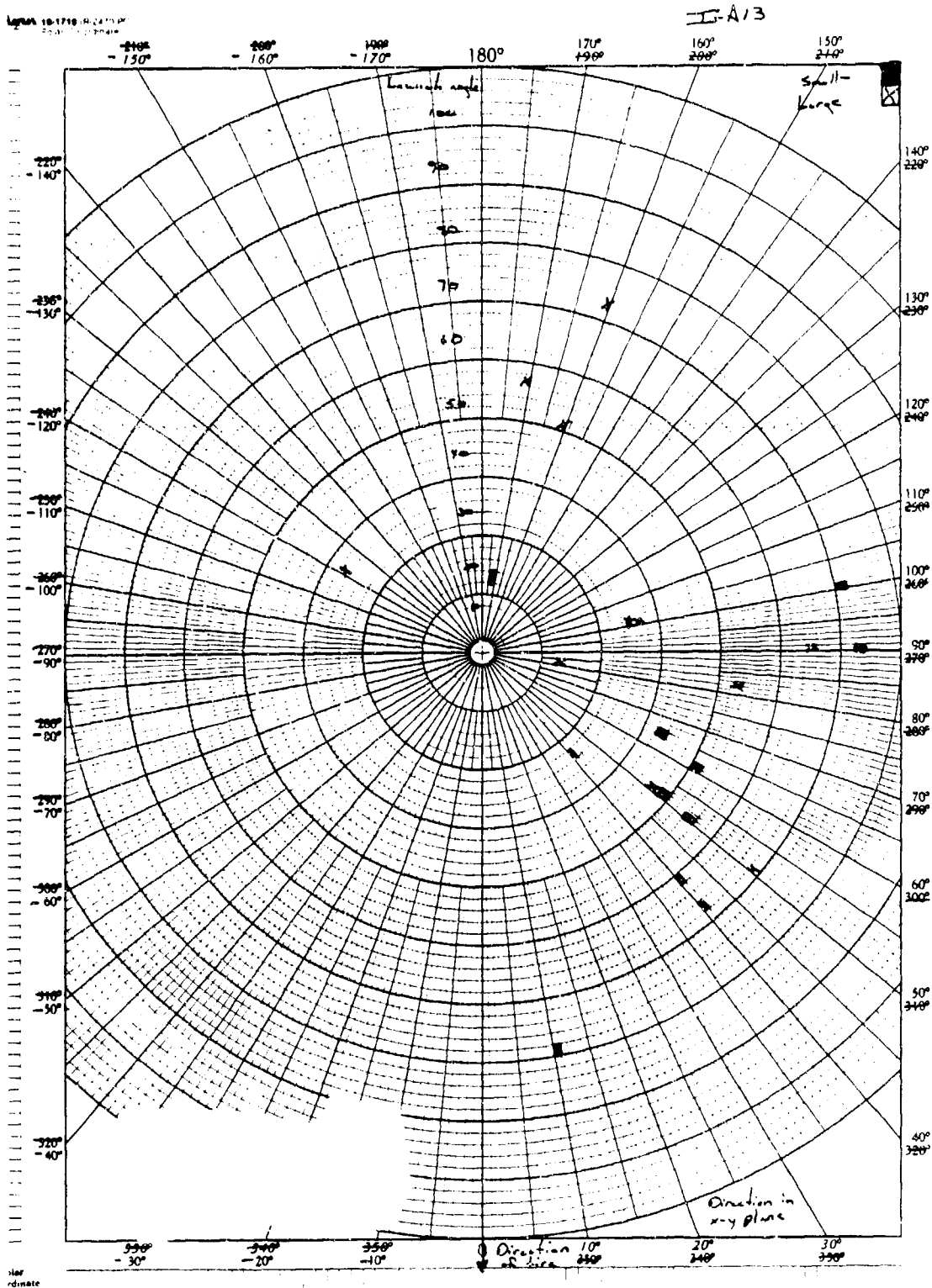


Figure B30. Test IA13, Baseline, Single-Wheel, Aggregate Bed, All Stones, Direction and Elevation Distribution.

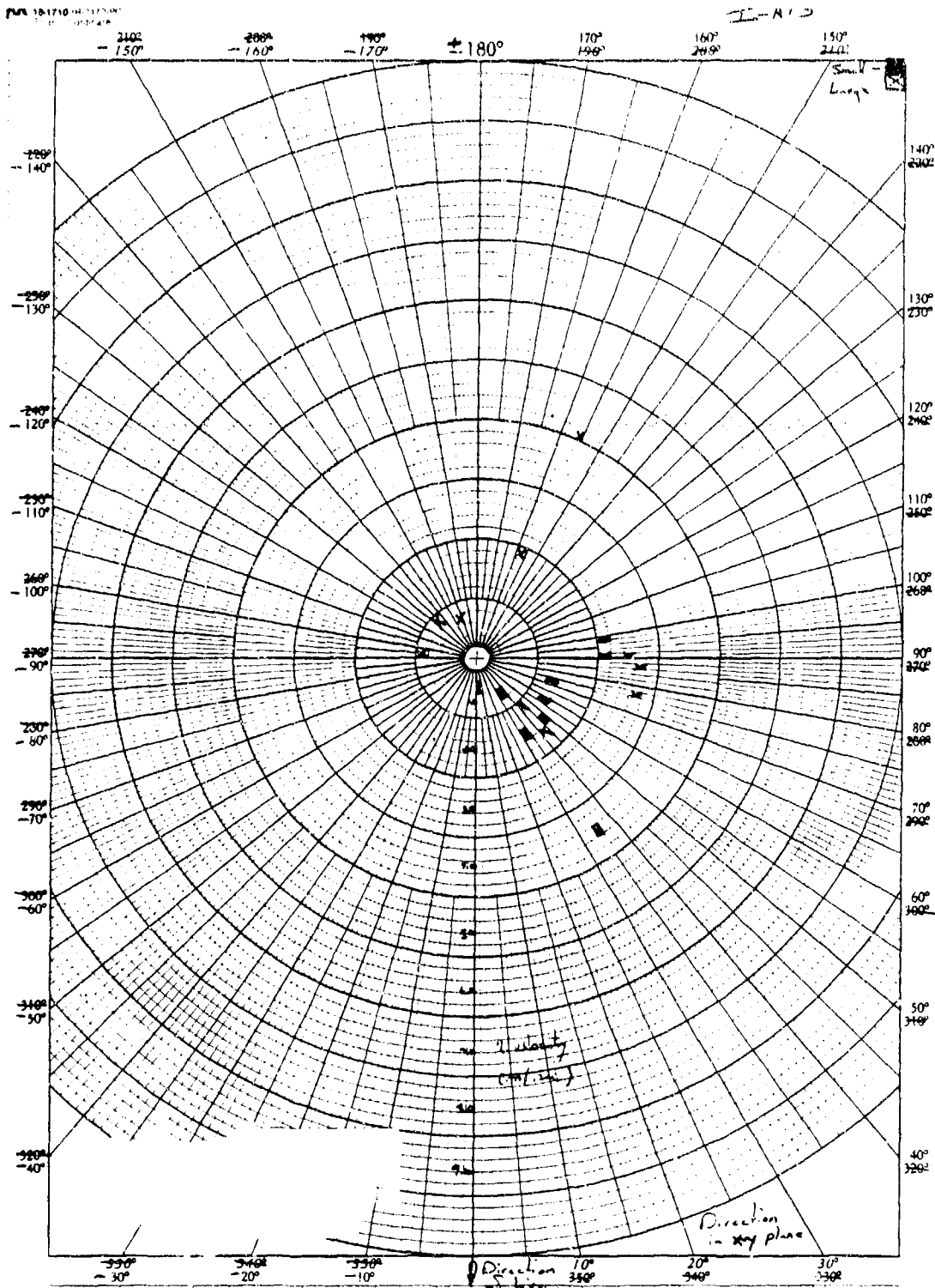


Figure B31. Test IA13, Baseline, Single-Wheel, Aggregate Bed, All Stones, Velocity and Direction Correlation.

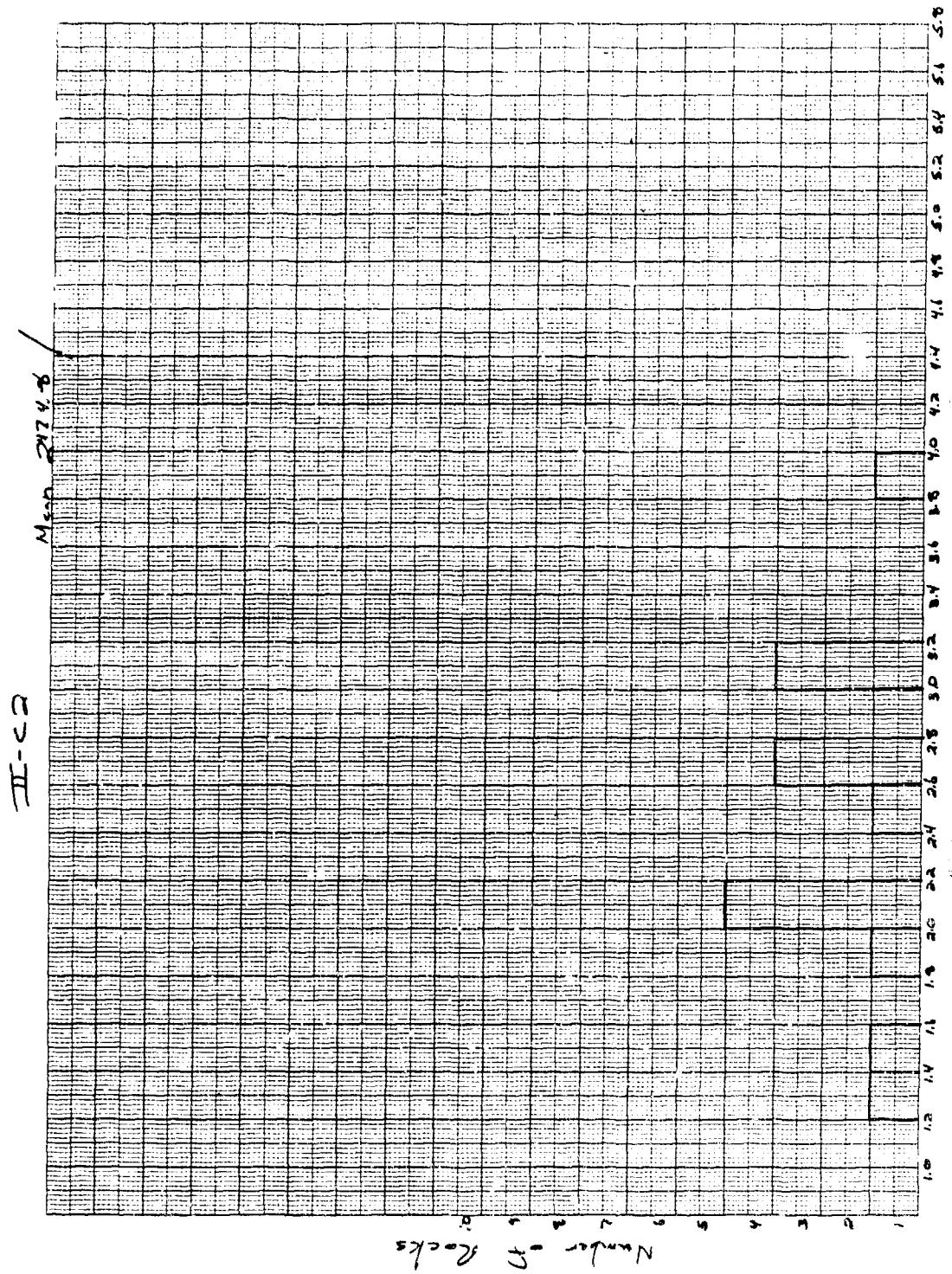


Figure B32. Test IIC2, Single-Wheel Baseline, 2% Coverage, Large Stones, Velocity Distribution.

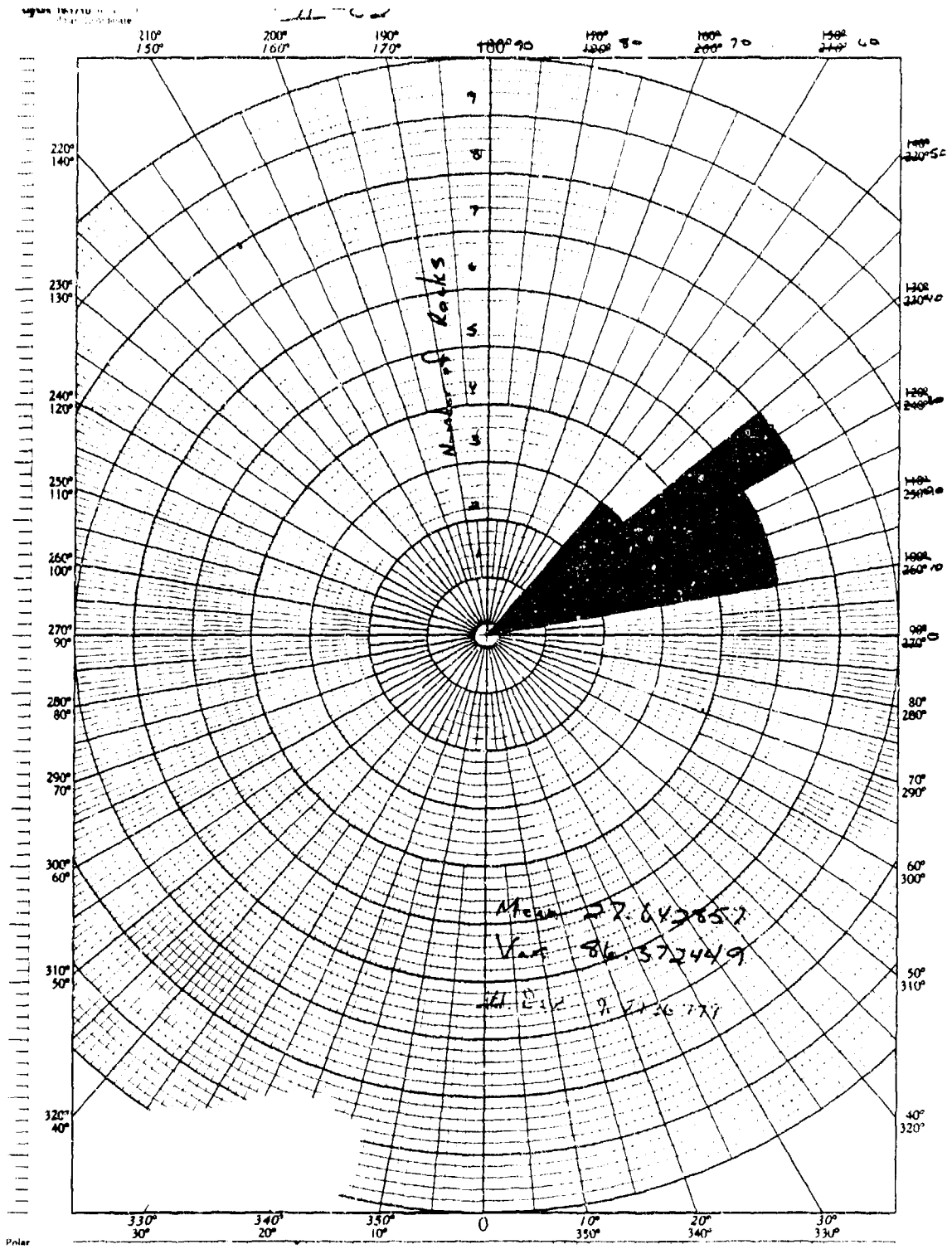


Figure B33. Test IIC2, Single-Wheel Baseline, 2% Coverage, Large Stones, Direction Distribution.

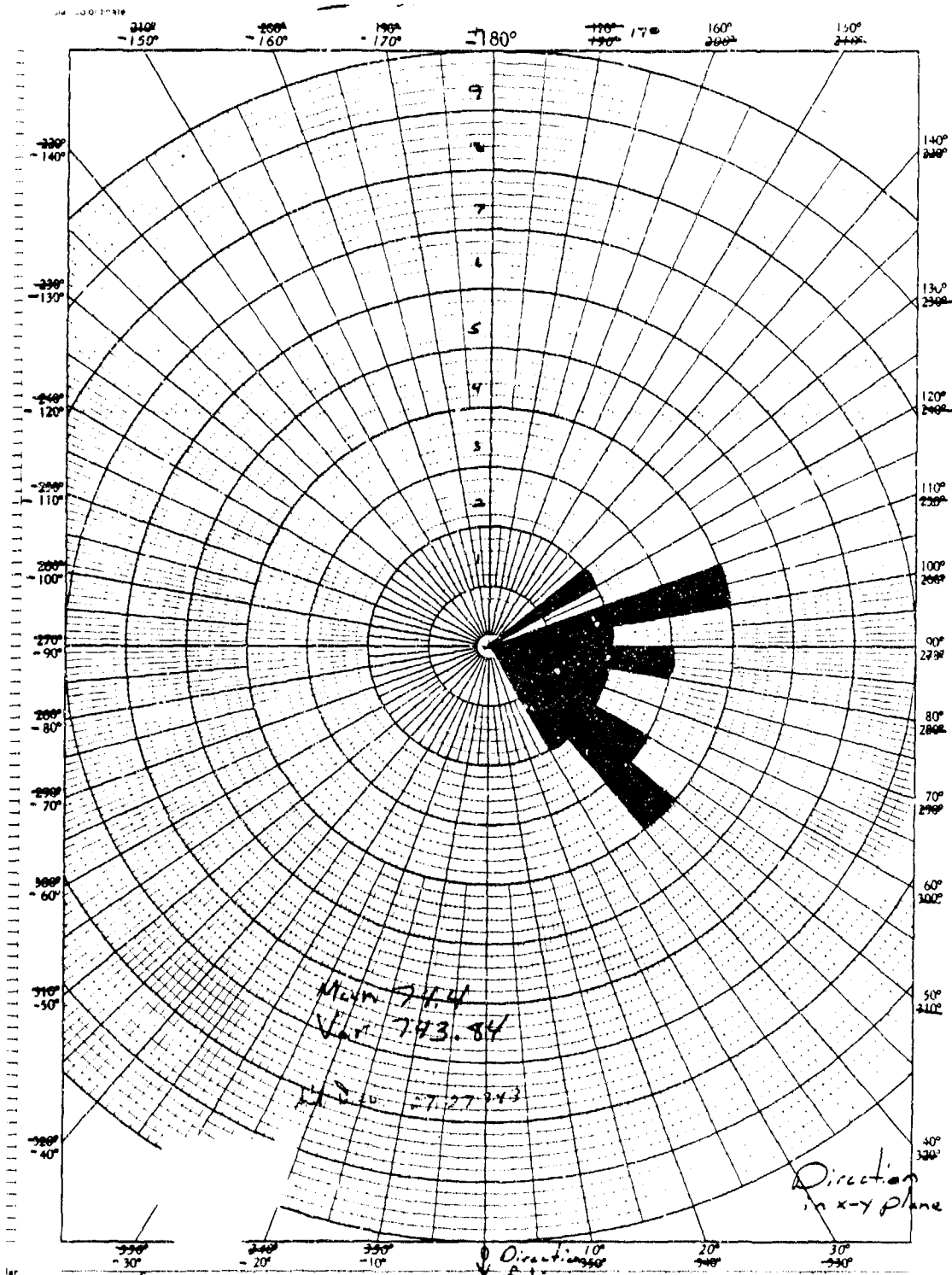


Figure B34. Test IIC2, Single Wheel Baseline, 2% Coverage, Large Stones, Direction Distribution.

II-C-2

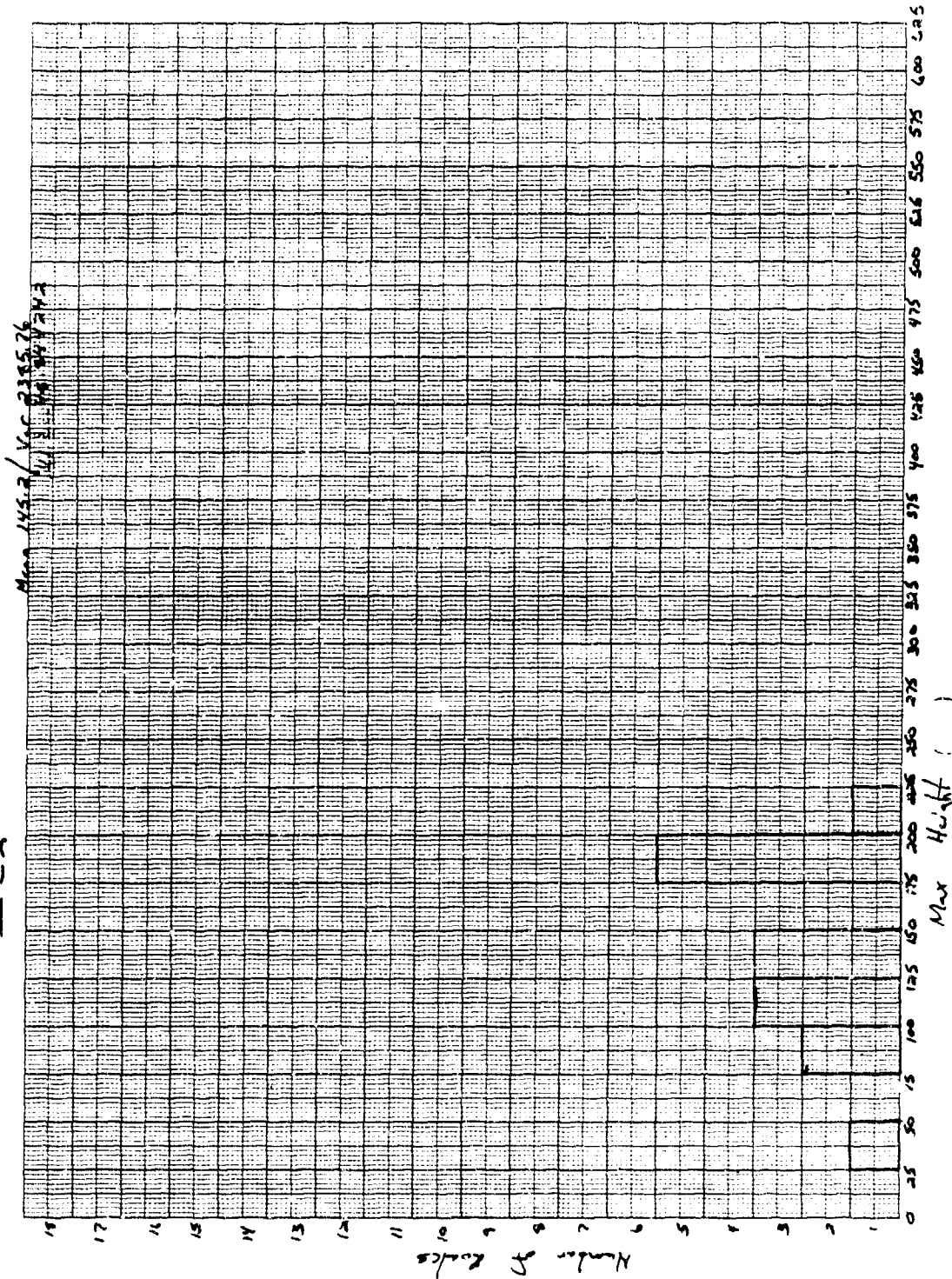


Figure B35. Test IIC2, Single Wheel Baseline, 2% Coverage, Large Stones, Maximum Height Distribution.

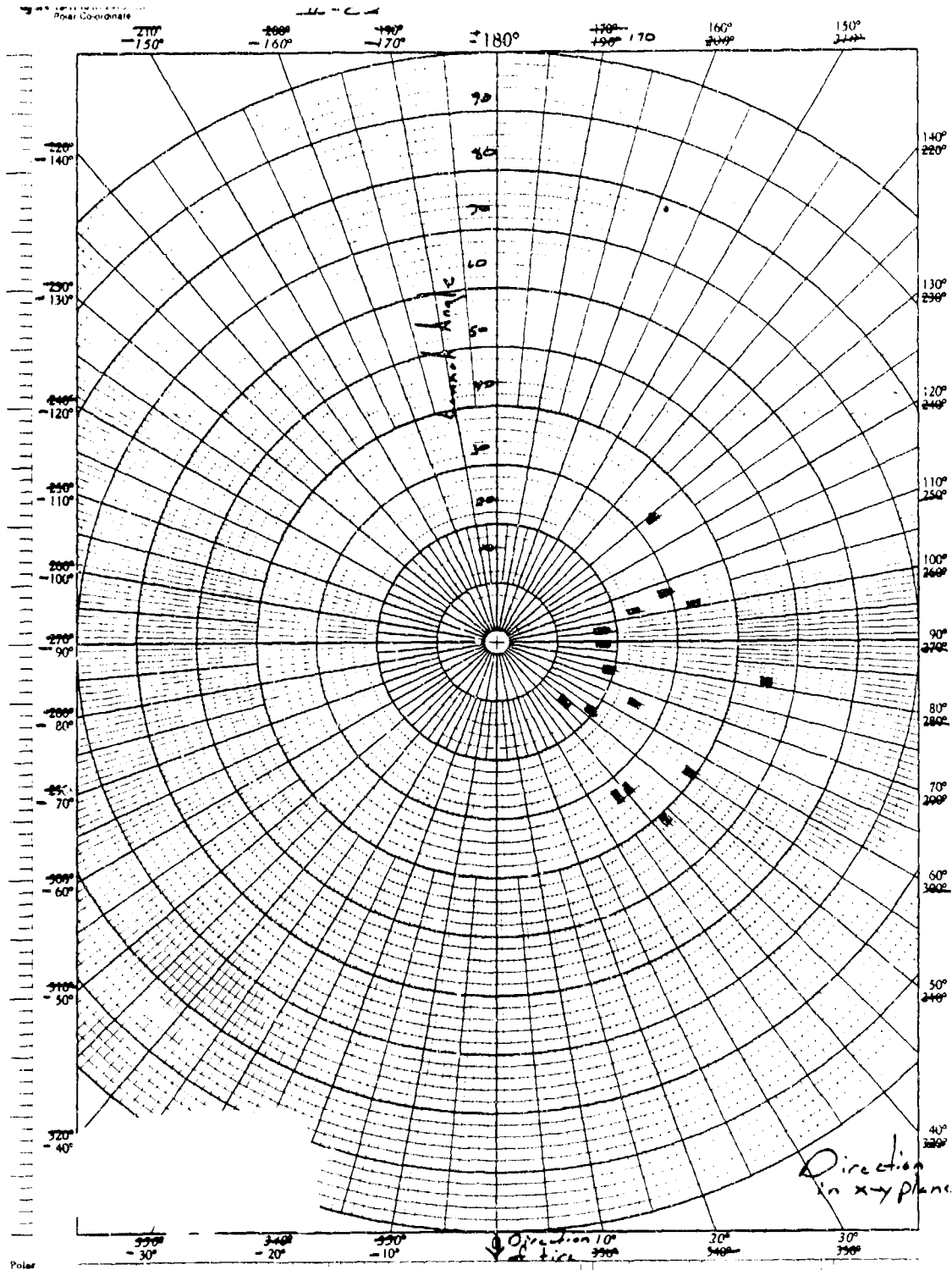


Figure B36. Test IIC2, Single Wheel Baseline, 2% Coverage, Large Stones, Direction and Launch Angle Distribution.

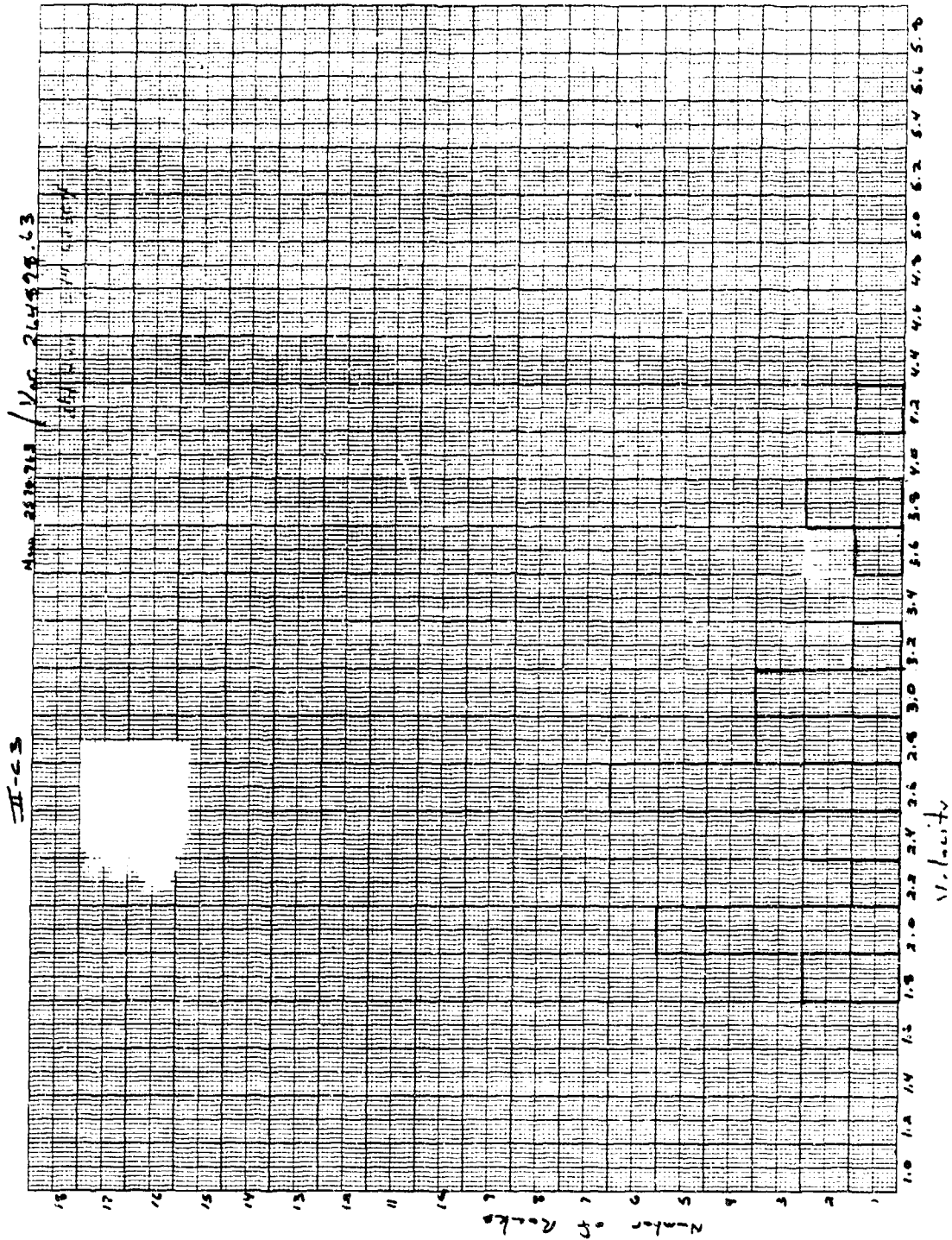


Figure B37. Test IIC3, Dual-Wheel Baseline, 2% Coverage, Large Stones, Velocity Distribution.

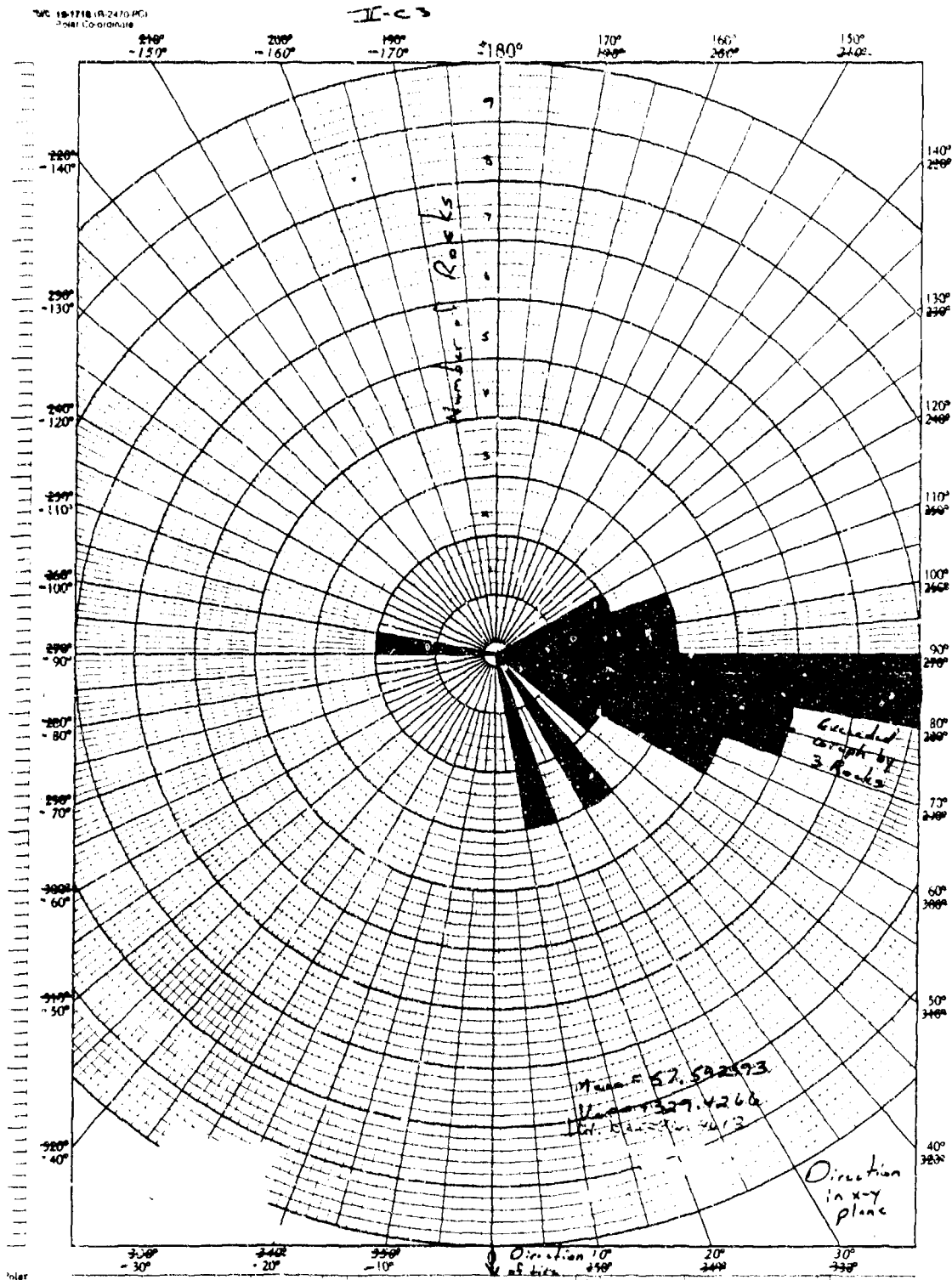


Figure B39. Test IIC3, Dual-Wheel Baseline, 2% Coverage, Large Stones, Direction Distribution.

II-C-3

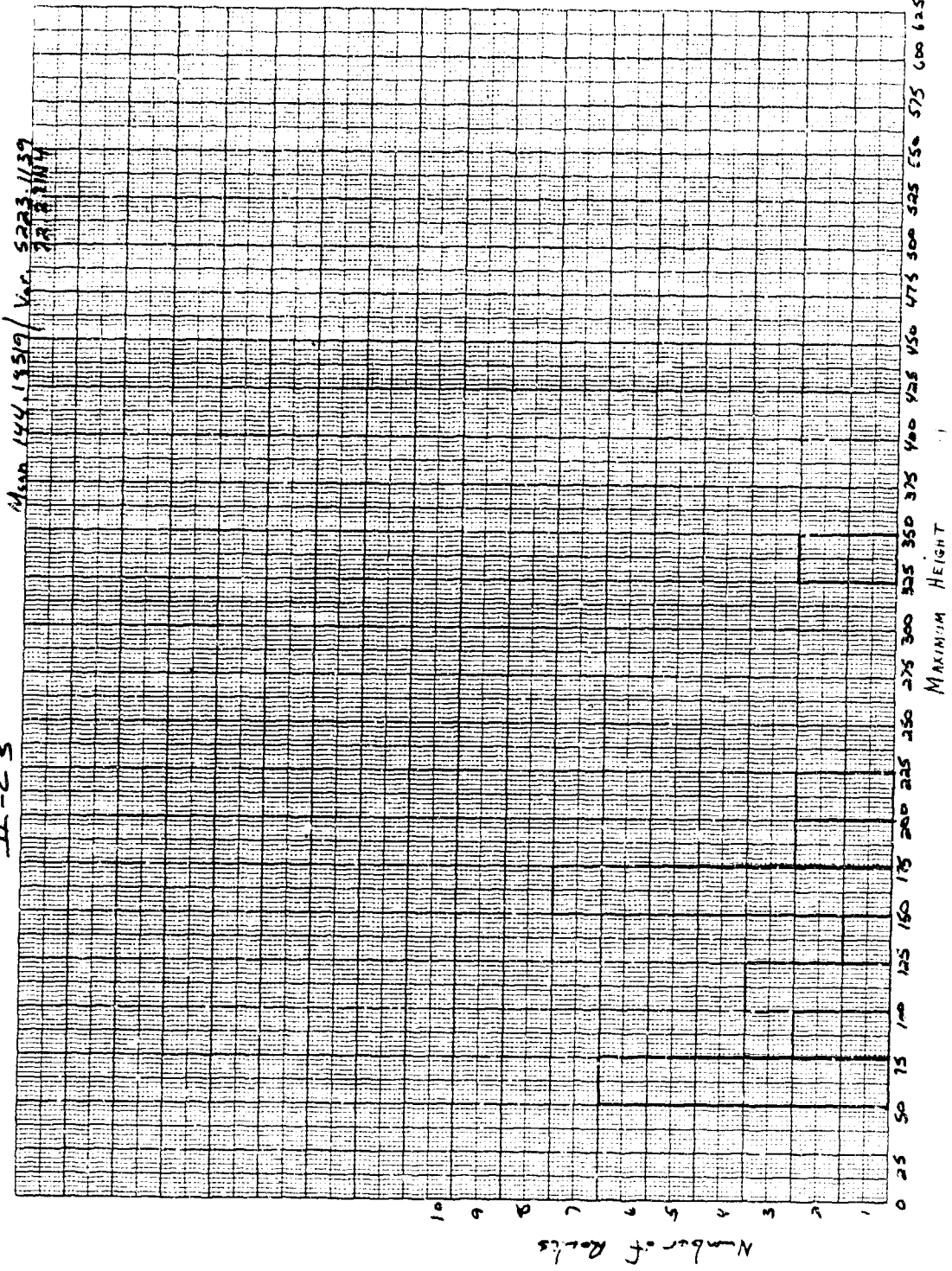


Figure B40. Test IIC3, Dual-Wheel Baseline, 2% Coverage, Large Stones, Maximum Height Distribution.

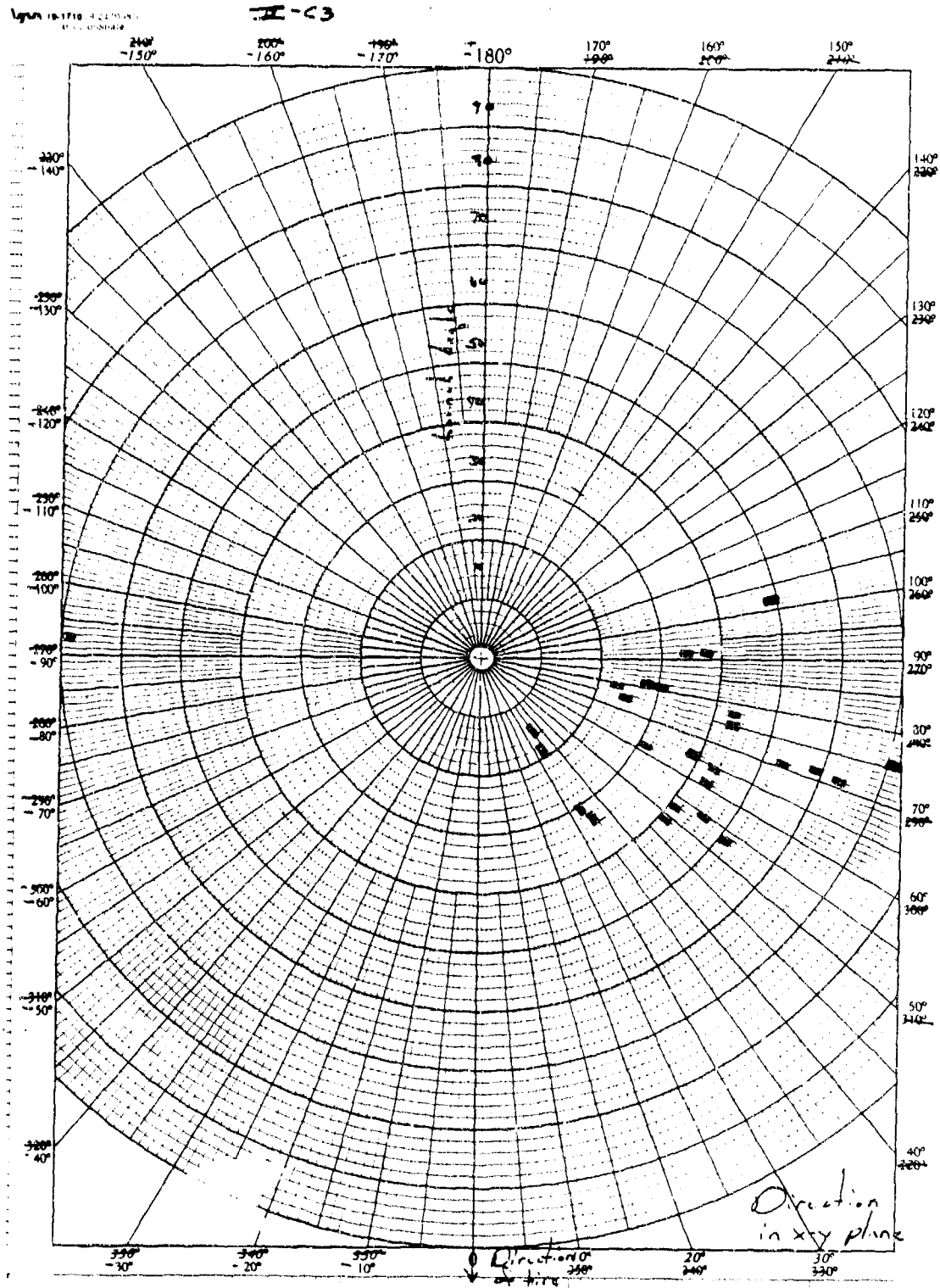


Figure B41. Test II-C3, Dual-Wheel Baseline, 2% Coverage, Large Stones, Direction and Angle Distribution.

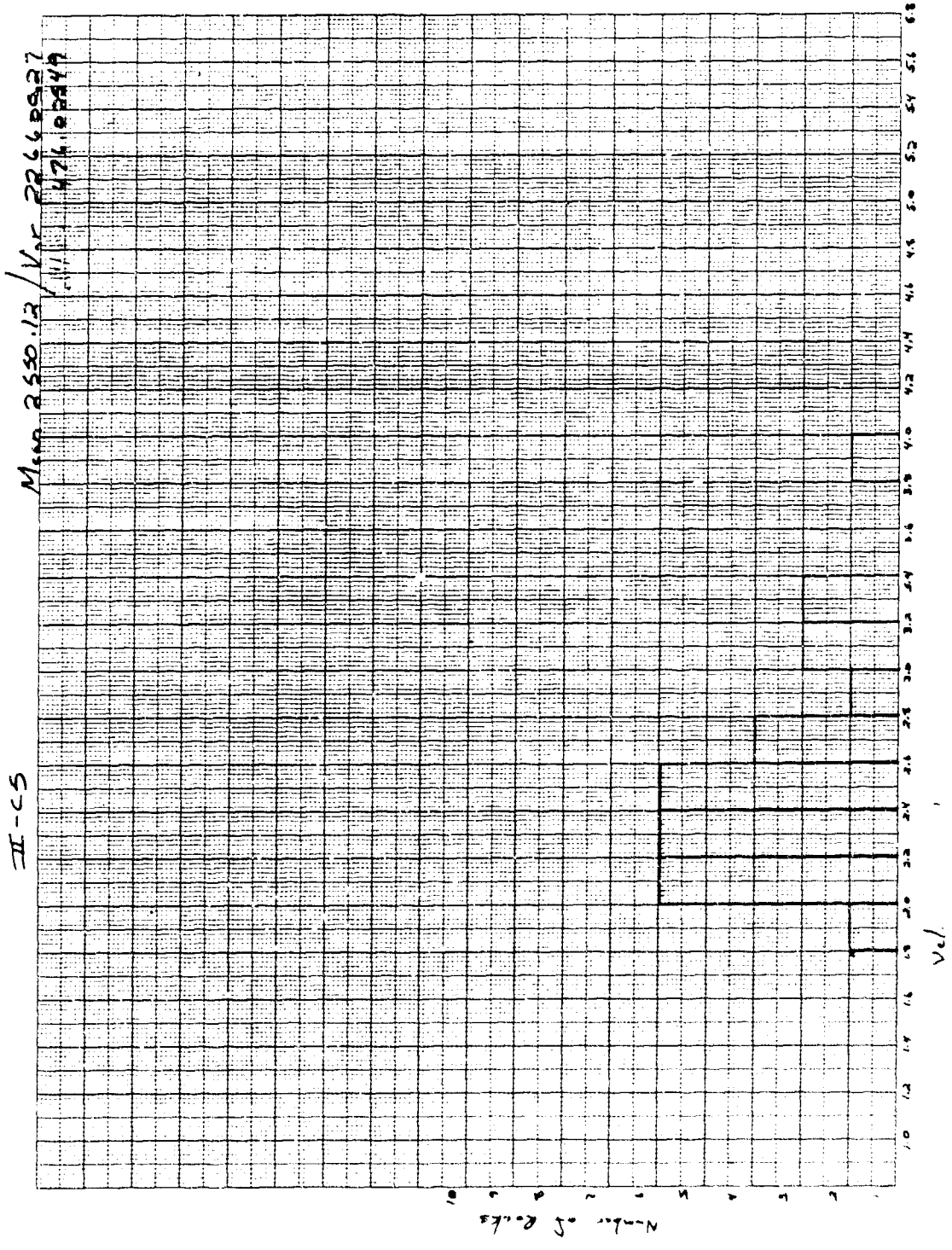


Figure B42. Test IIC5, Dual-Wheel 20% Coverage, Velocity Distribution.

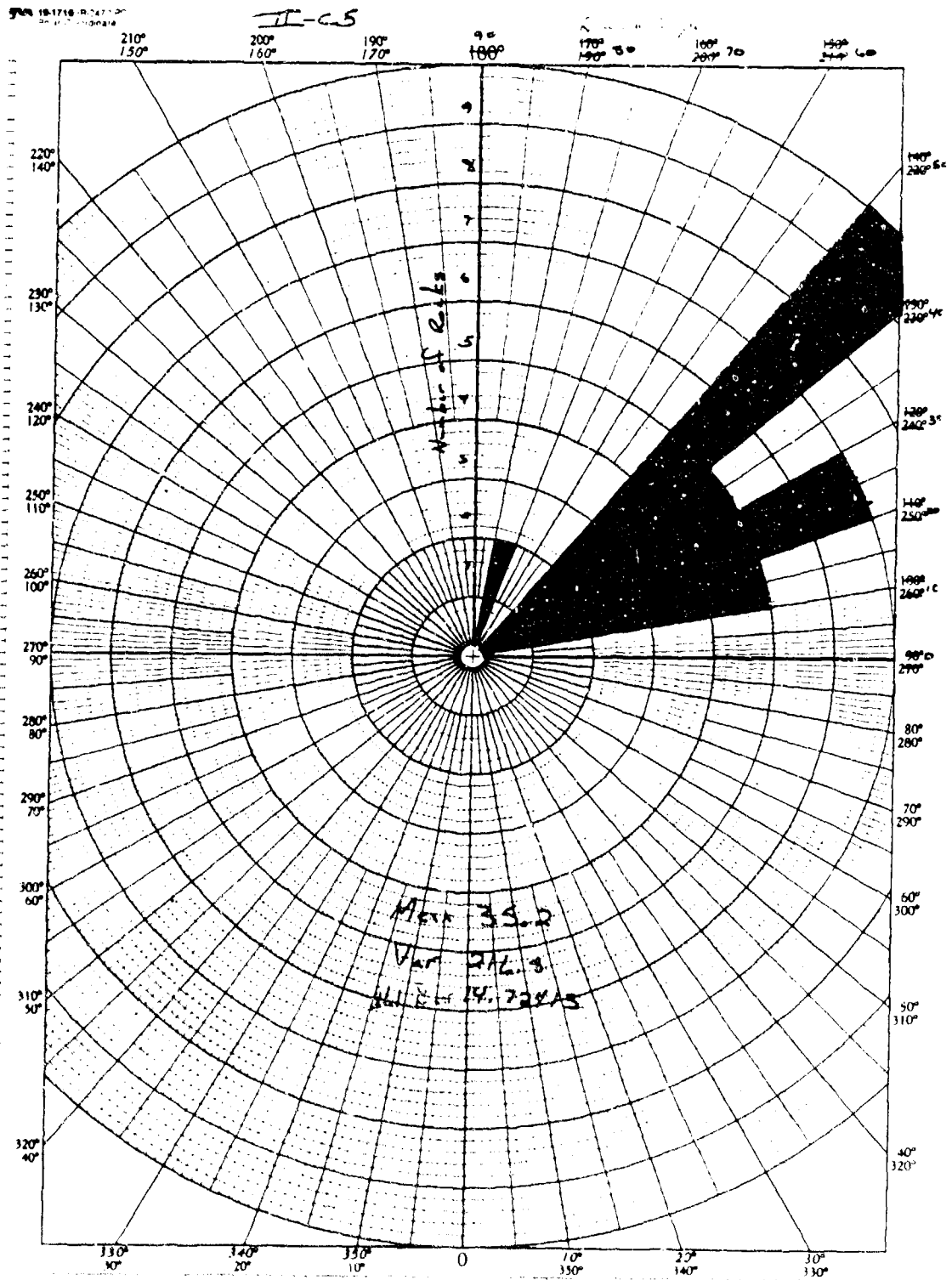


Figure B43. Test IIC5, Dual-Wheel, 20% Coverage, Elevation Angle Distribution.

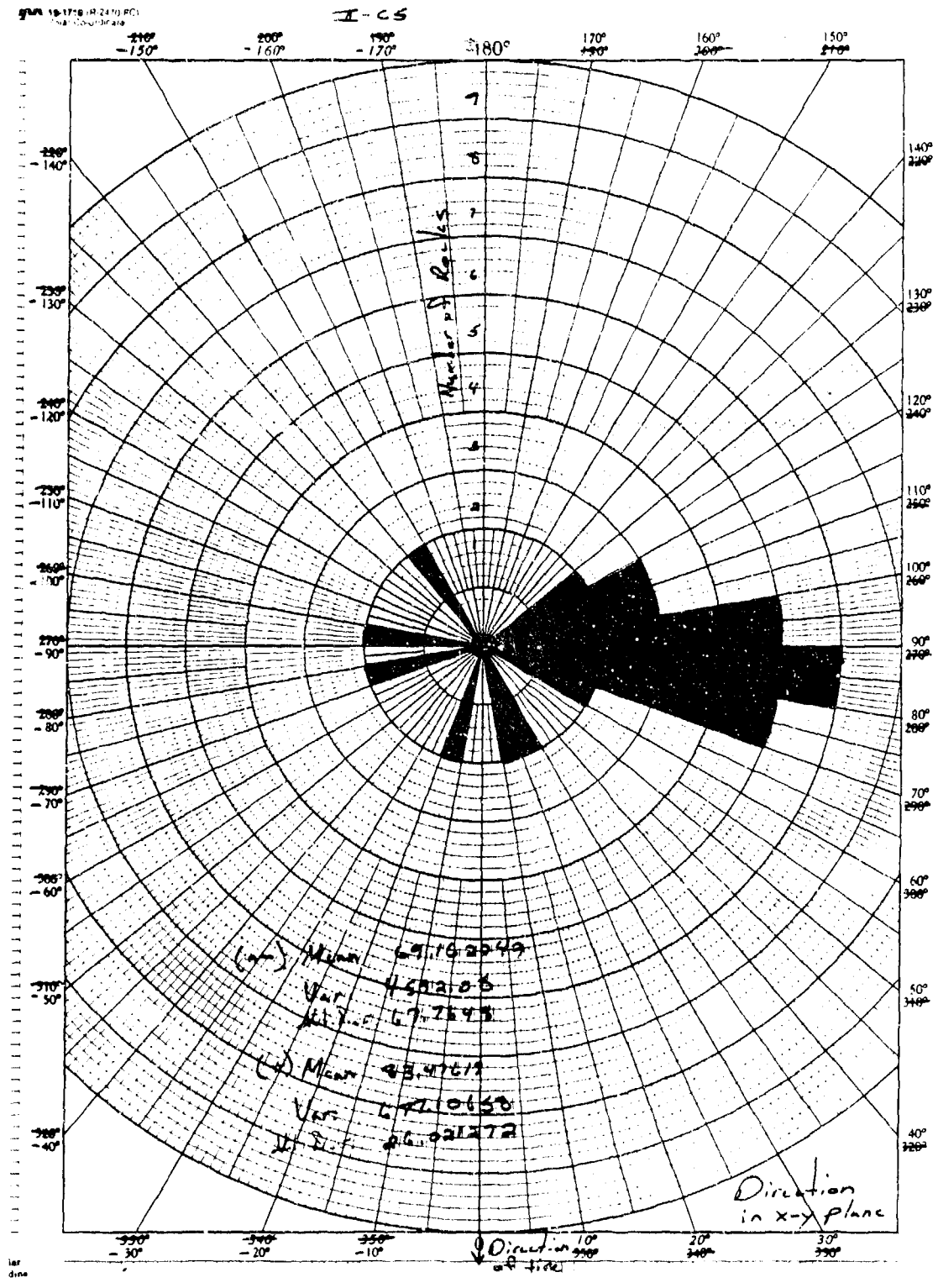


Figure B44. Test IIC5, Dual-Wheel, 20% Coverage, Direction Distribution.

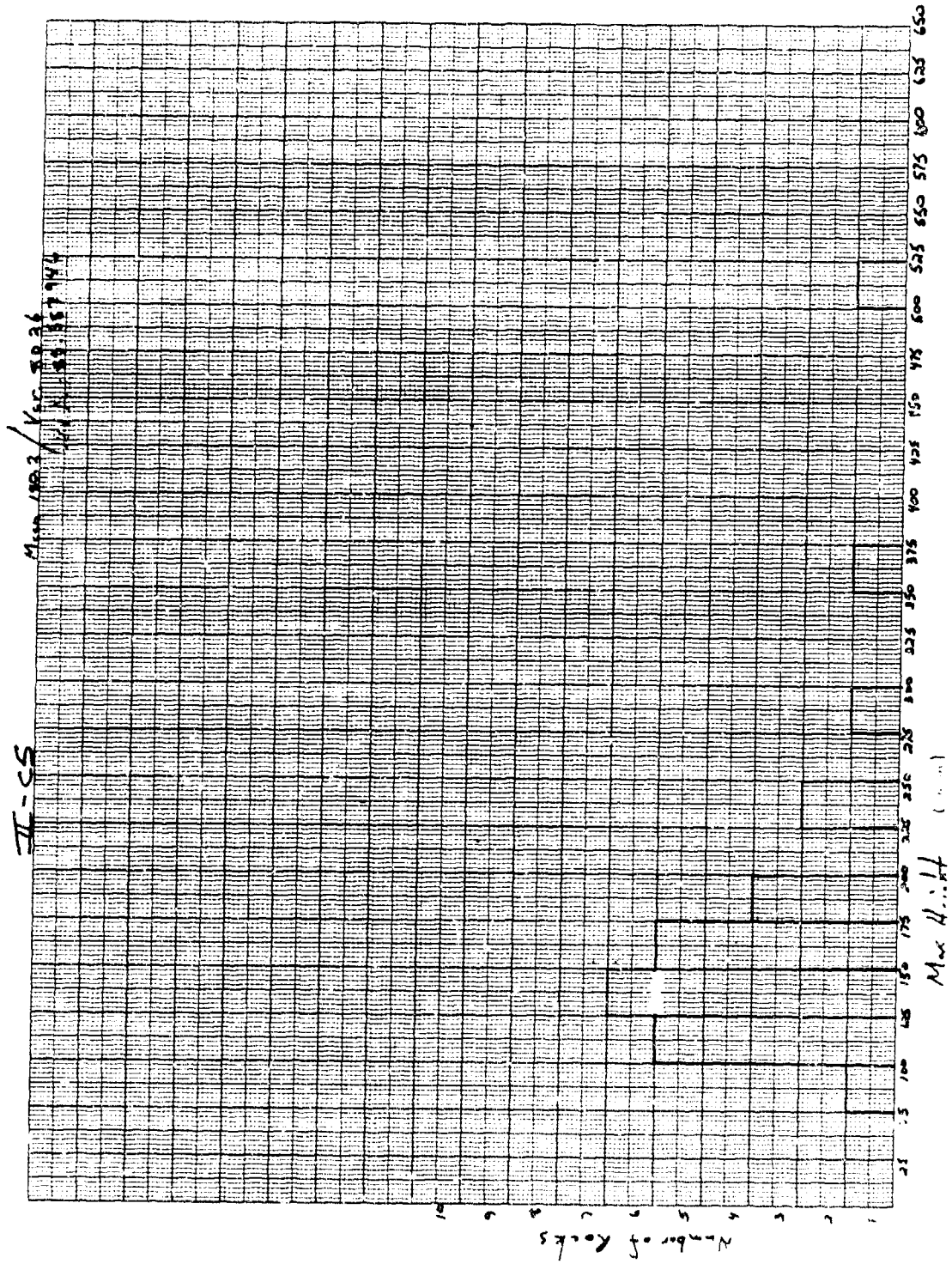


Figure B45. Test IIC5, Dual-Wheel, 20% Coverage, Maximum Height Distribution.

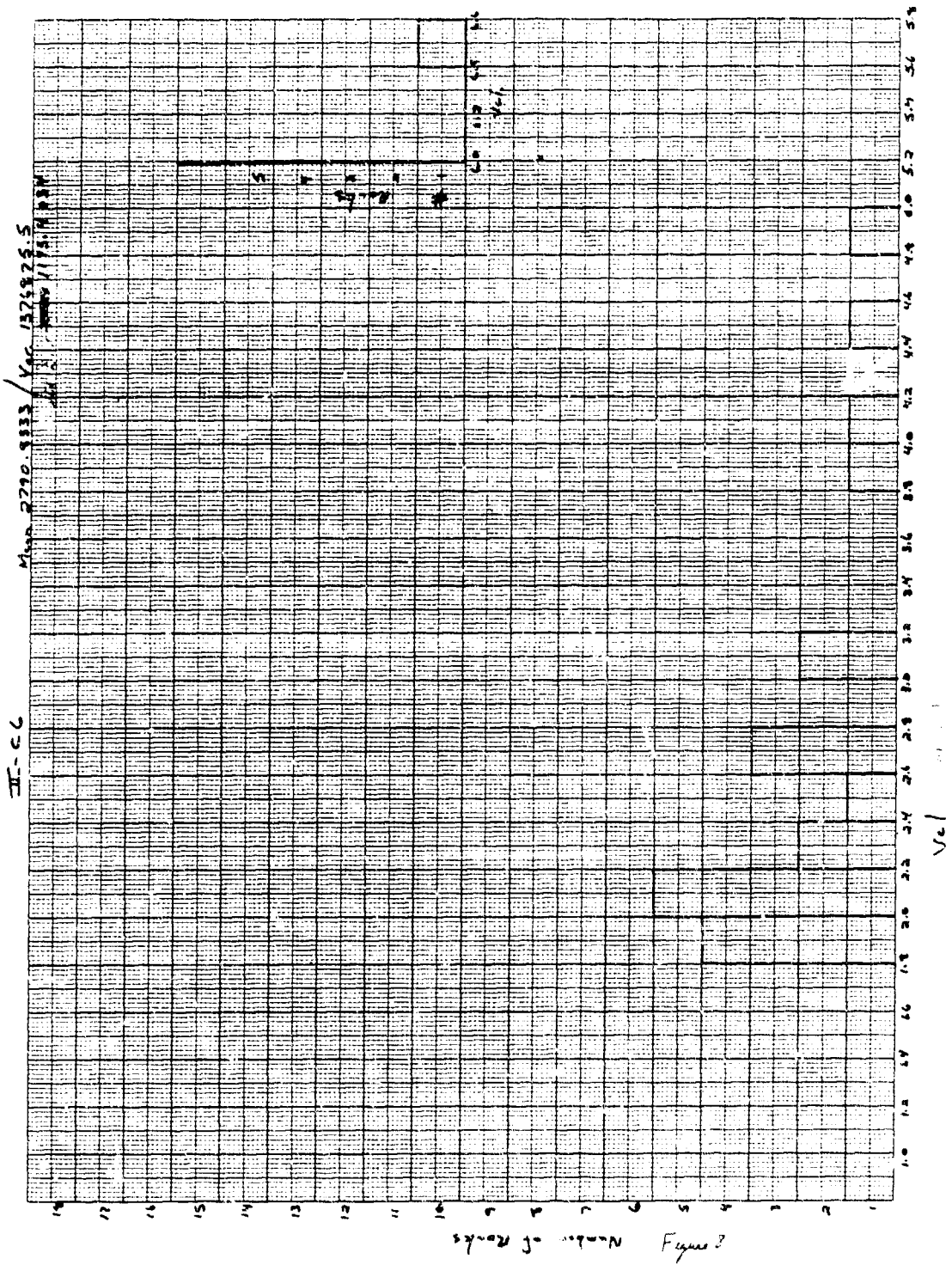


Figure B46. Test IIC6, Dual-Wheel, 10% Coverage, Velocity Distribution.

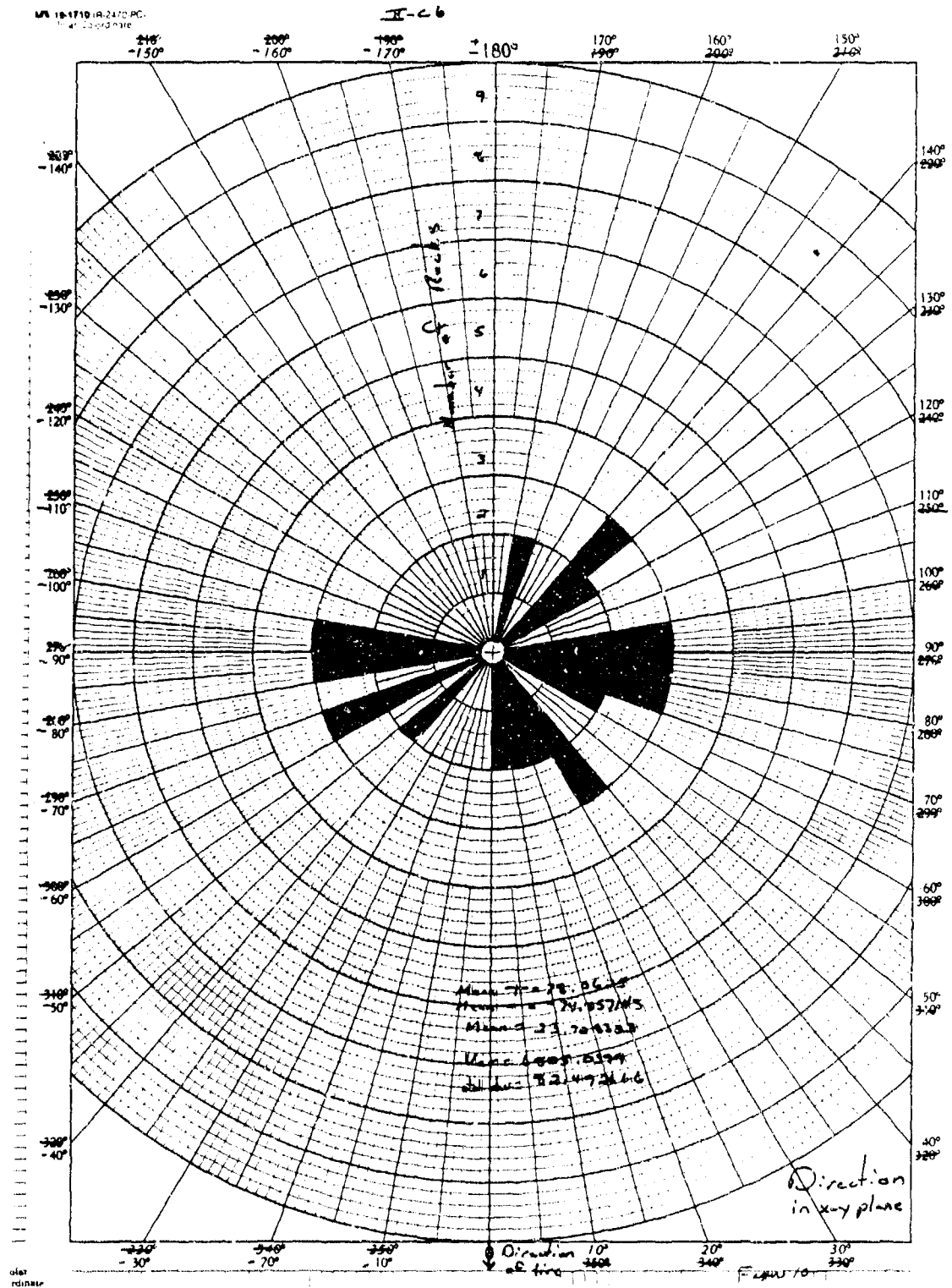


Figure B48. Test IIC6, Dual-Wheel, 10% Coverage, Direction Distribution.

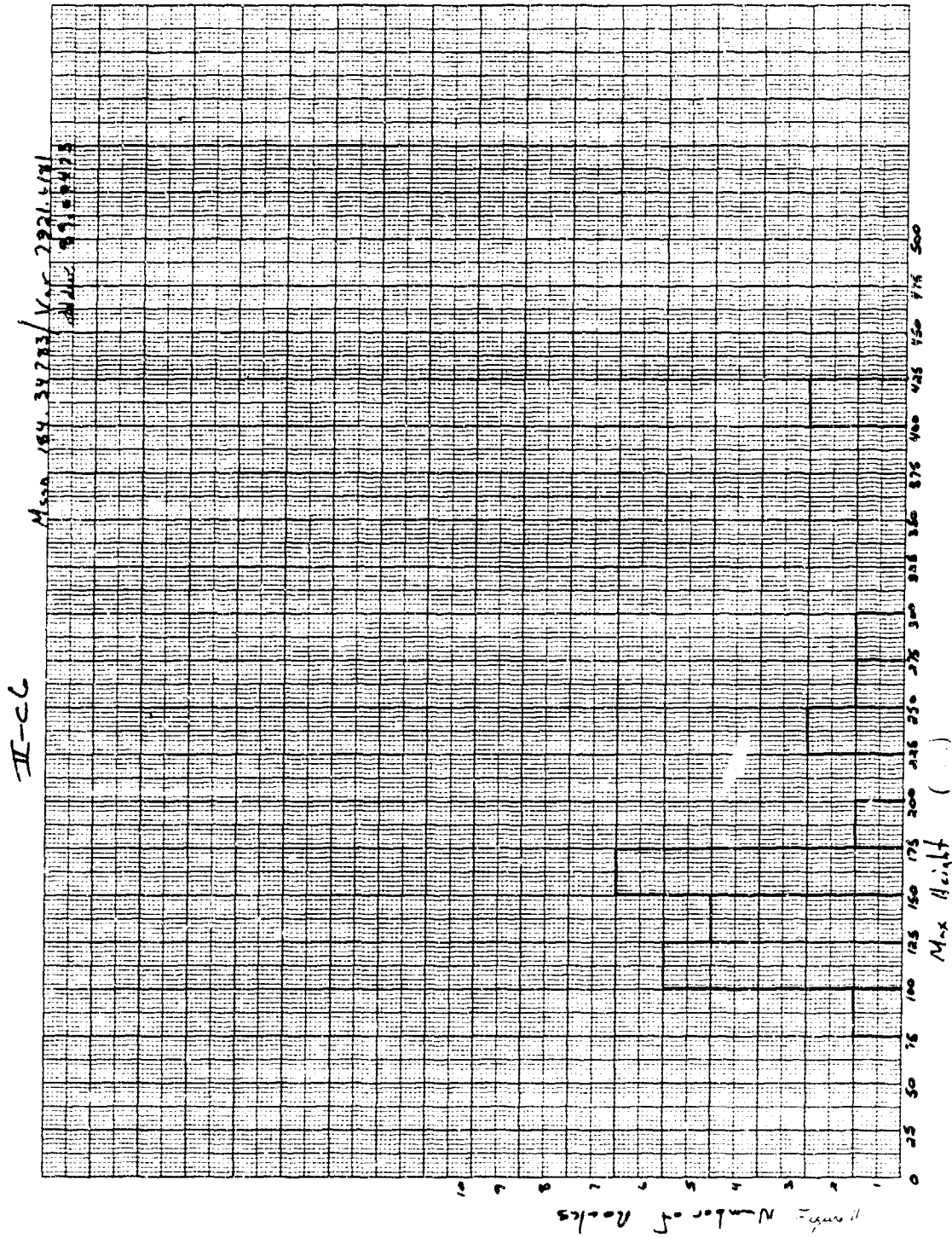


Figure B49. Test IIC6, Dual Wheel, 10% Coverage, Maximum Height Distribution.

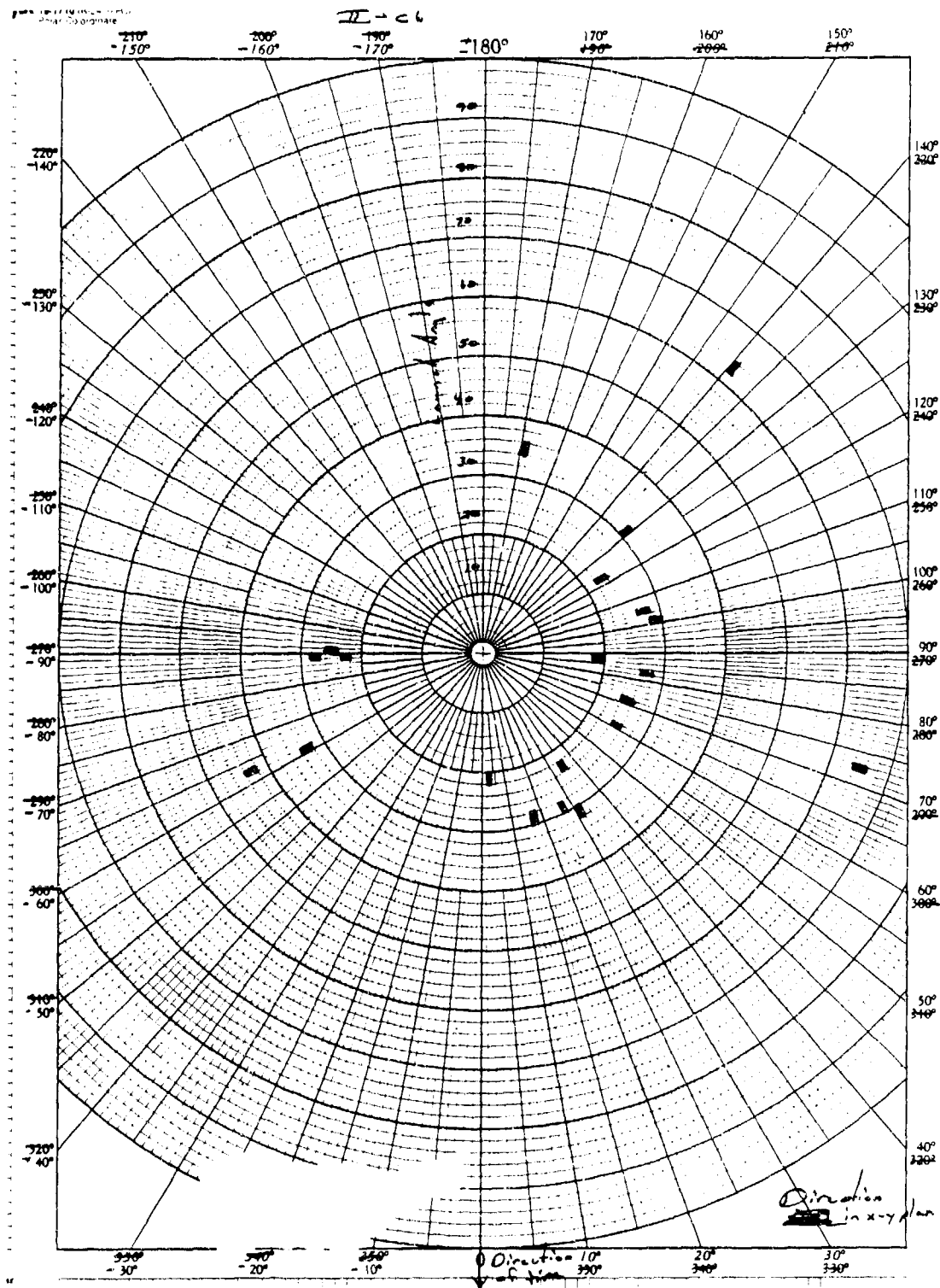


Figure B50. Test IIC6, Dual-Wheel, 10% Coverage, Direction and Launch Angle Distribution

II-c-2

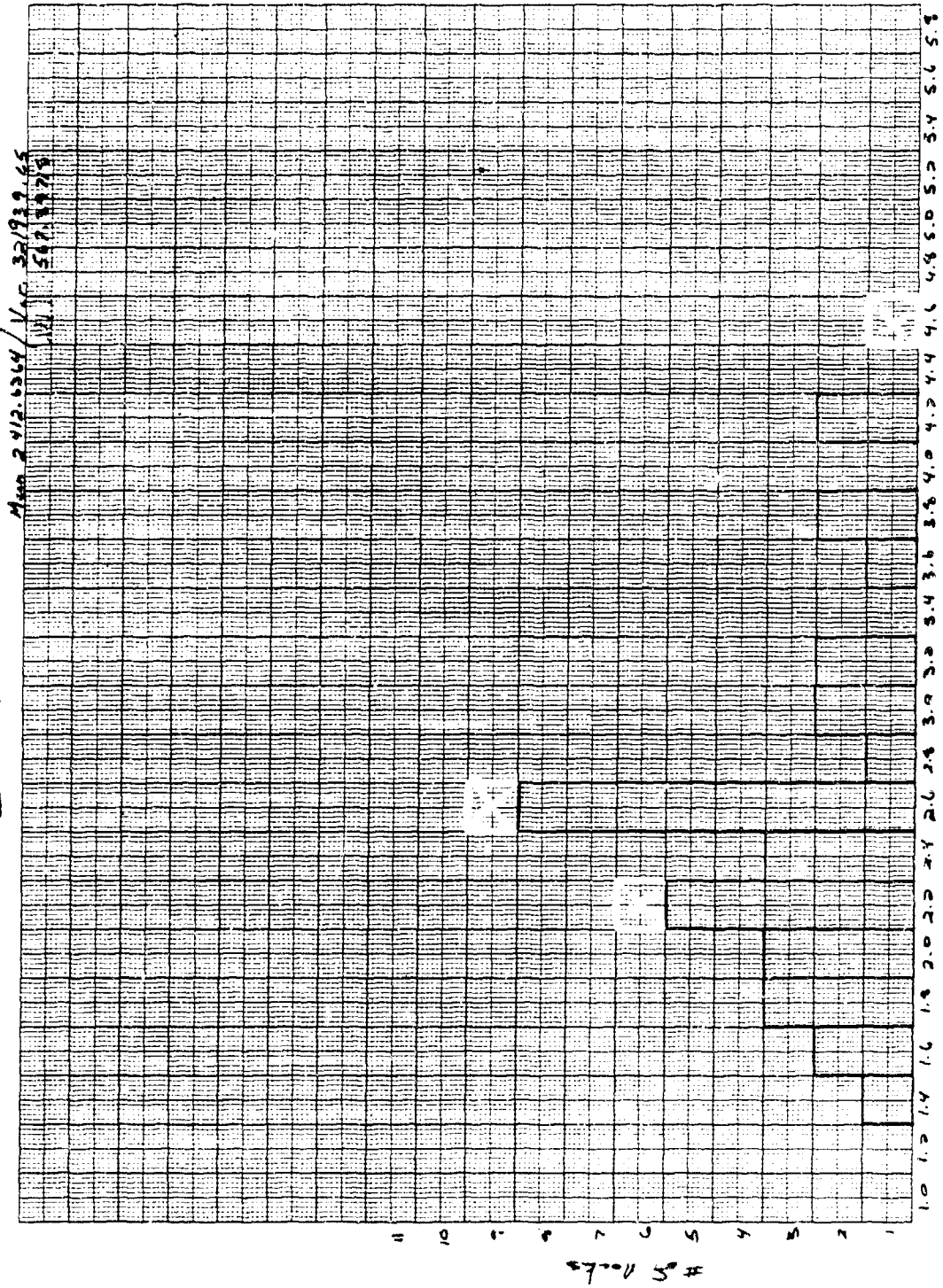


Figure B51. Test IIC7; Dual Wheels, 5% Coverage, Maximum Height Distribution.

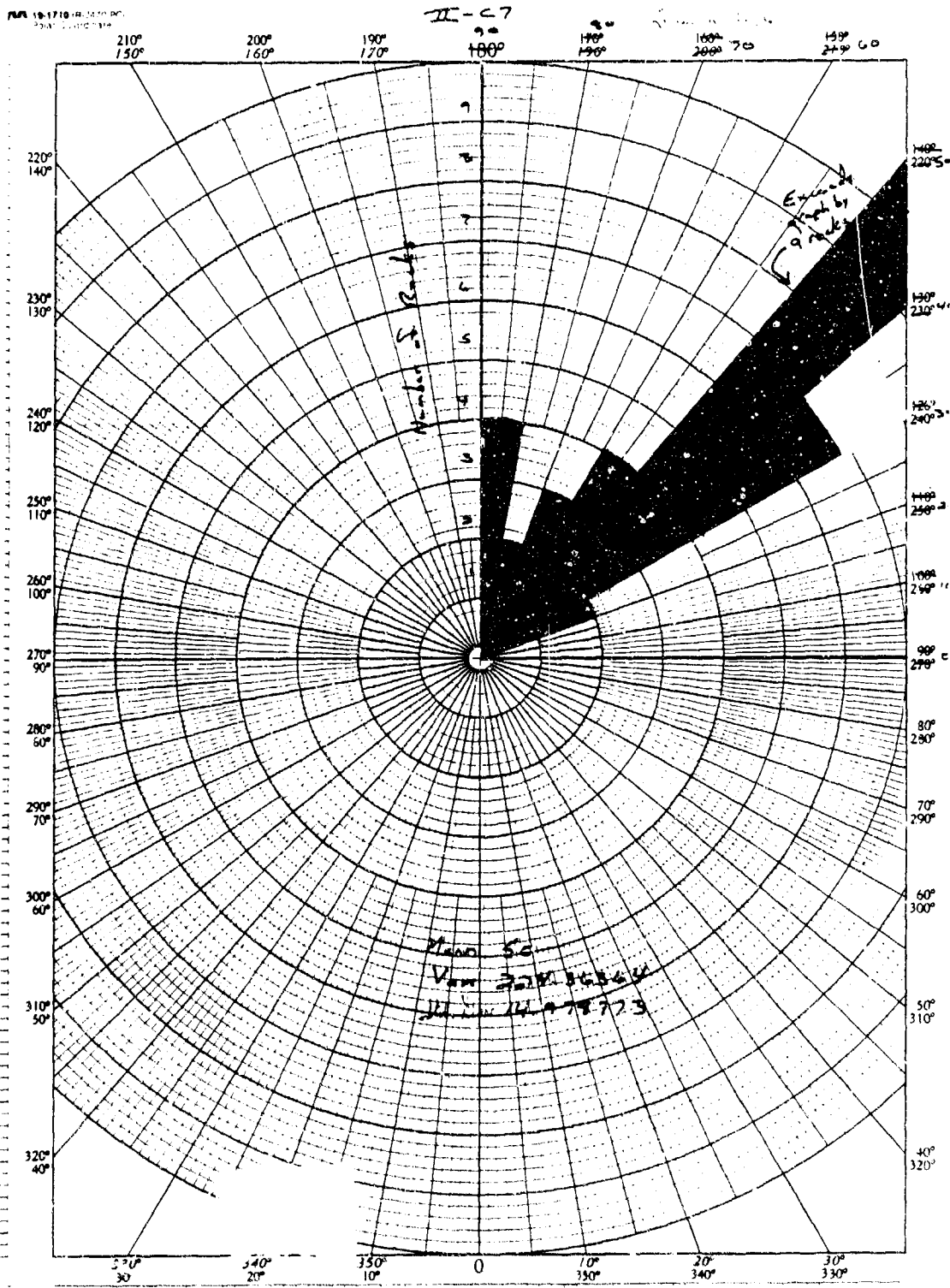


Figure B52. Test IIC7, Dual Wheels, 5% Coverage, Direction and Launch Angle Distribution.

II-47

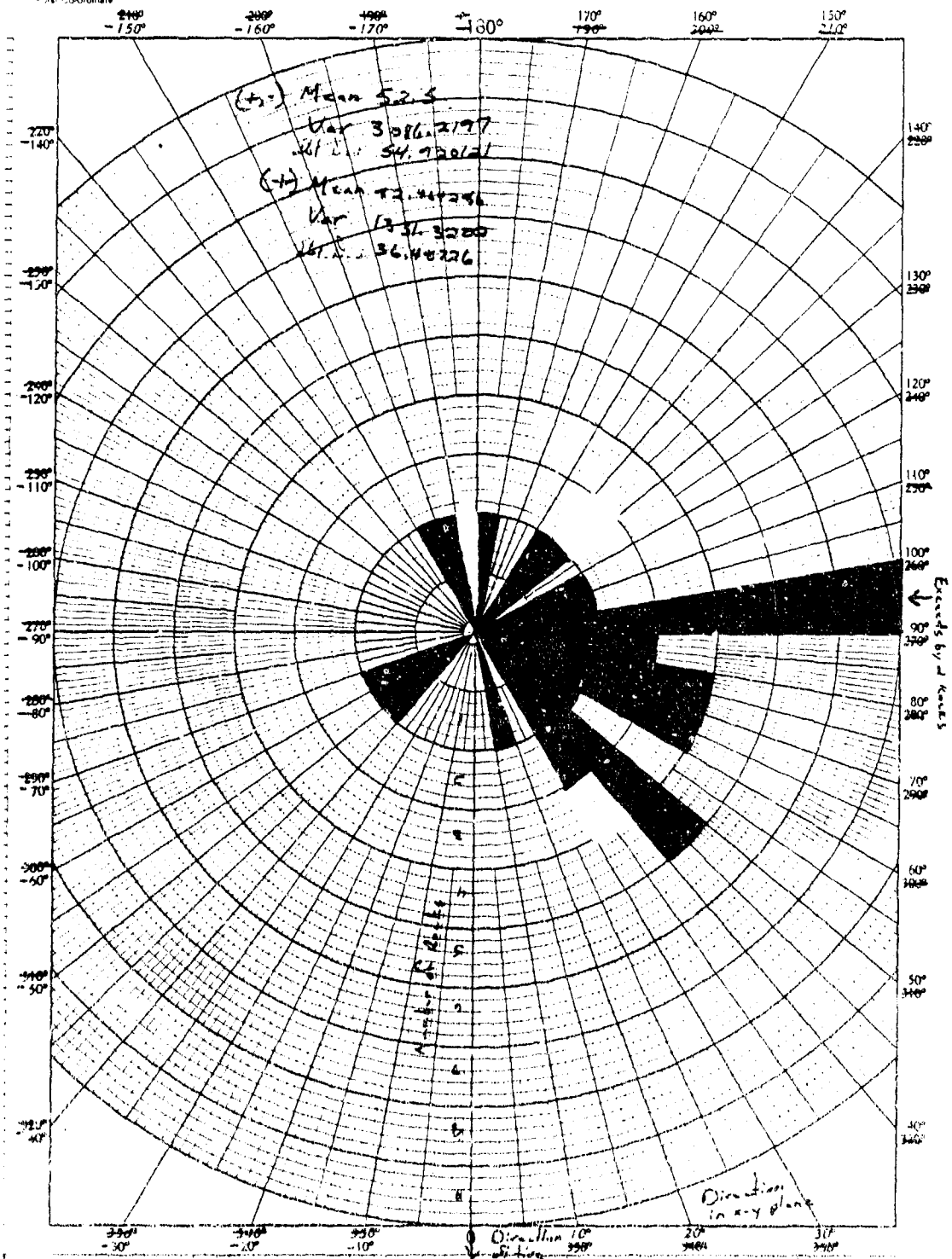


Figure B53. Test IIC7, Dual Wheels, 5% Coverage, Direction Distribution.

II-C7

Max 171.5 / Yr 8512.5441
107.1 / P.P. 26.348

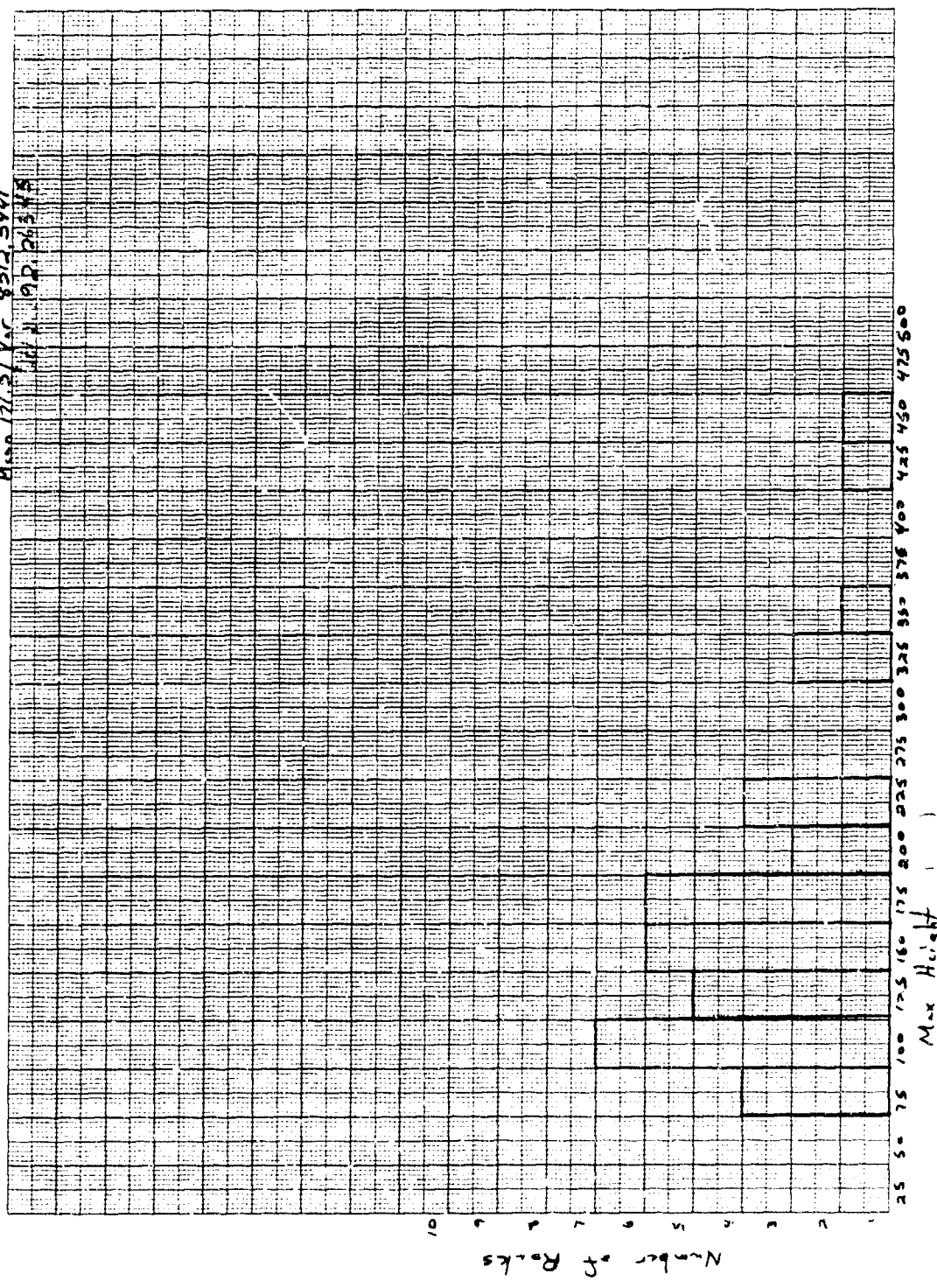


Figure B54. Test IIC7, Dual Wheels, 5% Coverage, Maximum Height Distribution.

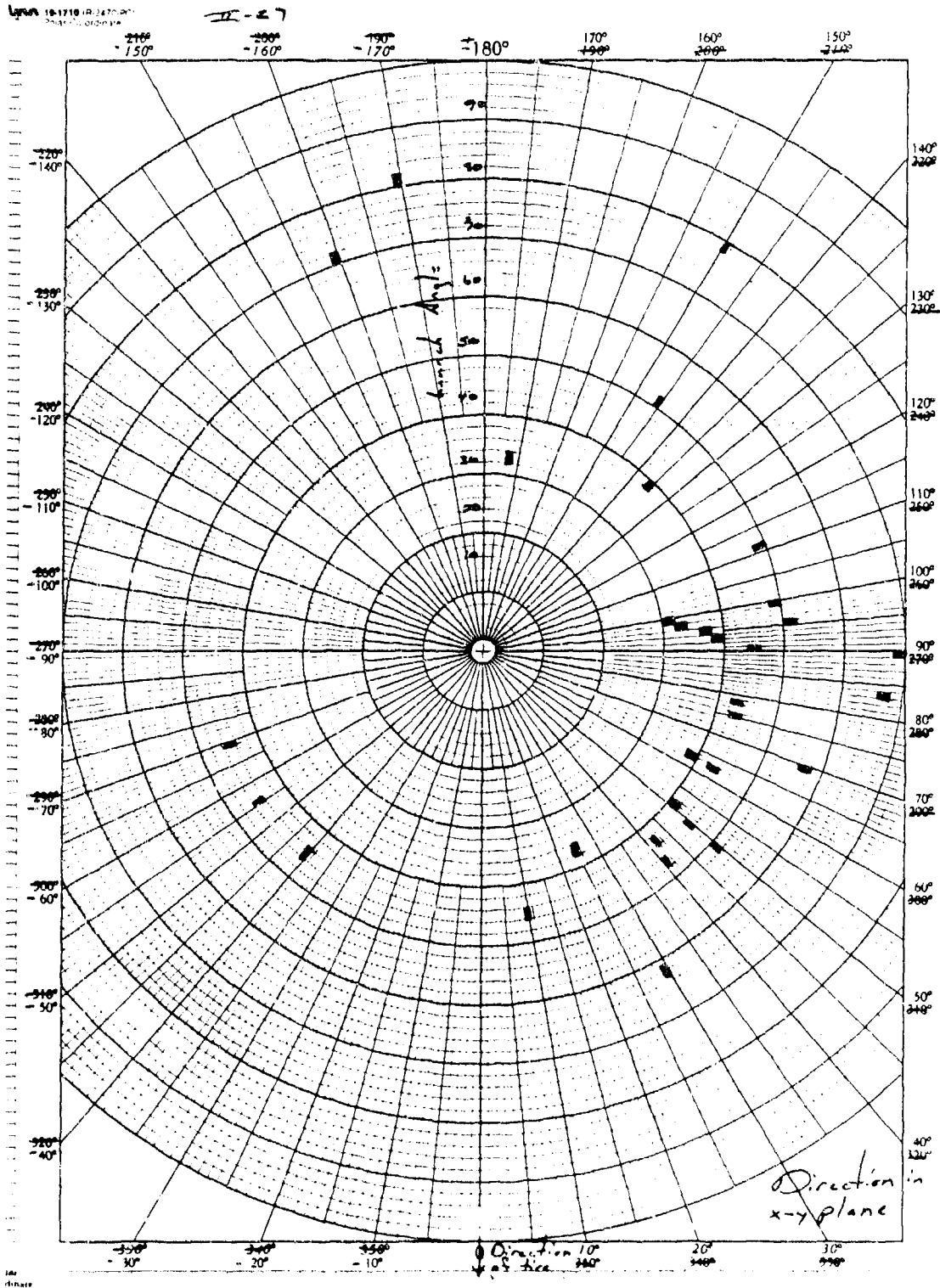


Figure B55. Test IIC7, Dual Wheels, 5% Coverage, Direction and Launch Angle Distribution.

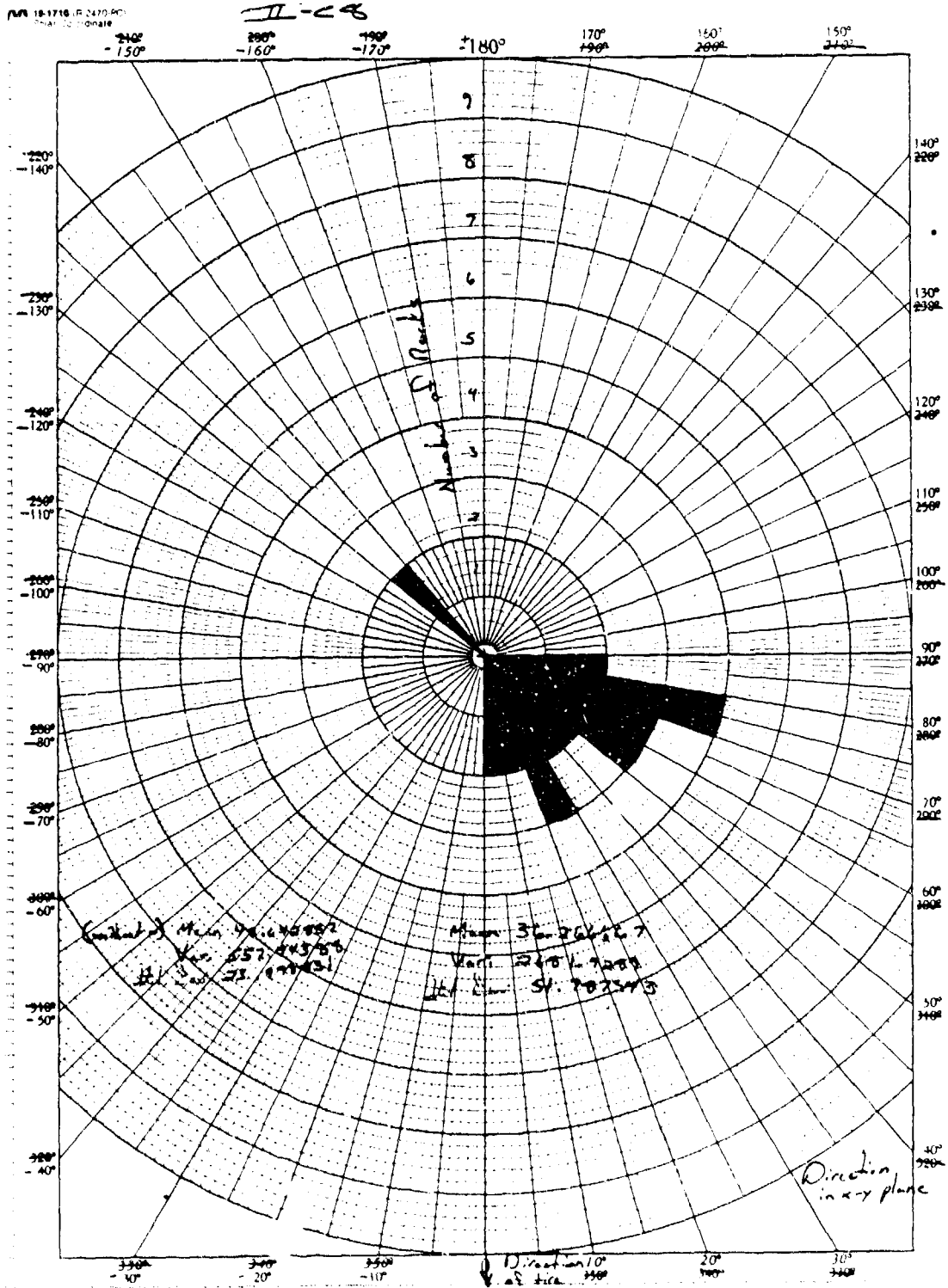


Figure B57. Test IIC8, Dual-Wheel, 1% Coverage, Direction Distribution.

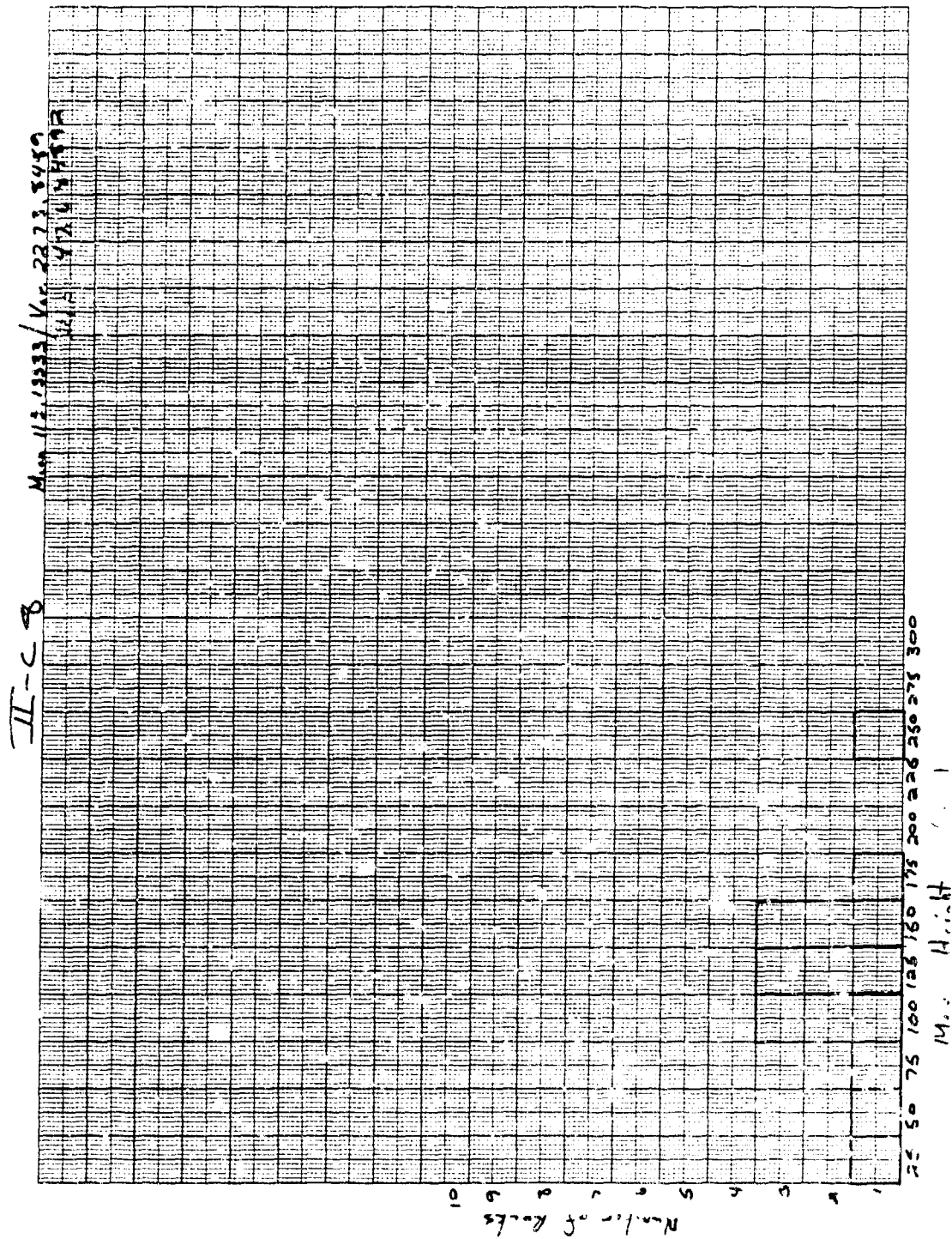


Figure B56. Test IIC8, Dual-Wheel, 1% Coverage, Maximum Height Distribution.

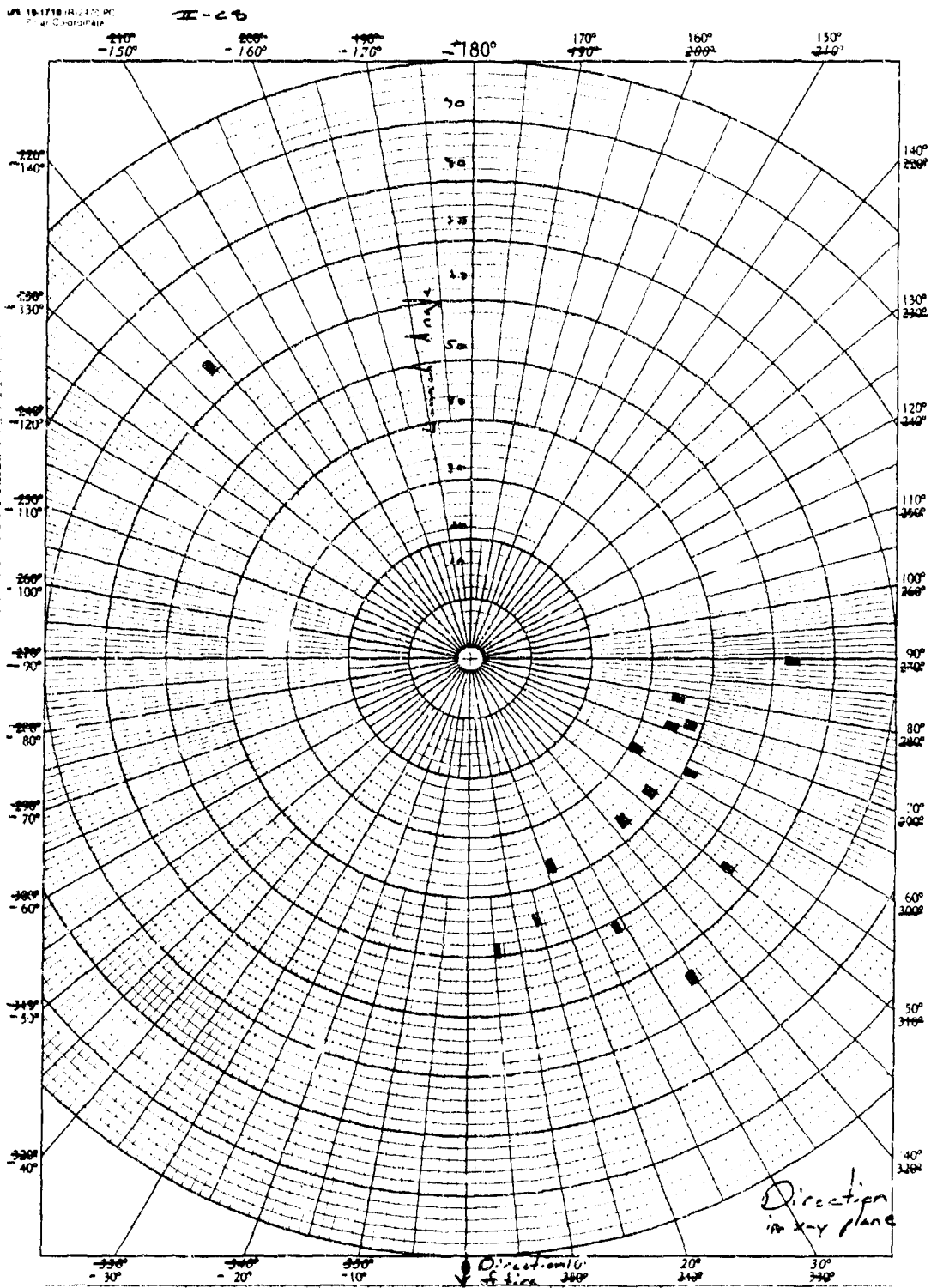


Figure B59. Test IIC8, Dual-Wheel, 1½ Coverage, Direction and Launch Angle Distribution.

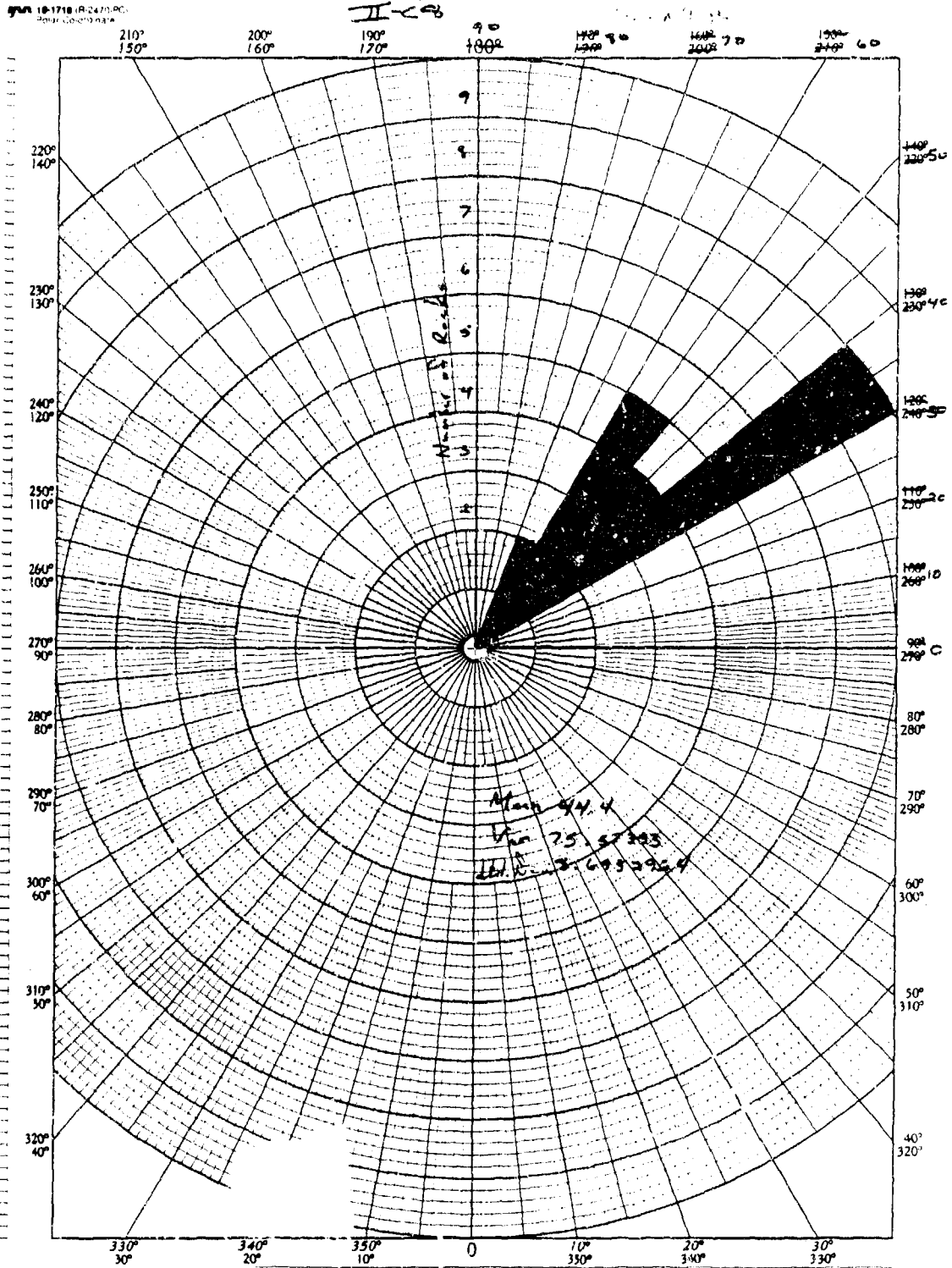


Figure B60. Test IIC8, Dual-Wheel, 1% Coverage, Elevation Angle Distribution.

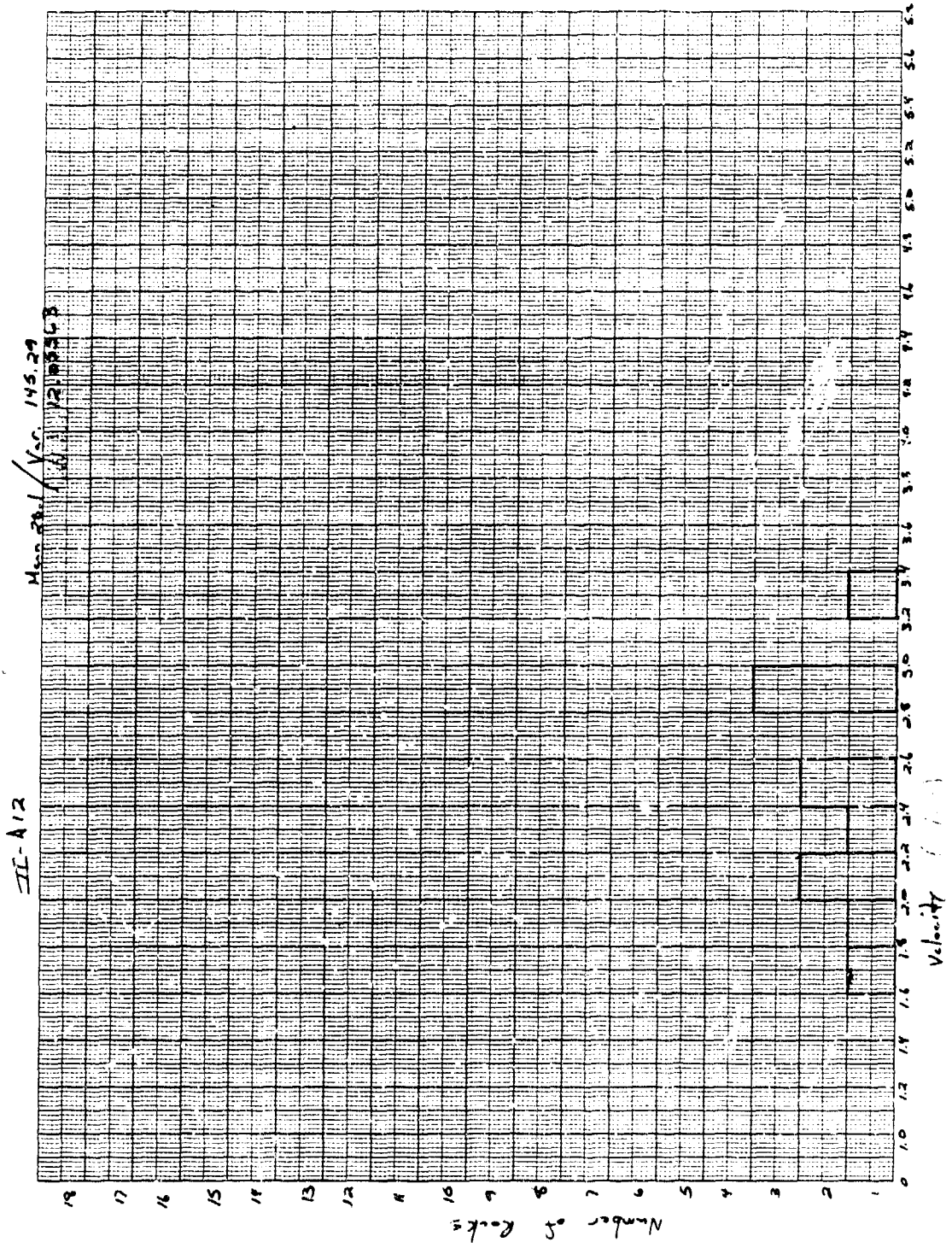


Figure B61. Test IIA12, Dual-Wheel, Aggregate Bed, 2% Coverage, Velocity Distribution.

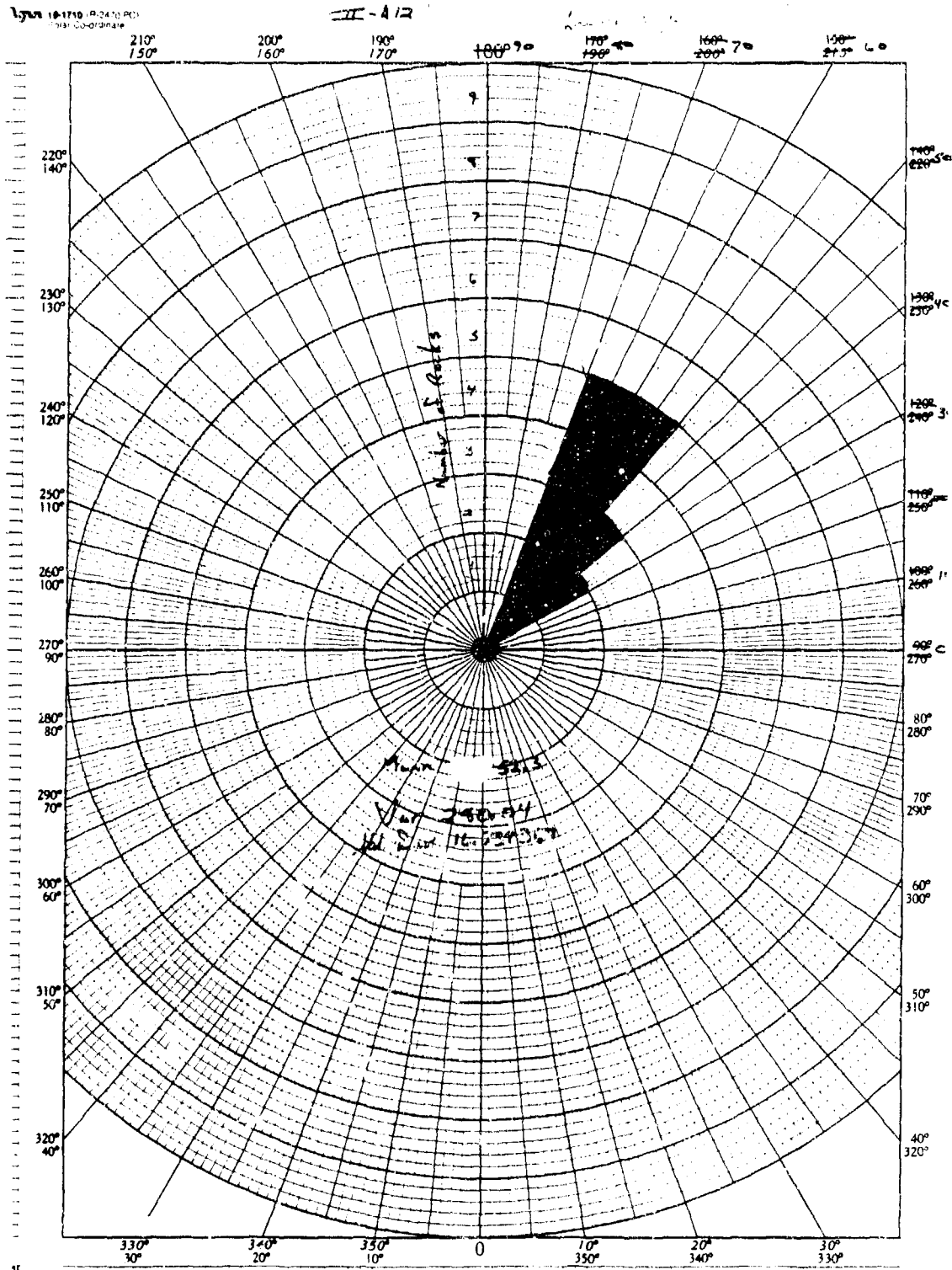


Figure B62. Test IIA12, Dual-Wheel, Aggregate Bed, 2% Coverage, Elevation and Angle Distribution.

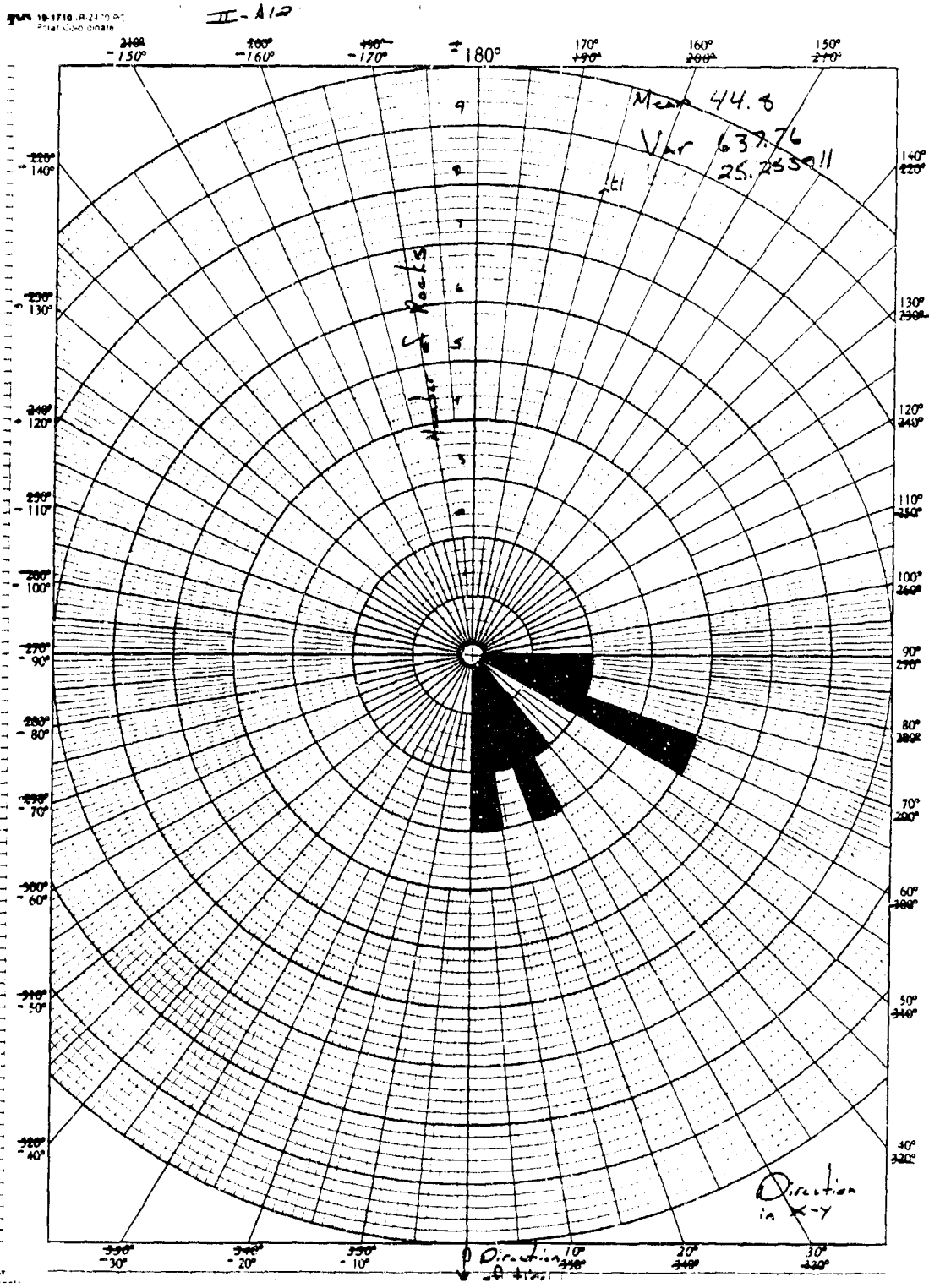


Figure B63. Test IIA12, Dual-Wheel, Aggregate Bed, 2% Coverage, Direction Distribution.

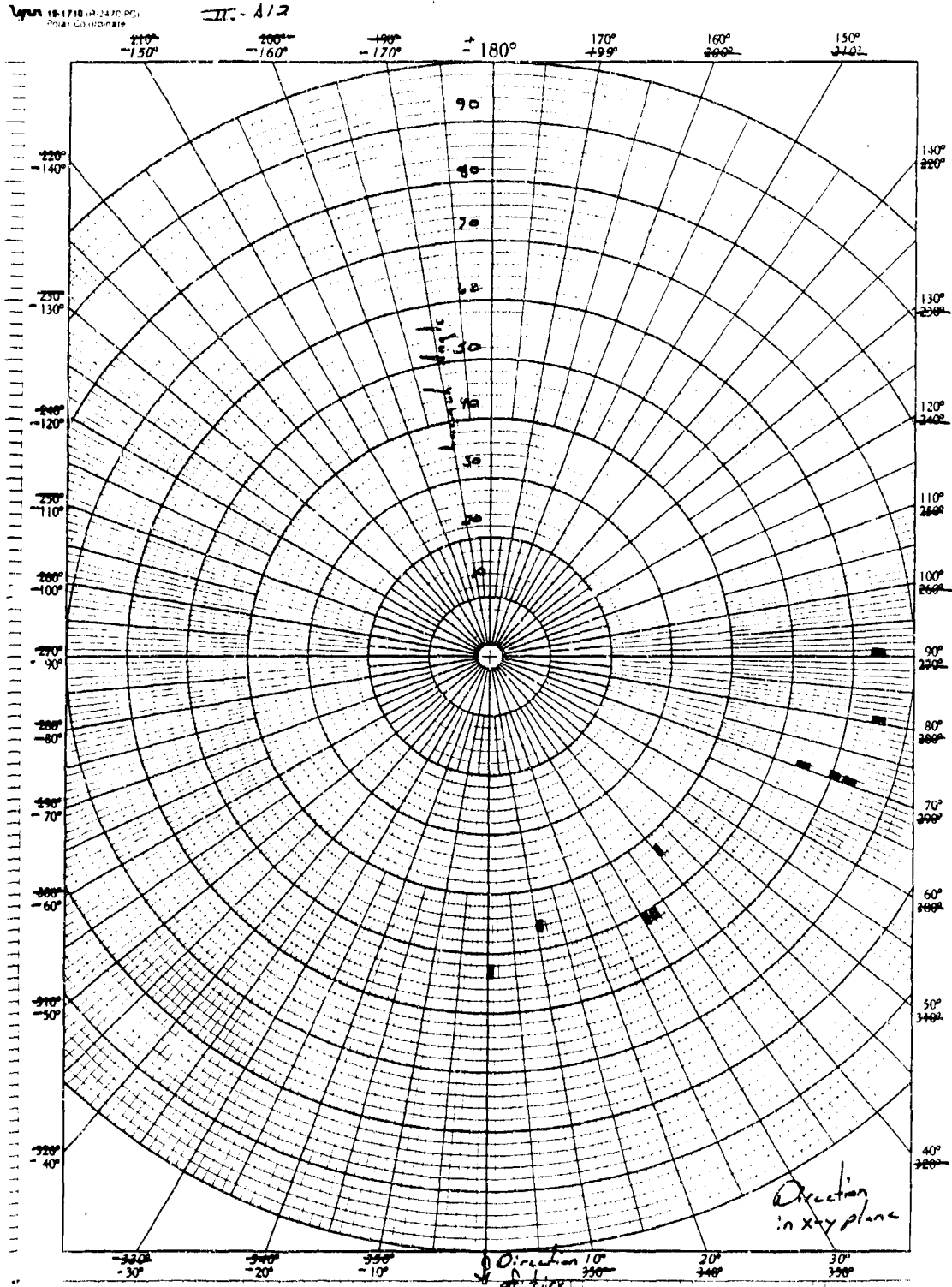


Figure B64. Test IIA12, Dual-Wheel, Aggregate Bed, 2% Coverage, Direction and Elevation Distribution.

II-A13

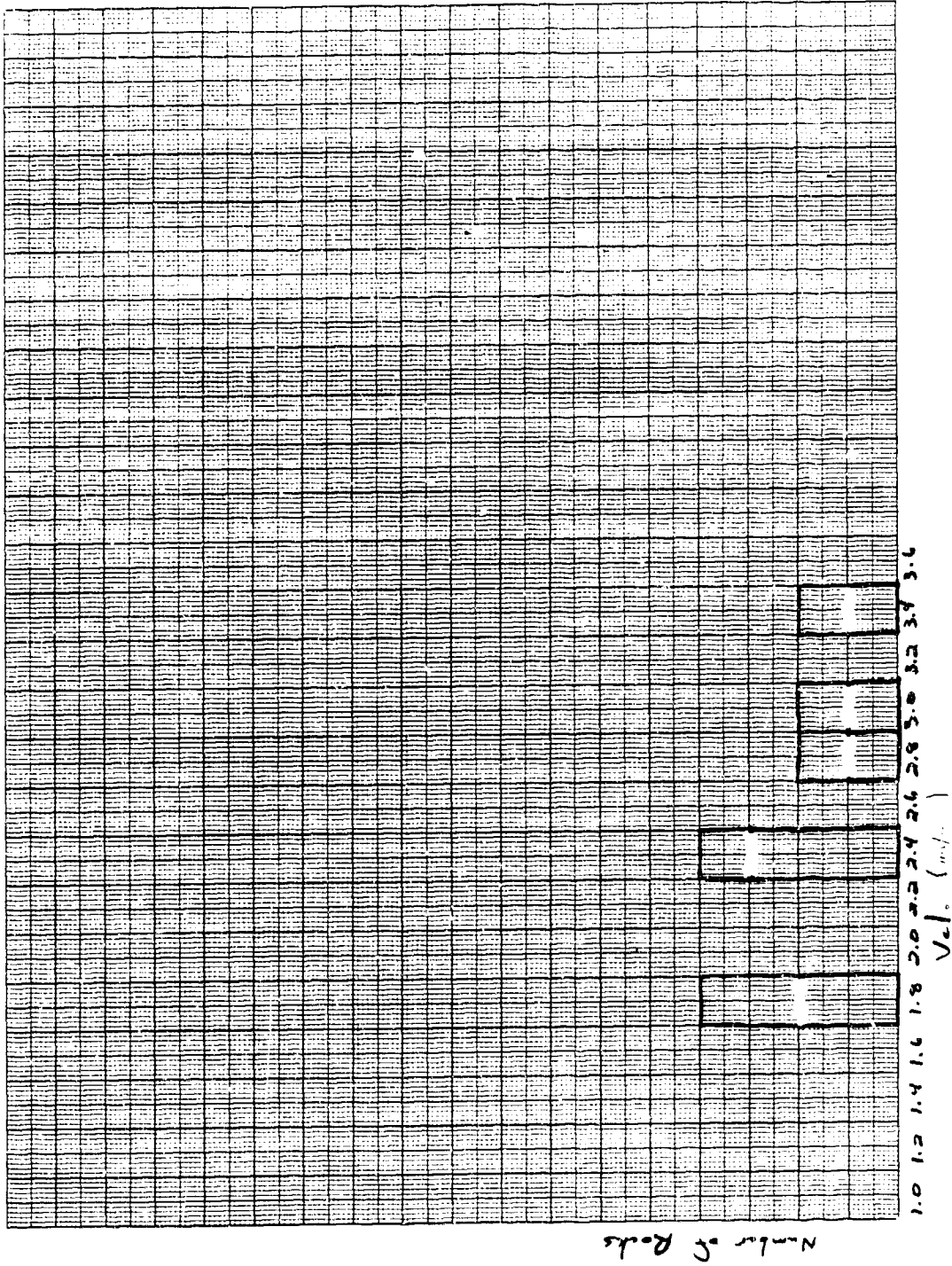


Figure B65. Test IIA13, Dual Wheels, Low-Pressure, Aggregate Bed, 2% Coverage, Velocity Distribution.

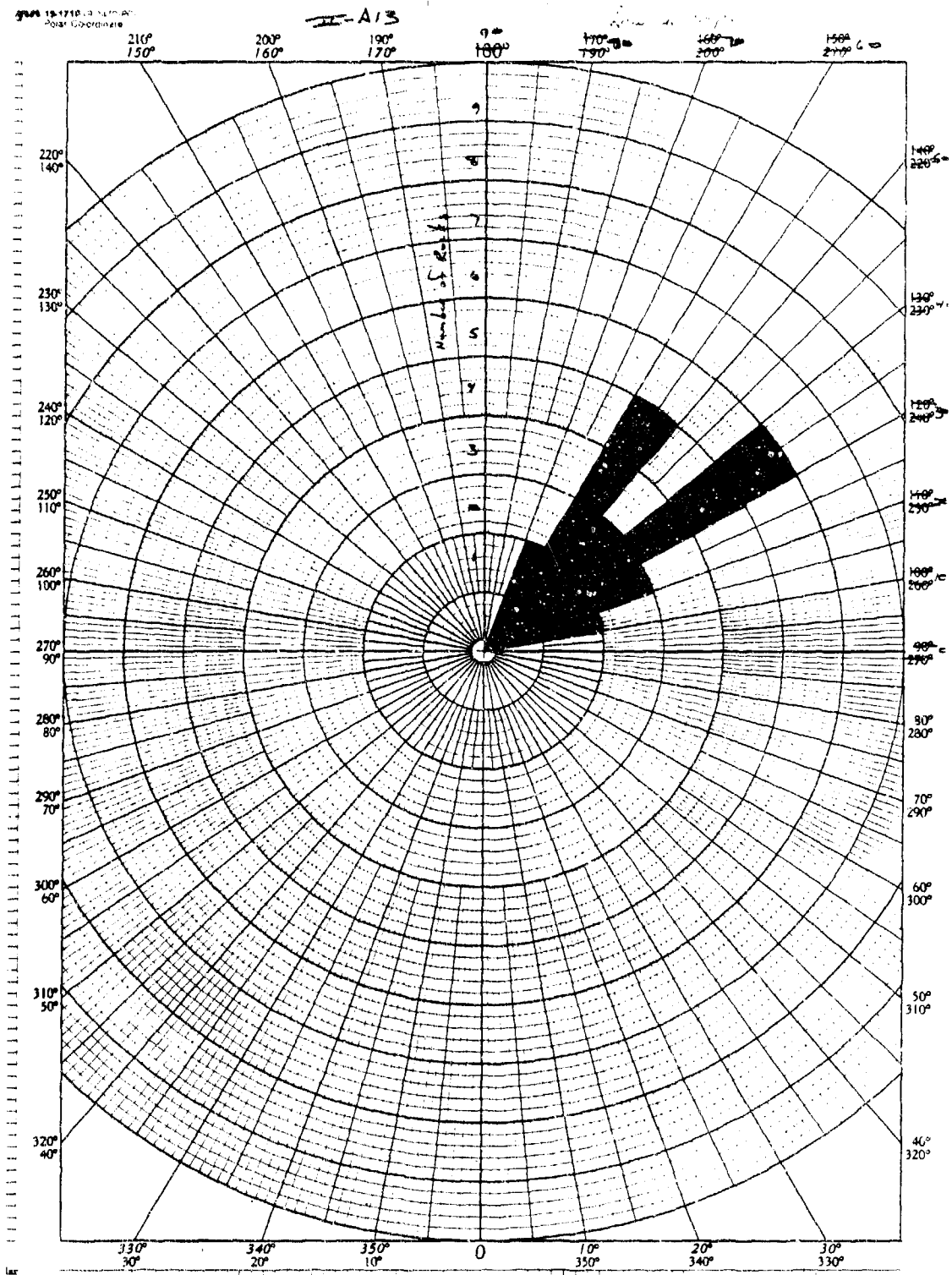


Figure B65. Test IIA13, Aggregate Bed, 2% Coverage, Elevation Angle Distribution.

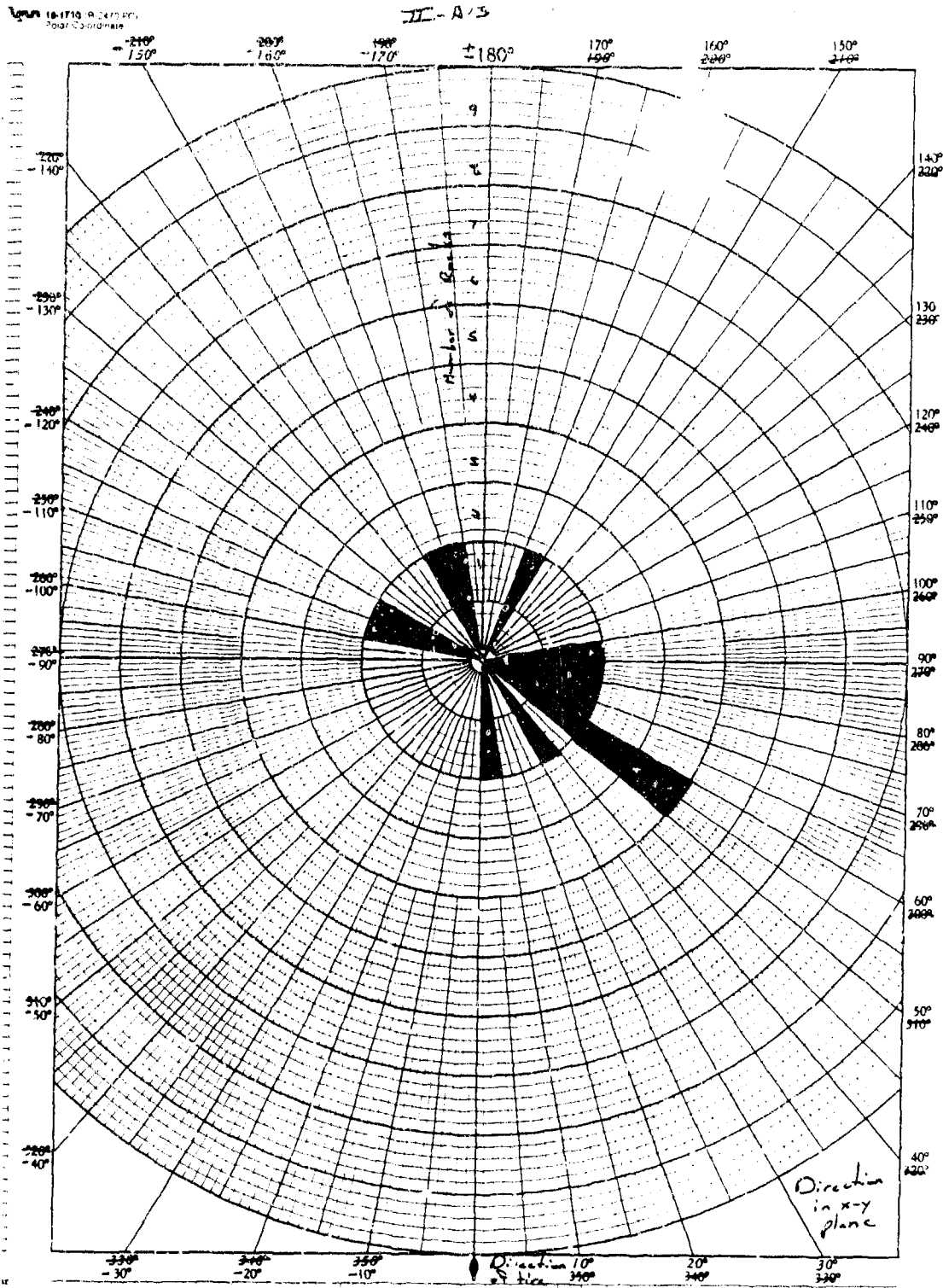


Figure B67. Test IIA13, Aggregate Bed, 2% Coverage, Direction Distribution.

ALL LARGE ROCKS MATRIX III

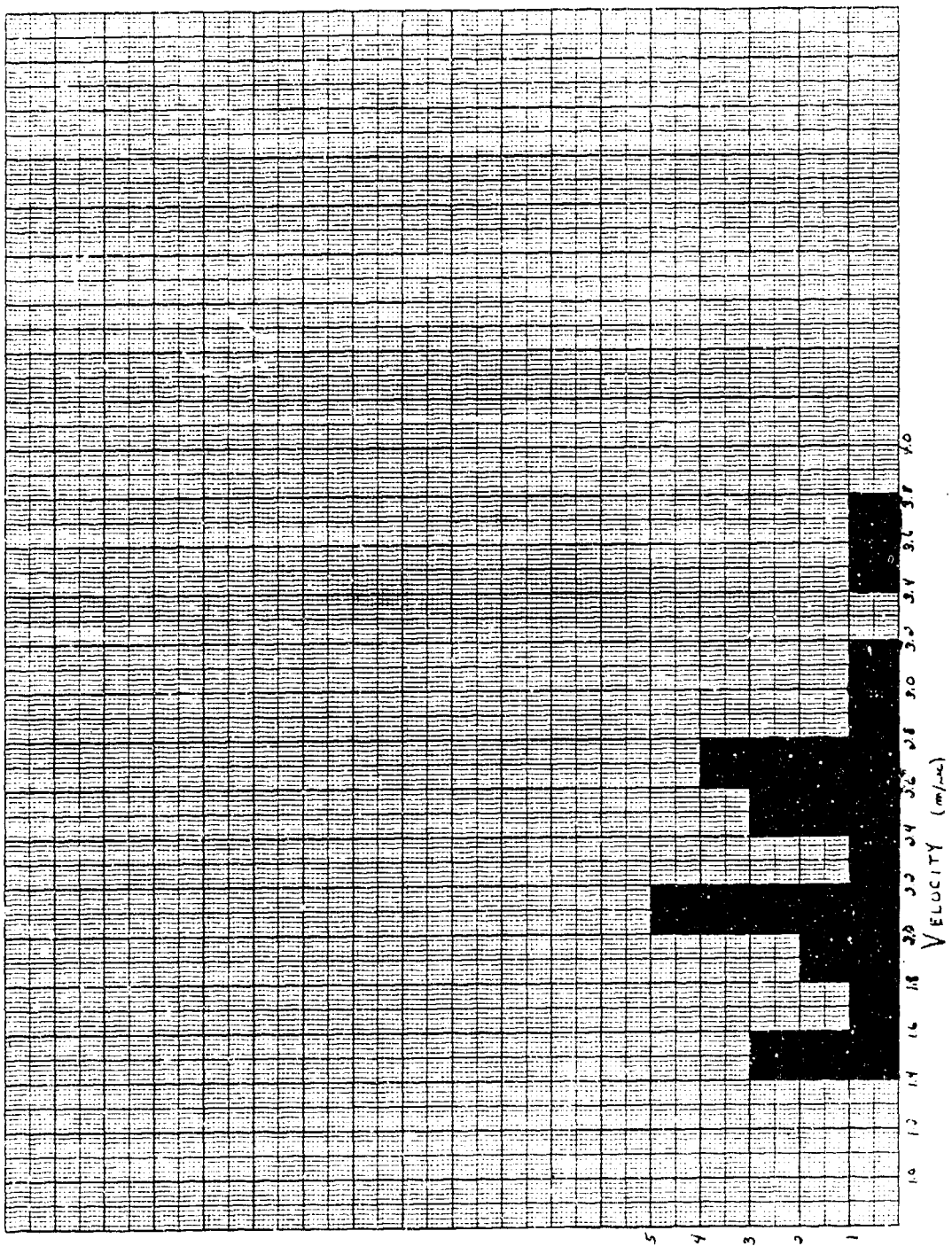


Figure B68. All Wet Tests, Test Matrix III, Large Rocks, Velocity Distribution.

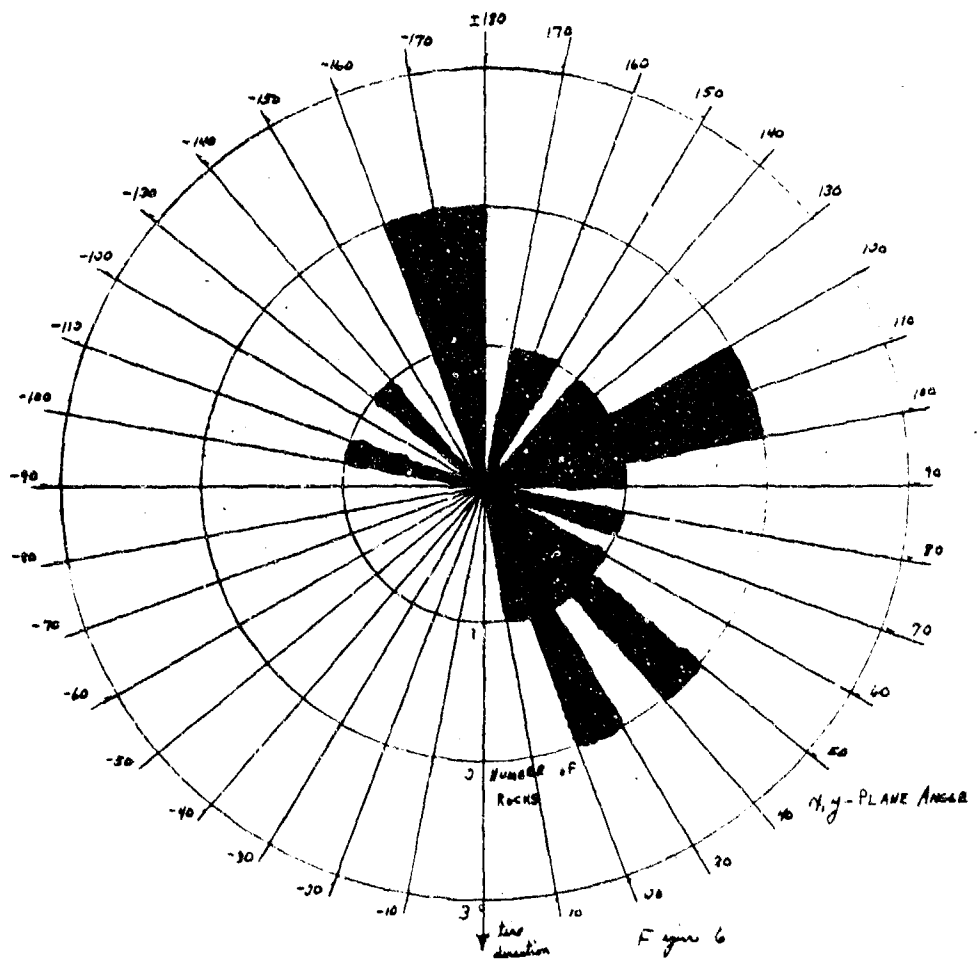
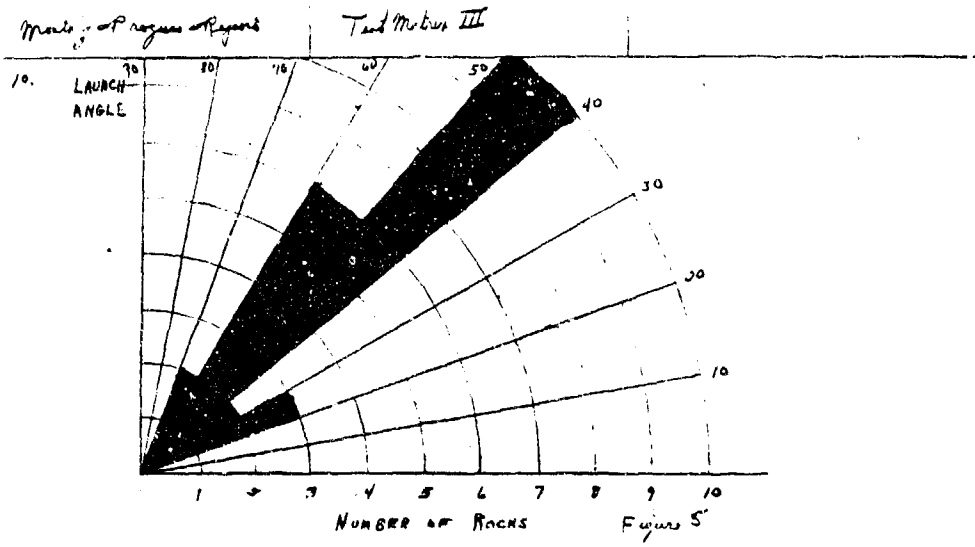


Figure B69. All Wet Tests, Test Matrix III, Large Rocks, Elevation Angle and Direction Distribution.

ALL LARGE ROCKS MATRIX III

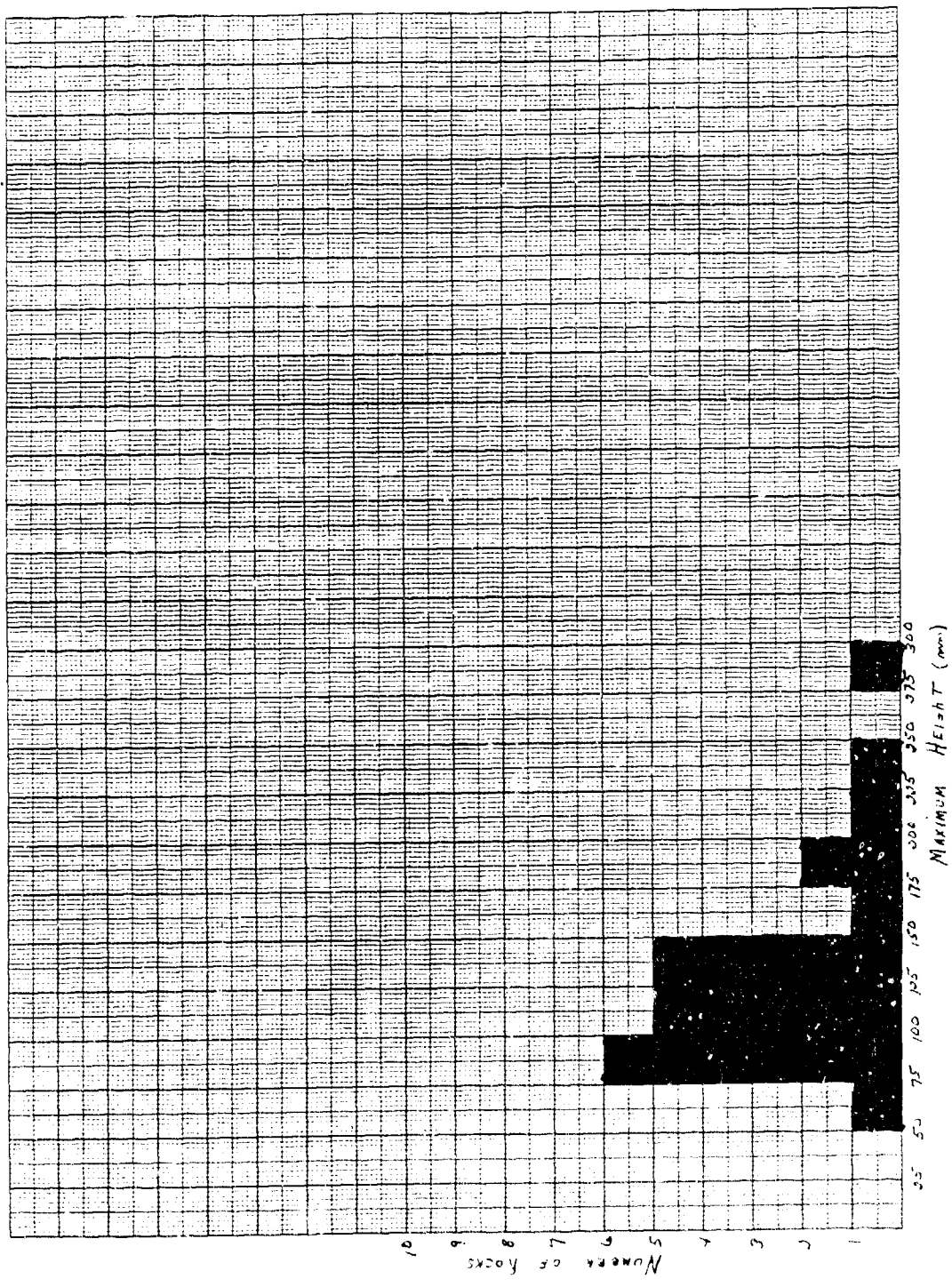


Figure B70. All Wet Tests, Test Matrix III, Large Rocks, Maximum Height Distribution.

```

*****
TEST # 3UC1B
*****
LAUNCH COORDINATES (ROT.,MM.)
*****
PEBBLE # 1      X      Y      Z      LAUNCH VEL.      LAUNCH ANGLE      ANGLE (X-Y PLANE)      MAX. HEIGHT
1      2.9667      212.4899      -0.0001      3632.4106      53.8250      78.3542      439.6465
*****
TEST # 3UC1B      PASS # 15
*****
LAUNCH COORDINATES (ROT.,MM.)
*****
PEBBLE # 1      X      Y      Z      LAUNCH VEL.      LAUNCH ANGLE      ANGLE (X-Y PLANE)      MAX. HEIGHT
1      -11.7774      214.8962      0.0000      4544.7524      48.6817      60.8382      594.4373
2      -5.4486      189.1000      0.0000      3377.2283      58.9928      65.3771      427.4937
3      -8.3195      214.3677      0.0000      2128.9600      58.5661      62.0481      168.4256
4      118.8637      243.5070      0.0000      2265.2061      66.6795      67.7342      220.7664
5      125.9835      235.4935      0.0000      1500.5898      62.7389      65.5984      90.7823
*****
* LOG
* LOFTING      loaded out at 5-OCT-1982 16128156.14
* Username:

```

323.4

66

53

3907

max

0

0

0

0

0

0

0

0

0

0

0

Figure B71. Sample Computer Printout.